

LOAN DOCUMENT

PHOTOGRAPH THIS SHEET

①

INVENTORY

AD-A252 127



DTIC ACCESSION NUMBER

LEVEL

Proceedings 14th Annual Gravity
Gradiometry Conference

DOCUMENT IDENTIFICATION

11-12 Feb 86

DISTRIBUTION STATEMENT A

Approved for public release;
Distribution Unlimited



DISTRIBUTION STATEMENT

ACCESSION FOR

NTIS GRA&I
DTIC TRAC
UNANNOUNCED
JUSTIFICATION



BY

DISTRIBUTION/

AVAILABILITY CODES

DISTRIBUTION AVAILABILITY AND/OR SPECIAL

A-1

DISTRIBUTION STAMP

DTIC
ELECTE
JUN 24 1992
S C D

DATE ACCESSIONED

DATE RETURNED

92 6 23 039

DATE RECEIVED IN DTIC

92-16507



REGISTERED OR CERTIFIED NUMBER

PHOTOGRAPH THIS SHEET AND RETURN TO DTIC-FDAC

H
A
N
D
L
E

W
I
T
H

C
A
R
E



DEPARTMENT OF THE AIR FORCE
AIR FORCE GEOPHYSICS LABORATORY (AFSC)
HANSCOM AIR FORCE BASE, MASSACHUSETTS 01731-5000

AD-A252 127



REPLY TO
ATTN OF LWG (Capt Fundak (617) 377-3486)

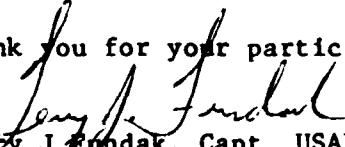
SUBJECT Gravity Gradiometer Conference Presentations

TO

Enclosed please find the 1986 Gravity Gradiometer Conference Presentations. I would like to apologize for taking my time in getting this out to you. I know a year late is a long time after my promised April 86 delivery. For those of you who are attending this years' conference, please remind me of how long it took, so I'll be embarrassed enough to get it out more promptly.

The experiment I tried with the "Question/Answer Sheets" was a partial success. However, as with any experiment there was experimental error. Some data points are missing, which leads me to believe that I did not stress the importance of experiment sufficiently to everyone. To all those speakers who may feel that their responses were not accurately recorded, you'll have to blame me. It is my hope, though, that no bias was introduced into the experiment. It was my conclusion that most errors were of a random nature and have not detracted from the resulting compilation. You will also have to blame me for typo's, spelling, grammatical errors and any other mistakes that went uncorrected. In some cases, I have altered the wording of the questions or responses for clarity.

Thank you for your participation at the 14th Gravity Gradiometer Conference.


Terry J. Fundak, Capt, USAF
Geodesy and Gravity Branch
Earth Sciences Division

**Proceedings of the
Fourteenth Annual Gravity Gradiometry Conference
United States Air Force Academy
Colorado Springs, Colorado**

11-12 February 1986

**Edited by:
1Lt Terry J Fundak**

Approved for public release; distribution unlimited.

AGENDA

Fourteenth Gravity Gradiometry Conference United States Air Force Academy Colorado Springs, Colorado

Tuesday 11 February

- 0730 - Buses depart USAFA Officers' Club for Fairchild Hall
- 0745 - Registration - 3rd floor Fairchild Hall, South End
- 0800 - Welcome/Introduction - 1Lt Terry J Fundak
- 0810 - Opening Remarks - Dr. Donald H. Eckhardt
- 0830 - " Development Experience of a Moving Base Gravity Gradiometer and Discussion of Future Applications "
Mr. Ernest H. Metzger
- 0900 - " Gradiometry & Geodesy, or Separating Inseparables "
Dr. Christopher Jekeli
- 0920 - " Requirements for the use of Airborne Gradiometry in Exploration Geophysics "
Dr. Klaus-Peter Schwarz
- 0945 - Break
- 1000 - " Applications of Superconducting Gravity Gradiometer System toward Inertial Guidance and Fundamental Science "
Dr. Hinghung A. Chan, Dr. Martin Vol Moody, Dr. Ho Jung Paik*
- 1030 - " Quick Review of Gradiometer-Aided Land Navigation "
Dr. Warren G. Heller
- 1050 - " Efficient Gravity Gradient Data Gathering "
Mr. Michel Bilello*, Dr. John B. Breakwell, Dr. Daniel B. DeBra
- 1110 - " Use of Terrain Elevation Data in Airborne Gradiometry "
Dr. Julian L. Center, Jr.
- 1145 - Buses depart Fairchild Hall for USAFA Officers' Club
- 1200 - Luncheon - Officers' Club
- 1315 - Buses depart Officers' Club for Fairchild Hall
- 1330 - " The Gravity Gradiometer Survey System "
1Lt Terry J. Fundak
- 1350 - " Airborne Gravity Gradiometer Data Processing "
Dr. William J. Hutcheson

- 1410 - " Isomorphic Geodetic and Electrical Networks: An Application to the Analysis of Airborne Gravity Gradiometer Survey Data "
Dr. Donald H. Eckhardt
- 1430 - " Stage II Processing of Airborne Gravity Gradiometer Data using Frequency Domain Techniques "
Mr. Anthony A. Vassiliou
- 1450 - Break
- 1505 - " Karhunen-Loeve Gravity Gradiometer Data Processing "
Dr. Sam C. Bose
- 1525 - " Gravity Gradiometer (GGSS) Test Planning and Test Data Treatment"
Dr. Warren G. Heller
- 1545 - " Gradient Integration Procedure for Path Error Reduction "
Mr. Alan E. Rufty
- 1615 - Buses depart Fairchild Hall for USAFA Officers' Club
- 1630 - Reception - USAFA Officers' Club

Wednesday 12 February

- 0800 - Buses depart USAFA Officers' Club for Fairchild Hall
- 0810 - " NASA Requirements for a Spaceborne Gravity Gradiometers - An Overview "
Mr. Charles J. Finley, Dr. David E. Smith
Presented by Mr. Werner D. Kahn
- 0825 - " Gravity Field Fine Structure Mapping using a Spaceborne Gravity Gradiometer "
Mr. Werner D. Kahn
- 0845 - " Superconducting Gravity Gradiometer on the Space Shuttle "
Dr. Samuel H. Morgan, Mr. Joe R. Parker*
- 0910 - " Development of Superconducting Gravity Gradiometer for Space Applications "
Dr. Hinghung A. Chan, Dr. Martin Vol Moody*, Dr. Ho Jung Paik
- 0930 - Break
- 0945 - " Platform Requirements and Error Compensation for a Superconducting Gravity Gradiometer "
Dr. Ho Jung Paik
- 1015 - " TLC for a Magnetically Floated Gravity Gradiometer "
Dr. Dave Sonnabend
- 1040 - " Development of a High-Sensitivity Non-Cryogenic Gravity Gradiometer for Spaceborne Use "
Dr. F. Bordoni, Dr. F. Fuligini*, Dr. B. V. Iafolla,
Dr. Enrico C. Lorenzini

- 1110 - " Common Mode Balancing Gradiometer with Monocrystalline Silicon
Suspension for High Sensitivity Gravity Measurements "
Dr. Jean-Paul Richard
- 1140 - " Liquid-Supported Torsion Balance as a Gradiometer"
Dr. James E. Faller, Mr. Paul T. Keyser*
- 1210 - Closing Remarks
1Lt Terry J Fundak
- 1230 - Buses leave for lunch at USAFA Officers' Club
- 1345 - Tour of Air Force Academy

Conference Participants by Organizational Affiliation

<u>Organization</u>	<u>Name</u>
Aero Services	Richard O. Crosby
Air Force 6585th Test Group	Richard Pearson
Air Force Geophysics Laboratory	*Don Eckhardt *Terry Fundak *Chris Jekeli Tom Rooney Andy Lazarewicz Brenda Schliniski
Air Force Intelligence Service	J. Edward Jones
Applied Sciences Analytics	*Sam Bose
Barringer Resources	Anthony Barringer George Hinton
Bell Aerospace Textron	*William John Hutcheson Albert Jircitano *Ernest Metzger Andrew Grierson Louis Pfohl John White
The Charles Stark Draper Laboratory	Milton Trageser
Colorado School of Mines	Harry Emrick Richard Hansen
Defense Mapping Agency	Randy Smith B. Louis Decker John J. Graham
Dynamics Research Corp	Don Benson Alan Zorn
Geodynamics Corp	Chris Harrison
Geospace Corp	Stan Jordan *Julian Center Scott Peacock
Honeywell Inc.	Michael Hadfield
Istituto di Fisica dello Spazio Interplanetario	*Franco Fuligni
Jet Propulsion Laboratory	*Dave Son nabend
Johns Hopkins University Applied Physics Laboratory	Jonathan Howland Paul Zucker

Astrophysics	Jim Faller
NASA/Goddard Space Flight Center	*Werner D. Kahn
NASA/Marshall Space Flight Center	*Joe Parker
National Bureau of Standards	Donald McDonald
National Oceanic and Atmosphere Administration	Robert Moose
Naval Surface Weapons Center	Peter Ugincius *Alan Rufty
Nortech Surveys	Gerald Lachapella
Smithsonian Astrophysical Observatory	Enrico Lorenzini
Stanford University	*Michel Bilello John Breakwell Dan DeBra
The Analytic Sciences Corp	*Warren Heller
University of Calgary	*Klaus-Peter Schwarz *Anthony Vassiliou
University of Maryland	*Ho Jung Paik *M. Vol Moody *Jean-Paul Richard
University of Texas	Wayne Peebles
U.S. Army Engineer Topographic Laboratories	Hans Baussus von Luetzow
U.S. Geological Survey	Lin Cordell Thomas Hildenbrand Larry Beyer
U.S. Navy Oceanographic Office	Don Parker Jim Strauss
U.S. Navy Strategic Systems Program Office	Bernard Epstein

* indicates conference speaker

Alphabetical Listing of Conference Participants

<u>Name</u>	<u>Organization</u>
Anthony Barringer	Barringer Resources
Hans Baussus von Luetzow	U.S. Army Engineer Topographic Laboratory
Don Benson	Dynamics Research Corp
Larry Beyer	U.S. Geological Survey
*Michel Bilello	Stanford University
*Sam Bose	Applied Science Analytics
John Breakwell	Stanford University
*Julian Center	Geospace Corp
Lin Cordell	U.S. Geological Survey
Richard Crosby	Aero Services
B. Louis Decker	Defense Mapping Agency
Dan DeBra	Stanford University
*Don Eckhardt	Air Force Geophysics Laboratory
Harry Emrick	Colorado School of Mines
Bernard Epstein	U. S. Navy Strategic Systems Program Office
Jim Faller	Joint Institute for Laboratory Astrophysics
*Franco Fuligni	Istituto di Fisica dello Spazio Interplanetario
*Terry Fundak	Air Force Geophysics Laboratory
John Graham	Defense Mapping Agency
Andy Grierson	Bell Aerospace Textron
Michael Hadfield	Honeywell Corp
Chris Harrison	Geodynamics Corp
Ricahrd Hansen	Colorado School of Mines
*Warren Heller	The Analytic Sciences Corp
Thomas Hildenbrand	U.S. Geological Survey
George Hinton	Barringer Resources
Jonathan Howland	Johns Hopkins University/Applied Physics Laboratory
*John Hutcheson	Bell Aerospace Textron
*Chris Jekeli	Air Force Geophysics Laboratory
Al Jircitano	Bell Aerospace Textron
J. Edward Jones	Air Force Intelligence Service
Stan Jordan	Geospace Systems Corp
*Werner Kahn	Goddard Space Flight Center
*Paul Keyser	Joint Institute for Laboratory Astrophysics
Gerard Lachapelle	Nortech Surveys
Andy Lazarewicz	Air Force Geophysics Laboratory
Enrico Lorenzini	Harvard-Smithsonian Center for Astrophysics
Donald McDonald	National Bureau of Standards
*Ernie Metzger	Bell Aerospace Textron
*Vol Moody	University of Maryland
Robert Moose	National Oceanic and Atmospheric Administration
*Ho Jung Paik	University of Maryland
Don Parker	Naval Oceanographic Office
*Joe Parker	Marshall Space Flight Center

Scott Peacock
Richard Pearson
Wayne Peebles
Lou Pfohl
*Jean-Paul Richard
Tom Rooney
*Alan Rufty
Brenda Schilinski
*Klaus-Peter Schwarz
Randy Smith
*Dave Sonnabend
Jim Strauss
Milton Trageser
Peter Ugincius
*Anthony Vassiliou
John White
Alan Zorn
Paul Zucker

Geospace Systems Corp
Air Force 6585th Test Group
University of Texas
Bell Aerospace Textron
University of Maryland
Air Force Geophysics Laboratory
Naval Surface Weapons Center
Air Force Geophysics Laboratory
University of Calgary
Defense Mapping Agency
Jet Propulsion Laboratory
U.S. Naval Oceanographic Office
The Charles Stark Draper Laboratory
Naval Surface Weapons Center
University of Calgary
Bell Aerospace Textron
Dynamics Research Corp
Johns Hopkins University/Applied Physics Laboratory

* indicates conference speaker

Papers presented at the 14th Gravity Gradiometry Conference

1. *Mr. Ernest H. Metzger " Development Experience of a Moving Base Gravity
Bell Aerospace Textron Gradiometer and Discussion of Future Applications"
2. *Dr. Christopher Jekeli " Gradiometry & Geodesy, or Separating Inseparables"
Air Force Geophysics Lab
3. *Dr. Klaus-Peter Schwarz " Requirements for the use of Airborne Gradiometry
University of Calgary in Exploration Geophysics"
- 3A. *Dr. Warren G. Heller " Quick Review of Gradiometer-Aided Land Navigation"
The Analytic Sciences Corp
4. *Dr. Ho Jung Paik " Applications of Superconducting Gravity
Dr. Martin Vol Moody Gradiometer System toward Inertial Guidance
Dr. Hinghung A. Chan and Fundamental Science"
University of Maryland
5. *Mr. Michel Bilello " Efficient Gravity Gradient Data Gathering"
Dr. John B. Breakwell
Dr. Daniel B. DeBra
Stanford University
6. *Dr. Julian L. Center, Jr. " Use of Terrain Elevation Data in Airborne
Geospace Corp. Gradiometry"
7. *1Lt Terry J. Fundak " The Gravity Gradiometer Survey System"
Air Force Geophysics Lab
8. *Dr. William J. Hutcheson " Airborne Gravity Gradiometer Data Processing"
Bell Aerospace Textron
9. *Dr. Donald H. Eckhardt " Isomorphic Geodetic and Electrical Networks:
Air Force Geophysics Lab An Application to the Analysis of Airborne
Gravity Gradiometer Survey Data "
10. *Mr. Anthony A. Vassiliou " Stage II Processing of Airborne Gravity
University of Calgary Gradiometer Data using Frequency Domain Techniques "
11. *Dr. Sam C. Bose " Karhunen-Loeve Gravity Gradiometer Data Processing "
Applied Sciences Analytics
12. *Dr. Warren G. Heller " Gravity Gradiometer (GGSS) Test Planning and Test
The Analytic Science Corp Data Treatment "
13. *Mr. Alan E. Rufty " Gradient Integration Procedure for Path Error Reduction
Naval Surface Weapons Center
14. Dr. David E. Smith " NASA Requirements for a Spaceborne Gravity Gradiometer
Goddard Space Flt Ctr - An Overview "
Mr. Charles J. Finley
NASA Headquarters (Presented by *Mr. Werner D. Kahn)

15. *Mr. Werner D. Kahn " Gravity Field Fine Structure Mapping using a
Goddard Space Flt Ctr Spaceborne Gravity Gradiometer "
16. Dr. Samuel H. Morgan " Superconducting Gravity Gradiometer on the Space
*Mr. Joe R. Parker Shuttle"
Marshall Space Flt Ctr
17. Dr. Hinghung A. Chan " Development of Superconducting Gravity Gradiometer
*Dr. Martin Vol Moody for Space Applications "
Dr. Ho Jung Paik
University of Maryland
18. *Dr. Ho Jung Paik " Platform Requirements and Error Compensation for a
University of Maryland Superconducting Gravity Gradiometer "
19. *Dr. Dave Sonnadend " TLC for a Magnetically Floated Gravity Gradiometer "
- Jet Propulsion Lab
20. *Dr. Jean-Paul Richard " Common Mode Balancing Gradiometer with
University of Maryland Monocrystalline Silicon Suspension for High
Sensitivity Gravity Measurements "
21. *Mr. Paul T. Keyser " Liquid-Supported Torsion Balance as a Gradiometer"
- Dr. James E. Fallor
Joint Institute for Lab Astrophysics
22. Dr. Enrico C. Lorenzini " Development of a High-Sensitivity, Non-Cryogenic
Smithsonian Astrophysical Gravity Gradiometer for Space-borne Use "
Observatory
*Dr. Franco Fuligini (Presently at SAO)
Dr. B. V. Iafolla
Dr. F. Bordoni
Istituto di Fisica dello
Spazio Interplanetario

* indicates conference speaker

DEVELOPMENT EXPERIENCE OF A MOVING BASE GRAVITY GRADIOMETER
AND DISCUSSION OF FUTURE APPLICATIONS

E. H. Metzger
Bell Aerospace Textron
P. O. Box One
Buffalo, NY 14240

ABSTRACT

A summary of the development experience of the rotating accelerometer gravity gradiometer from its conception to reduction to practice yielding accurate measurements aboard a moving vehicle is presented. Potential future applications of moving base gravity gradiometers are outlined and the technical difficulties to achieve these objectives are discussed.

MOVING BASE GRAVITY GRADIOMETER REVIEW

**DEVELOPMENT EXPERIENCE OF A
MOVING BASE GRAVITY GRADIOMETER
and
DISCUSSION OF FUTURE APPLICATIONS**

Air Force Academy

Report No. 6501 927150 • FEBRUARY 11-12, 1986

Bell Aerospace **TEXTRON**

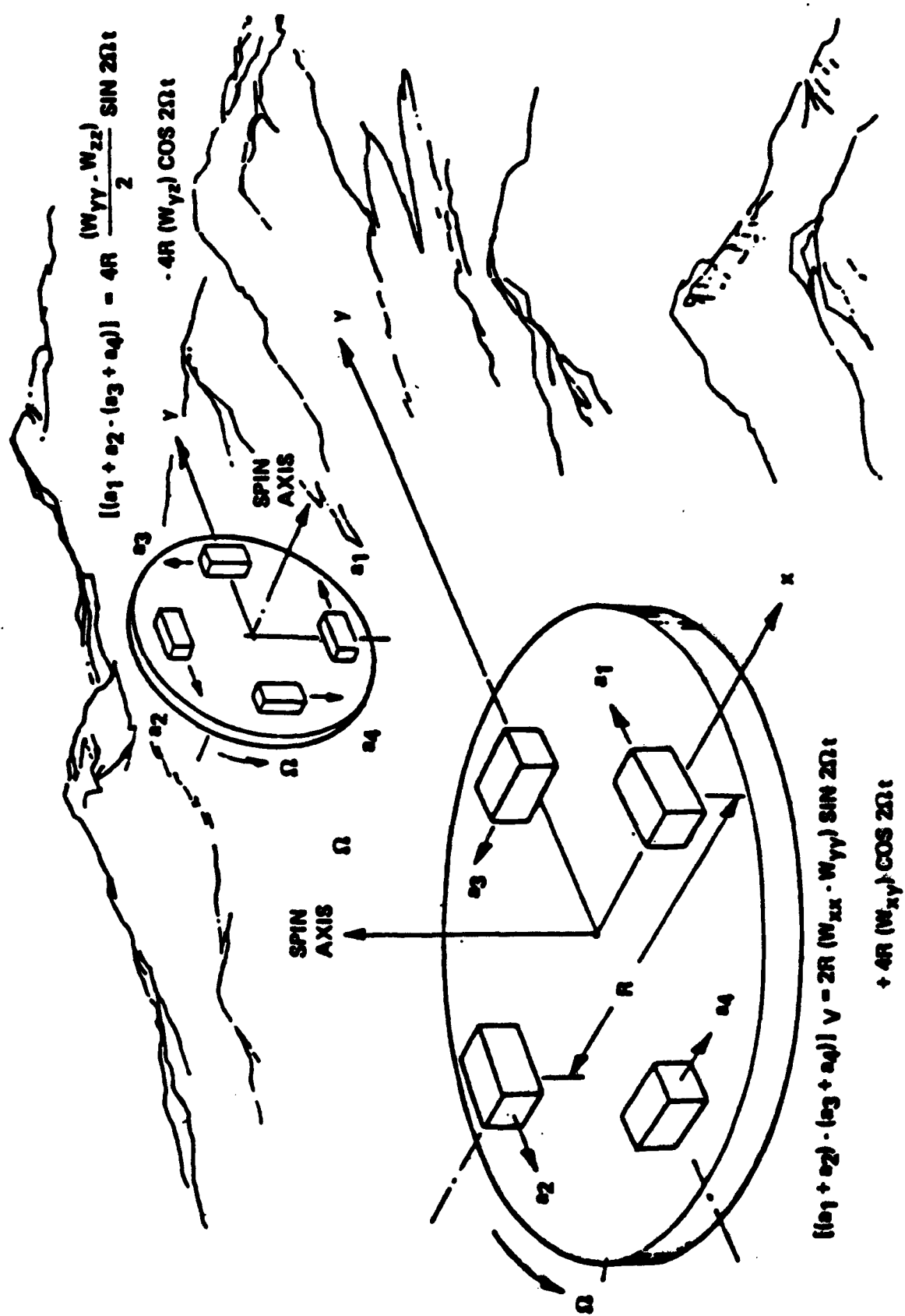
Division of Textron Inc.

POST OFFICE BOX ONE • BUFFALO, NEW YORK 14240

Gravity Gradiometer System Development Experience

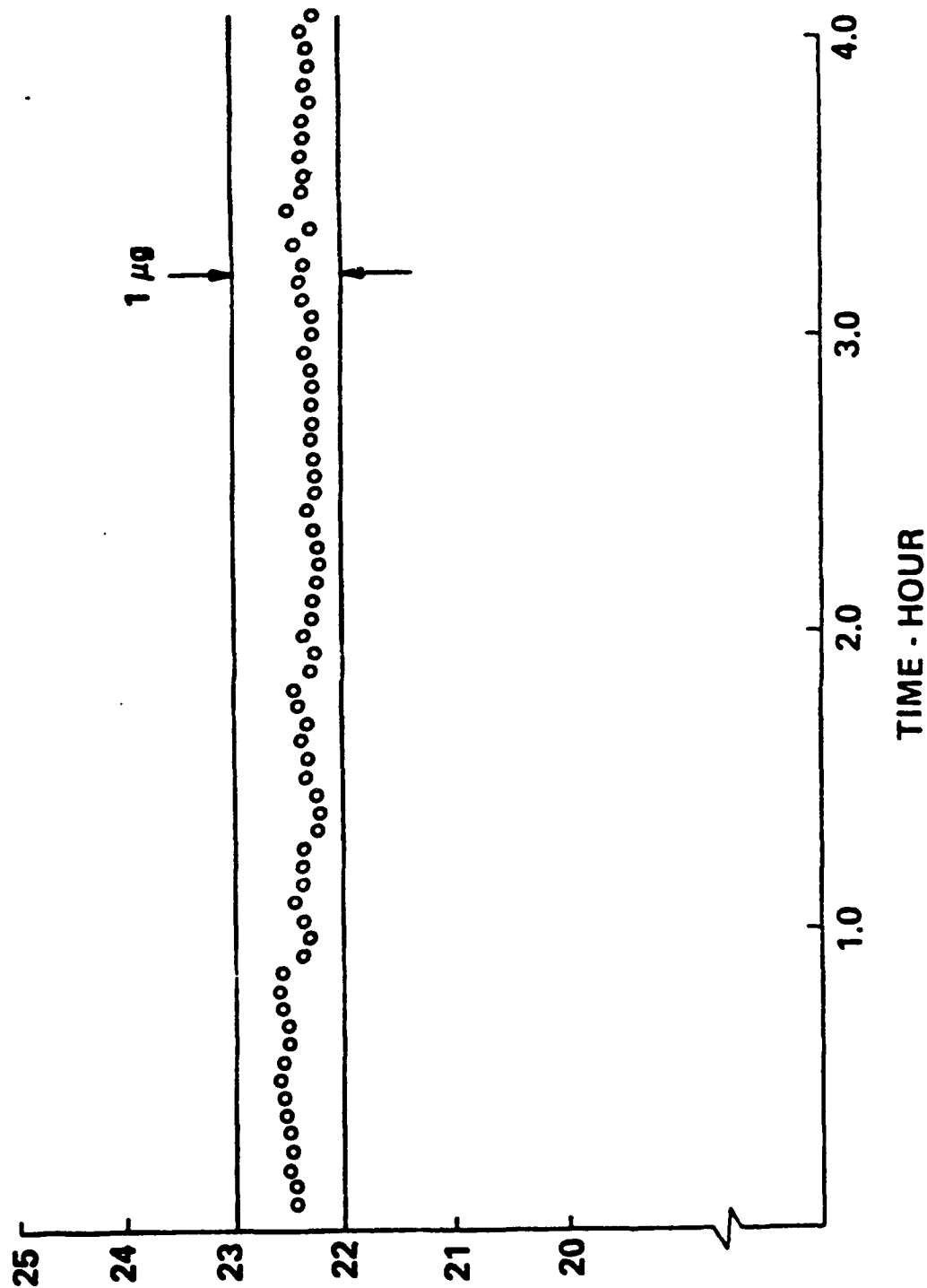
Bell Aerospace **TEXTRON**

SCHEMATIC ILLUSTRATION OF ROTATING FIXTURE

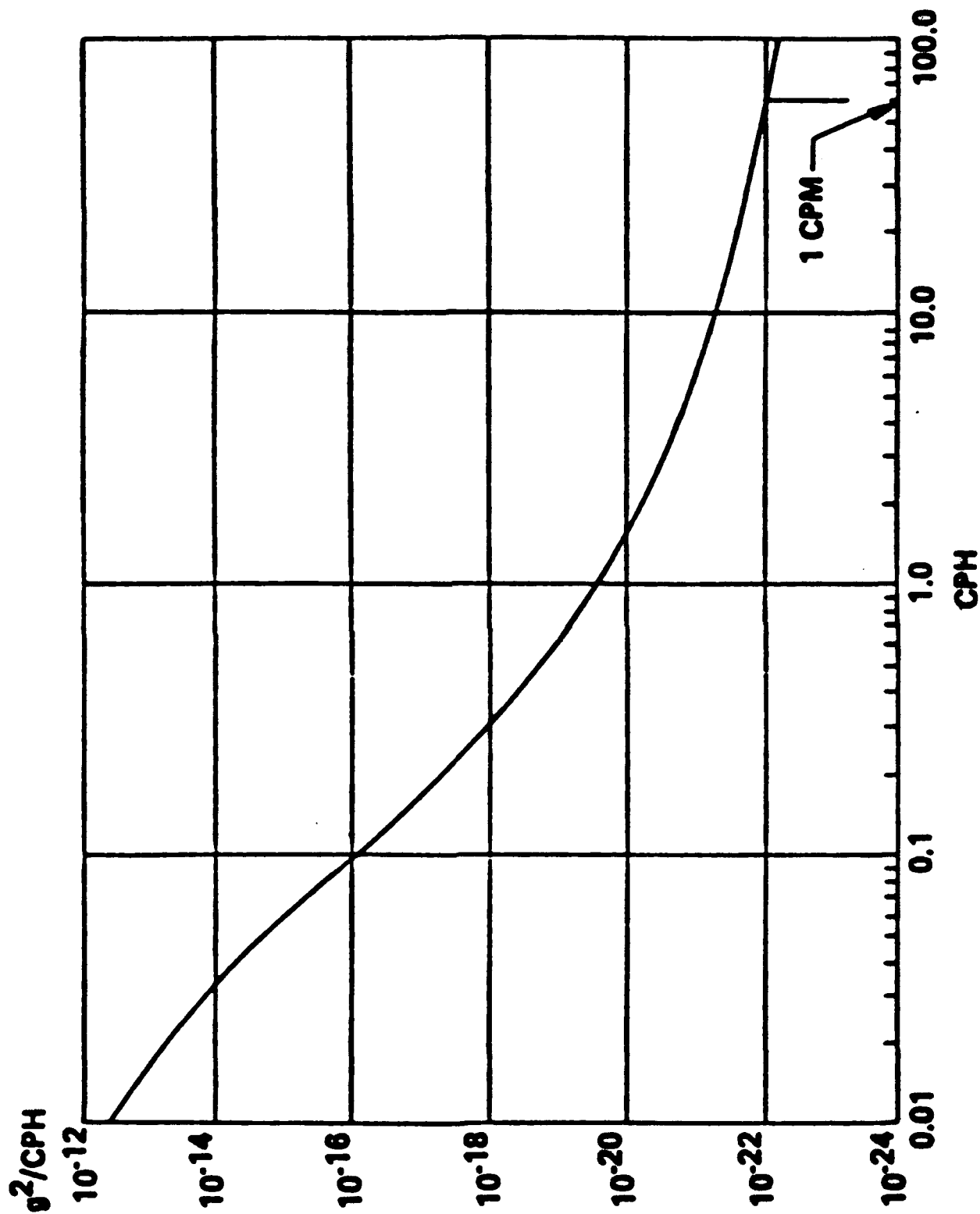


TYPICAL ACCELEROMETER NULL BIAS

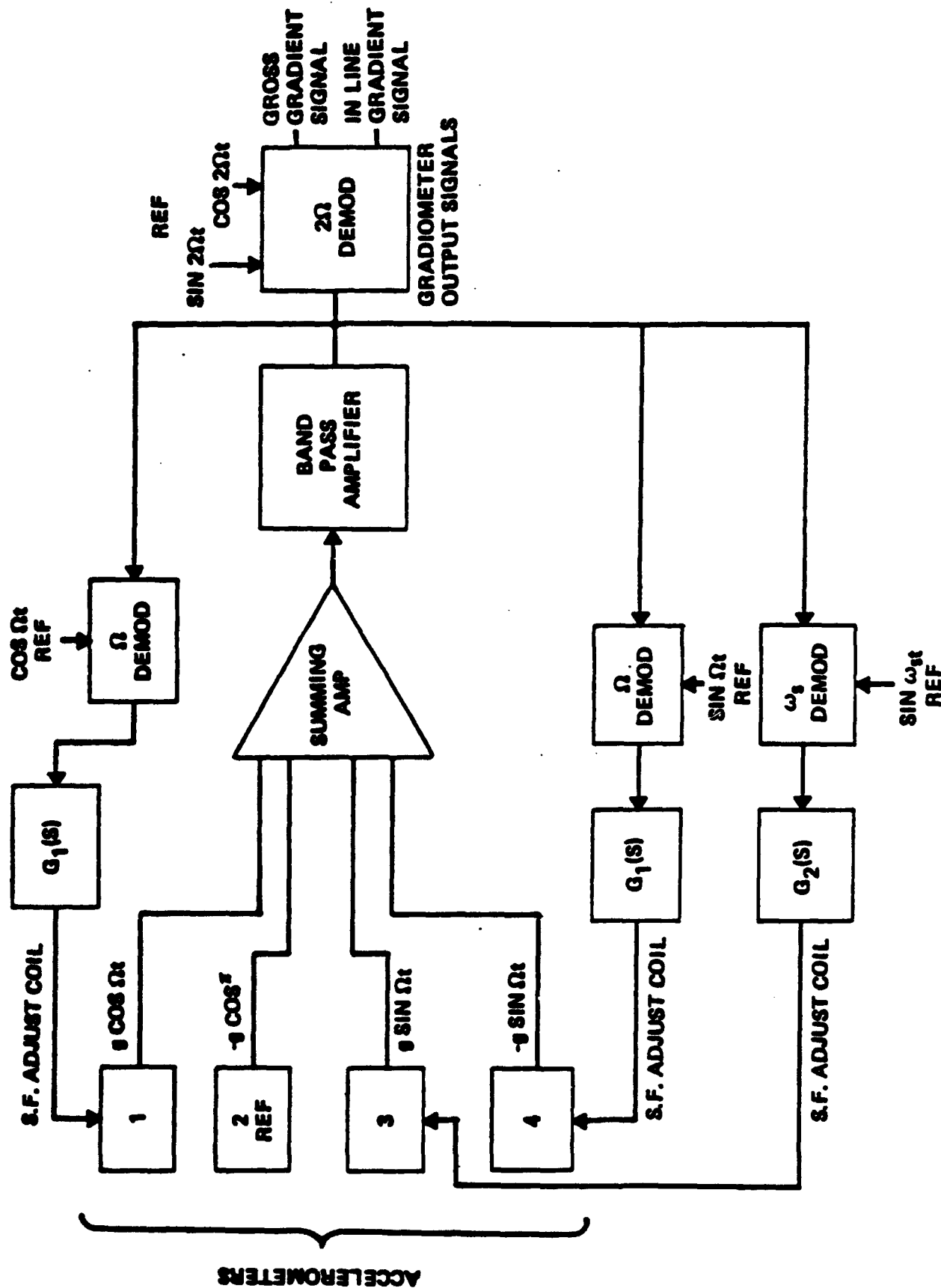
ACCELEROMETER BIAS - MICRO "g"



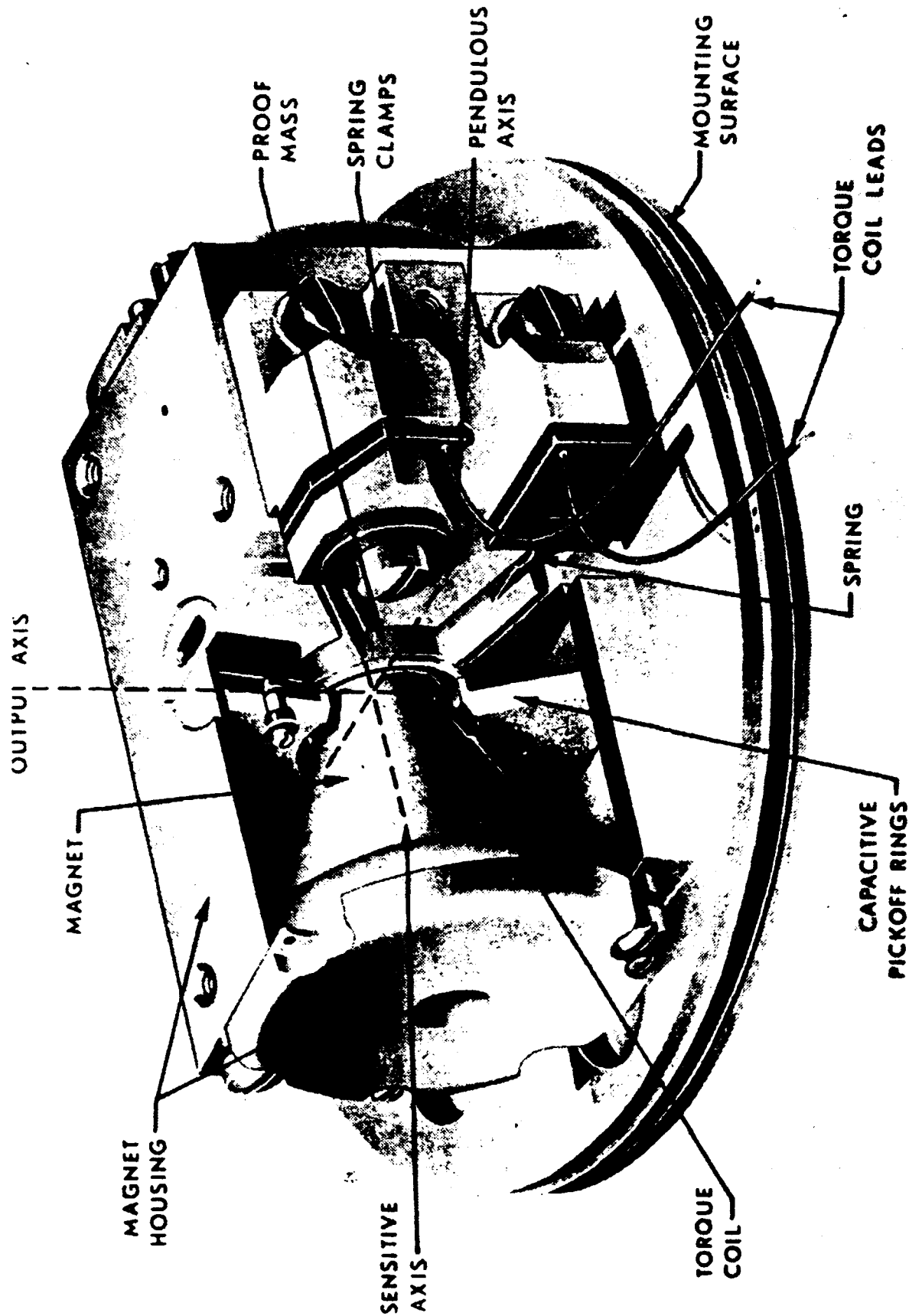
TYPICAL ACCELEROMETER NULL BIAS POWER SPECTRUM



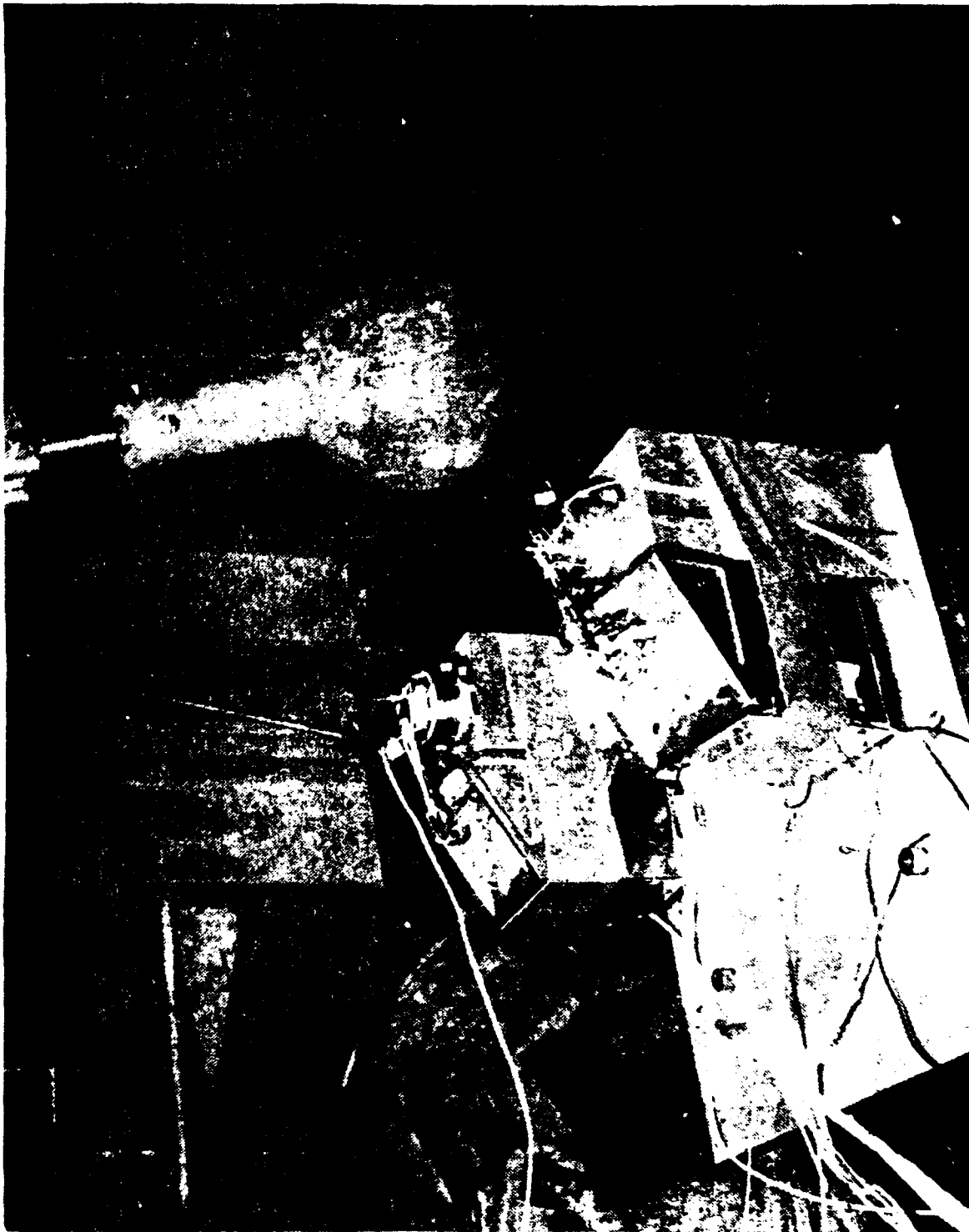
GGI SIGNAL PROCESS BLOCK DIAGRAM



MODEL VIIB ACCELEROMETER

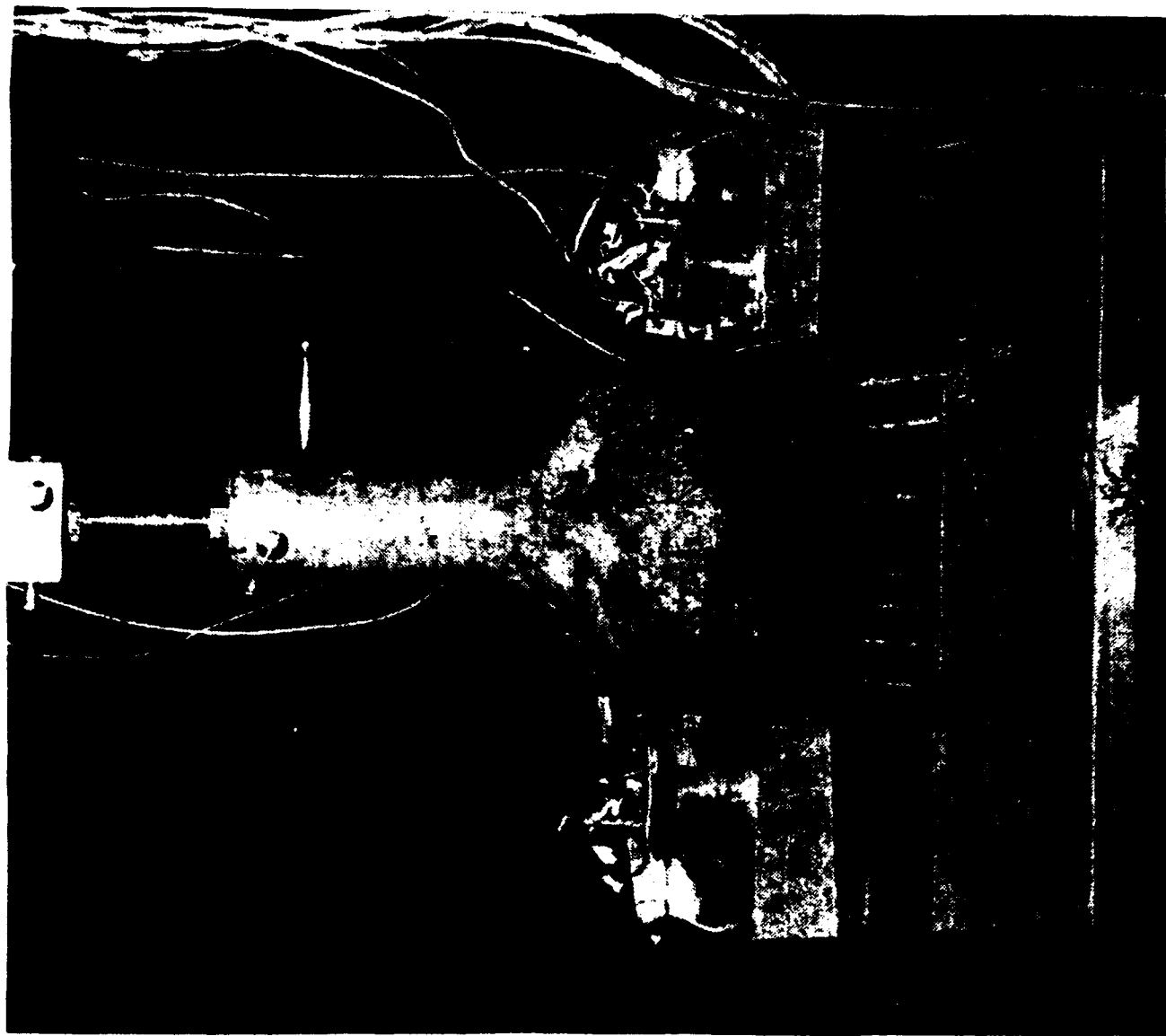


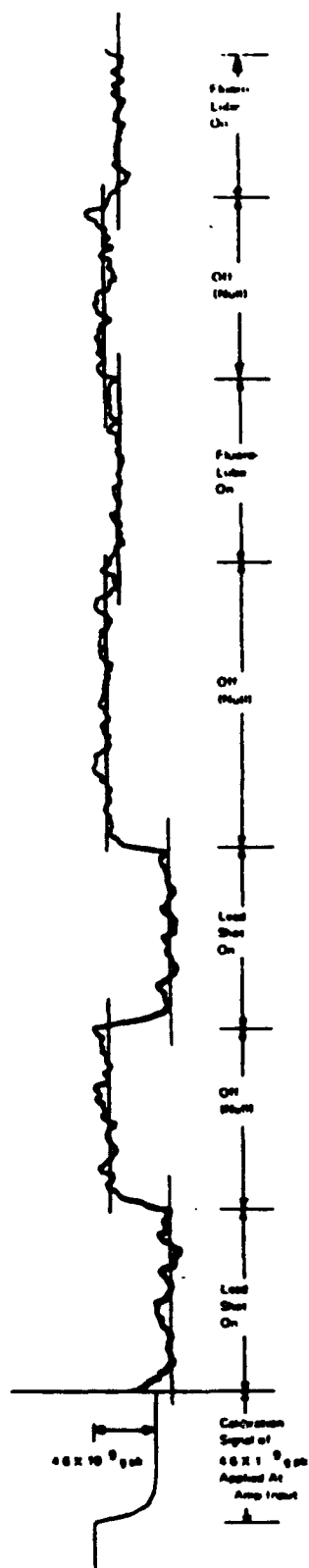
MASS ATTRACTION TEST - MODEL VII ACCELEROMETERS, FIBERGLASS COATED FLASK OUTSIDE ACCELEROMETERS



Bell Aerospace **TEXTRON**

MASS ATTRACTION TEST - MODEL VII ACCELEROMETERS, FIBERGLASS COATED FLASK BETWEEN ACCELEROMETERS





RESULTS OF MASS DETECTION EXPERIMENT

Material	Weight	Calculated Value	Measured Value
Lead	15.2 lb	3.4×10^{-9} g	15 mm = 4.4×10^{-9} g
Fluorolube	5.06 lb	1.1×10^{-9} g	3.5 mm = 1.1×10^{-9} g

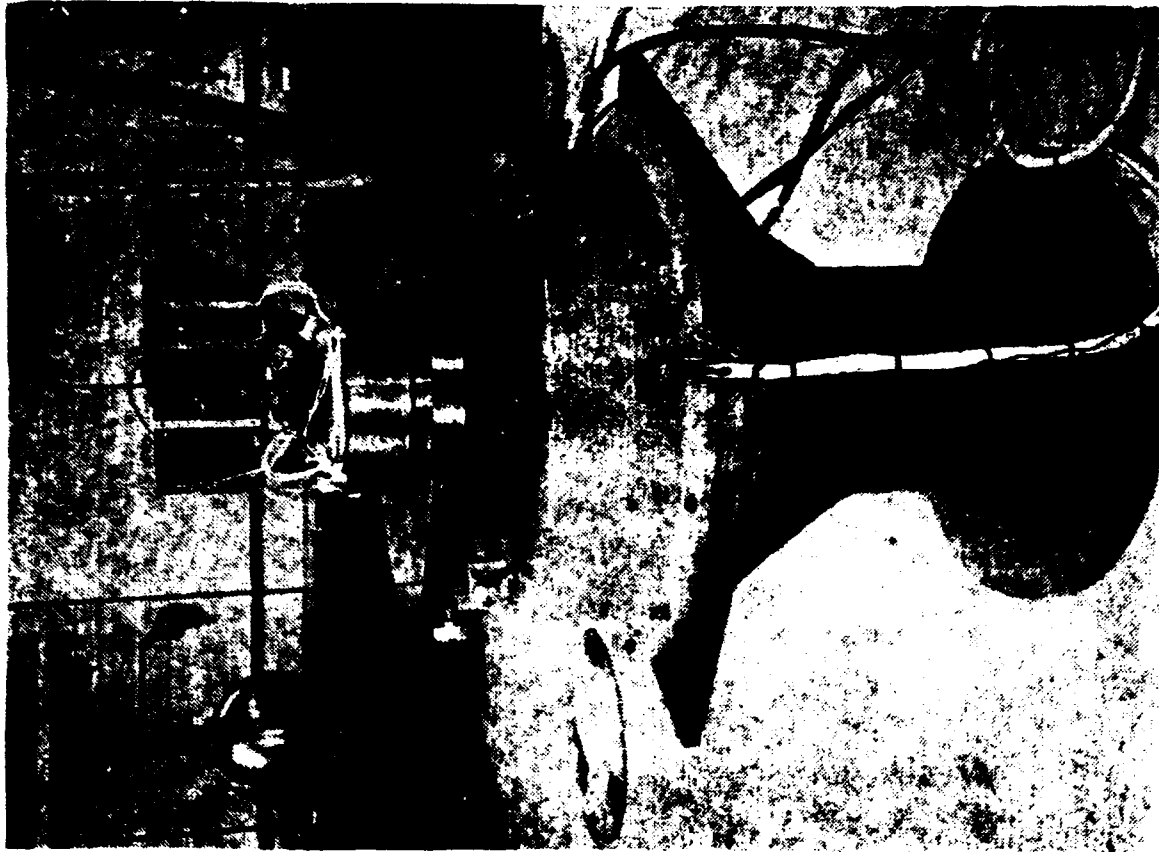
COMPARISON OF THEORETICAL AND MEASURED THERMAL NOISE

10 SECOND TIME CONSTANT

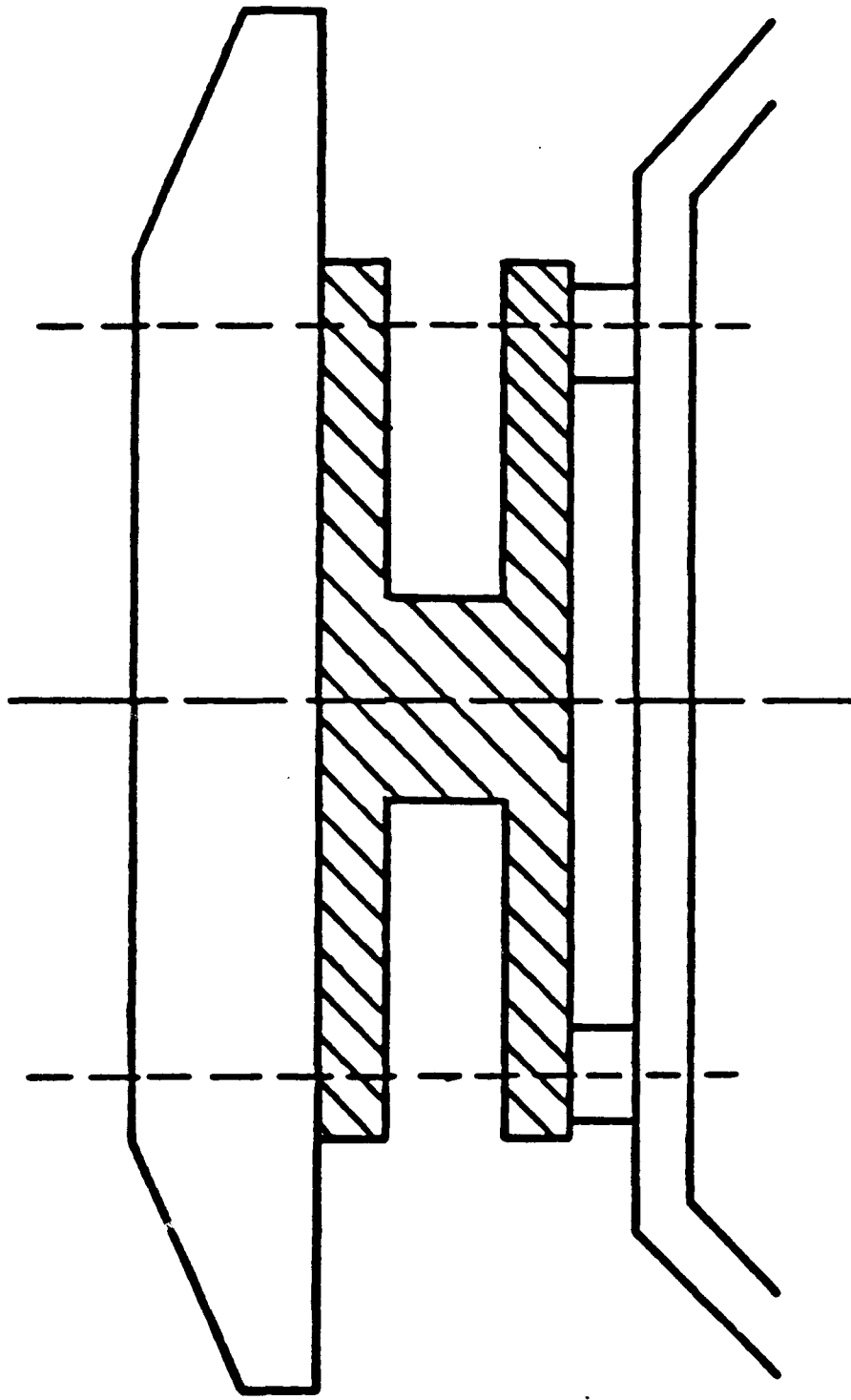
	THEORETICAL NOISE	MEASURED NOISE
PAIR OF STANDARD MODEL ACCELEROMETERS C = 360 DYNE CM · SEC	$9.1 \times 10^{-9} \text{ g}$	$1.2 \times 10^{-8} \text{ g}$
PAIR OF MODIFIED MODEL VII ACCELEROMETERS C = 0.9 AND 1.4 DYNE CM · SEC	$5.3 \times 10^{-10} \text{ g}$	$4.5 \times 10^{-10} \text{ g}$

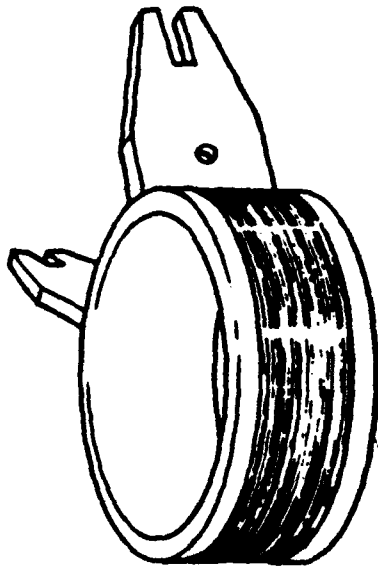
TABLE I

ROTATING ACCELEROMETER GRAVITY GRADIOMETER
ON HOLLOMAN RATE TABLE

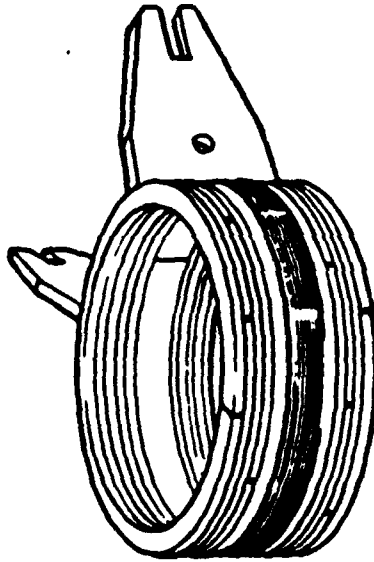


MOUNTING BLOCK DECOUPLING INTERFACE

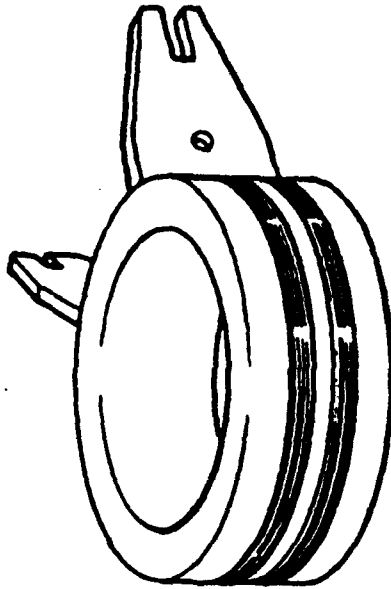




STANDARD
MODEL VII
PROOFMASS



LAMINATED
TANTALUM-ALLOY
PROOFMASS

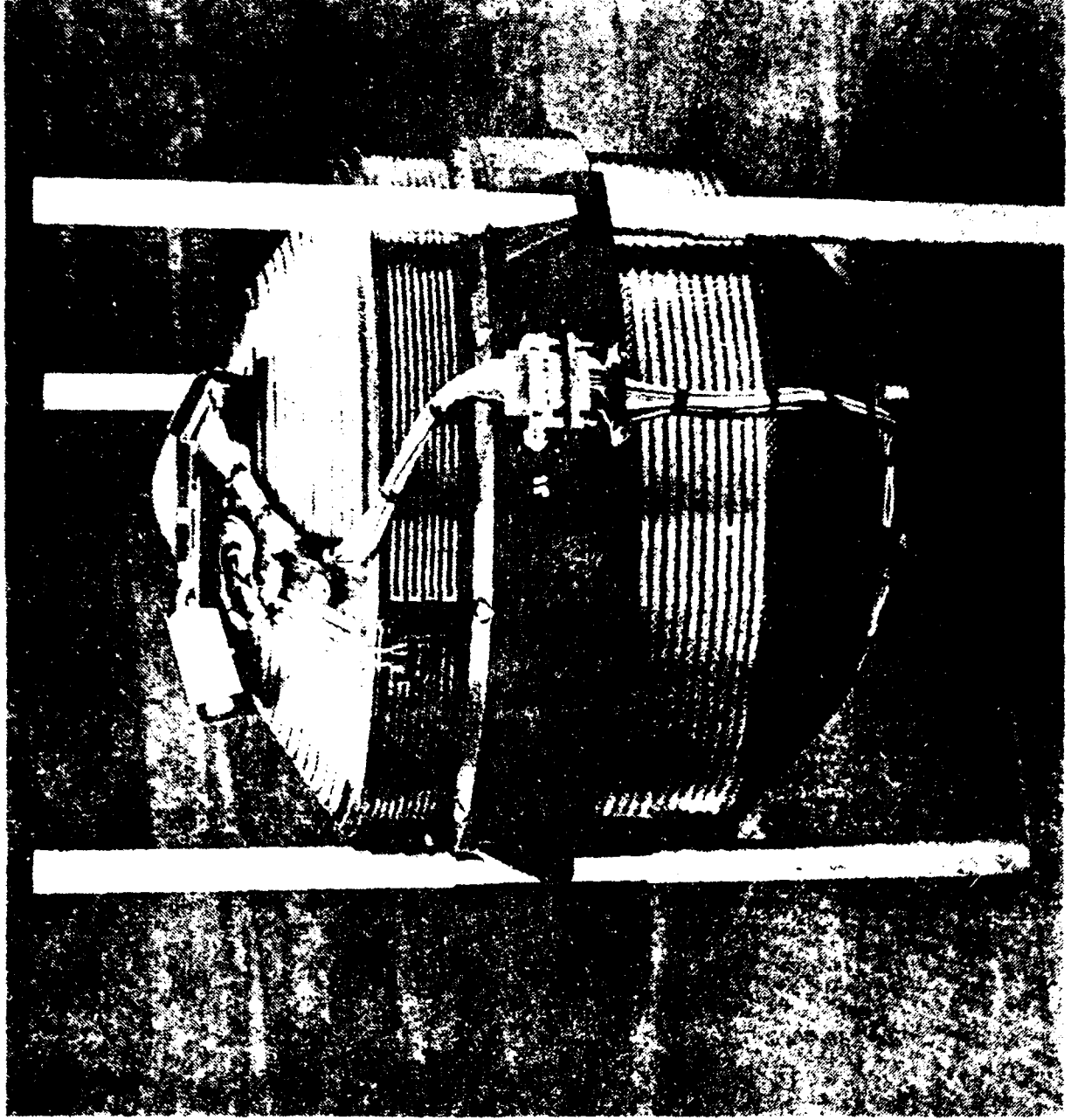


HI-DENSITY
CERAMIC
PROOFMASS

Gravity Sensors System Trident Program

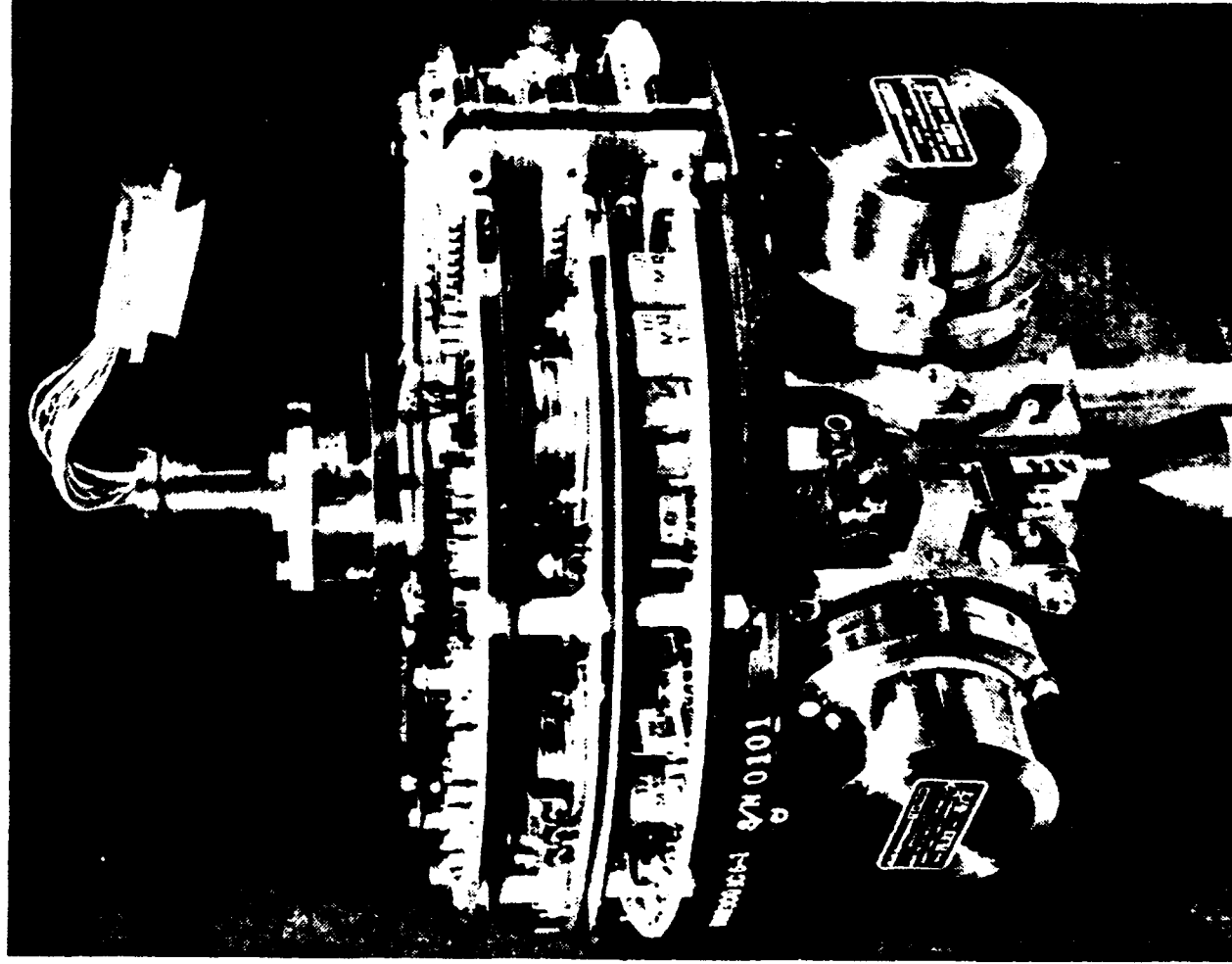
Sperry/SP 24 USN

ADM GGI



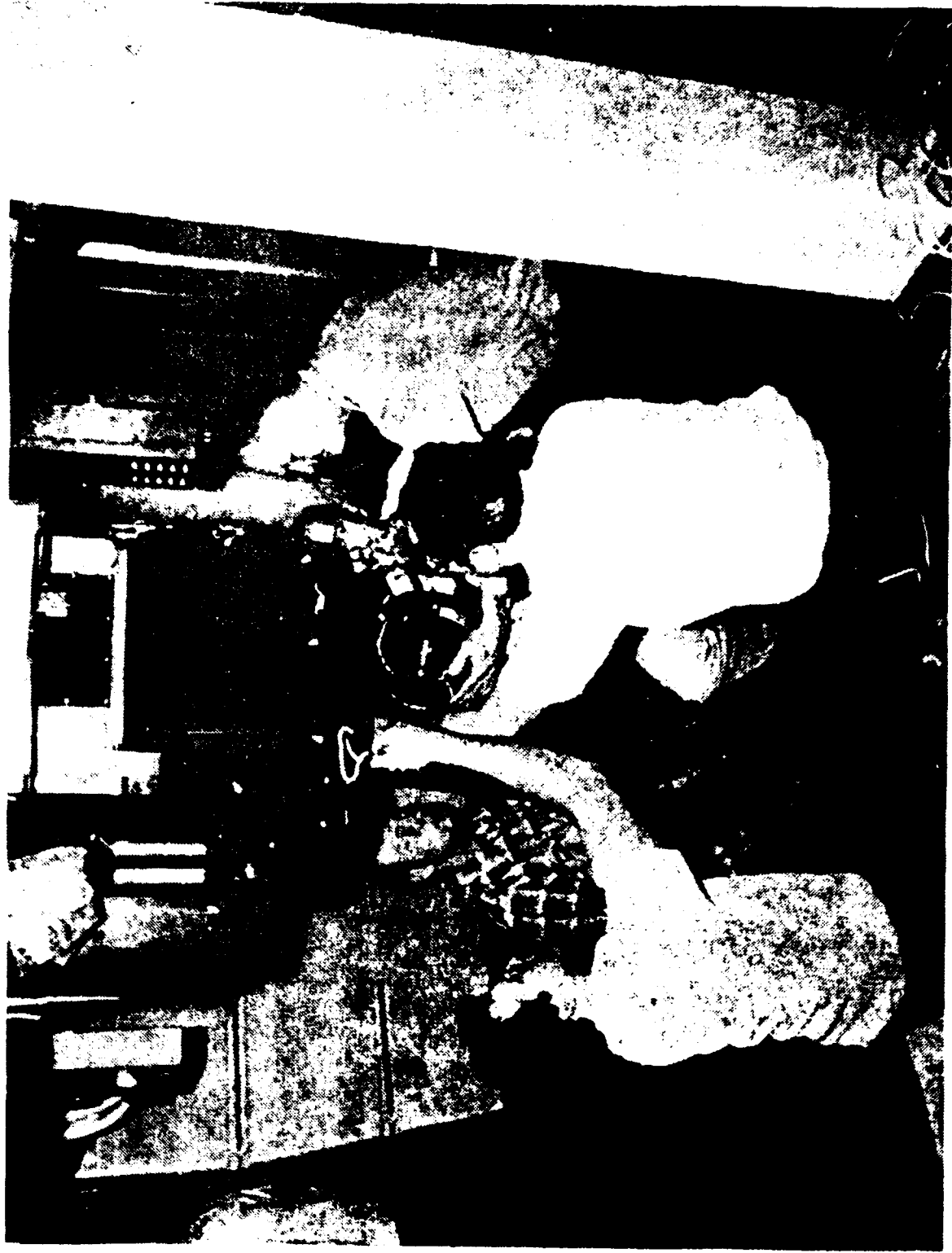
Bell Aerospace **TEXTRON**

INSTRUMENT BLOCK AND ELECTRONICS



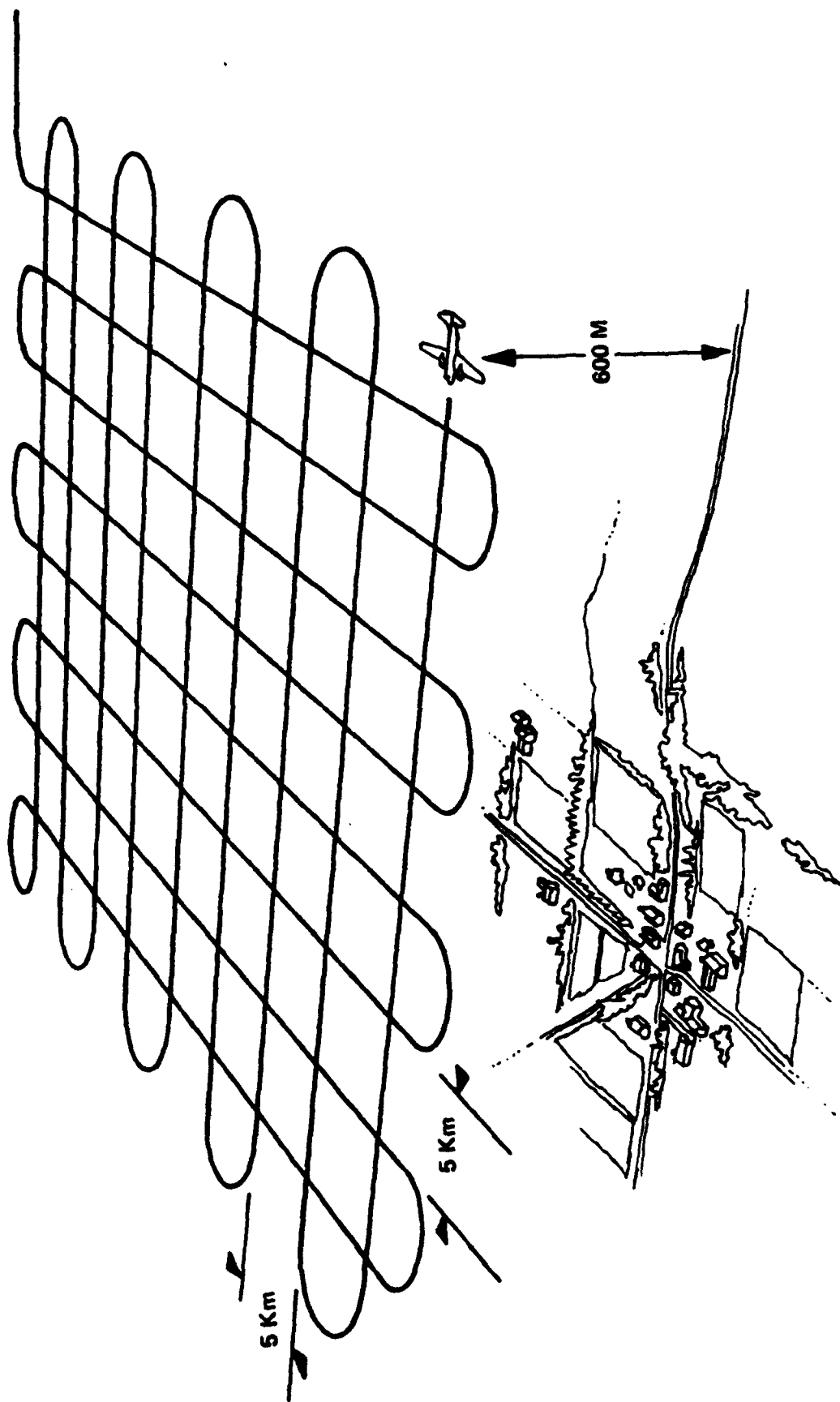
Bell Aerospace **TEXTIRON**

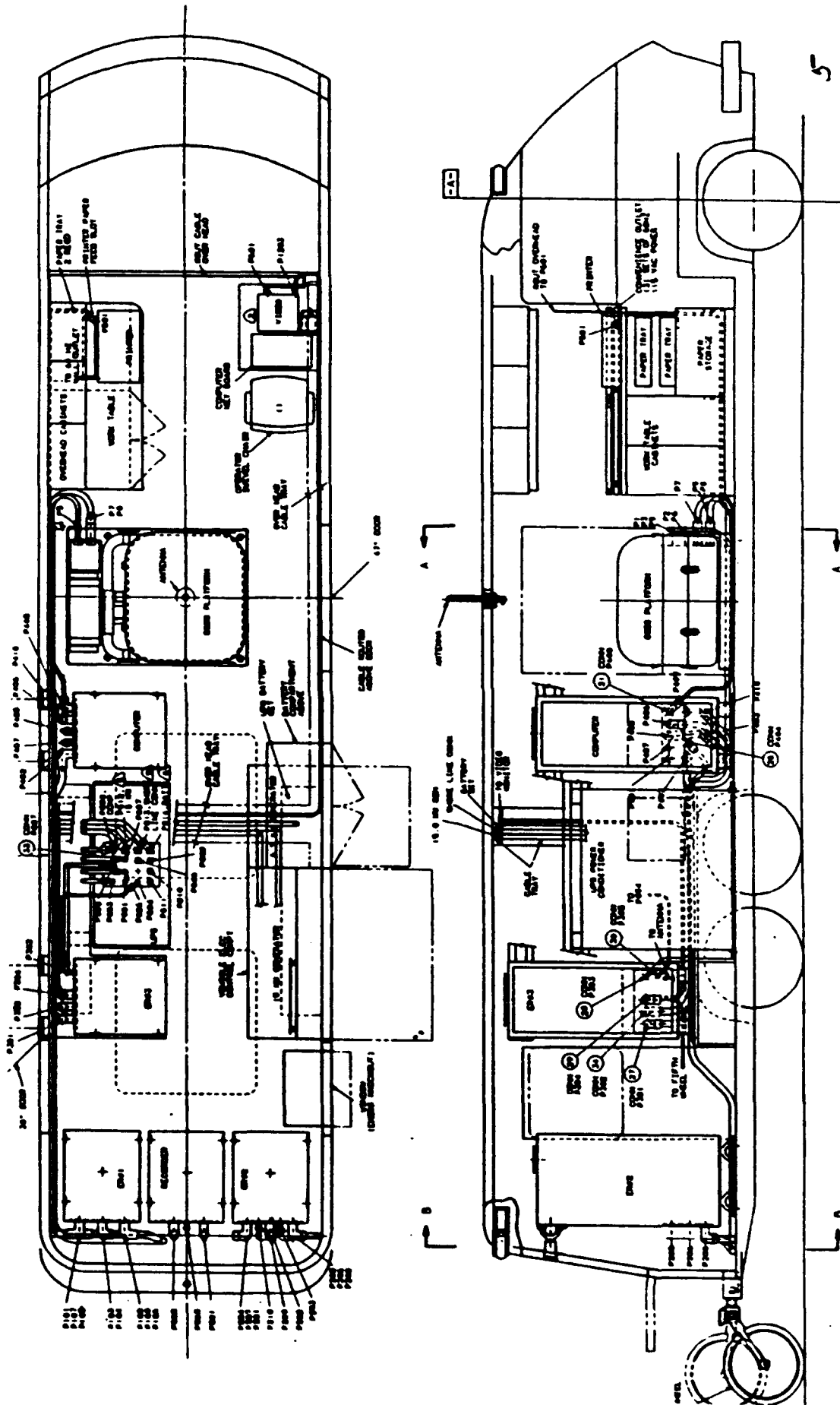
GSS ADM PLATFORM AND GGI BEING INSTALLED ON THE USNS VANGUARD



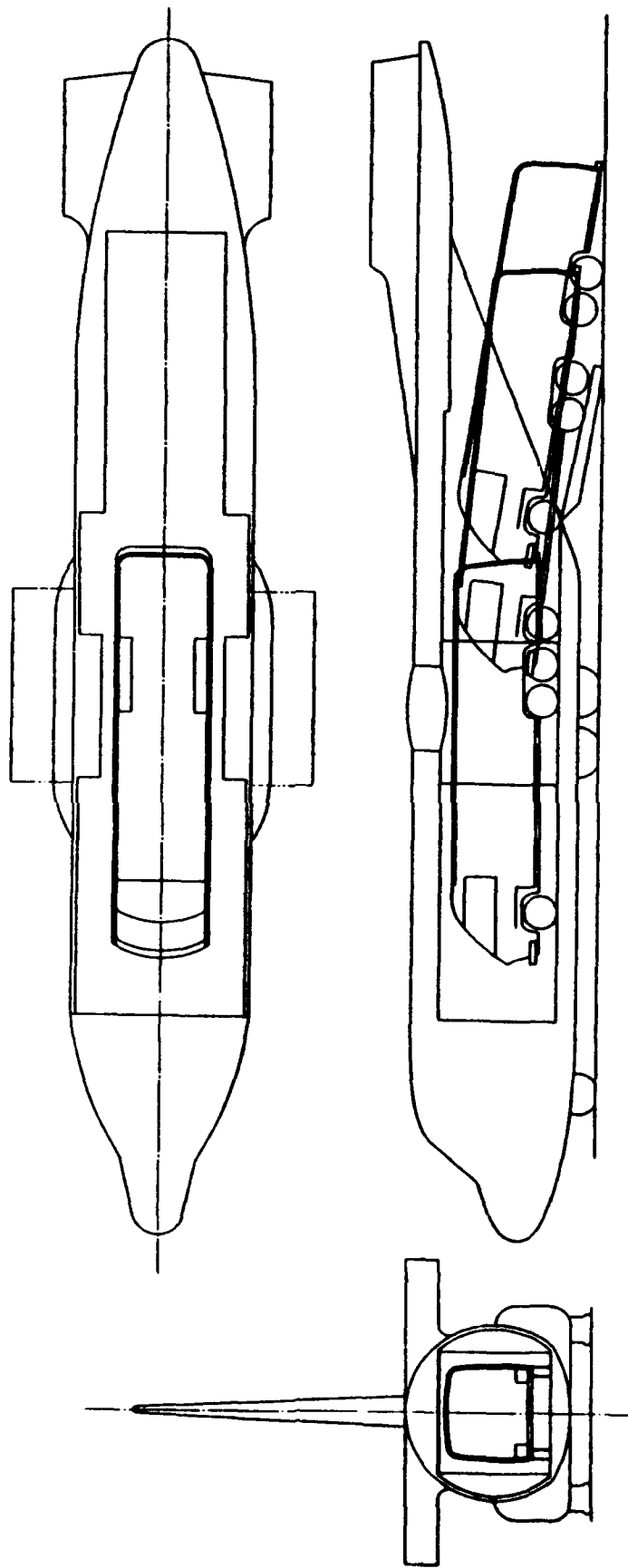
Airborne And Land Vehicle Gravity Gradiometer Survey System For AFGL

Bell Aerospace **TEXTRON**





C130 INSTALLATION



Gravity Sensor System Facility

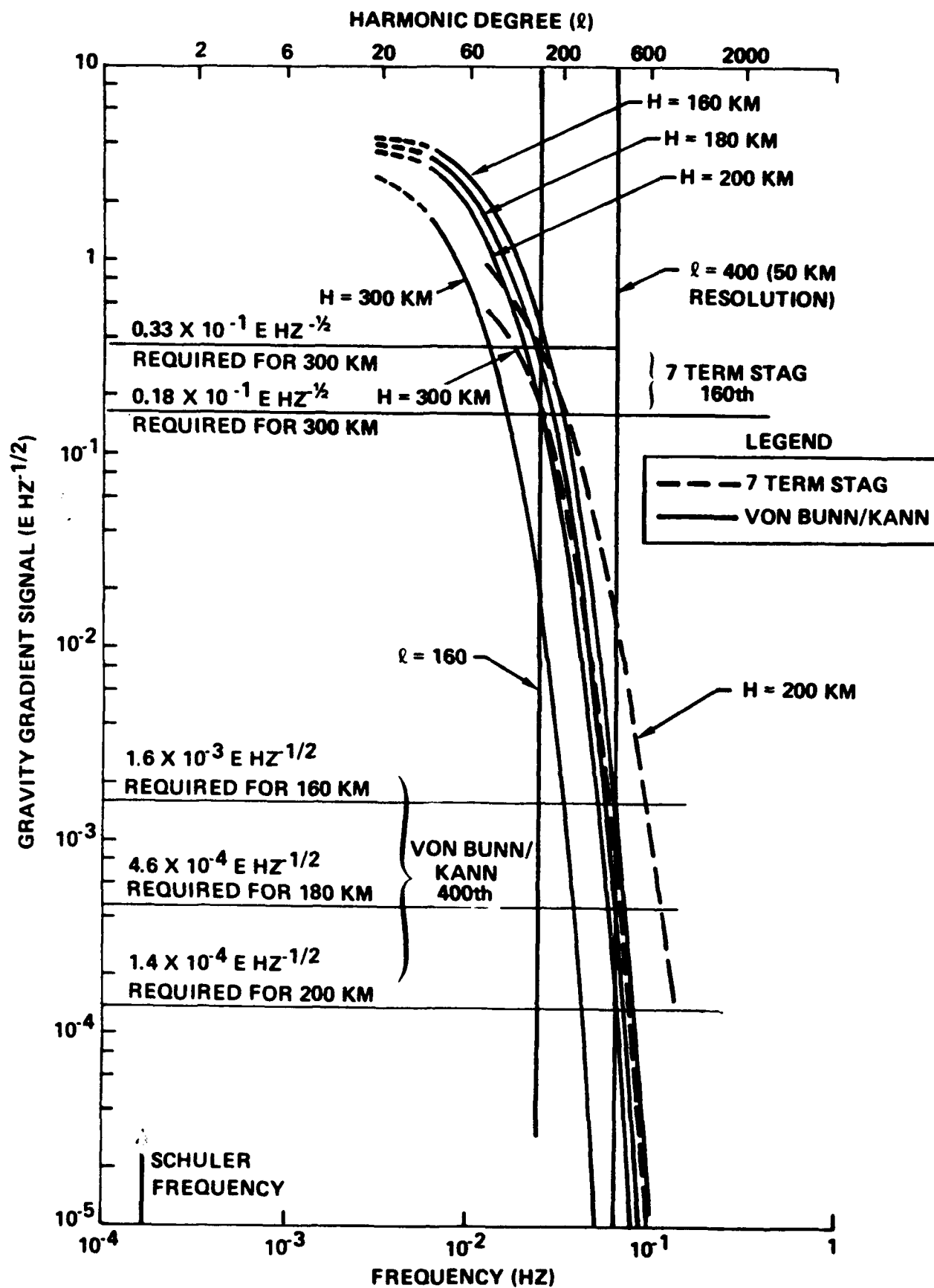
Potential Future Moving Base Gravity Gradiometer Applications Space

LONG WAVE LENGTH GRAVITY DISTURBANCE VECTOR DETERMINATION

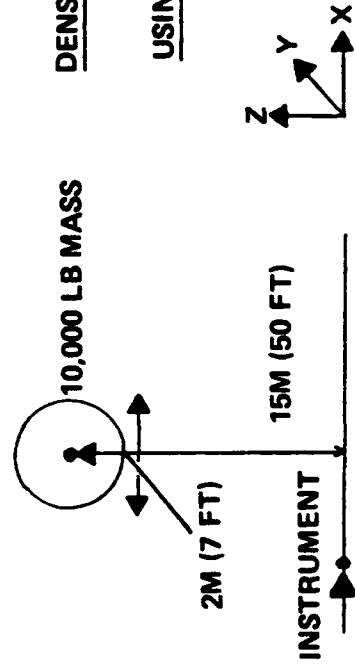
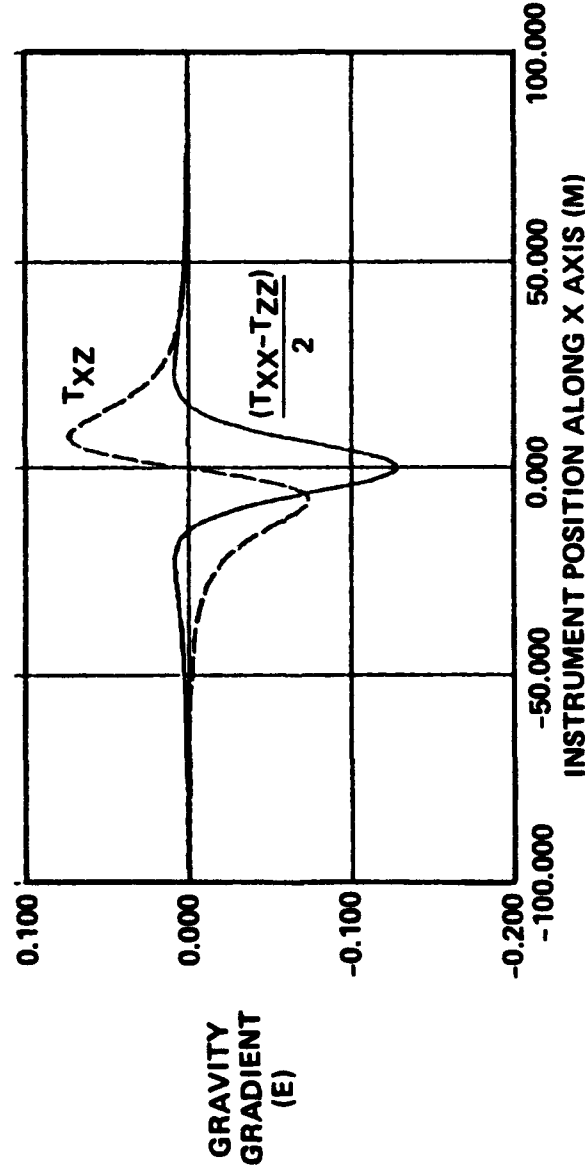
- LONG WAVE LENGTH GRAVITY DISTURBANCE VECTOR INFORMATION NOT CURRENTLY AVAILABLE ACCURATELY OVER LAND MASSES
- SEASAT AND GEOSAT HAVE PROVIDED LONG WAVE LENGTH GRAVITY DISTURBANCE VECTOR DATA OVER OCEANS THROUGH RADAR ALTIMETRY
- GGSS IS SPECIFIED TO MEASURE THE GRAVITY DISTURBANCE VECTOR FOR WAVE LENGTH SHORTER THAN 500 KM OR THE 80 HARMONIC DEGREE OF THE EARTH
- SATELLITE GRAVITY GRADIENT MEASUREMENTS YIELDING ACCURATE DATA TO THE 160 HARMONIC DEGREE OF THE EARTH WOULD ELIMINATE THE NEED FOR TIE POINTS FOR THE 500 KM SQUARE GGSS DERIVED GRAVITY DISTURBANCE VECTOR MAPS
- THIS REQUIRES GRAVITY GRADIOMETERS WITH VERY LOW NOISE, 10^{-2} TO 5×10^{-6} $E^2/RAD/SEC$ DEPENDING ON MODEL OF GRAVITY GRADIENTS AT ORBITAL ALTITUDES AND THE ORBITAL ALTITUDE

GRAVITY GRADIOMETER NOISE LEVEL REQUIRED TO DETERMINE GRAVITY DISTURBANCE VECTOR TO THE 160TH HARMONIC DEGREE

GRAVITY GRADIENT MODEL		ORBITAL ALTITUDE	
VON BUN/KANN	ALLOWABLE NOISE LEVEL $E^2/RAD/SEC$	200 KM 3×10^{-2}	300 KM 5×10^{-5}
	ALLOWABLE NOISE LEVEL $E^2/RAD/SEC$	10^{-1} 3×10^{-2}	



- AS PART OF SDI IT MAY BE DESIRABLE TO INSPECT THE MASS OF A SATELLITE WITHOUT DISTURBING IT
- A GRAVITY GRADIOMETER SATELLITE FLY BY COULD DETERMINE THE DENSITY OF THE SATELLITE TO BE INSPECTED TO A FRACTION OF A GM/CM^3 AT DISTANCES OF MANY TENS OF FEET WITH A GRADIOMETER NOISE LEVEL OF $0.01 \text{ E}^2/\text{RAD}/\text{SEC}$
- A ROTATING MESA GRAVITY GRADIOMETER COULD PROVIDE THIS PERFORMANCE

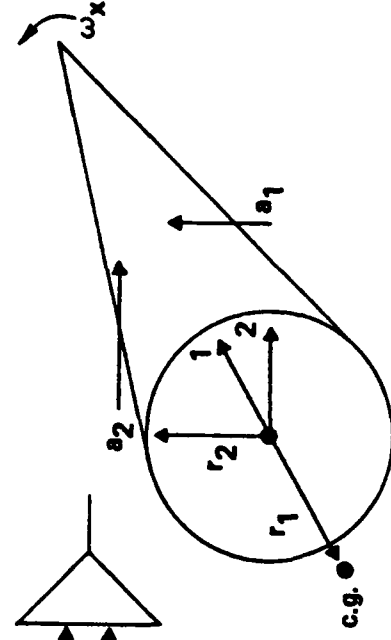


DENSITY DETERMINATION BY
MASS FLY BY
USING A GRADIOMETER

SATELLITE OR REENTRY BODY VERTICAL ERECTION SYSTEM

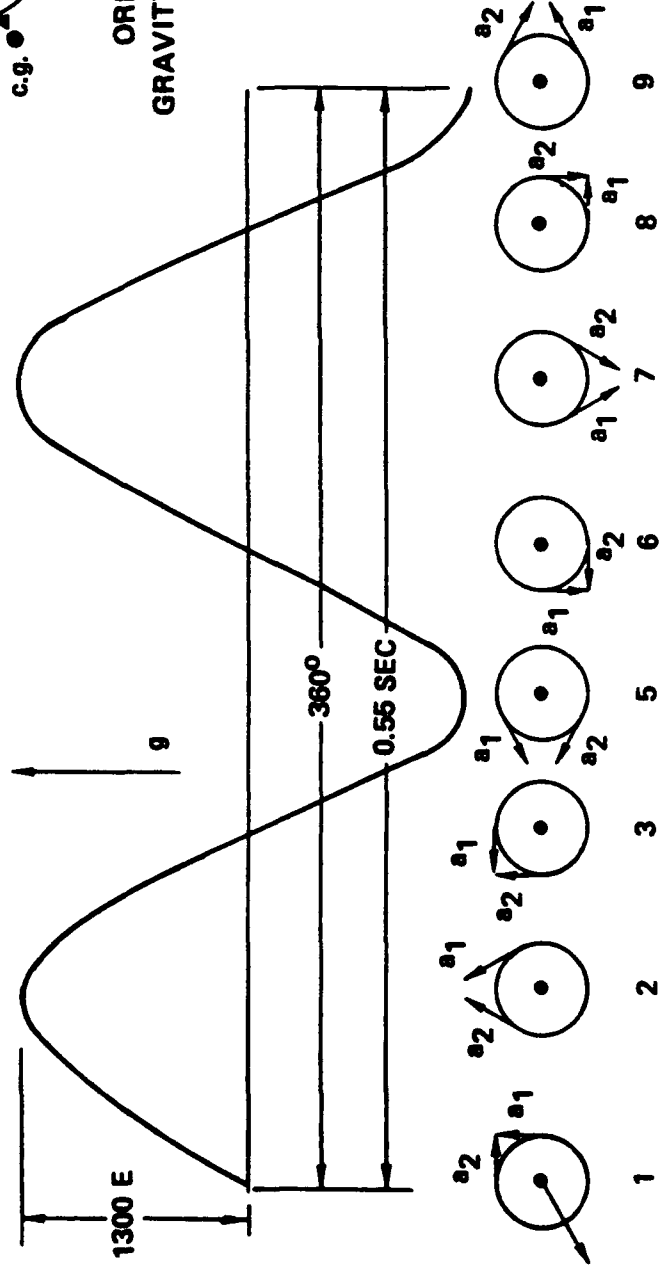
- A GRAVITY GRADIOMETER COULD FIND THE VERTICAL IN A REENTRY BODY OR SATELLITE, SELF CONTAINED, TO A MINUTE OF ARC.
- AT ORBITAL ALTITUDES (300 KM) THE NOMINAL GRAVITY GRADIENT IS 1300 E.
- A BIAS CALIBRATION OF THE GRADIOMETER IN ORBIT MAY BE REQUIRED.

SUMMARY OF ACCELERATIONS SENSED BY GRAVITY GRADIENT ROLL ERECTION ACCELEROMETERS.



ORIENTATION AND LOCATION OF GRAVITY GRADIOMETER ACCELEROMETERS ON REENTRY BODY

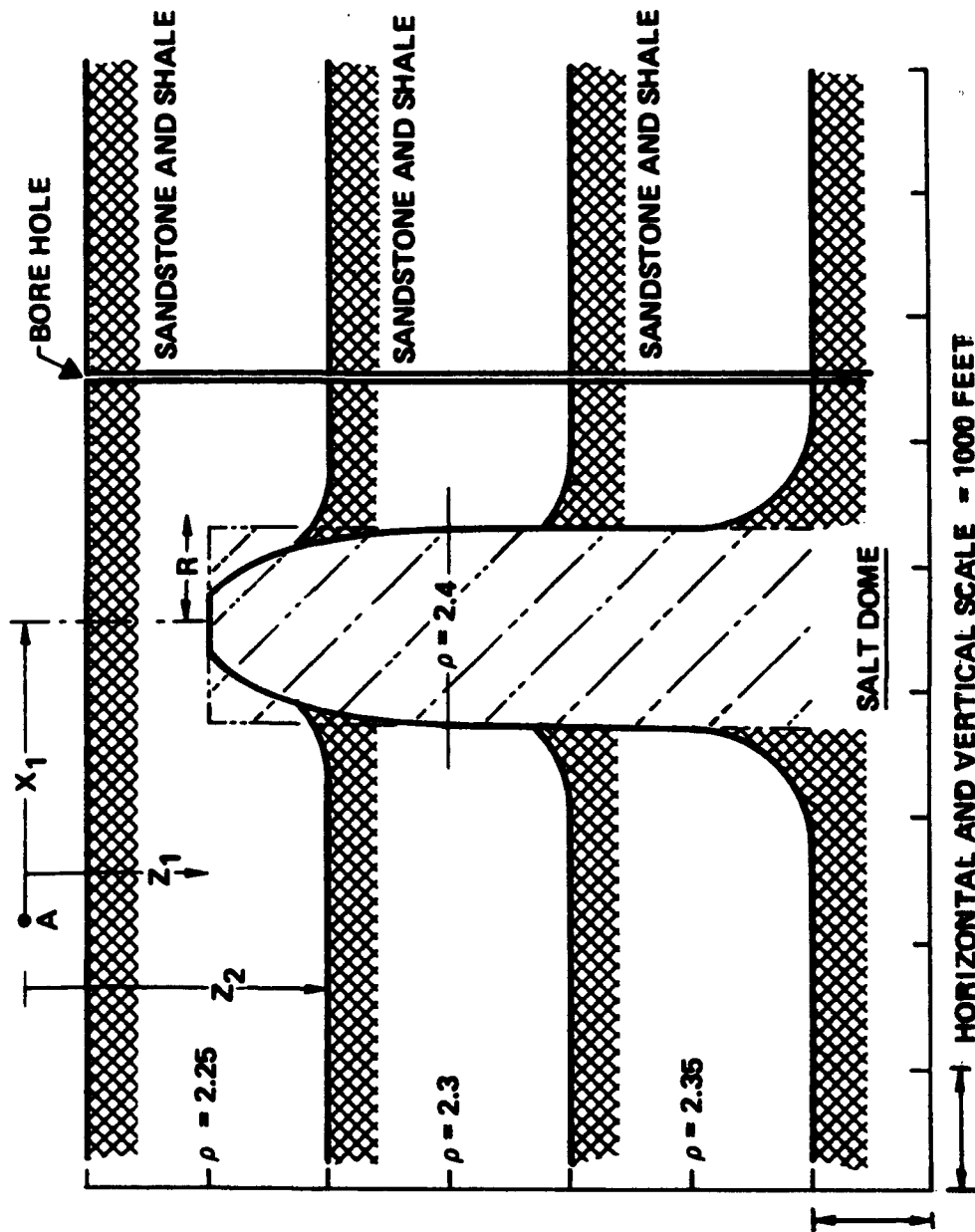
GRAVITY GRADIENT SIGNAL AS A FUNCTION OF REENTRY BODY ROLL ATTITUDE AND G VECTOR



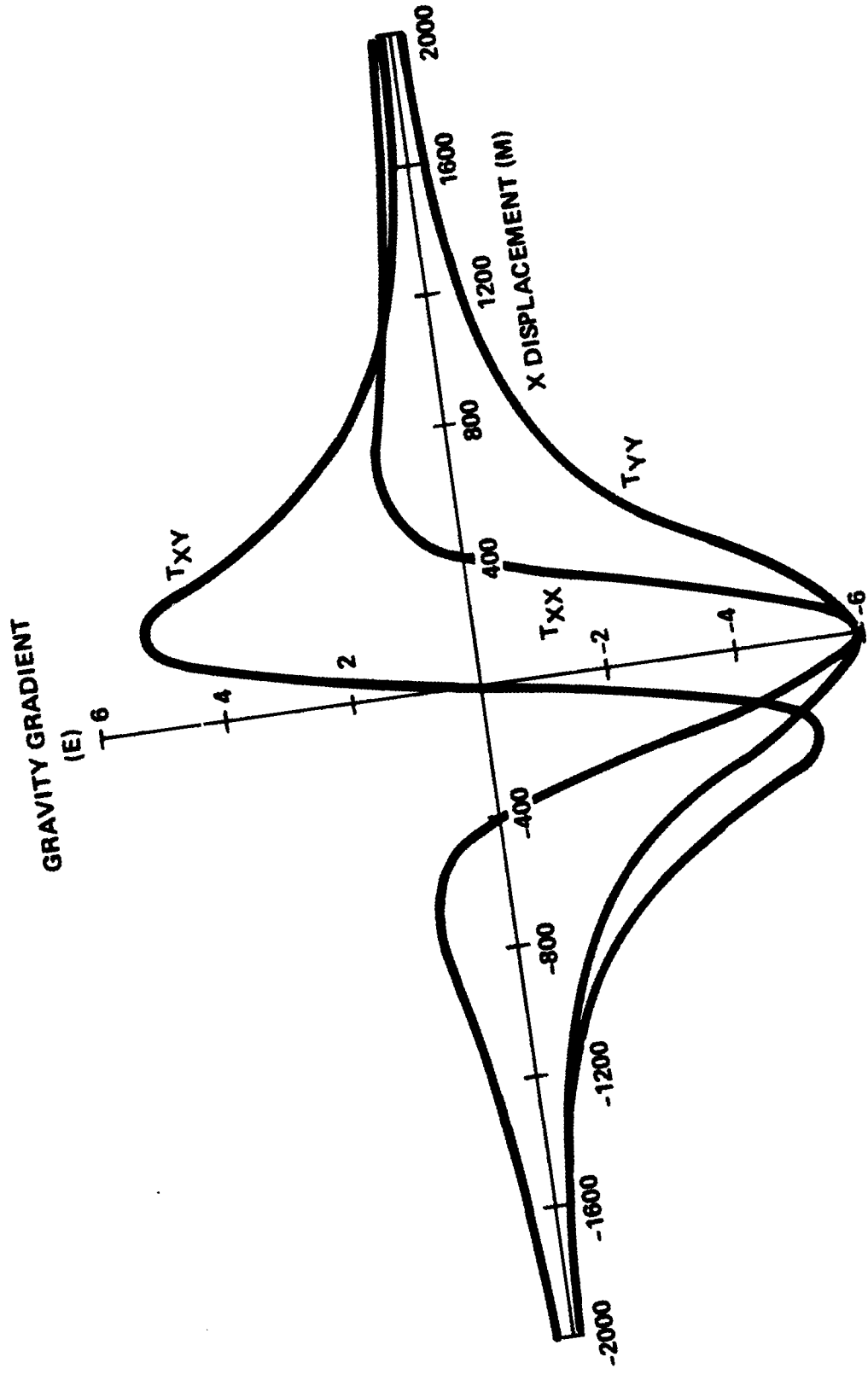
Potential Future Moving Bass Gravity Gradiometer Applications Terrestrial

OIL EXPLORATION FROM AIRBORN/LANDVEHICLE GRAVITY GRADIENT MEASUREMENTS

- DEVELOP GRAVITY GRADIENT SIGNALS DEVELOPED BY GEOLOGICAL FEATURES ASSOCIATED WITH OIL DEPOSITS – SALT DOMES' ANGLE FAULTS OR DRAPE FOLDS ETC.
- DEVELOP OPTIMAL PROCESS WHICH WILL EXTRACT THOSE FROM OTHER GRADIENT SIGNALS (TOPOGRAPHY ETC.) AND NOISE
- GGSS PERFORMANCE APPEARS MORE THEN ADEQUATE



GRAVITY GRADIENT DUE TO A SALT DOME



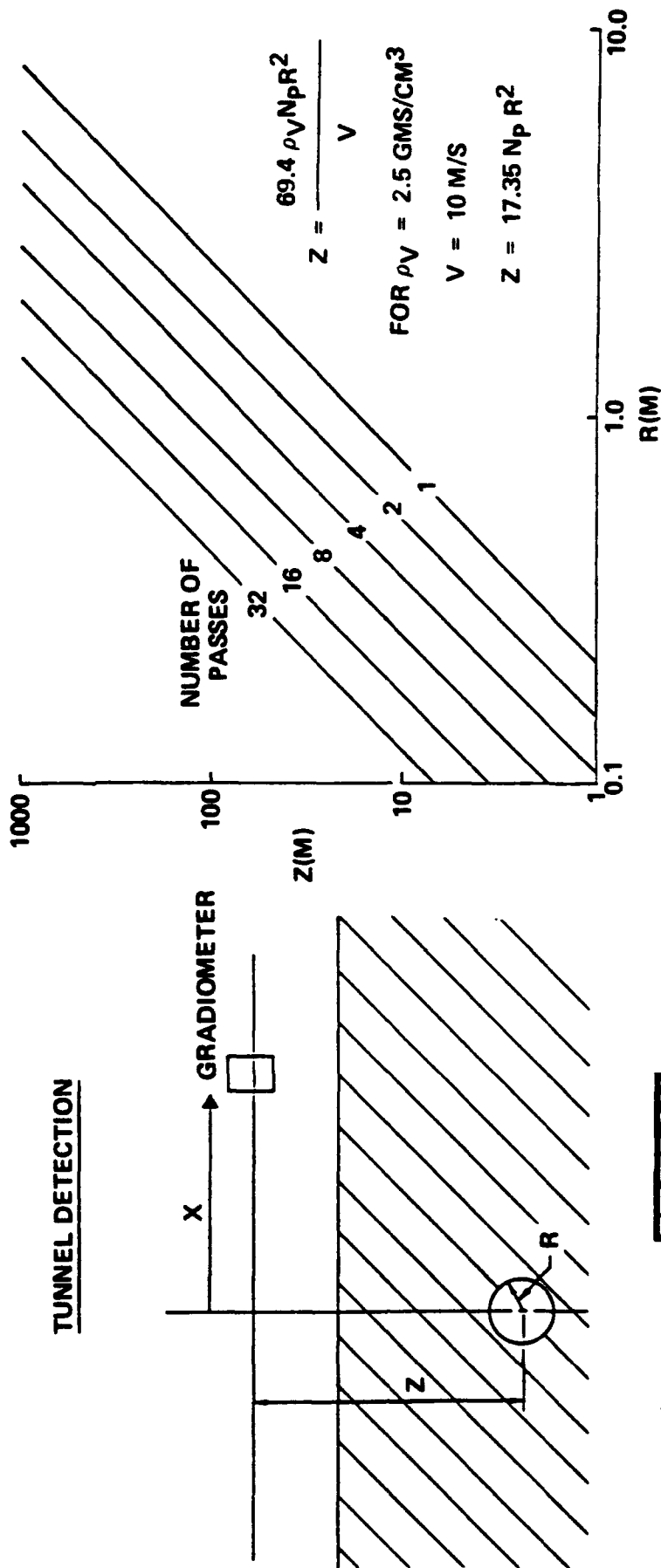
Bell Aerospace **TEXTIRON**

OIL EXPLORATION THROUGH BORE HOLE GRAVITY GRADIENT MEASUREMENTS

- WILL PERMIT EXPLORATION THOUSANDS OF FEET BEYOND BORE HOLE WALL
- REQUIRES SIGNIFICANT GRAVITY GRADIOMETER SIZE REDUCTION
- THERMAL ENVIRONMENT SEVERE IN DEEP HOLES - 350°F
- METHOD TO CALIBRATE BORE HOLE SELF GRADIENTS REQUIRED

DETECTION OF COVERT TUNNELS

- VERY DIFFICULT TO DETECT AT THIS TIME
- GGSS IN LAND VEHICLE OR HELICOPTER COULD DETECT 1 METER RADIUS TUNNEL AT 15M DEPTH WITH SINGLE PASS. REPETITIVE TRACKS COULD EXTEND DEPTH MANY FOLD



POSITION LOCATION USING GRAVITY GRADIENT MAP MATCHING

- REQUIRES GOOD GRAVITY GRADIENT MAPS
- POSITION LOCATION TO TENS OF FEET OVER ROUGH GRAVITY AREAS FEASIBLE
- POSITION LOCATION TO HUNDREDS OF FEET OVER QUIET AREAS FEASIBLE
- POSITION FIXES FOR BOTH LATITUDE AND LONGITUDE MAY REQUIRE SPECIFIC TRAVEL PATTERN, CIRCULAR ETC.

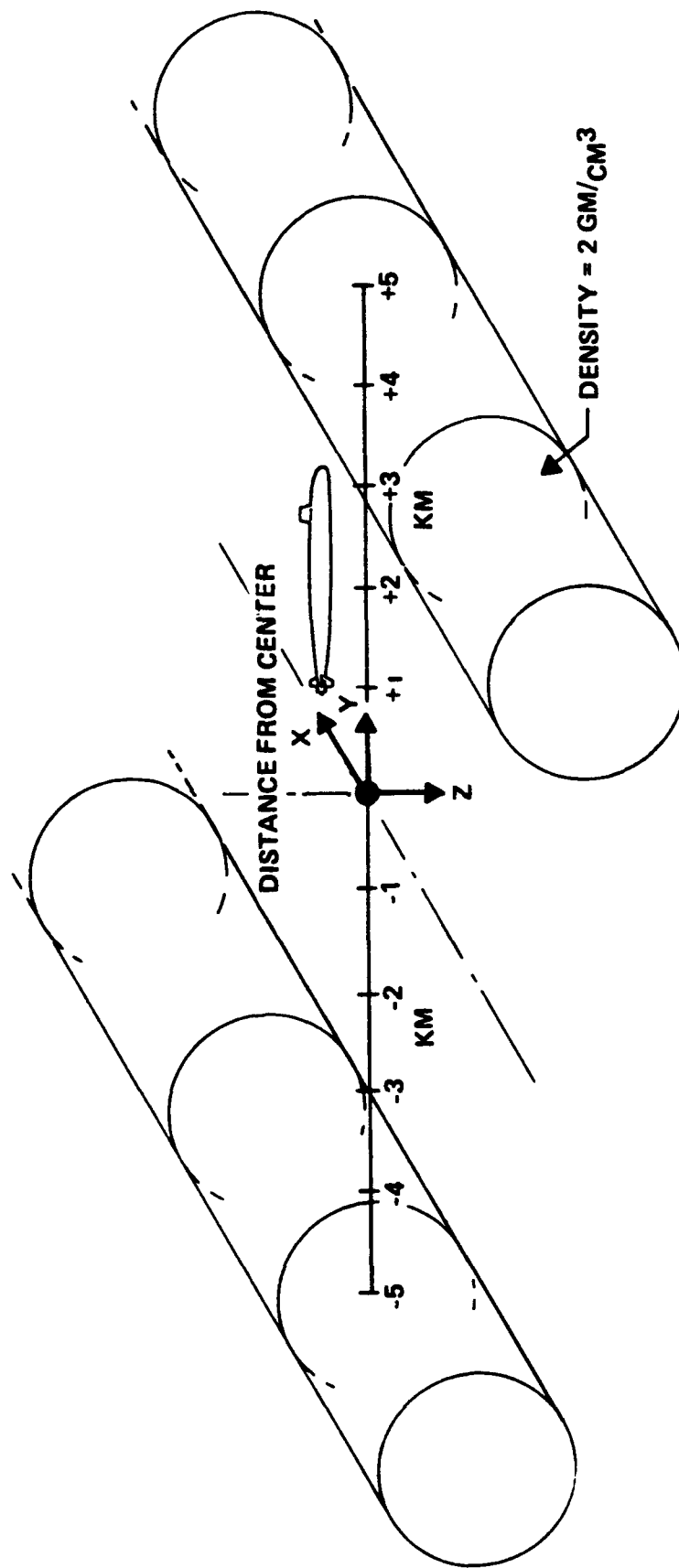


TERRAIN AVOIDANCE

GSS WILL GIVE STRONG GRADIENT RATE OF CHANGE SIGNALS TO APPROACHING MOUNTAINS.

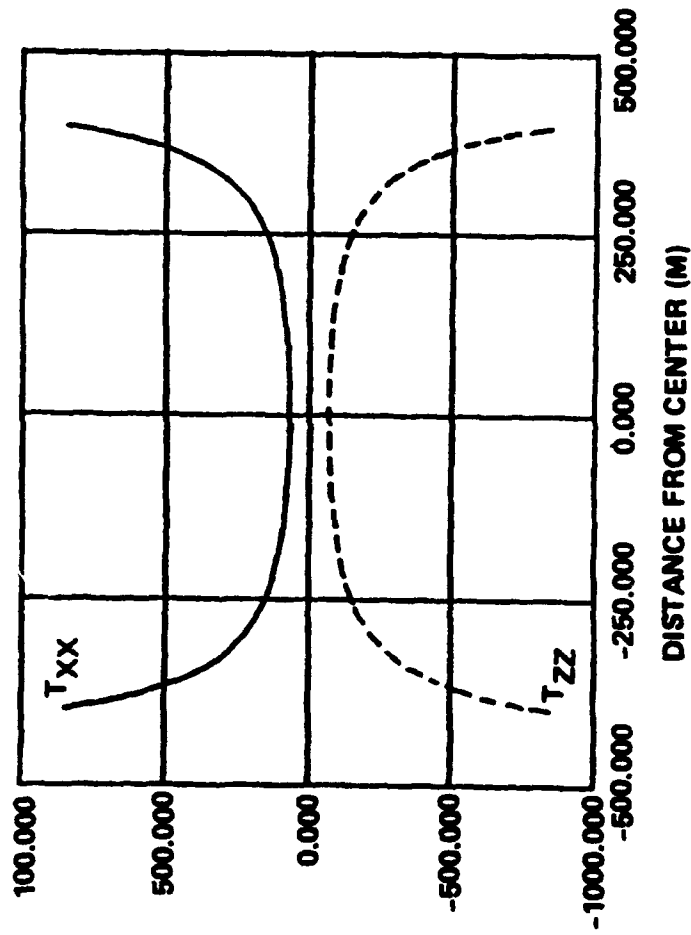
GRADIENTS AMPLITUDE (E) AND GRADIENTS RATE OF CHANGE (E/M) WILL INDICATE DIRECTION AND PROXIMITY TO MOUNTAINS.

THE NARROWNESS OF A PASSAGEWAY THAT CAN BE IDENTIFIED WITH GRAVITY GRADIENTS WILL REQUIRE ANALYSIS.



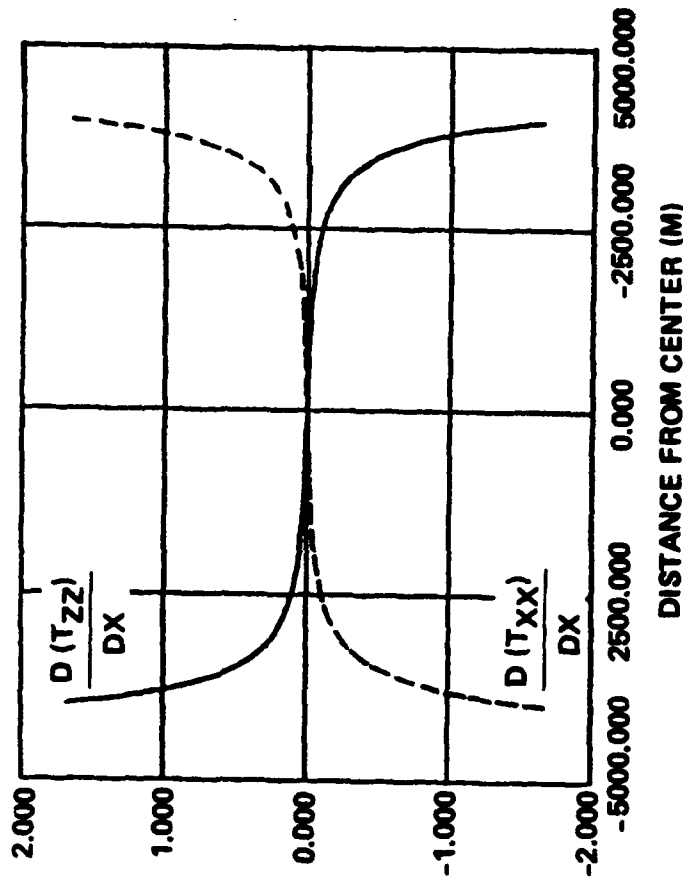
TERRAIN AVOIDANCE

GRAVITY
GRADIENT
(E)



GRAVITY GRADIENTS AS A FUNCTION
OF POSITION BETWEEN MOUNTAINS

CHANGE IN
GRADIENT/M
(E/M)



CHANGE IN GRADIENT/M AS A FUNCTION
OF POSITION BETWEEN MOUNTAINS

PAPER TITLE: DEVELOPMENT EXPERIENCE OF A MOVING BASE GRAVITY GRADIOMETER
AND DISCUSSION OF FUTURE APPLICATIONS

SPEAKERS NAME: Ernest H. Metzger

Questions and Comments:

Milton Trageser: I have never seen data which show your Gradiometer's quick time response and noise. Can you show some data on this?

→ SPEAKERS RESPONSE: (No Response Noted)

Daniel DeBra: What is/are the principle hardware differences in the Navigation GGS and the Mapping GGS?

SPEAKERS RESPONSE: The Mapping GGS is more sensitive. The accelerometers have fewer turns on the proof mass to require more A/g (Amperes per unit of gravity). This has produced a significantly better signal to noise ratio. It is not needed for the navigation application.

GRADIOMETRY AND GEODESY, OR SEPARATING INSEPARABLES

C. Jekeli

Air Force Geophysics Laboratory

Earth Sciences Division

Hanscom AFB, MA 01731-5000

ABSTRACT

The purpose of geodesy is to determine the size and shape of the earth and to determine the exterior gravity field. These two facets of geodesy are tightly interwoven. In fact, a knowledge of the gravity field is a prerequisite for terrestrial positioning, and vice versa. In the most comprehensive solutions (integrated geodesy), both are determined simultaneously from all available measurements.

Two methodologies being proposed for rapid local gravity mapping are airborne gravimetry and airborne gravity gradiometry. In addition to the classic chicken-egg problem mentioned above, there is the problem that airborne gravity instruments sense not only gravity (gravity gradients) but also various effects of an accelerated coordinate frame.

A rudimentary analysis shows how gravity gradiometry mitigates these problems of inseparability.

GRADIOMETRY & GEODESY, OR SEPARATING INSEPARABLES

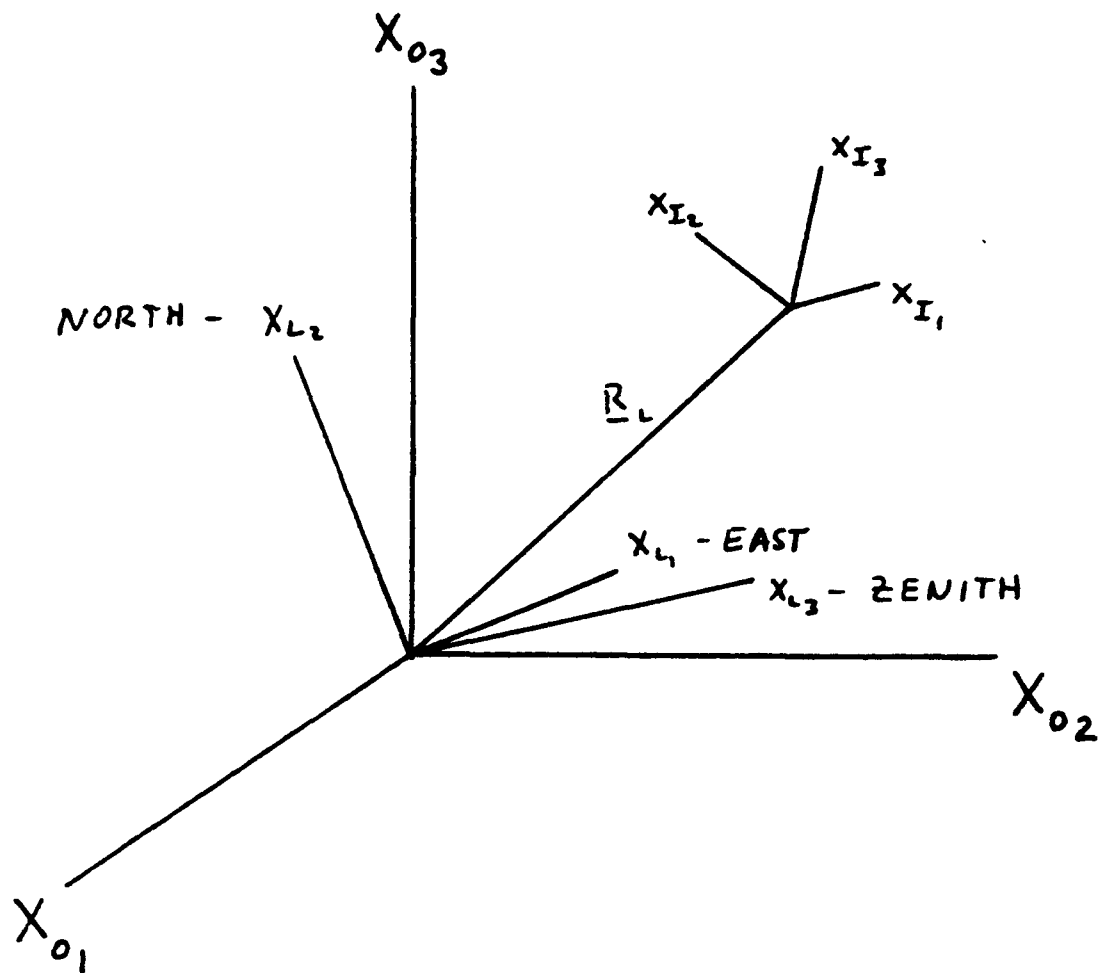
PROBLEMS OF MOVING-BASE GRAVITY MAPPING:

- INSTRUMENTS IN AN ACCELERATED FRAME
- GRAVITY FIELD IS A FUNCTION OF POSITION

SIMPLIFIED ANALYSIS:

- USE SPHERICAL APPROXIMATION
- LINEARIZE OBSERVATIONAL MODEL
- ASSUME LOCAL LEVEL STABILIZATION
- ASSUME NO HORIZONTAL ACCELERATIONS, CONSTANT ALTITUDE
- GRAVITY (GRAVITY GRADIENT) DETERMINATION AT ALTITUDE TO

ACCURACY OF 1 MGAL (1 E)



$$\underline{X}_0 = [\alpha_{ij}] \underline{X}_L = [\alpha_{ij}] (\underline{R}_L + [\beta_{kl}] \underline{X}_I)$$

\underline{X}_0 - INERTIAL FRAME

\underline{X}_L - LOCAL LEVEL FRAME

\underline{X}_I - INSTRUMENT FRAME

MATH. MODELS FOR MEASURED QUANTITIES

GENERAL FORM:

$$\ddot{x}_{In} = g_{In} - \alpha_{km} \beta_{mn} \left[\ddot{\alpha}_{ki} (R_{Li} + \beta_{ij} x_{Ij}) - 2 \dot{\alpha}_{ki} (\dot{R}_{Li} + \dot{\beta}_{ij} x_{Ij} + \beta_{ij} \dot{x}_{Ij}) - \alpha_{ki} (\ddot{R}_{Li} + \ddot{\beta}_{ij} x_{Ij} + 2 \dot{\beta}_{ij} \dot{x}_{Ij}) \right]$$

$$G_{Inl} = \Gamma_{Inl} - \alpha_{km} \beta_{mn} \frac{d^2}{dt^2} (\alpha_{ki} \beta_{il})$$

INERTIAL STABILIZATION: $\beta_{mn} = \alpha_{mn}^{-1}$

$$\ddot{x}_{In} = g_{In} - \alpha_{nk} \left[(\dot{w}_{ki} - w_{mk} w_{mi}) R_{Li} + \ddot{R}_{Lk} \right], \quad w_{jk} = \alpha_{ij} \dot{\alpha}_{ik}$$

$$G_{Inl} = \Gamma_{Inl}$$

LOCAL LEVEL STABILIZATION: $\beta_{mn} = \delta_{mn}$

$$\ddot{x}_{In} = g_{In} - (\dot{w}_{ni} - w_{kn} w_{ki}) R_{Li} - \ddot{R}_{Ln}$$

$$G_{Inl} = \Gamma_{Inl} - (\dot{w}_{nl} - w_{kn} w_{kl})$$

OBSERVATIONAL MODEL FOR AIRBORNE GRAVIMETRY

$$\begin{aligned}
 \Delta \ddot{r} = & \Delta g + \left[\frac{1}{r^2} (V_N^2 + (V_E + \omega_e r \cos \varphi)^2 + \frac{2KM}{r^3}) \right]_0 \Delta r \\
 & - \frac{2}{r_0^2} \left[V_E^2 \tan \varphi + 2\omega_e r V_E \sin \varphi + \omega_e^2 r^2 \sin \varphi \cos \varphi \right]_0 \Delta \varphi \\
 & + \left[\frac{2 \cos \varphi}{r} (V_E + \omega_e r \cos \varphi)^2 \right]_0 \Delta V_E \\
 & + 2 \left[\frac{V_N}{r} \right]_0 \Delta V_N \\
 & - \Delta \ddot{h} \\
 & + r_0 \Delta \beta
 \end{aligned}$$

WITH NOMINAL ZERO-ORDER VALUES:

$$\begin{aligned}
 \Delta \ddot{r} = & \Delta g + .3086 \Delta r - 8.56 \times 10^{-4} r \Delta \varphi + 2.57 \Delta V_E + .771 \Delta V_N - \Delta \ddot{h} + g(1 - \cos \omega t) \\
 & (\text{ALL TERMS IN MGAL} ; \Delta r, r \Delta \varphi \text{ IN } \underline{M} ; \Delta V_E, \Delta V_N \text{ IN } \underline{KM/HR})
 \end{aligned}$$

OBSERVATIONAL MODEL FOR AIRBORNE GRADIOMETRY

$$\begin{bmatrix} \Delta G_{11} \\ \Delta G_{12} \\ \Delta G_{13} \\ \Delta G_{22} \\ \Delta G_{23} \\ \Delta G_{33} \end{bmatrix} = \begin{bmatrix} \Delta \Gamma_{11} \\ \Delta \Gamma_{12} \\ \Delta \Gamma_{13} \\ \Delta \Gamma_{22} \\ \Delta \Gamma_{23} \\ \Delta \Gamma_{33} \end{bmatrix} + \frac{3 \text{ km}}{r_0^4} \begin{bmatrix} 0 & 0 & -1 \\ 0 & 0 & 0 \\ -1 & 0 & 0 \\ 0 & 0 & -1 \\ 0 & -1 & 0 \\ 0 & 0 & 2 \end{bmatrix} \begin{bmatrix} r_0 \Delta \varphi \\ r_0 \cos \varphi_0 \Delta \lambda \\ \Delta r \end{bmatrix}$$

WITH NOMINAL ZERO-ORDER VALUES:

$$= \begin{bmatrix} \Delta \Gamma_{11} \\ \Delta \Gamma_{12} \\ \Delta \Gamma_{13} \\ \Delta \Gamma_{22} \\ \Delta \Gamma_{23} \\ \Delta \Gamma_{33} \end{bmatrix} + 7.25 \times 10^{-4} \begin{bmatrix} 0 & 0 & -1 \\ 0 & 0 & 0 \\ -1 & 0 & 0 \\ 0 & 0 & -1 \\ 0 & -1 & 0 \\ 0 & 0 & 2 \end{bmatrix} \begin{bmatrix} r_0 \Delta \varphi \\ r_0 \cos \varphi_0 \Delta \lambda \\ \Delta r \end{bmatrix}$$

(GRADIENT RESIDUALS, ANOMALIES IN E ;

$r_0 \Delta \varphi$, $r_0 \cos \varphi_0 \Delta \lambda$, Δr IN M)

GENERALIZED GEODETIC BOUNDARY CONDITION:

OBSERVED GRAVITY ANOMALY:

$$\Delta g = -\frac{\partial T}{\partial r} - \frac{2}{r} T + \frac{2}{r} \Delta W$$

- LINEAR FUNCTIONAL OF T PLUS ΔW

OBSERVED QUANTITY:

$$\Delta \Gamma_{zz} - \frac{3}{r} \Delta g = \frac{\partial^2 T}{\partial r^2} + \frac{3}{r} \frac{\partial T}{\partial r}$$

- LINEAR FUNCTIONAL OF T ONLY

- AVOID HEIGHT DATUM PROBLEM

SATELLITE GRADIOMETRY

OBSERVED QUANTITY:

$$\Delta \Gamma_{xy} = \frac{\partial^2 T}{\partial x \partial y}$$

$$\Delta \Gamma_{xx} - \Delta \Gamma_{yy} = \frac{\partial^2 T}{\partial x^2} - \frac{\partial^2 T}{\partial y^2}$$

- LINEAR FUNCTIONALS OF T ONLY

- AVOID COMPLICATED ORBIT
DETERMINATION

REQUIREMENTS FOR THE USE OF AIRBORNE
GRAVITY GRADIOMETRY IN GEOPHYSICAL EXPLORATION

K. P. Schwarz

A. A. Vassiliou

The University of Calgary

Division of Surveying Engineering

2500 University Drive N.W.

Calgary, Alberta T2N 1N4

CANADA

ABSTRACT

Gravity methods in geophysical exploration exploit the fact that density variations in rocks give rise to variations in the anomalous gravity potential. Interpretation of these variations gives information on rock formations that may be of geophysical interest. The anomalous gravity potential of some typical formations are specified in terms of wavelengths and amplitude and the requirements for resolving these signals by single axis or multi-axis gravity gradiometers are stated. Simple numerical examples are used to show the effect of downward continuation, aliasing, and profile spacing. Finally, the noise spectra of current gravity gradiometers are discussed with view to their potential use in these applications.

REQUIREMENTS
FOR THE USE OF AIRBORNE
GRAVITY GRADIOMETRY IN GEOPHYSICAL
EXPLORATION

by

K.P. SCHWARZ AND A.A. VASSILIOU
UNIVERSITY OF CALGARY

GRAVITY METHODS IN EXPLORATION

1. MAJOR EXPLORATION AREAS

- PETROLEUM EXPLORATION
- MINERAL EXPLORATION
- WATER RESOURCE EXPLORATION

2. MAJOR EXPLORATION METHODS

- SEISMIC (PETROLEUM)
- ELECTROMAGNETIC (MINERAL)
- MAGNETIC
- GRAVIMETRIC

3. GRAVITY METHODS

- COMPLEMENT SEISMIC AND ELECTROMAGNETIC METHODS
- ARE INEXPENSIVE
- GIVE MULTIPLE SOLUTIONS (NON-UNIQUENESS OF POTENTIAL METHODS)
- GIVE LITTLE GEOMETRIC INFORMATION
- ARE SLOW

4. ADVANTAGES OF AIRBORNE GRAVITY GRADIOMETRY

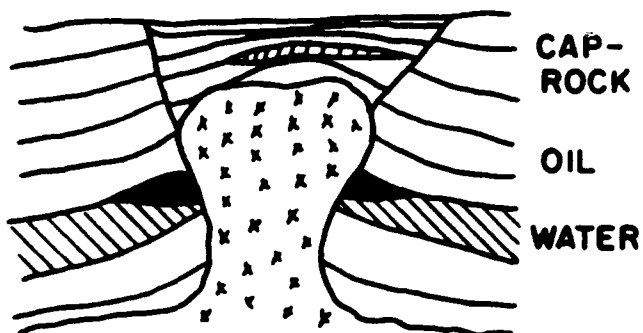
- MORE COMPLETE INFORMATION (FULL TENSOR)
- HIGHER RESOLUTION POSSIBLE
- FASTER DATA ACQUISITION
- LARGER AREAS
- IDEAL COMBINATION WITH AEROMAGNETICS

5. INTEGRATED APPROACH

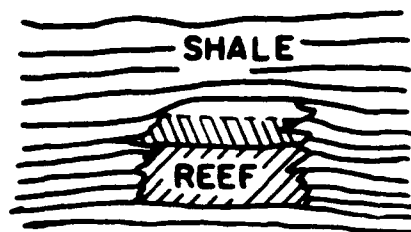
APPROACH

- 1. REQUIREMENTS IN TERMS OF WAVELENGTH AND AMPLITUDE**
 - TYPICAL STRUCTURES
 - RESULTING WAVELENGTHS AND AMPLITUDES
- 2. SIGNAL DETECTION AT FLYING ALTITUDE**
 - ATTENUATION OF SECOND-ORDER GRADIENTS WITH ALTITUDE
 - DETECTABILITY OF OFF-PROFILE SOURCES
 - GEOLOGICAL AND TOPOGRAPHICAL NOISE
 - SAMPLING RATE AND MEASURING ACCURACY
- 3. DOWNWARD CONTINUATION**
 - AMPLIFICATION OF NOISE
 - RECOVERY OF DESIRED SIGNALS
- 4. USE OF CURRENT AND FUTURE SYSTEMS**
 - CURRENT ROOM TEMPERATURE SYSTEMS
 - FUTURE ROOM TEMPERATURE SYSTEMS
 - CURRENT SUPERCONDUCTING SYSTEM
 - FUTURE SUPERCONDUCTING SYSTEM

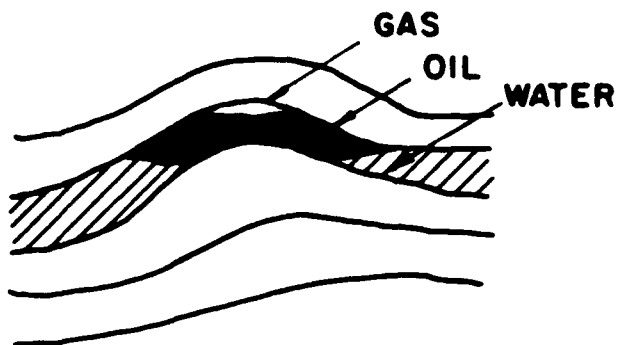
OIL TRAPS IN SEDIMENTARY STRUCTURES



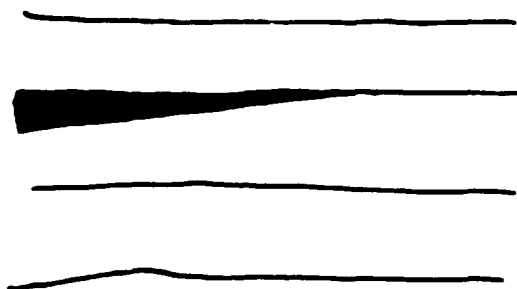
SALT DOME



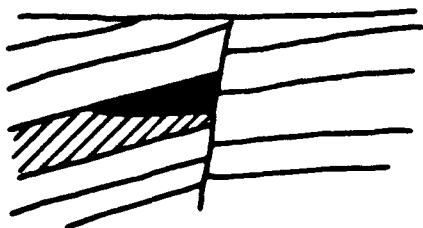
LIMESTONE REEF



ANTICLINE



PINCHOUT



FAULT TRAP



UNCONFORMITY TRAP

TYPICAL WAVELENGTHS AND AMPLITUDES

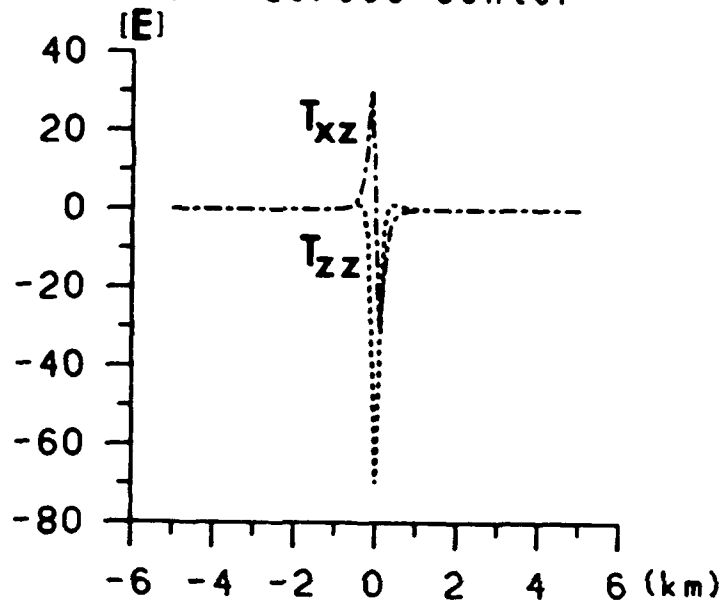
STRUCTURE	RANGE		GRAVITY METHODS USEFUL?
	WAVELENGTH *	AMPLITUDE *	
SALT DOME	3 - 10 KM	5 - 30 E	YES
REEF	0.5- 5 KM	0.3- 5 E	OFTEN
ANTICLINE	3 - 15 KM	3 - 10 E	YES
FAULT	1 - 5 KM	1 - 30 E	YES
PINCHOUT	1 - 5 KM	1 - 5 E	} ONLY IF DENSITY CONTRAST IS SUFFICIENT
UNCONFORMITY	1 - 5 KM	1 - 10 E	
ORE BODY	0.3 - 0.5 KM	0.5 - 100 E	YES

* SIGNAL AMPLITUDE AND WAVELENGTH AT THE SURFACE
OF THE EARTH.

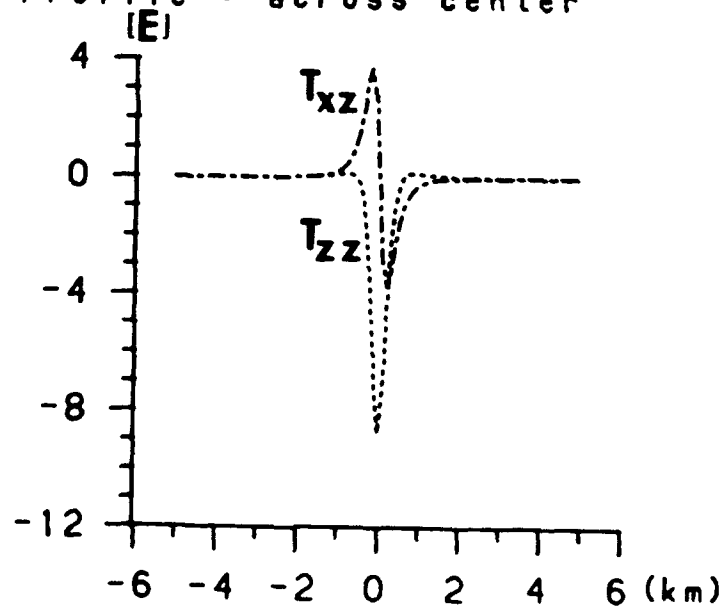
STRONG ATTENUATION WITH ALTITUDE

EXAMPLE : ORE BODY

Depth : 200 m below ground
 radius=100m
 density contrast = 1.0 gr/cm³
 flying altitude = 0.0 m
 Profile : across center



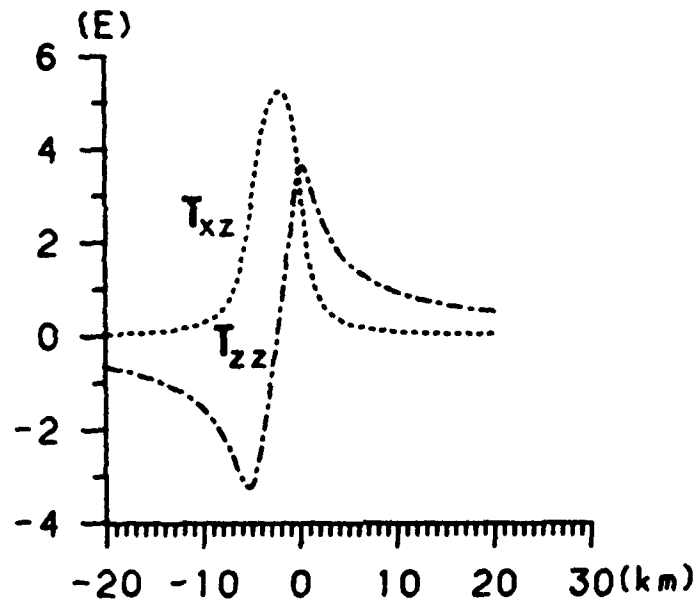
Depth : 200 m below ground
 radius=100m
 density contrast = 1.0 gr/cm³
 flying altitude = 200.0 m
 Profile : across center



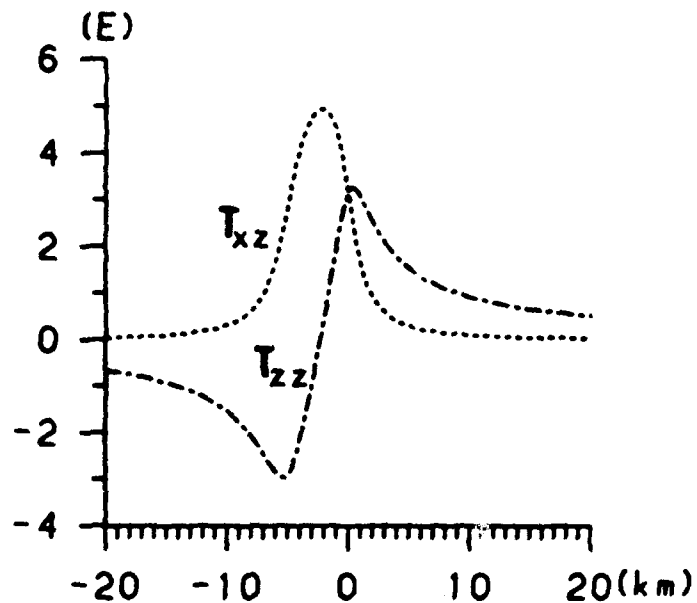
WEAK ATTENUATION WITH ALTITUDE

EXAMPLE : FAULT TRAP

Example : Fault trap
length=5.0 km , depth = 1.0 km
density contrast = 0.2 gr/cm³
flying altitude = 0.0 km



Example : Fault trap
length=5.0 km , depth = 1.0 km
density contrast = 0.2 gr/cm³
flying altitude = 0.2 km



POOR DETECTABILITY OF OFF-PROFILE SOURCES

EXAMPLE : ORE BODY

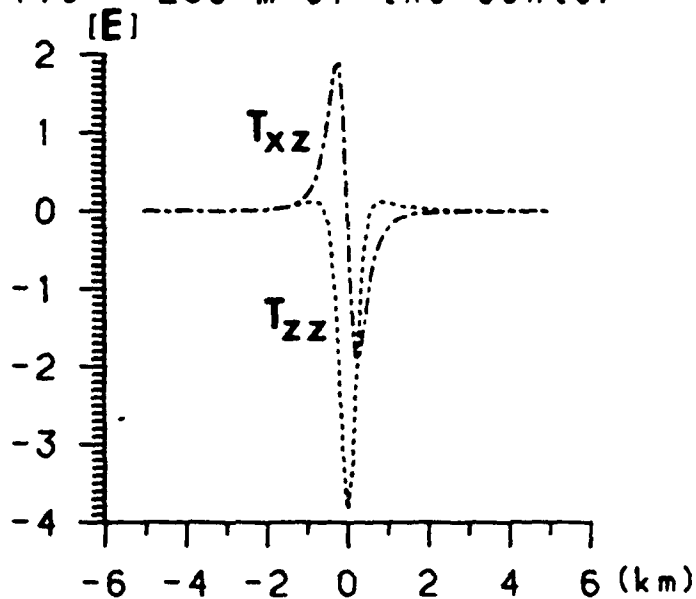
Depth : 200 m below ground

radius=100m

density contrast = 1.0 gr/cm³

flying altitude = 200.0 m

Profile : 250 m of the center



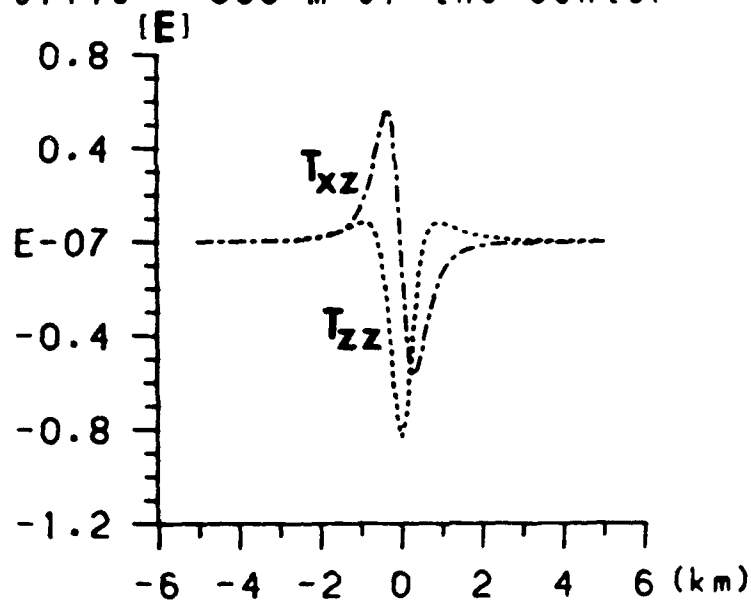
Depth : 200 m below ground

radius=100m

density contrast = 1.0 gr/cm³

flying altitude = 200.0 m

Profile : 500 m of the center

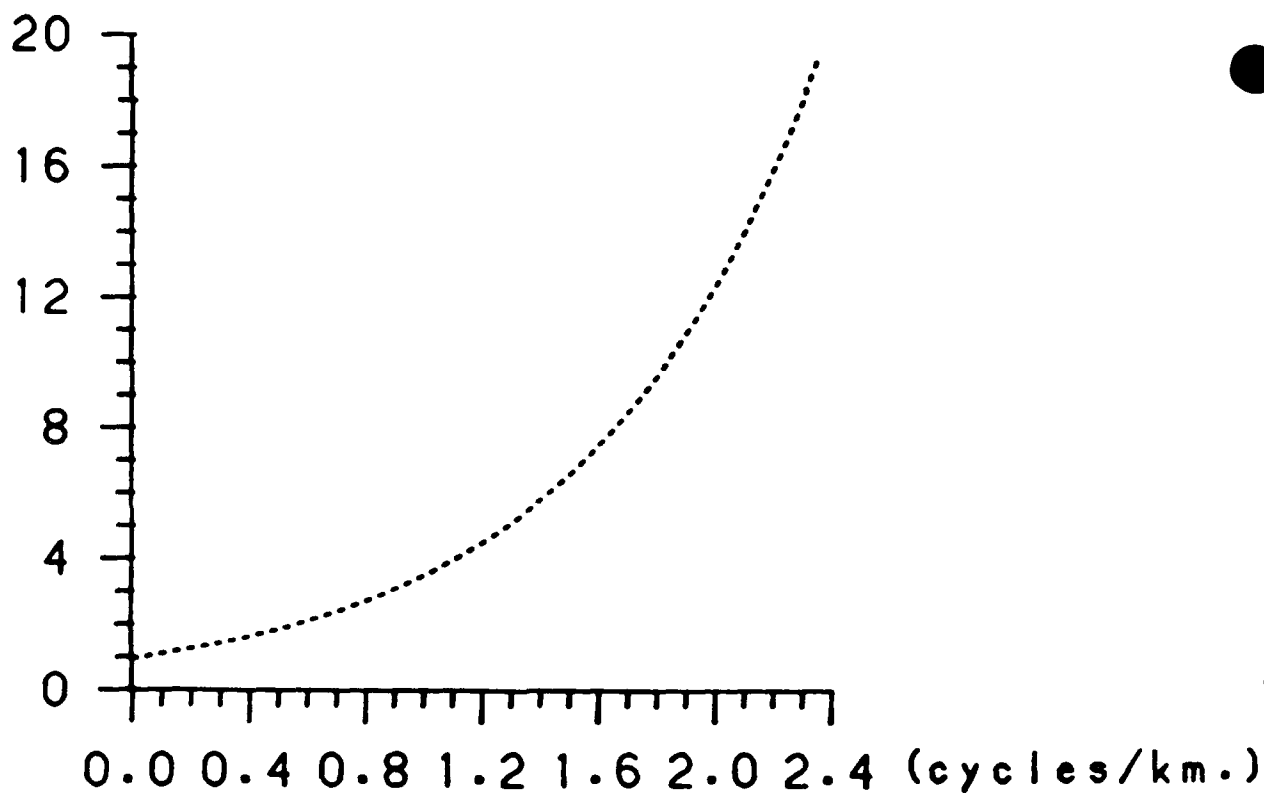


NOTE: LARGER STRUCTURES ARE MUCH BETTER TO DETECT. SOURCES AT A HORIZONTAL DISTANCE OF FIVE TIMES THE SOURCE DEPTH CAN STILL BE SENSED.

DOWNWARD CCNTINUATION

FIGURE GIVES THE AMPLIFICATION FACTOR FOR WAVELENGTHS
RANGING FROM ABOUT 10 KM (1) TO 0.4 KM (20)

downward continuation operator of T_{zz}
flying altitude = 200.0 m
grid spacing = 300.0 m



SIGNAL DETECTION AT FLYING ALTITUDE

ATTENUATION: STRONG ATTENUATION OF SHORT WAVELENGTH SIGNALS (< 0.5 KM) WITH ALTITUDE. IF A SPECIFIC FREQUENCY BAND IS WANTED, FLYING ALTITUDE CAN BE USED AS A LOW-PASS FILTER.

DETECTION OF OFF-PROFILE SIGNALS: MIXED GRADIENTS ARE USEFUL TO DETECT SIGNAL SOURCES WHICH ARE NOT DIRECTLY BELOW THE FLIGHT PROFILE. IN GENERAL, SIGNALS CAN STILL BE DETECTED AT A HORIZONTAL DISTANCE THAT IS TWICE THE DEPTH OF THE SOURCE. THIS WOULD FAVOUR A FULL TENSOR GRADIOMETER OVER A ONE AXIS GRADIOMETER (T_{zz}).

NOISE REDUCTION

GEOLOGICAL NOISE: CAUSE BY 'UNWANTED' DENSITY CHANGES IN THE UPPER CRUST. WAVELENGTHS AND AMPLITUDES ARE SIMILAR. ELIMINATION ONLY POSSIBLE BY JOINT INTERPRETATION OF ALL RELEVANT DATA.

TOPOGRAPHICAL NOISE: CAUSED BY SURFACE TOPOGRAPHY. AIRBORNE MEASUREMENTS MUST BE REDUCED USING DEM AND DENSITY ASSUMPTIONS. SMALLER FEATURES CAN BE FILTERED OUT BY FLYING ALTITUDE. RESIDUAL SYSTEMATIC EFFECTS HAVE TO BE EXPECTED BUT WILL USUALLY BE SMALLER THAN GEOLOGICAL NOISE.

SAMPLING RATE AND MEASURING ACCURACY

ASSUMPTIONS : 10 DATA POINTS PER SMALLEST PERIOD

FLIGHT SPEED : 100 KNOTS

FLYING HEIGHT : 200 M (660 FT)

SIGNAL TO NOISE RATIO : 5 : 1

STRUCTURE	SAMPLING RATE		MEASURING
	(M)	(S)	ACCURACY* (E)
SALT DOMES ANTICLINES	300 - 1500	6 - 30	4 - 7
ORE BODIES PINNACLE REEFS	30 - 50	0.6 - 1.0	0.3 - 0.5
ALL OTHERS	100 - 500	2 - 10	1.0 - 2.0

* TO RESOLVE MINIMUM AMPLITUDE AT FLIGHT LEVEL.

DOWNWARD CONTINUATION

STRONG AMPLIFICATION OF NOISE AND SHORT WAVELENGTH FEATURES MAKE THE INTERPRETATION OF THE DOWNWARD CONTINUED SIGNAL MUCH MORE DIFFICULT. SIGNAL DETECTION AND INTERPRETATION AT FLYING ALTITUDE ARE THEREFORE PREFERABLE. AVAILABLE GROUND GRAVITY CAN BE UPWARD CONTINUED TO FACILITATE LONG WAVELENGTH DETECTION.

USE OF CURRENT AND FUTURE SYSTEMS

CURRENT ROOM TEMPERATURE (BELL SYSTEM)

NOISE: $9 \text{ E } \text{Hz}^{-\frac{1}{2}}$, .1 HZ AVERAGING

——> LARGE SALT DOMES AND ANTICLINES

FLYING ALTITUDE OF 600 M IS ACCEPTABLE FOR THESE FEATURES.

FUTURE ROOM TEMPERATURE

——> LOWER NOISE LEVEL WITH ROOM TEMPERATURE SYSTEMS SEEMS TO BE FEASIBLE. HOWEVER, NOISE REDUCTION HAS TO BE ACCOMPANIED BY A HIGHER SAMPLING RATE, TO MAKE THEM ADAPTABLE TO THESE APPLICATIONS.

CURRENT SUPERCONDUCTING (PAIK)

NOISE: $0.7 \text{ E } \text{Hz}^{-\frac{1}{2}}$, < 1 HZ SAMPLING

——> ALL SIGNALS OF EXPLORATION INTEREST ARE DETECTABLE
A ONE AXIS GRADIOMETER IS SUFFICIENT IF THE SIGNAL SOURCE IS DIRECTLY BELOW THE FLIGHT PASS. FULL TENSOR GRADIOMETER WOULD INCREASE CHANCES FOR DETECTION OF OFF-PROFILE SOURCES.

FUTURE SUPERCONDUCTING

NOISE: $0.07 \text{ Hz}^{-\frac{1}{2}}$, < 1 HZ SAMPLING RATE

——> OFFERS RESOLUTION OF MUCH SHORTER WAVELENGTHS AND POSSIBLY NEW APPLICATIONS.

HIGHER FLYING ALTITUDE AND WIDER PROFILE SPACING
POSSIBLE FOR EXPLORATORY SURVEY.

CONCLUSIONS

- SPEED, RESOLUTION, AND AREA COVERAGE ARE DECISIVE ADVANTAGES OF AIRBORNE GRADIOMETRY OVER CONVENTIONAL GRAVITY EXPLORATION METHODS.
- ATTENUATION OF GRADIENTS WITH HEIGHT IS A PROBLEM FOR SHORT WAVELENGTH FEATURES. A FLYING ALTITUDE OF 200 M IS REQUIRED TO RESOLVE WAVELENGTHS DOWN TO 300 M.
- CURRENT AND NEAR FUTURE SYSTEMS CAN RESOLVE MOST SIGNALS IMPORTANT IN PETROLEUM PROSPECTING AT FLYING ALTITUDES OF 200 - 300 M.
- FULL TENSOR SYSTEMS ARE BETTER THAN ONE AXIS SYSTEMS FOR INTERPRETING SPECIFIC STRUCTURES AND FOR DETECTING OFF-PROFILE SIGNALS.
- ELIMINATION OF TOPOGRAPHICAL AND GEOLOGICAL NOISE IS NECESSARY TO $< 0.5 \text{ E PER KM}$ AT FLYING ALTITUDE.
- SIGNAL DETECTION AT FLIGHT LEVEL IS PREFERABLE TO DOWNWARD CONTINUATION.
- SUPERCONDUCTING GRADIOMETERS ARE ADVANTAGEOUS IN THESE APPLICATIONS BECAUSE OF HIGH SAMPLING RATE AND LOWER NOISE LEVEL.

PAPER TITLE: REQUIREMENTS FOR THE USE OF AIRBORNE GRAVITY GRADIOMETRY
IN GEOPHYSICAL EXPLORATION

SPEAKERS NAME: Klaus-Peter Schwarz

Questions and Comments:

Anthony R. Barringer: In airborne geophysical surveys it is quite normal to fly at survey heights as low as 600 ft. However, turbulence increases a great deal at these heights. What are your comments?

SPEAKERS RESPONSE: It may be possible to stabilize aircraft using wingtip devices. The problem is appreciated and there is a trade-off between flying height and turbulence problems.

Ho Jung Paik: If you have a gradiometer with higher sensitivity, could you take advantage of the sensitivity and fly at a higher altitude to suppress the air turbulence noise?

SPEAKERS RESPONSE: Yes, one can always take advantage of higher sensitivity.

Dave Sonnbend: What is the effect of near surface features causing gravity noise masking signals from deeper features - maybe we want to fly a little higher.

SPEAKERS RESPONSE: Agree that one must optimize altitude; but even with full tensor measured everywhere, cannot sort this out completely.

QUICK REVIEW OF GRADIOMETER-AIDED LAND NAVIGATION

W. G. Heller

The Analytic Sciences Corporation

One Jacob Way

Reading, MA 01867

ABSTRACT

Real-time inertial navigation compensation for gravity disturbances is one of the most demanding applications of gradiometry. This discussion reviews the potential contribution of existing gradiometer instruments to land navigation, namely the benefits which accrue to gravity vector estimation and inertial platform tilt determination. Real-time gravity vector recovery accuracy is seen to be strongly dependent on the quality of initialization gravity data, inertial system and gradiometer accuracy as well as elapsed time from initialization. Position and velocity accuracy is observed not to be significantly enhanced with a gradiometer. The sharp contrast between real-time determination of the gravity field and the accuracy obtainable through post-traverse smoothing motivates combining the gravity gradiometer measurements with gravity vector map. The sensitivity of real-time gravity determination to gradiometer errors also motivates further development of terrestrial gradiometer instruments to achieve noise densities better than $1.0 \text{ E}^2/\text{Hz}$.

SP-4423-30

**QUICK REVIEW OF
GRADIOMETER-AIDED
LAND NAVIGATION**

11-12 February 1986

Prepared for:

FOURTEENTH MOVING BASE GRAVITY GRADIOMETER REVIEW
United States Air Force Academy
Colorado

Prepared by:

W.G. Heller

LAND NAVIGATION BACKGROUND

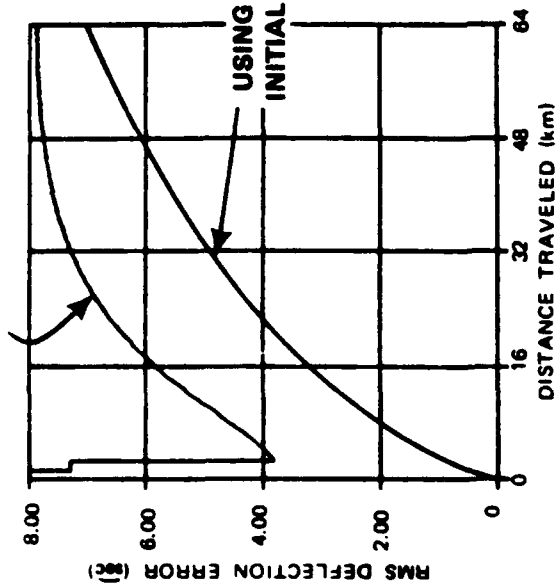
A-34645

- PRIMARILY MILITARY
- CHARACTERIZED BY "REAL TIME" GRAVITY DISTURBANCE RECOVERY
(VS SURVEY OPERATIONS)
- KEY OUTPUTS
 - POSITION AND VELOCITY DETERMINATION
 - GRAVITY AND DEFLECTION RECOVERY
 - INERTIAL SYSTEMS INITIALIZATION (PLATFORM ATTITUDE, AZIMUTH, DRIFT PARAMETERS)
- GRADIOMETER OFFERS MARGINAL BENEFIT TO INERTIALLY-DETERMINED
POSITION AND VELOCITY
- PROVIDES SIGNIFICANT BENEFIT TO THE ACCURACY OF RECOVERED GRAVITY
AND TILT-RELATED QUANTITIES

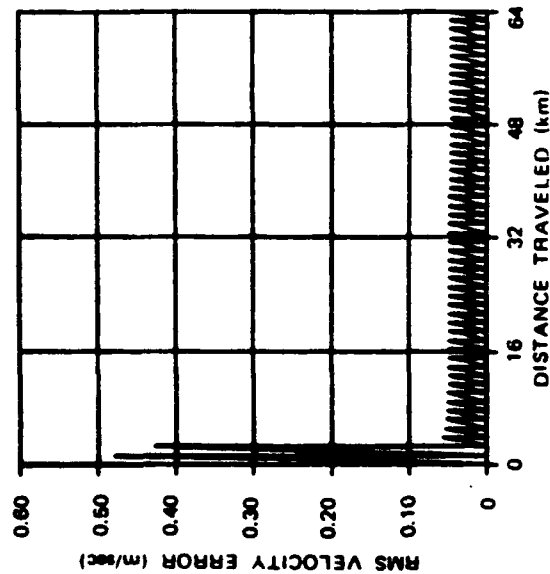
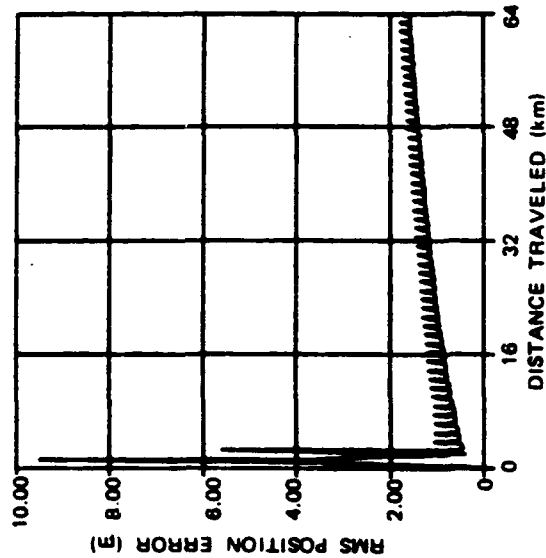
TASC
THE AIRCRAFT SYSTEMS CORPORATION

TYPICAL REAL-TIME LAND INERTIAL NAVIGATION WITH ZUPTS*

NO INITIAL DEFLECTION VALUE



A-34629



- OPTIMAL KALMAN FILTERING
- TYPICAL AUTOSURVEYOR**
- ERROR SOURCES
- FILTER INITIALIZED BY ZUPTS (3 MINUTE DASH; 1 MINUTE DWELL)
- ACCURATE INITIAL POSITION AND VELOCITY
- CRUISE SPEED = 30 km/hr

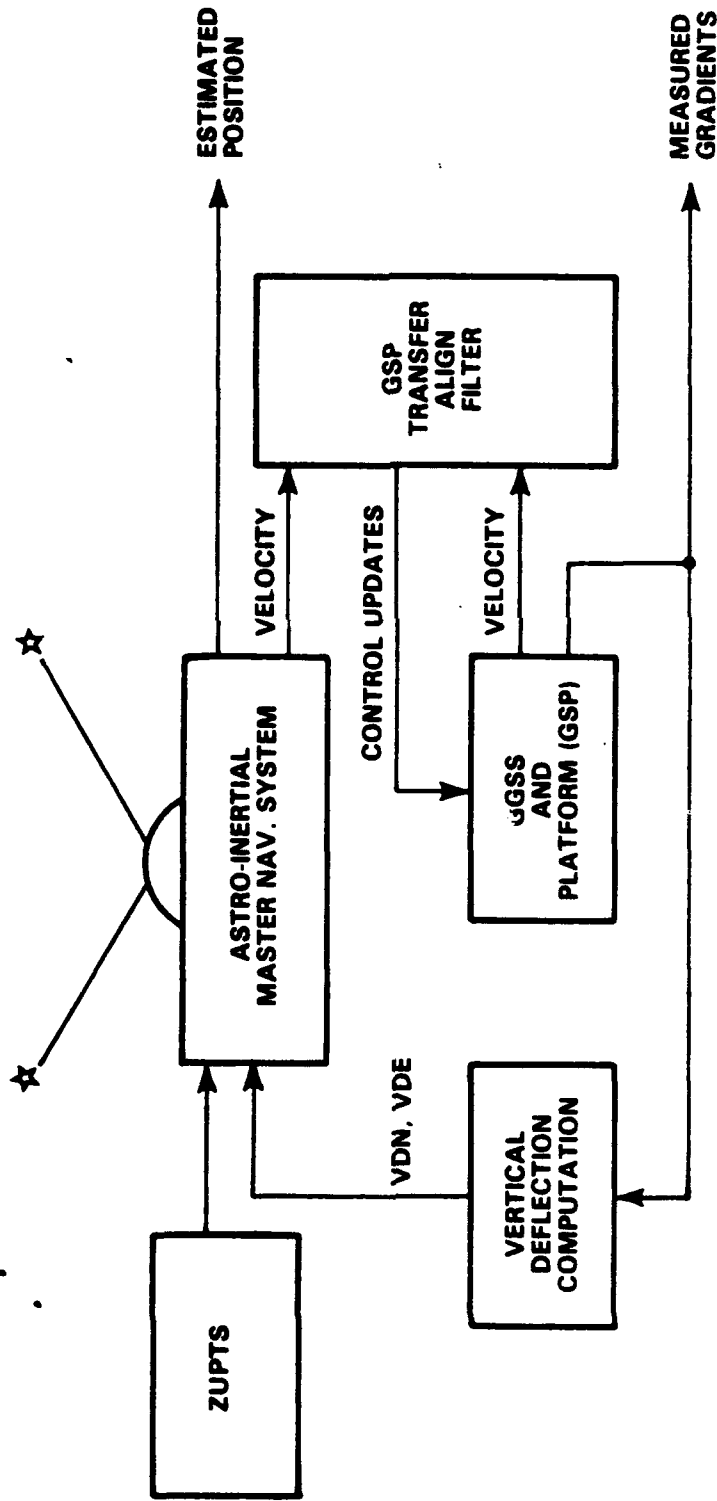
**TRADEMARK - LITTON INDUSTRIES

TASC
THE ADAPTIVE SURVEILLANCE COMPANY

*ZERO VELOCITY UPDATES

GGSS/INS MECHANIZATION (SURFACE SURVEY MODE)

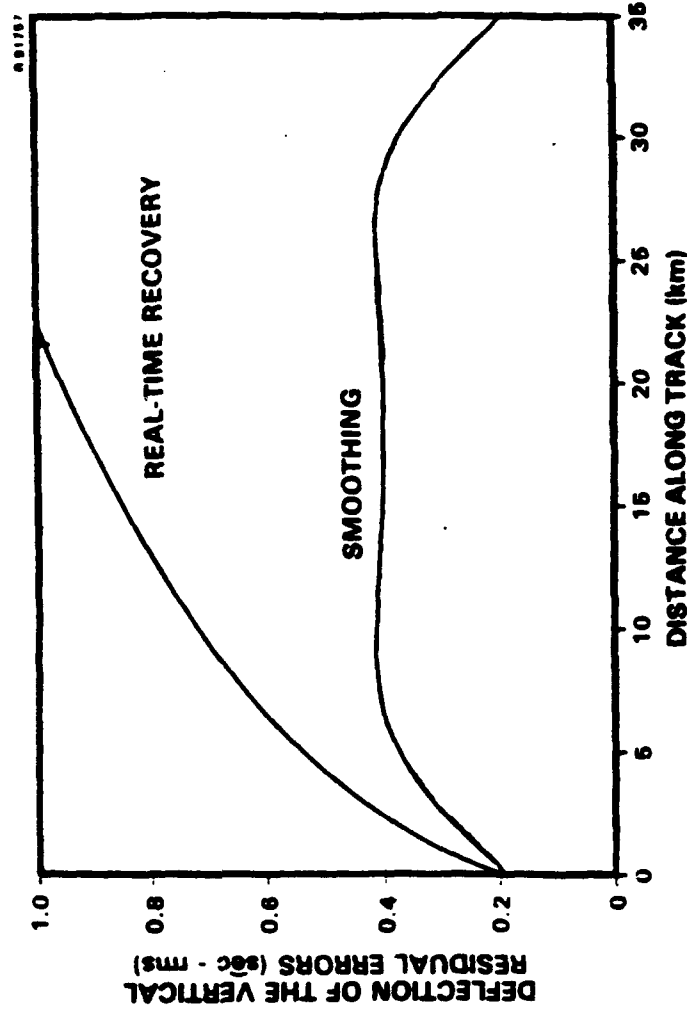
A-9307



TASC
THE ANALYTICAL SYSTEMS CORPORATION

BENEFITS OF ADDING A GRADIOMETER

- DEFLECTION/TILT RECOVERY IN REAL TIME IS DIFFICULT
- IMPROVEMENT WITH SMOOTHING/TERMINAL POINT GRAVITY VECTOR IS DRAMATIC
- MOTIVATES HYBRID GRADIOMETER/MAP MECHANIZATIONS
- DEFLECTION ACCURACY AT ENDPOINTS - 0.2 ARC SEC
- RESULTS BASED ON USE OF STATE-OF-THE-ART ASTRO-INERTIAL SYSTEM



SUMMARY AND ADDITION OBSERVATIONS

A-34648

- REAL-TIME, GRADIOMETER-AIDED INERTIAL NAVIGATION IS DIFFICULT FOR INSTRUMENTS THAT ARE CURRENTLY OPERATIONAL
- CURRENT TECHNOLOGY MOTIVATES USE OF MAPS AND PRESURVEYED GRAVITY AND DEFLECTION TIE POINTS
- GRADIOMETER NOISE LEVELS BETTER THAN $1.0 \text{ E}^2/\text{Hz}$ NEEDED FOR PRACTICAL REAL-TIME RECOVERY AND INS TILT COMPENSATION WITHOUT RECOURSE TO MAPS

TASC
THE AIRCRAFT SYSTEMS CORPORATION

APPLICATIONS OF SUPERCONDUCTING GRAVITY GRADIOMETER SYSTEM
TOWARD INERTIAL GUIDANCE AND FUNDAMENTAL SCIENCE

H. A. Chan

M. V. Moody

H. J. Paik

Dept of Physics and Astronomy

University of Maryland

College Park, Maryland 20742

ABSTRACT

In addition to the gravity survey application which is the primary objective of the NASA program, the superconducting gravity gradiometer system can be used as a gradiometer-aided inertial navigation system and as a detector for a series of fundamental physics experiments both in the laboratory and in the earth orbit. These applications will be discussed.

APPLICATIONS OF SUPERCONDUCTING GRAVITY GRADIOMETER SYSTEM TOWARD INERTIAL GUIDANCE AND FUNDAMENTAL SCIENCE

H. A. Chan, M. V. Moody and H. J. Paik

2/11/86

I. Principle of Gravity and Acceleration Measurement

II. Precision Gravity Experiments

A. Null Test of R^{-2} Law

B. Tests of General Relativistic Effects

III. Superconducting Gravity Gradiometer Systems

A. Prototype Superconducting Gradiometer

B. Advanced 3-axis Superconducting Gradiometer

C. 6-axis Superconducting Accelerometer

IV. Applications of Superconducting Gravity Gradiometers

A. Spaceborne and Airborne Gravity Survey

B. Inertial Guidance and Attitude Stabilization

(Colorado Springs, Colorado)

I. Principle of Gravity and Acceleration Measurement

Specific force on a single proof mass:

$$\begin{aligned}\vec{g}'(\vec{r}, t) &\equiv \left(\frac{d^2 \vec{r}}{dt^2} \right)_{pl} \\ &= -\vec{\nabla} \phi(\vec{r}, t) - \vec{\Omega} \times (\vec{\Omega} \times \vec{r}) - 2\vec{\Omega} \times \left(\frac{d\vec{r}}{dt} \right)_{pl} - \left(\frac{d\vec{\Omega}}{dt} \right)_{pl} \times \vec{r} - \vec{a}(t) \\ &\equiv -\vec{\nabla} \phi(\vec{r}, t) - \vec{a}(\vec{r}, t).\end{aligned}$$

\Rightarrow Acceleration and gravity cannot be distinguished.
(by accelerometer)
"Equivalence Principle".

Differential specific force measurements:

$$\Gamma'_{ij}(\vec{r}, t) = \Gamma_{ij}(\vec{r}, t) - (\Omega_i \Omega_j - \Omega^2 \delta_{ij}) + \sum_k \epsilon_{ijk} \alpha_k.$$

Symmetric component:

$$\Gamma'_{(ij)}(\vec{r}, t) = \Gamma_{ij}(\vec{r}, t) - (\Omega_i \Omega_j - \Omega^2 \delta_{ij})$$

\Rightarrow Gravity gradiometer (2 or 4 proof masses)

Antisymmetric component:

$$\Gamma'_{[ij]}(\vec{r}, t) = \sum_k \epsilon_{ijk} \alpha_k(t)$$

\Rightarrow Angular accelerometer (4 proof masses)

II. Precision Gravity Experiments

A. Null Test of R^{-2} Law

Theoretical challenges :

{ Supersymmetry \Rightarrow gravitinos, graviphotons
{ Unified field theory \Rightarrow axions, goldstone bosons, etc.

\Downarrow

Violation of R^{-2} law

Violation of Equivalence Principle

Experimental challenges :

Violation of R^{-2} Law (Long, Stacey)

Violation of Equivalence Principle (Fischbach et al)

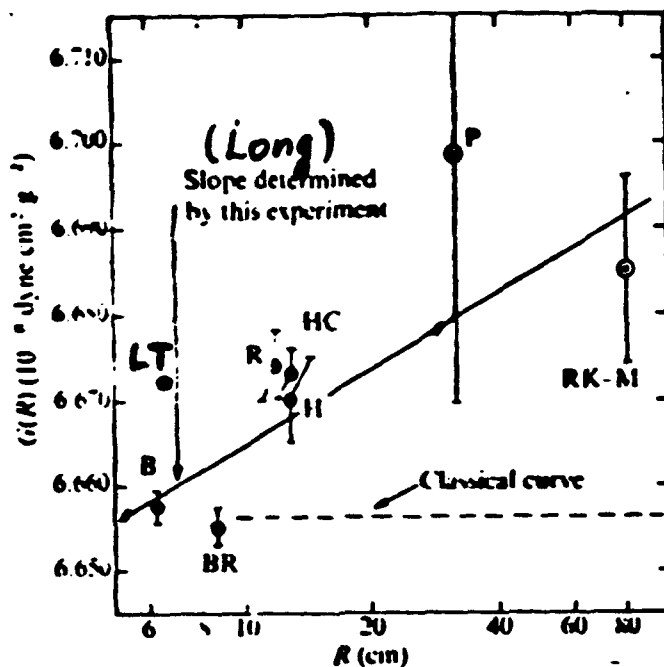
New Null Test of R^{-2} Law :

$$\nabla^2 \phi = 4\pi G \rho$$

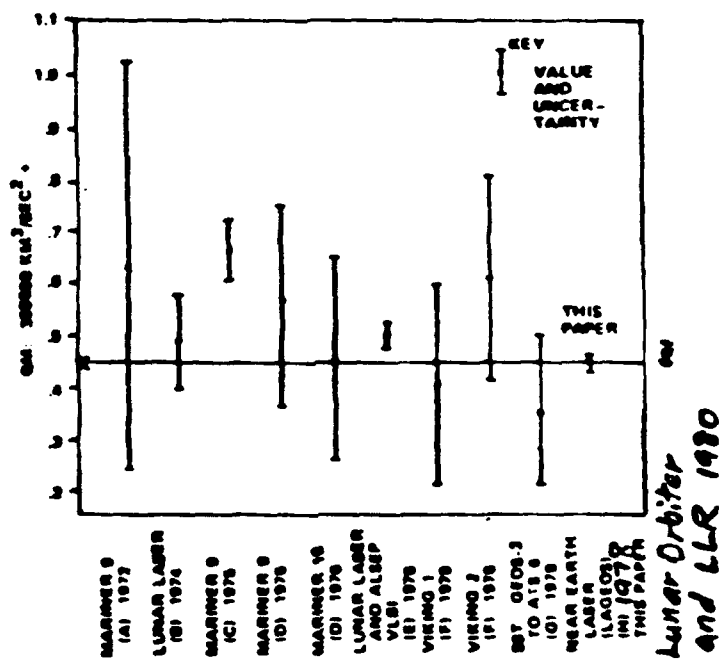
\Rightarrow Laboratory, geological scale, earth-orbit experiments

Status of G and G(r) Measurements

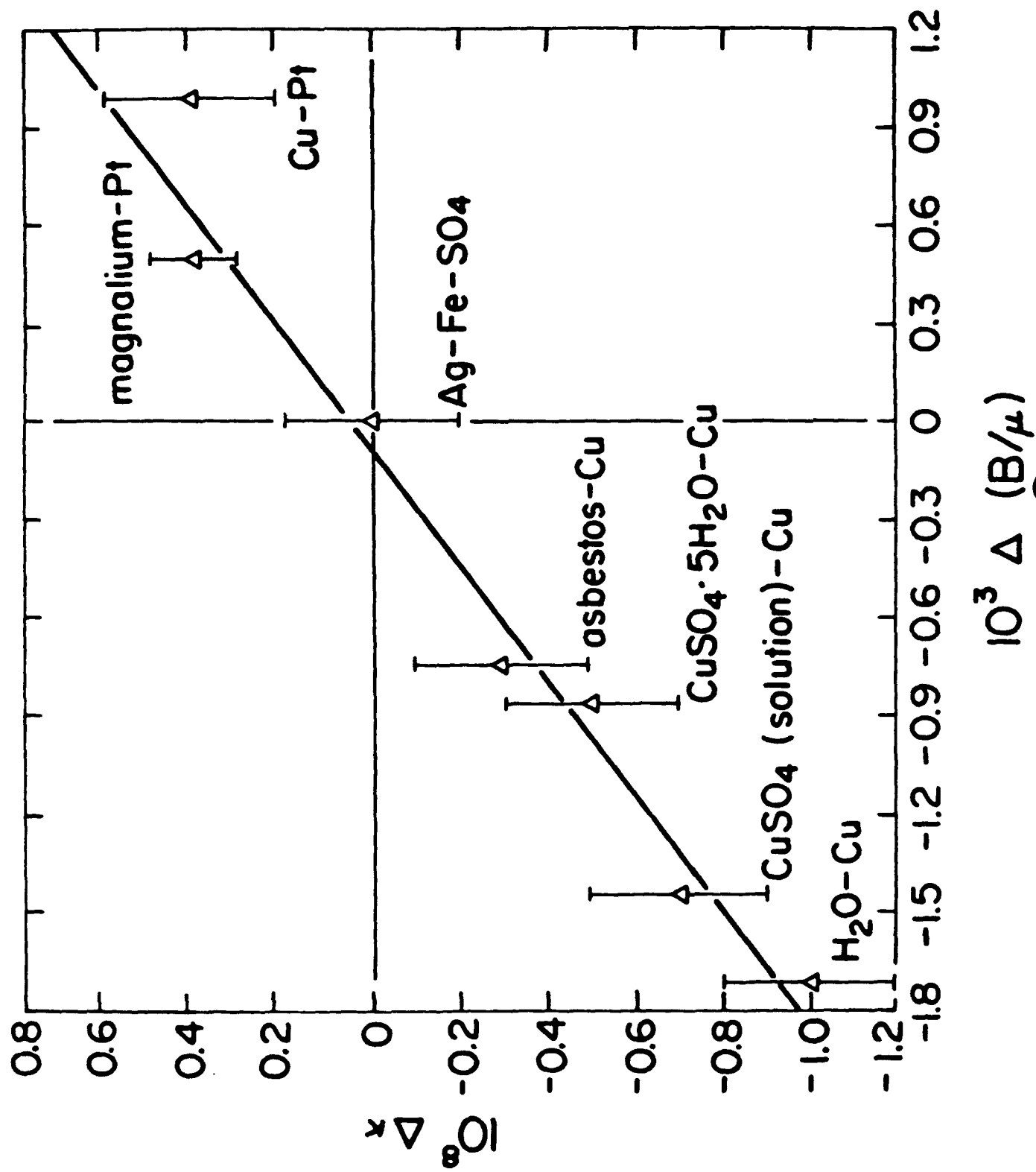
Absolute G Measurements (Cavendish Exps.)



GM_{\oplus} Measurements (Spacecraft Exps)



Lunar Orbiter
and LLR 1980



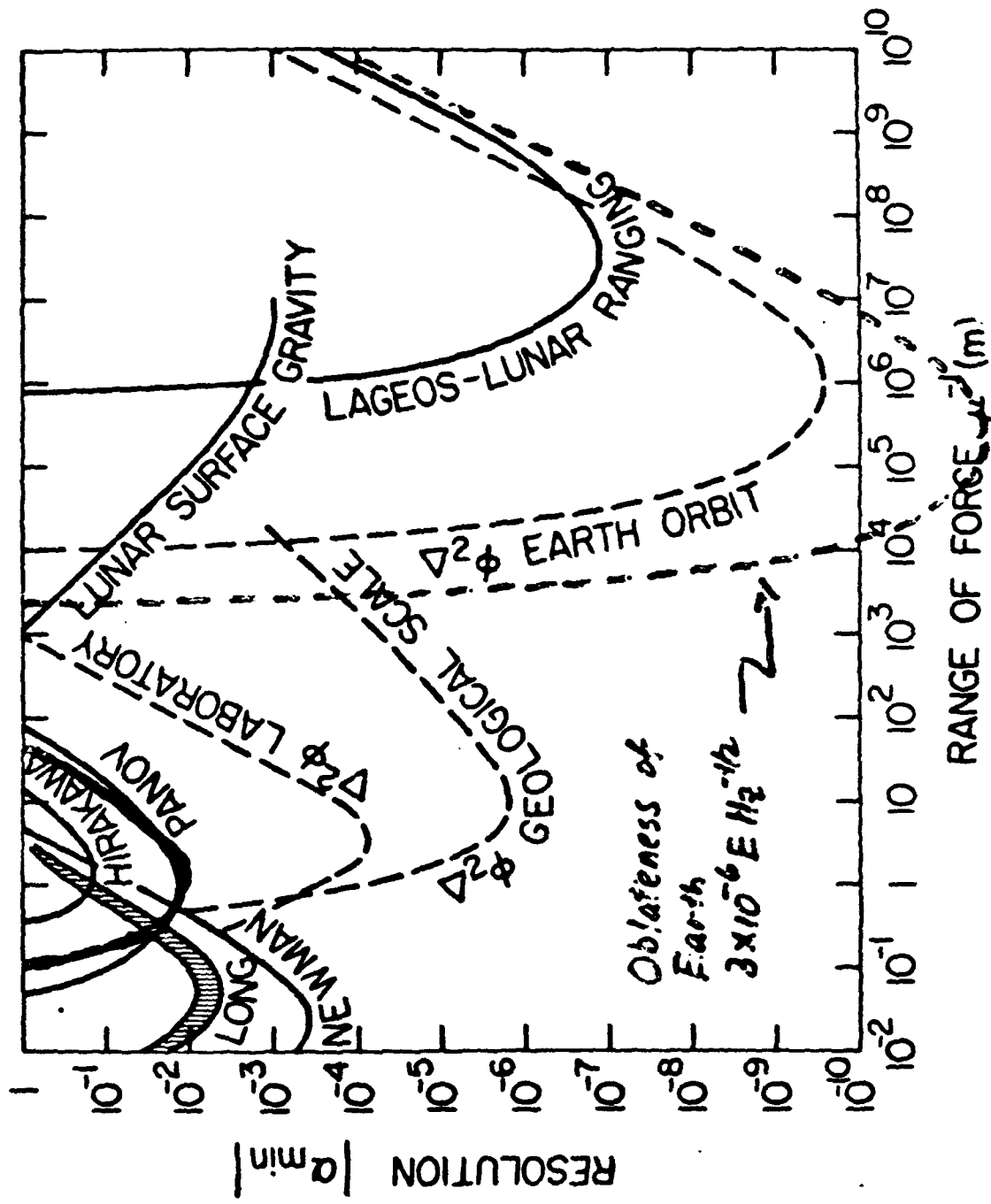


Figure 7

$$\phi(r) = -\frac{1}{64\pi} (1 + i e^{-\mu r})$$

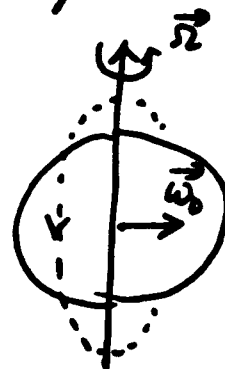
B. Tests of General Relativistic Effects

"Magnetic" component of gravity gradients
due to Earth's rotation (Brazinsky & Polnarev):

$$(\Gamma_{11})_{\text{mag}} \cong (\Gamma_{11})_{\text{el}} \times \frac{v_E}{c} \times \frac{v_S}{c}$$

$$\cong \frac{2GM\Omega\omega_0}{c^2} \frac{R_\oplus^2}{R^3}$$

$$\frac{(\Gamma_{11})_{\text{mag}}}{(\Gamma_{11})_{\text{el}}} \cong 8 \times 10^{-13}$$



Anomalous resonant term (Mashhoon & Theiss):

$$\Gamma_{ij} = \frac{GM}{R^3} \begin{bmatrix} -2-3\chi & -3\alpha p \sin \eta & 0 \\ -3\alpha p \sin \eta & 1+3\chi & 0 \\ 0 & 0 & 1 \end{bmatrix},$$

where $\chi \cong \frac{GM}{R_\oplus c^2} - \frac{2GJ}{R_\oplus^3 c^2 \omega_0}$

$$p = \frac{J}{MR_\oplus^2 \omega_0^2}$$

$$\eta = \omega\tau + \eta_0 \Rightarrow \text{anomalous resonance}$$

α : orbit inclination.

III. Superconducting Gravity Gradiometer Systems

A. Prototype Superconducting Gravity Gradiometer

Performance: $0.7 \text{ E Hz}^{-1/2}$ in certain frequency windows below 1 Hz

Error Modelling \Rightarrow noise spectrum understood.

B. Advanced 3-axis Superconducting Gradiometer

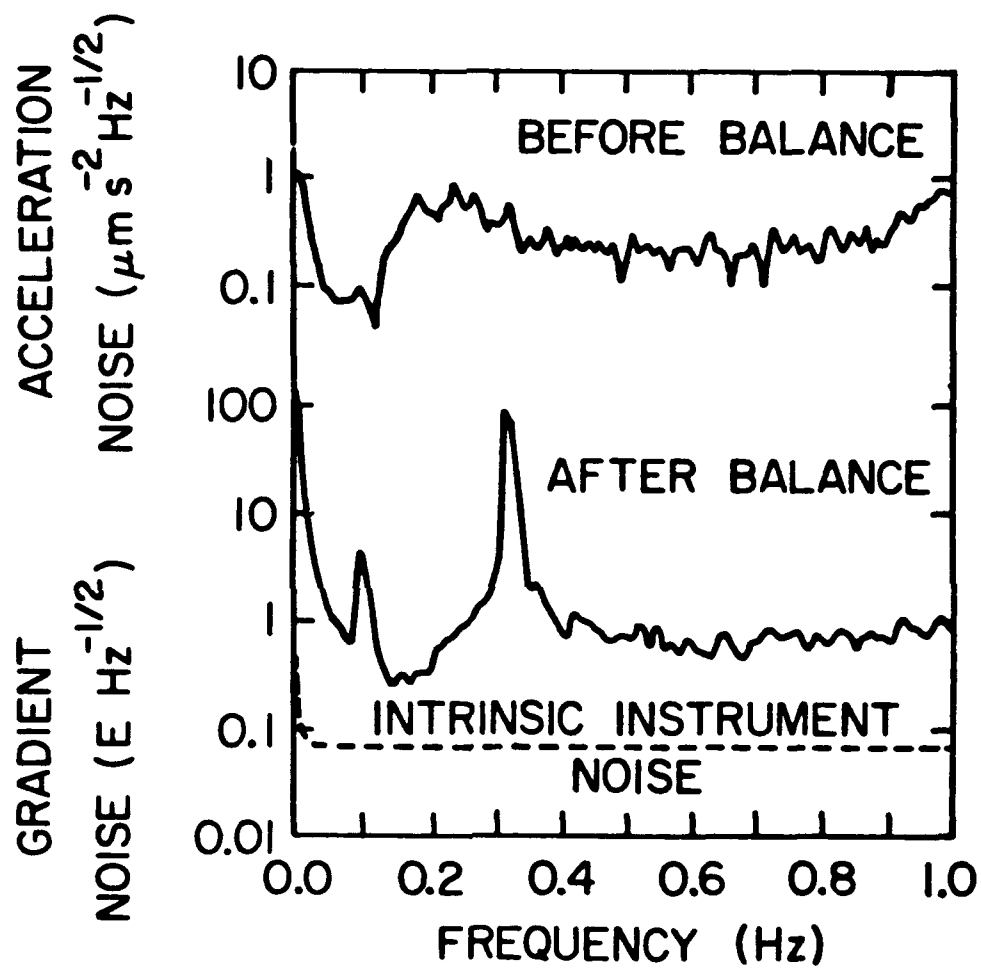
Performance: $< 10^{-3} \text{ E Hz}^{-1/2}$ aimed

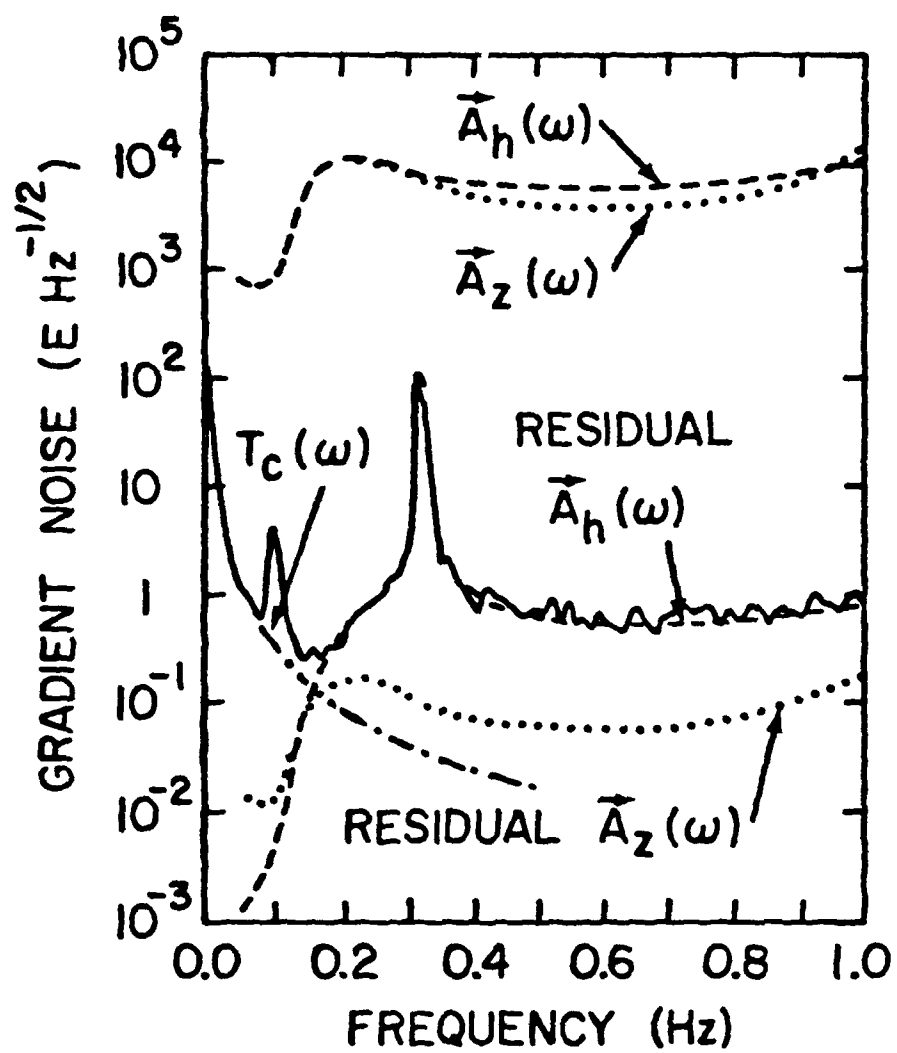
Many error sources are suppressed by improved design.

Complete navigation capability.

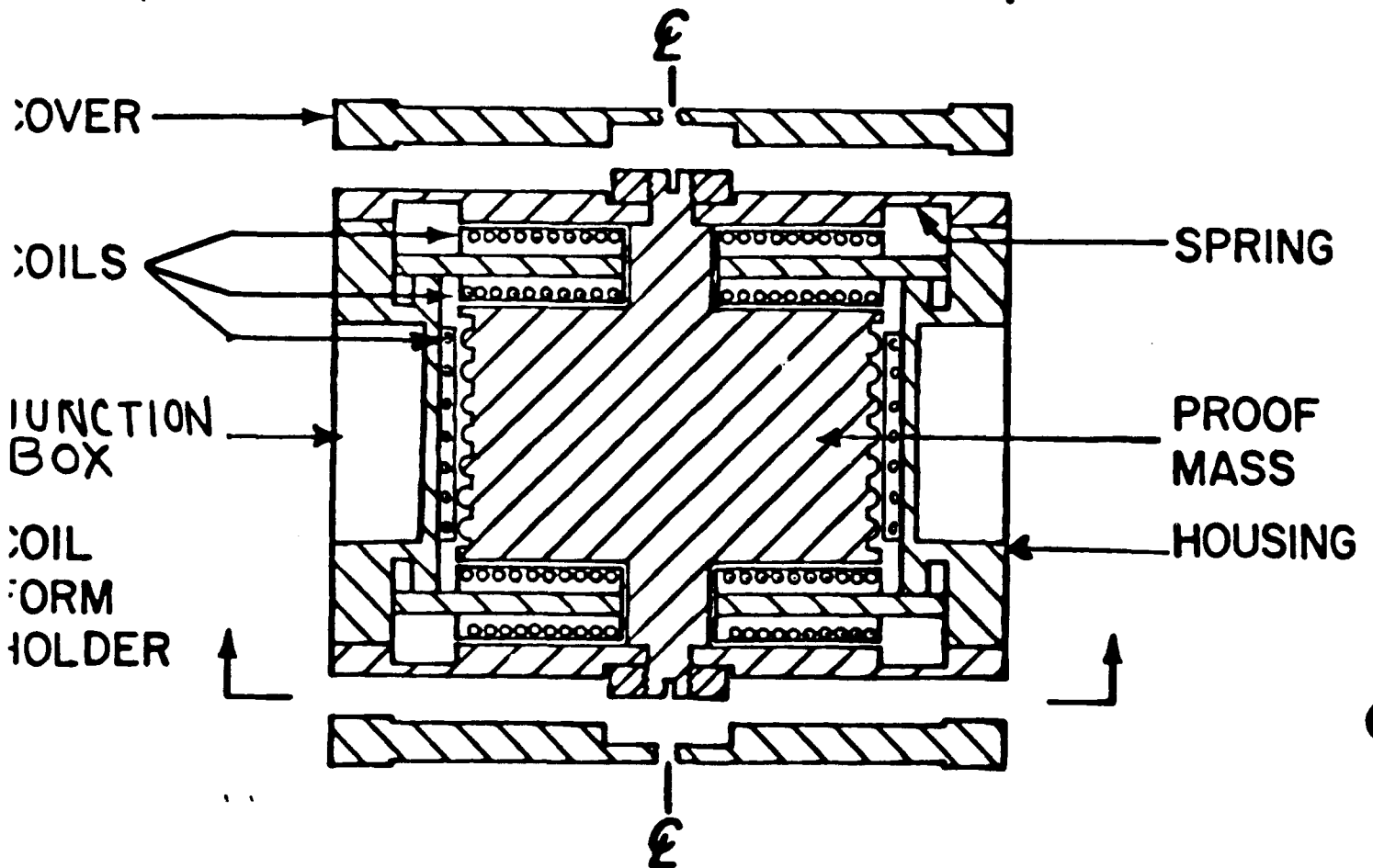
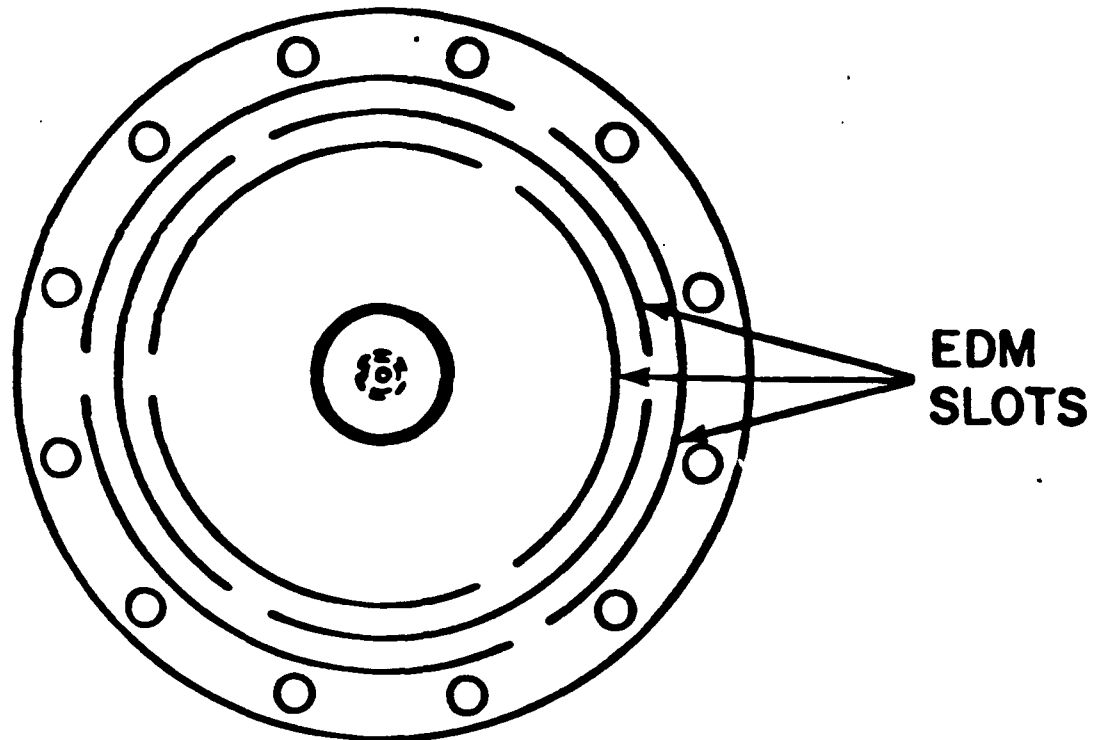
C. 6-axis Superconducting Accelerometer

Performance: $< 10^{-13} \text{ g}_E \text{ Hz}^{-1/2}$ expected
 $< 10^{-11} \text{ rad s}^{-2} \text{ Hz}^{-1/2}$ "

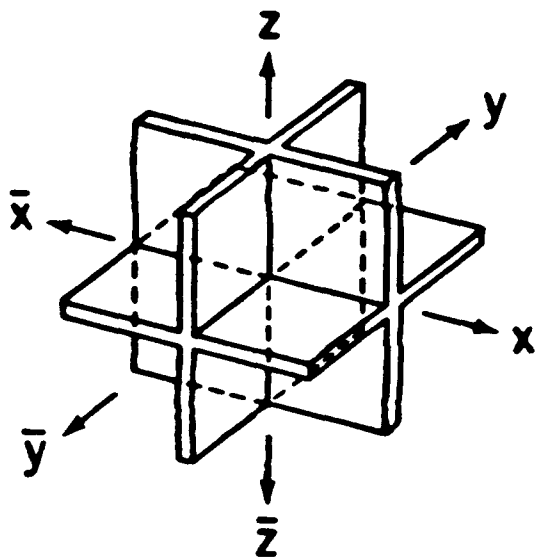




3-AXIS SUPERCONDUCTING GRAVITY GRADIOMETER DESIGN FOR ONE OF SIX IDENTICAL UNITS

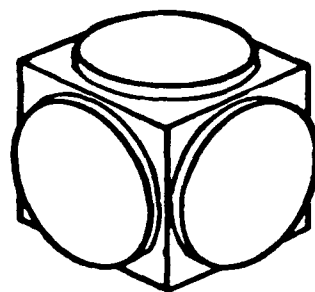


Design



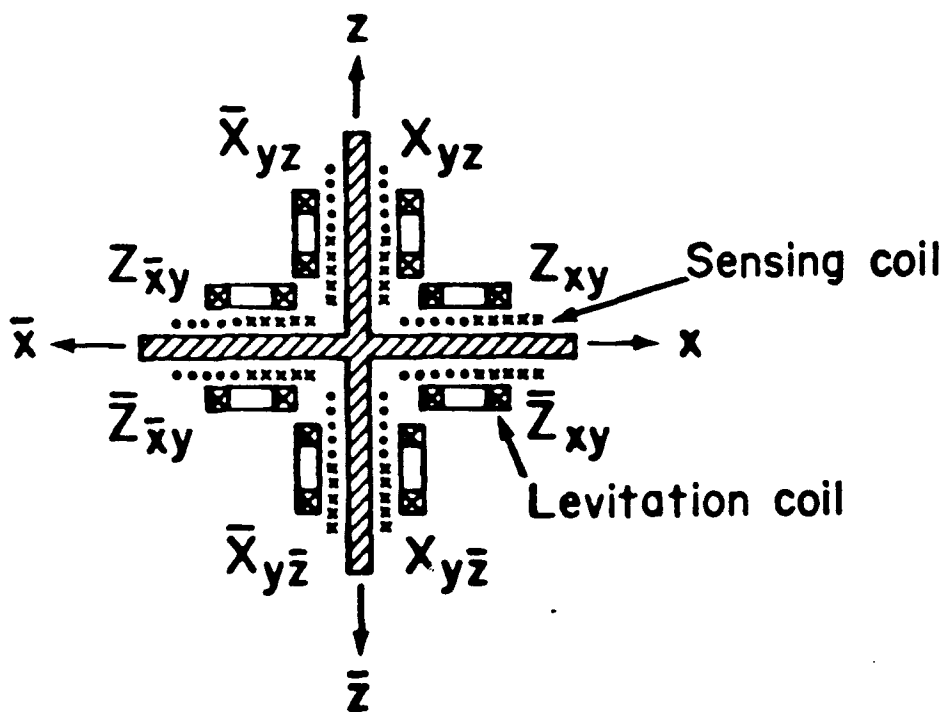
Proof mass (Niobium)

(a)



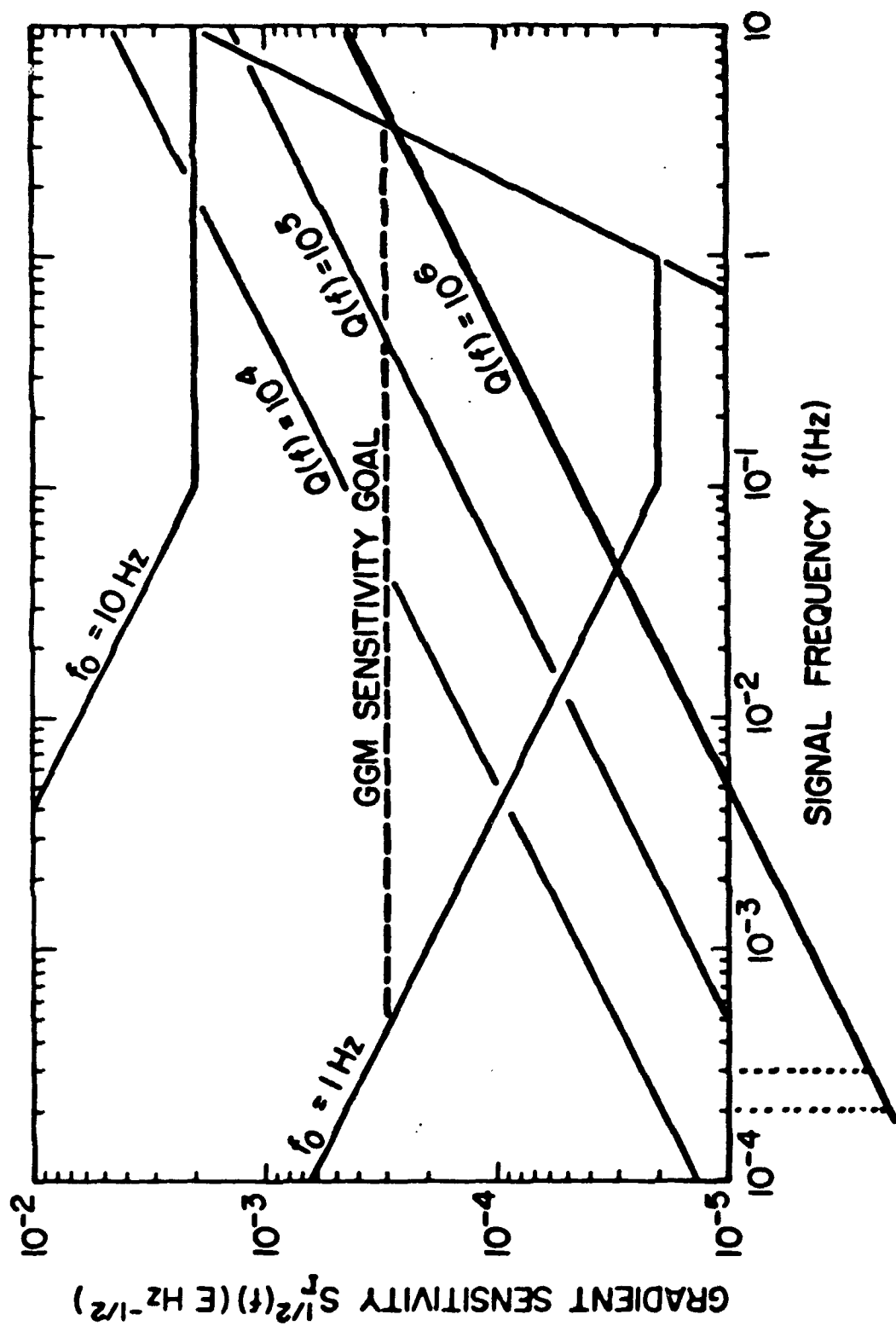
Coil form (Macor ceramic)

(b)



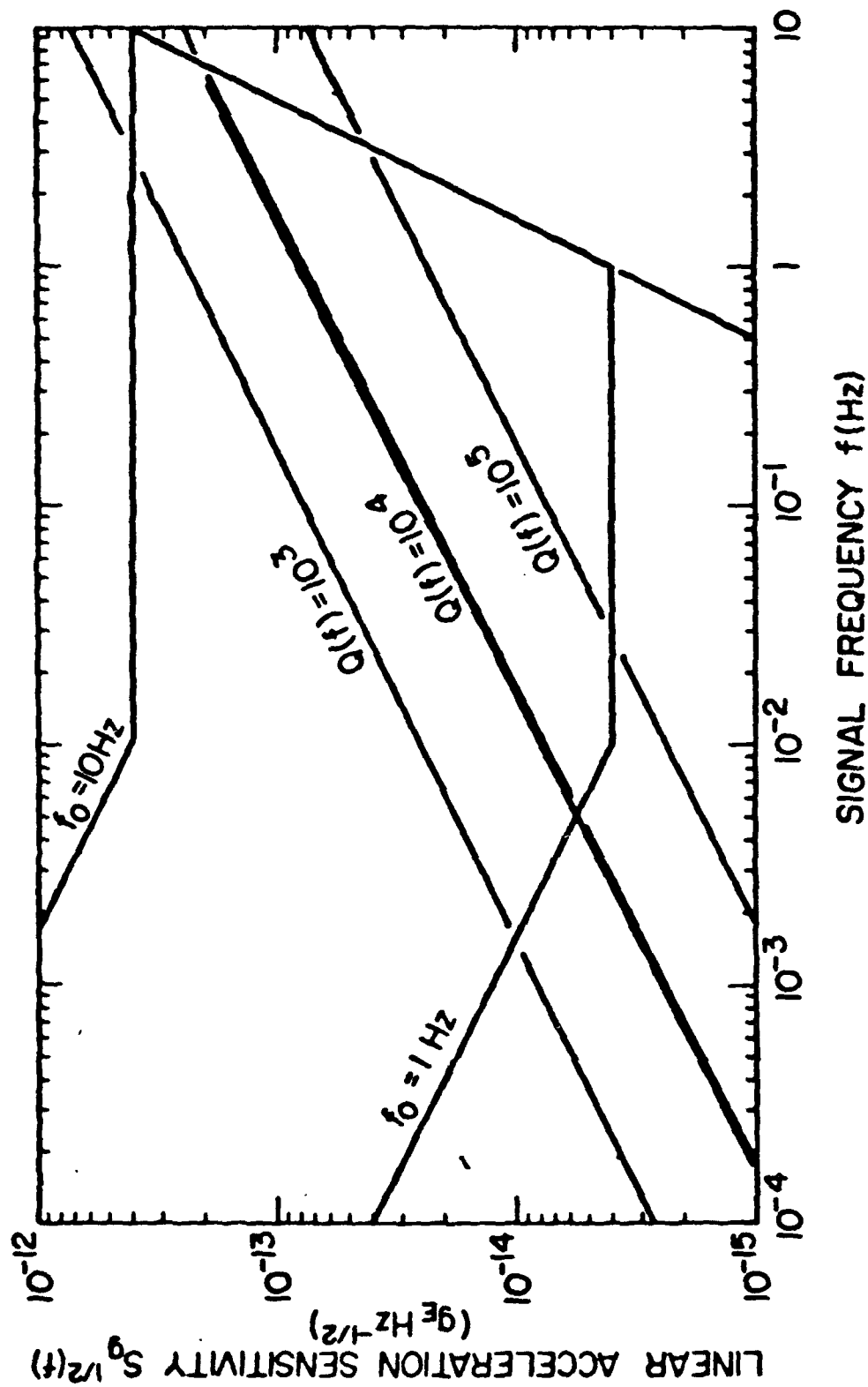
Coils (24 sensing coils + 24 levitation coils)

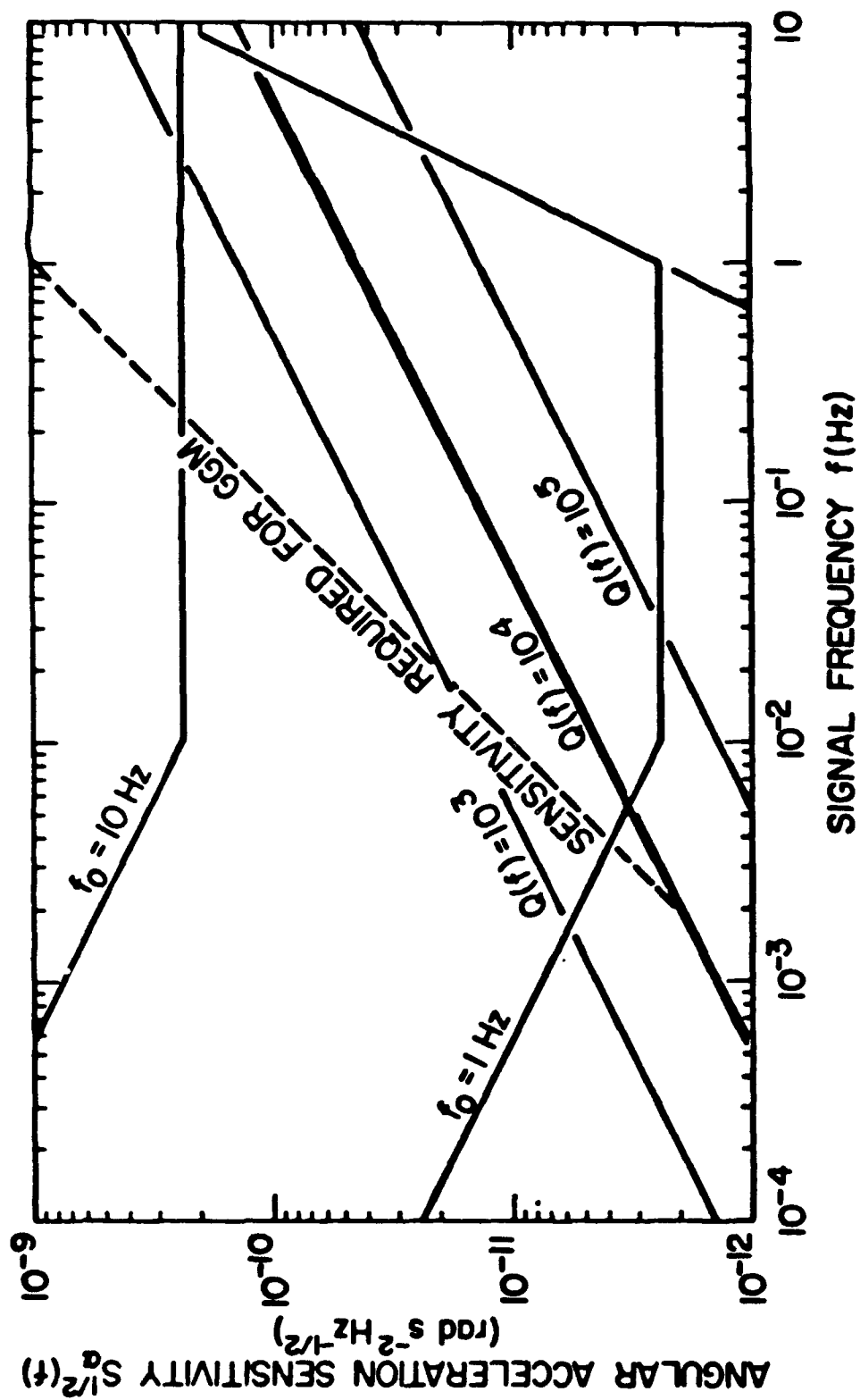
(c)



10^{-10}

Required for GGM





IV. Applications of Superconducting Gravity Gradiometers

A. Spaceborne and Airborne Gravity Survey

Space application: $10^{-6} \sim 10^{-4} \text{ E Hz}^{-1/2}$ eventually

Airborne application: $10^{-2} \sim 1 \text{ E Hz}^{-1/2}$

B. Inertial Guidance and Attitude Stabilization

3-axis gradiometer and 6-axis accelerometer

\Rightarrow gradiometer-aided INS.

Gradiometer in synchronous earth orbit

\Rightarrow precision stabilized platform.

PAPER TITLE: APPLICATIONS OF SUPERCONDUCTING GRAVITY GRADIOMETER SYSTEM
TOWARD INERTIAL GUIDANCE AND FUNDAMENTAL SCIENCE

SPEAKERS NAME: Ho Jung Paik

Questions and Comments:

Chris Harrison: The Stacey and Eötvös experiments (as revised by Fischbach) disagree by a factor of about 20. This is an order of magnitude disagreement.

SPEAKERS RESPONSE: Speaker thought I (Chris Harrison) was talking about the Dicke experiment.

Milton Trageser: You showed a slide showing the response to the swinging pendulum. Over how many pendulum swings was this average?

SPEAKERS RESPONSE: 500 swings --- 2000 second.

Paul Keyser: With regard to the inconsistency between Dicke and Fischback's version of Eötvös, it is important to realize that Fischback's postulates a short-range force so that only Eötvös' results are applicable. It is also important to note that Fischback left out a number of data points which make his curve less impressive, as I will mention in my talk.

Daniel DeBra: How can there be violation for characteristic lengths on either side of Panov's data which claims no violation?

SPEAKERS RESPONSE: Panov's data doesn't overlay the length-sensitivity where violation is claimed.

EFFICIENT GRAVITY GRADIENT DATA GATHERING

M. Bilello

J. B. Breakwell

D. B. DeBra

Department of Aeronautics and Astronautics

Stanford University

Stanford, California 94305

ABSTRACT

We are interested in how one can separate the variations in gravity field from the measurement noise when making a survey. Given a survey pattern in which the path of the instrument crosses itself (as it does in a series of orthogonal tracks), there are a discrete number of instants at which the measurements should be identical. We have examined a number of different sequences in generating the survey pattern to vary the times at which these identical conditions occur. The conjecture was that an appropriate choice of pattern could take advantage of the time characteristics of the measurement noise in permitting a separation of noise from gravity data. We show the results as a function of the correlation time of the measurement noise for a simple model of the gravity field. For noise varying from uncorrelated to a correlation time comparable to the survey time, the variation is approximately 10%. Large differences in accuracy of reconstruction do not appear likely since our results give variation between paths of approximately 2% for two very dissimilar paths through the same grid. Thus the conjecture has not been borne out.

Efficient Gravity Gradient Data Gathering

Introduction

The modern interest in measuring gravity gradients began in the late 1950s motivated by determining the vertical in a satellite. Early papers considering the analytical aspect of gradient determination were followed in the next decade by a number of innovative approaches in how such an instrument might be built. The revolution in gradiometry was to make the measurements in a moving vehicle and/or in a satellite without the gravity needed for the geophysical pendulum instruments. An instrument developed at the Bell Aerosystems was chosen for field application for improvements in navigation. This instrument has been very successful in its early field tests and is in production for deployment. As a result of this success for the navigation mission, the Defense Mapping Agency (DMA) through the Air Force Geophysical laboratory (AFGL) began the modification of this instrument for gravity gradient measurements for gravity survey work. Many people have subsequently contributed to the development of a survey plan and techniques for utilization of such an instrument. In this paper we explore the possibility that given an area to be surveyed and a track spacing that has been determined by the necessary resolution of gravity data, there might be improvements in accuracy depending upon the form of a grid pattern used in overflying the area. The conjecture is based on the fact that instrument noise, whether described in the time domain or spectrally, may be different than the equivalent noise associated with gravity fields for a given velocity of the vehicle during the survey. When a survey is performed with a grid in which tracks cross each other, there are a discrete number of crossings at which the measurements should be the same in both directions. Different patterns provide a different distribution in time of when these points of identical measurement occur. It is this variation in the distribution and time which could make a difference in being able to separate signal from noise.

Models

As indicated in the introduction, the spectral characteristics of the gravity field and of the instrument will have an influence on the separability of the gravity information from the instrument noise. With the amount of experimental data that exists from the laboratory and early field trials, it would be possible to give a good model of the expected noise from a gravity gradiometer. However, to investigate the potential for improvement one can start with a much simpler model of the instrument noise and vary its parameters to see whether or not significant improvements are possible. We have chosen the latter approach to investigate the feasibility of improvement with the expectation that if significant improvements appear possible we would then improve the model using available empirical data.

Spectral Characteristics of the Field

We have used a model of the gravity gradient field that allows us to determine the spatial correlations of the gravity gradient. (J.V. Breakwell [1]).

Using an approximation of flat earth, we can write:

$U(\vec{\omega}, h) = e^{-h\omega} U(\vec{\omega}, 0)$ where $U(\vec{\omega}, 0)$ is the Fourier transform of $U(x, y, 0)$, potential on the reference surface of the earth and $U(\vec{\omega}, h)$ is the Fourier transform of $U(x, y, h)$, gravity potential at altitude h .

Then the gravity gradients components are given by:

$$\begin{bmatrix} U_{xx}(\vec{\omega}, h) \\ U_{yy}(\vec{\omega}, h) \\ U_{zz}(\vec{\omega}, h) \\ U_{xy}(\vec{\omega}, h) \\ U_{xz}(\vec{\omega}, h) \\ U_{yz}(\vec{\omega}, h) \end{bmatrix} = e^{-h\omega} \begin{bmatrix} -\omega_x^2 \\ -\omega_y^2 \\ \omega^2 \\ -\omega_x\omega_y \\ -j\omega_x\omega \\ -j\omega_y\omega \end{bmatrix} U(\vec{\omega}, 0) \quad (1)$$

where

$$\vec{\omega} = (\omega_x, \omega_y) \\ \omega = \sqrt{\omega_x^2 + \omega_y^2}$$

From Heller's model referenced in [1], we get the spectral density of $U(x, y, 0)$ with correlation distance D_i :

$$\phi_{U_o}(\vec{\omega}) = \phi_{U_o}(\omega) = \sum_{i=1}^3 \phi_i e^{-2\omega D_i}$$

Equation (1) can be viewed as a representation of a linear system with $U(\vec{\omega}, 0)$ as input and

$$e^{-h\omega} \begin{bmatrix} -\omega_x^2 \\ -\omega_y^2 \\ \omega^2 \\ -\omega_x\omega_y \\ -j\omega_x\omega \\ -j\omega_y\omega \end{bmatrix}$$

as the transfer function.

Then we can compute the spectral densities of the gravity gradient components at altitude h :

$$\begin{bmatrix} \phi_{U_{xx}}(\vec{\omega}, h) \\ \phi_{U_{yy}}(\vec{\omega}, h) \\ \phi_{U_{zz}}(\vec{\omega}, h) \\ \phi_{U_{xy}}(\vec{\omega}, h) \\ \phi_{U_{xz}}(\vec{\omega}, h) \\ \phi_{U_{yz}}(\vec{\omega}, h) \end{bmatrix} = e^{2\omega h} \begin{bmatrix} \omega_x^4 \\ \omega_y^4 \\ \omega^4 \\ \omega_x^2\omega_y^2 \\ \omega_x^2\omega^2 \\ \omega_y^2\omega^2 \end{bmatrix} \phi_{U_o}(\omega)$$

By taking the inverse Fourier transform, we can determine the auto-correlation functions for the gradients, say $S_U(x, y, h)$.

Example: Say we want to compute $S_{U_{..}}(x, y, h)$

we have

$$\phi_{U_{..}}(\bar{\omega}, h) = e^{2\omega h} \omega^4 \phi_{U_{..}}(\omega) = \sum_{i=1}^3 \phi_i \omega^4 e^{-2\omega(h+D_i)}$$

then

$$S_{U_{..}}(x, y, h) = \sum_{i=1}^3 \phi_i \int \int_{-\infty}^{+\infty} e^{j(\omega_x x + \omega_y y)} \omega^4 e^{-2\omega(h+D_i)} d\omega_x d\omega_y$$

or

$$S_{U_{..}}(r, \theta, h) = \sum_{i=1}^3 \phi_i \int_0^{2R} \int_0^{+\infty} e^{j r \omega \cos(\theta - \alpha)} \omega^5 e^{-2\omega(h+D_i)} d\omega d\alpha$$

that is

$$S_{U_{..}}(r, h) = \sum_{i=1}^3 \phi_i 2\pi \int_0^{+\infty} \omega^5 e^{-2\omega(h+D_i)} J_0(r\omega) d\omega$$

In the special case of a flight path over a point grid, we need to compute $s_p = E[s_p s_p^T]$,

where S_p is the sequence of signals we want to estimate $s_p = \begin{bmatrix} s_{p1} \\ \vdots \\ s_{pN} \end{bmatrix}$.

Let's suppose that we are measuring the component $U_{..}$ of the gradient then:

$$E[s_{pi} s_{pj}] = S_{U_{..}}(r_{ij}, h)$$

where

$$r_{ij} = \|\overrightarrow{P_i P_j}\|,$$

is the distance between points P_i and P_j .

Gravity Survey

To perform a gravity survey, the craft which carries the instruments follows a particular path. In the simple case of a square survey area, a possible strategy is to fly parallel tracks as shown in Figure 1.

However, in order to remove drifts and red noise from the measurements, a better way is to make cross checks, taking two measurements at two different times at the same point. The grid of Figure 2.1 is an example of this type of flight. Also shown is the time of second crossing, Figure 2.2, and the time between the two crossings versus the point

of interest, Figure 2.3. One can see that for the path of Figure 2.2, the crossings occur essentially during the second half of the total survey time T and that when they begin to occur, it is in such a way that they are close to each other in space.

In order to get a better time and space distribution of second crossings, a path such as the one shown in Figure 3.1 might be of interest. Here, a row or column is skipped at each pass, and the effect can be seen in Figures 3.2 and 3.3. Basically, second crossings occur earlier and two consecutive ones are more likely to be spread in time. Another advantage of this kind of path is the possibility to continue to make measurements while turning between two tracks. If one row or column (or more) is skipped, then the radius of curvature in the turning is bigger, so that both the bank angle and the induced acceleration are smaller. This may allow the instrument platform to remain in tolerable perturbations and compensations may be possible.

In view of the disappointing results that we are about to give, we did not pursue the question of efficiency due to variations in the radius of turns, nor did we carry the study to include the effect of mass attraction and error modeling on the instrument.

Criteria for Comparison

Our purpose is to get an estimate of the gravity gradient at the grid points with the smallest error-standard deviation. Since all points are a priori of equal importance, we take as the performance criterion the arithmetic mean of the standard deviation obtained at each point, that is:

$$\sigma_{per} = \frac{1}{N} \sum_{i=1}^N \sigma_i$$

where $\sigma_i = \sqrt{P_i}$ and P_i is the variance of the error in the gravity quantity at point i : $P_i \equiv E[(s_{p_i} - \hat{s}_{p_i})^2]$. N is the number of points on the grid. Thus, we will be considering as the best path the one that minimizes the criterion σ_{per} .

Theory

The gradiometer output signals consist of the sum of a signal to be estimated (gravity quantity) and the noise inherent in the instrument.

$y = s + n$ where s is any one of the gravity gradient components and n is the instrument noise. If we take M measurements at M different times, we have in vector form:

$$y = s + n \text{ where } y = \begin{bmatrix} y_1 \\ \vdots \\ y_M \end{bmatrix} ; s = \begin{bmatrix} s_1 \\ \vdots \\ s_M \end{bmatrix} ; n = \begin{bmatrix} n_1 \\ \vdots \\ n_M \end{bmatrix}$$

where n_j is the instrument noise at time t_j , etc. ...

If the pattern is a square grid with intersecting points, then $M = 2p^2$ where p is the number of points on the side of the square grid.

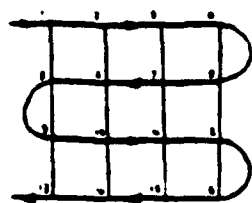


Fig. 1

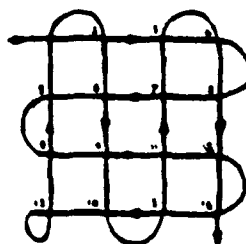


Fig. 2.1

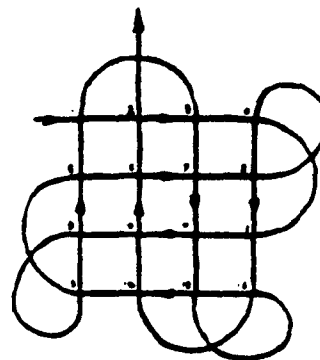


Fig. 3.1

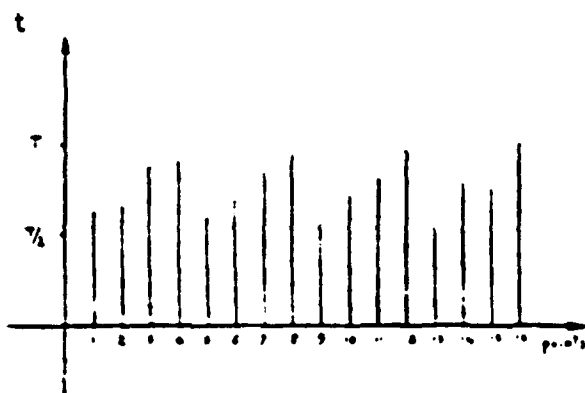


Fig. 2.2

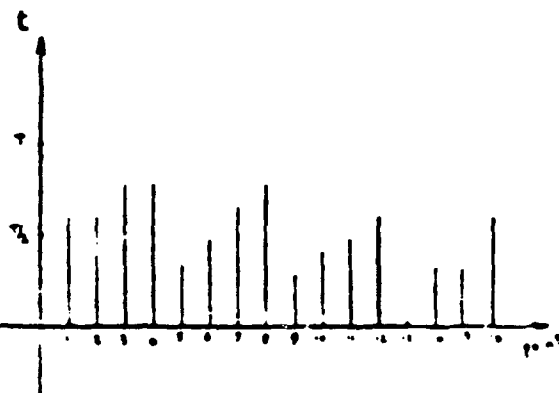


Fig. 2.3

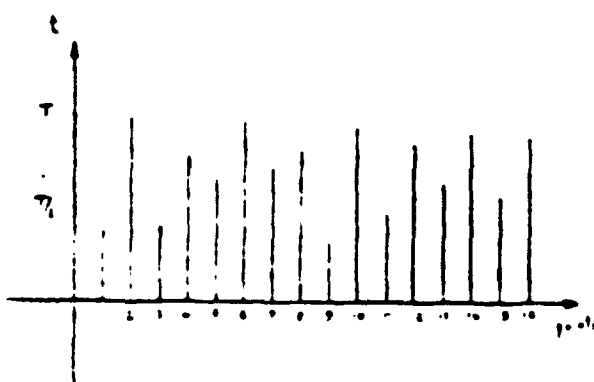


Fig. 3.2

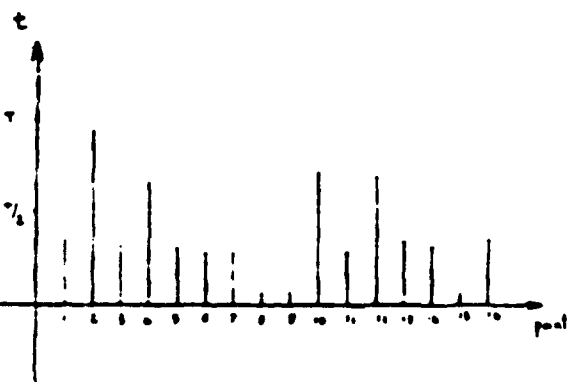


Fig. 3.3

Figs.

The sketches above show 4 by 4 grids. The speed of the craft is uniform and the turning times are neglected. In Fig. 2.2 and 3.2, the time of the second crossing at each point (from 1 to 16) is plotted, while Figs. 2.3 and 3.3 show the time between the two crossings for each point (from 1 to 16).

We assume for simplicity a linear estimate from the observations:

$\hat{z} = Ky$ where K is an $M \times M$ gain matrix. This is a smoothing formula where we use all the collected data to estimate the gravity quantity at each point.

The error in the estimate is $\bar{s} \triangleq s - \hat{z}$ or $\bar{s} = (I - K)s - Kn$.

Then the covariance matrix of the error, say P , can be computed:

$$P = E[\bar{s}\bar{s}^T] = (I - K)S(I - K)^T + K N K^T - (I - K)E[sn^T]K^T - K E[ns^T](I - K)^T$$

where $S \triangleq E[ss^T]$ and $N \triangleq E[nn^T]$.

The gravity signal S and the instrument noise being uncorrelated, the formula reduces to:

$$P = (I - K)S(I - K)^T + K N K^T$$

Then we choose the gain matrix K that minimizes the trace of P (least squares estimate) that is:

$$d(\text{tr}(P)) = \text{tr}[(-(I - K)S + KN)dK^T + dK(-S(I - K)^T + NK^T)] = 0$$

This yields $-(I - K)S + KN = 0$ or $K = S(S + N)^{-1}$ whenever the inverse exists and in this case K exists and is unique. We remark that if $(S + N)$ is non invertible then $E[yy^T]$ is non invertible. Minimising every term P_{ii} leads to the same gain matrix K . The linear least squares estimate is then deduced $\hat{z} = S(S + N)^{-1}y$. The performance of the estimate is judged upon the error covariance matrix and more precisely on the diagonal entries of this matrix. Substituting for K in the expression of P , we get:

$$P = S(S + N)^{-1}N$$

In addition to the fact that n and s are uncorrelated, we have implicitly assumed that s and n are zero-mean signals. If this is not the case, ($E(s) \neq 0$ and/or $E[n] \neq 0$ but still $E[ns^T] = E[sn^T] = 0$), then the formulae are modified in such a way that we replace the random variables with their centered counterparts, namely:

where ($y = s + n$)

$$\begin{cases} \hat{z} = E(s) + K(y - E(y)) \\ K = S^*(S^* + N^*)^{-1} \\ P = S^*(S^* + N^*)^{-1}N^* \end{cases}$$

with

$$S^* \triangleq E[ss^T] - E[s]E[s^T]$$

$$N^* \triangleq E[nn^T] - E[n]E[n^T]$$

Then for a particular pattern that links times to points, we associate the variance $P(t_j, t_j)$ with the point which is flown over at time t_j .

However, for a grid with crossed points, it turns out that it is never necessary to take the inverse of the $M \times M$ matrix $(S + N)$ because as can be expected, there are a lot of redundancies in the matrix P computed as $P = S(S + N)^{-1}N$. For example, if at times j and k the same point is flown over (with $j \neq k$), then obviously $P(t_j, t_i) = P(t_k, t_i) \forall i$; in particular, $P(t_j, t_j) = P(t_k, t_k)$.

We detail this in the next section on preliminary numerical results.

Numerical Results

We take for our example $p = 4$ and there are $16 = p^2$ points on the grid and we show first how to reduce the size of the matrix to be inverted $(S + N)$ (the path lasts M units of time).

Let

$$s_t = \begin{bmatrix} s_{t1} \\ \vdots \\ s_{tM} \end{bmatrix} \quad \text{and} \quad S_p = \begin{bmatrix} s_{p1} \\ \vdots \\ s_{pN} \end{bmatrix} \quad \text{also} \quad n_t = \begin{bmatrix} n_{t1} \\ \vdots \\ n_{tM} \end{bmatrix} \quad n_p = \begin{bmatrix} n_{p1} \\ \vdots \\ n_{pN} \end{bmatrix}$$

where the subscripts t stand for time and p for points ($N = p^2$)

then

$$\begin{cases} s_t = F s_p \\ n_t = F n_p \end{cases}$$

where F is the $M \times p^2$ matrix that maps the points to the times, i.e., $F(i, j) = 1$ if point j is flown over at time t_i and 0 otherwise.

F is full rank and let F_i be the pseudo-inverse of F (F_i is $p^2 \times M$) then we can write

$$\begin{cases} S_t = F S_p F^T \\ N_t = F N_p F^T \end{cases} \quad \begin{cases} S_p = F_i S_t F_i^T \\ N_p = F_i N_t F_i^T \end{cases}$$

where

$$S = E[ss^T]$$

$$N = E[nn^T]$$

From previous results we had:

$$P_t = S_t(S_t + N_t)^{-1}N_t$$

which yields

$$P_i = FS_p F^T [FS_p F^T + FN_p F^T]^{-1} FN_p F^T$$

or

$$P_i = FS_p F^T [F(S_p + N_p)F^T]^{-1} FN_p F^T$$

but

$$F^T [F(S_p + N_p)F^T]^{-1} F = (S_p + N_p)^{-1}.$$

Then

$$P_i = FS_p (S_p + N_p)^{-1} N_p F^T = F P_p F^T \text{ where } P_p \triangleq S_p (S_p + N_p)^{-1} N_p.$$

P_p is a $p^2 \times p^2$ matrix the diagonal entries of which are repeated in the diagonal of P_i . P_p gives directly the covariance of the gravity gradient at the points of interest.

For the numerical example, we chose a 4×4 grid with two different paths and we wish to compare the performances using the criterion mentioned earlier. We have first to define the covariance matrices N and S and to construct the F matrix for the two different paths.

The models used for the random signals n and s are exponentially correlated. That is, the entries of the covariance matrix N_i vary as the exponential of the time difference and the entries of the covariance matrix S_p vary as the exponential of the distance, namely:

$$N_i(i, j) = e^{\frac{-|t_i - t_j|}{\tau}} \text{ and } S_p(i, j) = e^{\frac{-|r_i - r_j|}{\delta}}$$

where τ and δ are correlation time and correlation distance, respectively.

These models do not claim to be accurate but represent only a first try to get numerical performance.

Then we compute $P_p = S_p (S_p + N_p)^{-1} N_p$ to determine the variance of the error associated with the gravity gradient at each point of the grid.

For the two paths, we plot the mean of the standard deviation versus τ ($\tau = 0$ corresponds to a white noise).

Conclusion:

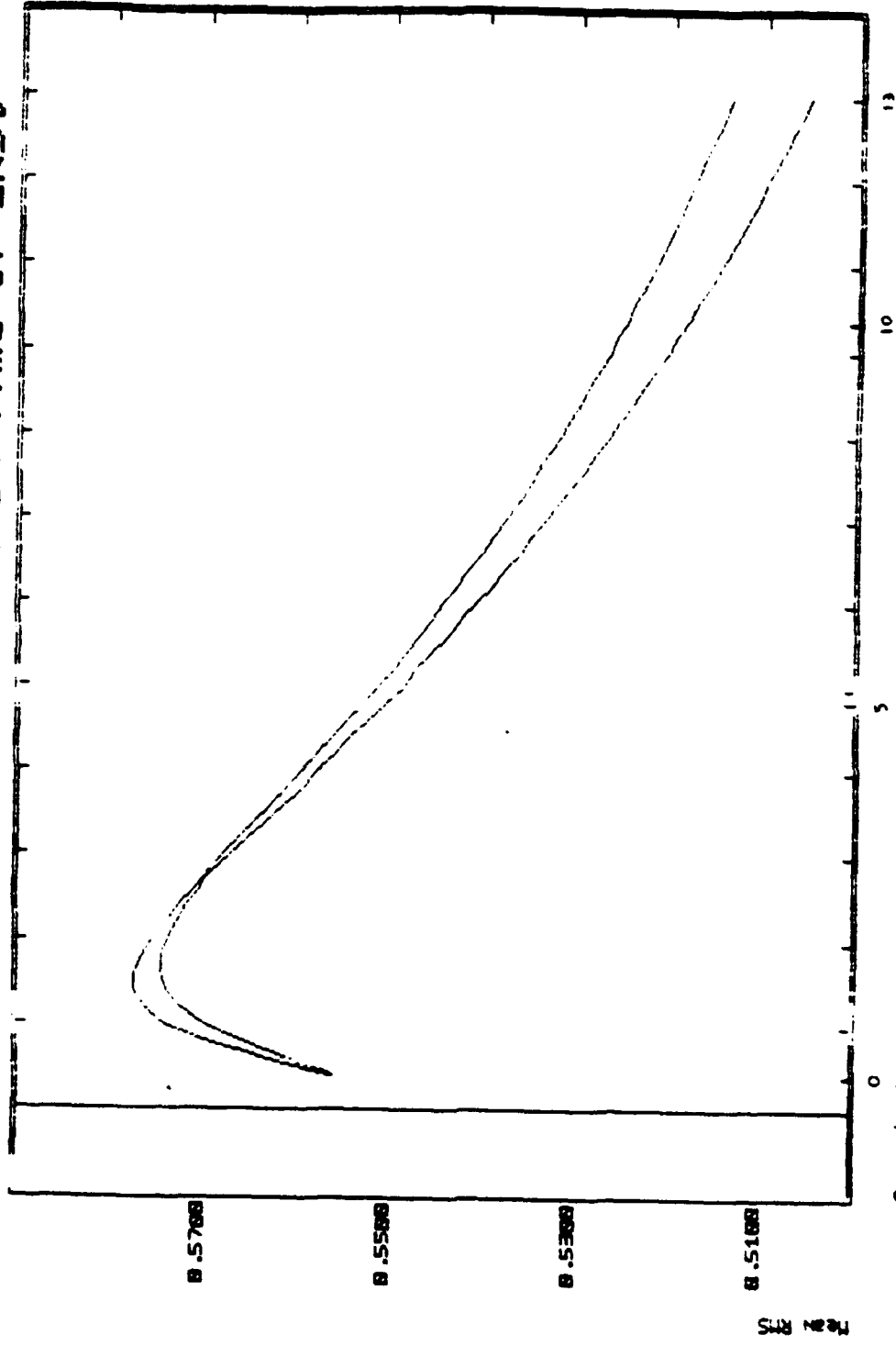
The spectral models of instrument noise and gravity gradient signal we used in our simulations may not be realistic and this marks the limitation of the results we got. However, in the special case of exponential correlated signals, they allow us to answer the question of the best path (among specified ones) according to the criterion we defined. In terms of times of second crossing and times between crossings, the two paths chosen for the simulation can be described as "very" different. Surprisingly enough, the performances for the two paths are close to each other for the range of correlation times we have run.

However, the gap is getting wider in favor of path 1 when the correlation time gets larger but the performance of path 1 is only 1.5 % better for $r = 13$ units of time.* In these conditions, the choice of a "better" path appears not to be an issue.

Our final remark concerns the nature of the instrument noise. The way it has been modelled assumed that it was stationary (in particular constant variance at any time); if this is not the case, quite different results may occur; for example, the importance of early crossings increases.

* 1 unit of time is the time required to fly from a point to the next one.

Mean RMS versus Correlation Time of Inst



Correlation time
Plot #1 4 Jan-86 20:12

[1] Breakwell, J.V., "Satellite Determination of Short Wavelength Gravity Variations,"
J. of the Astronautical Sciences, No. 4, pp. 329-344, Oct-Dec. 1979.

PAPER TITLE: EFFICIENT GRAVITY GRADIENT DATA GATHERING

SPEAKERS NAME: Michel Bilello

Questions and Comments:

Peter Uginčius: 1. If the noise were not correlated, would there be any difference for different survey patterns? 2. What determines the position of the maximum in the plot of error covariance vs. noise correlation time?

SPEAKERS RESPONSE: 1. No. 2. The ratio of correlation times for noise and signal.

USE OF TERRAIN ELEVATION DATA IN AIRBORNE GRADIOMETRY

J. L. Center, Jr.

Geospace Systems Corporation

Wellesley Office Park

40 William Street

Wellesley, Mass. 02181

ABSTRACT

Terrain elevation data is needed to relate airborne survey data to ground data.

This paper quantifies the errors introduced if terrain effects are ignored. It also suggests a method for operational use of terrain elevation data.

USE OF TERRAIN ELEVATION DATA IN AIRBORNE GRADIOMETRY

DR. JULIAN L. CENTER, JR.

Geospace Systems
CORPORATION

OVERVIEW

- THE NEED FOR TERRAIN ELEVATION DATA
- COMPUTATIONAL METHODS
- ERROR ANALYSIS METHODS

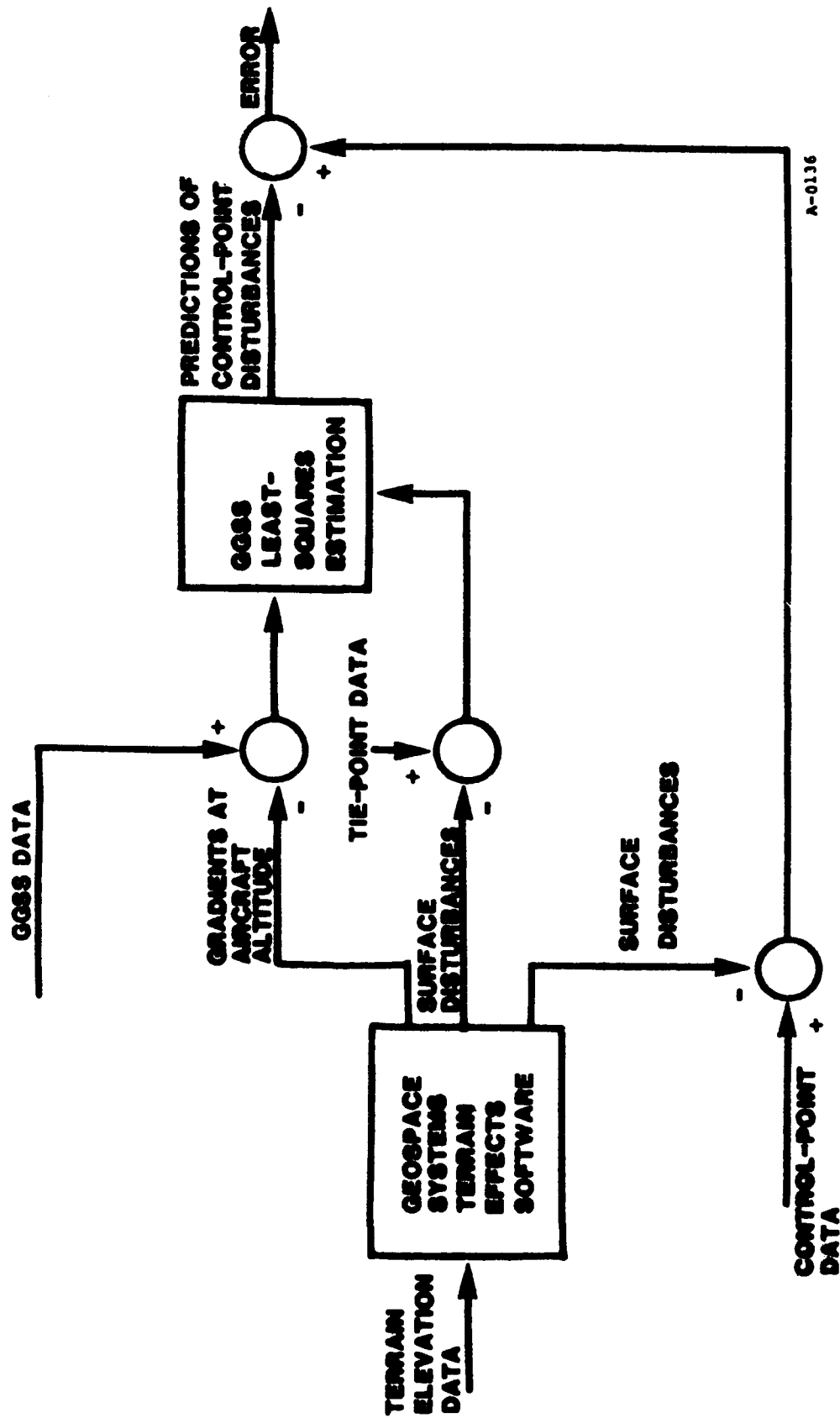
THE NEED FOR TERRAIN ELEVATION DATA

Geospace Systems
CORPORATION

WHY ARE TERRAIN EFFECTS IMPORTANT?

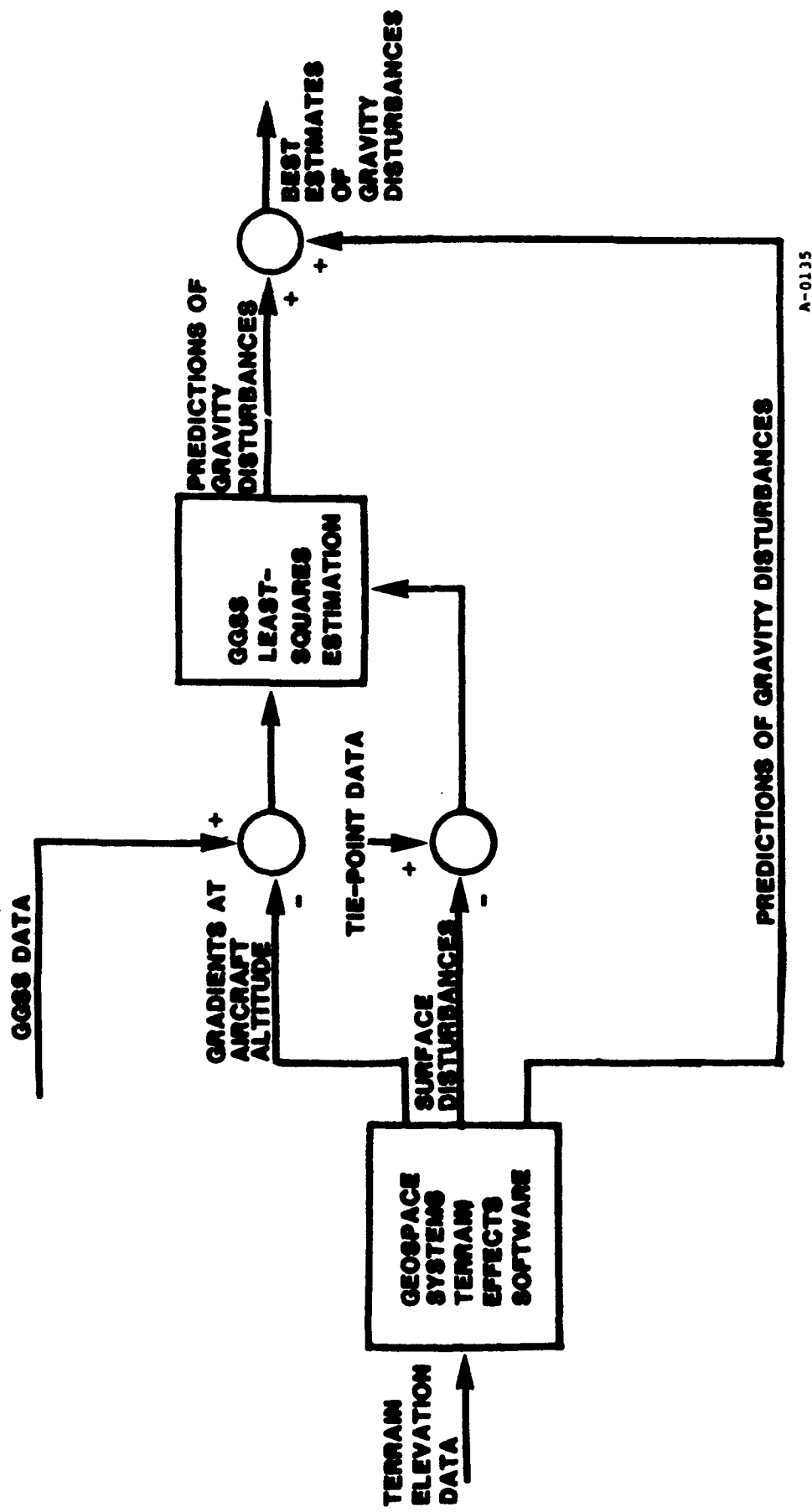
- **THEY ARE CRUCIAL TO RELATING AIRBORNE DATA TO SURFACE DATA.**
- **THEY CONTAIN HIGH FREQUENCIES NOT OBSERVED AT SURVEY ALTITUDES.**
- **THEY ENTER INTO UPWARD AND DOWNWARD CONTINUATION DIFFERENTLY -
BOUNDARY VALUE PROBLEM INVOLVING POISSON'S EQUATION, NOT
LAPLACE'S EQUATION.**

USE OF TERRAIN DATA IN GGSS TESTING



A-0136

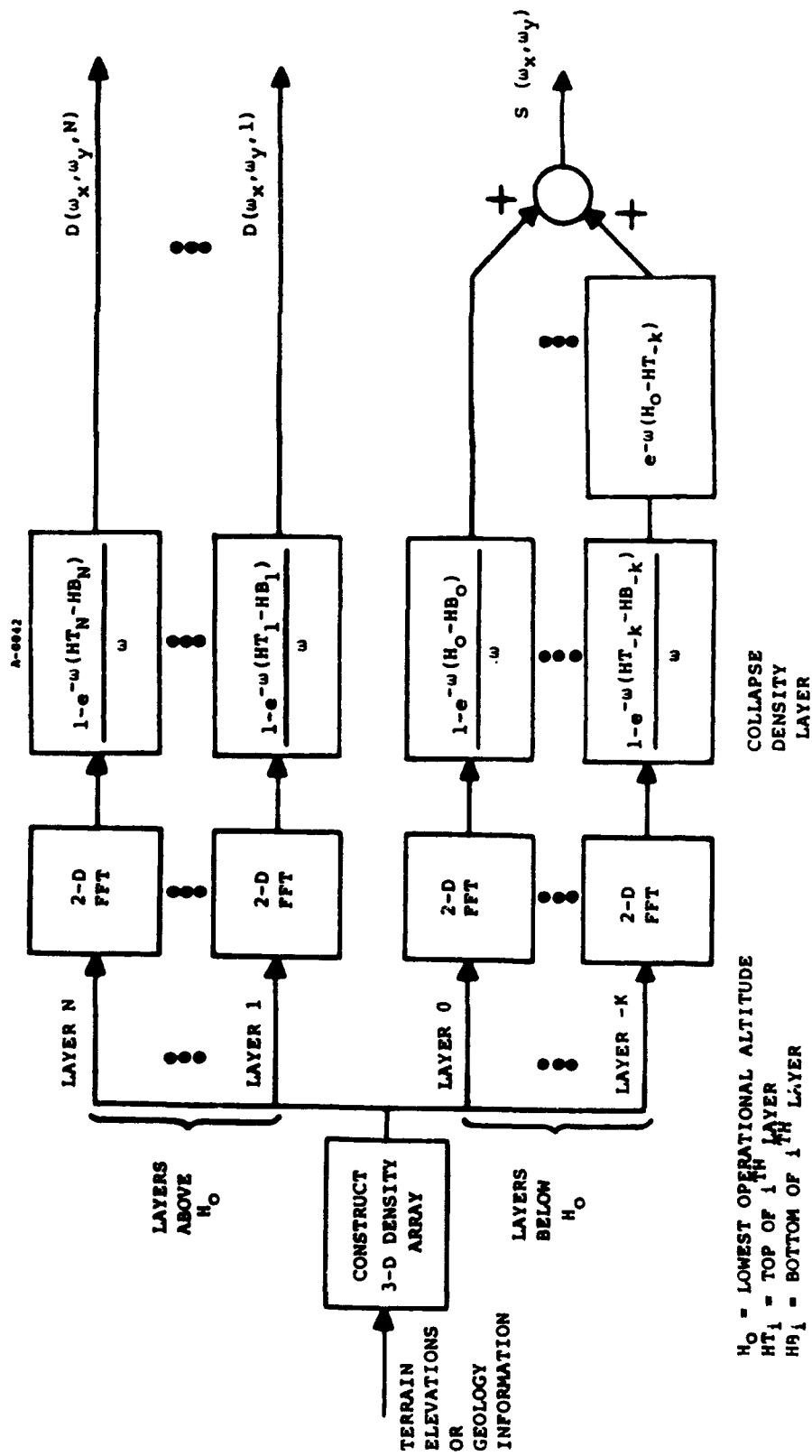
OPERATIONAL USE OF TERRAIN DATA WITH GGSS DATA



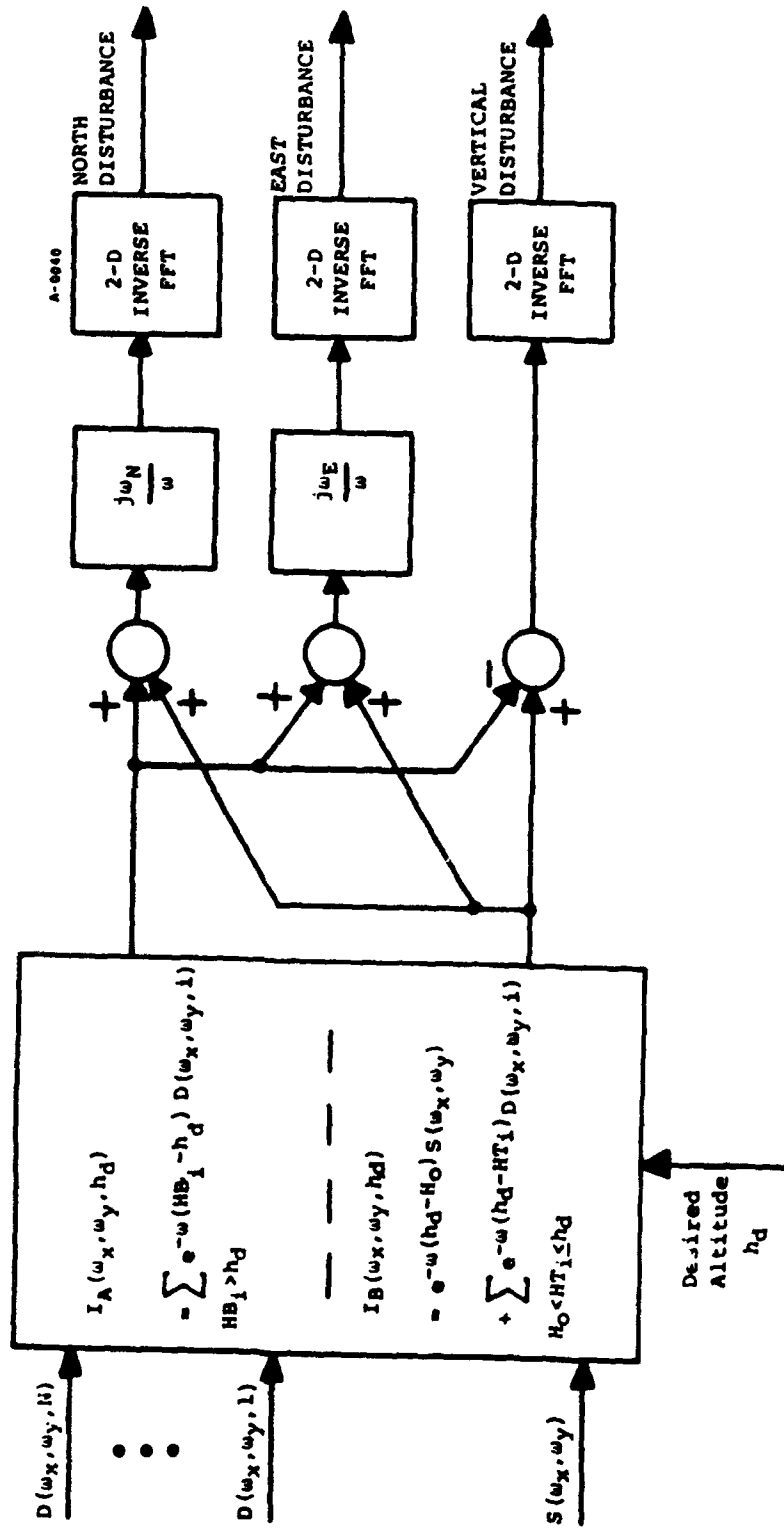
COMPUTATIONAL METHODS

Geospace Systems
CORPORATION

THREE-DIMENSIONAL FFT TERRAIN MODELLING



COMPUTATION OF GRAVITY DISTURBANCE VECTOR DUE TO TERRAIN

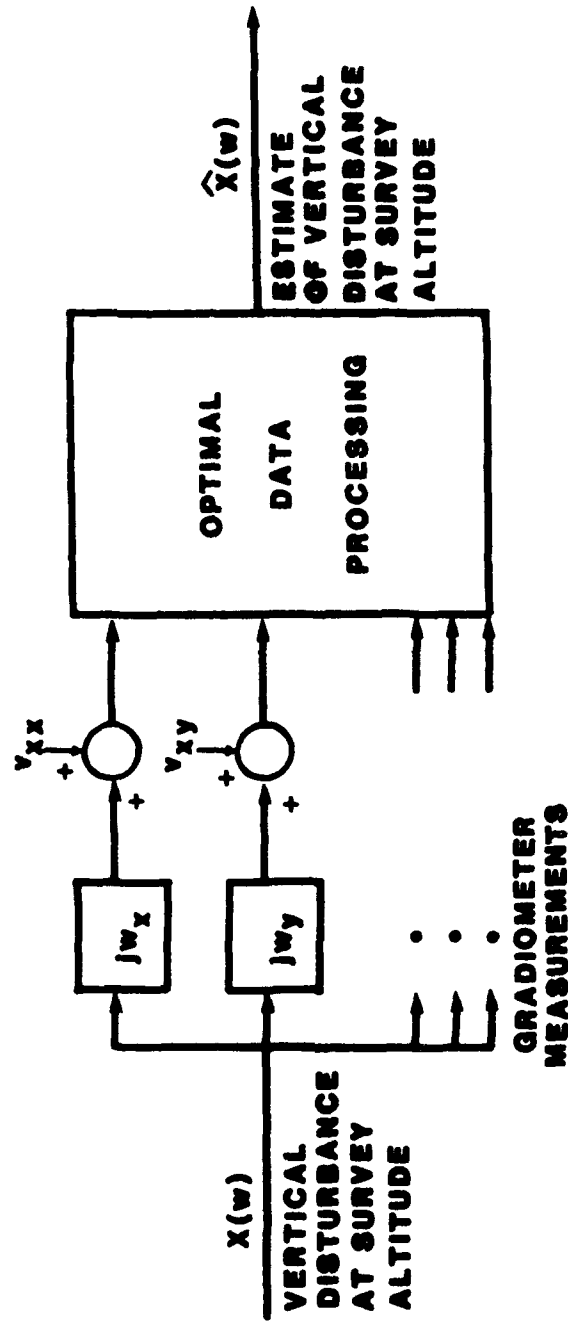


ERROR ANALYSIS METHODS

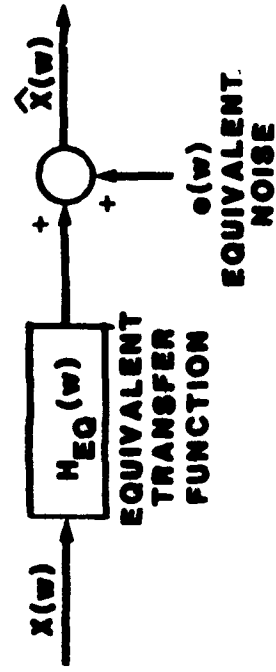
Geospace Systems
CORPORATION

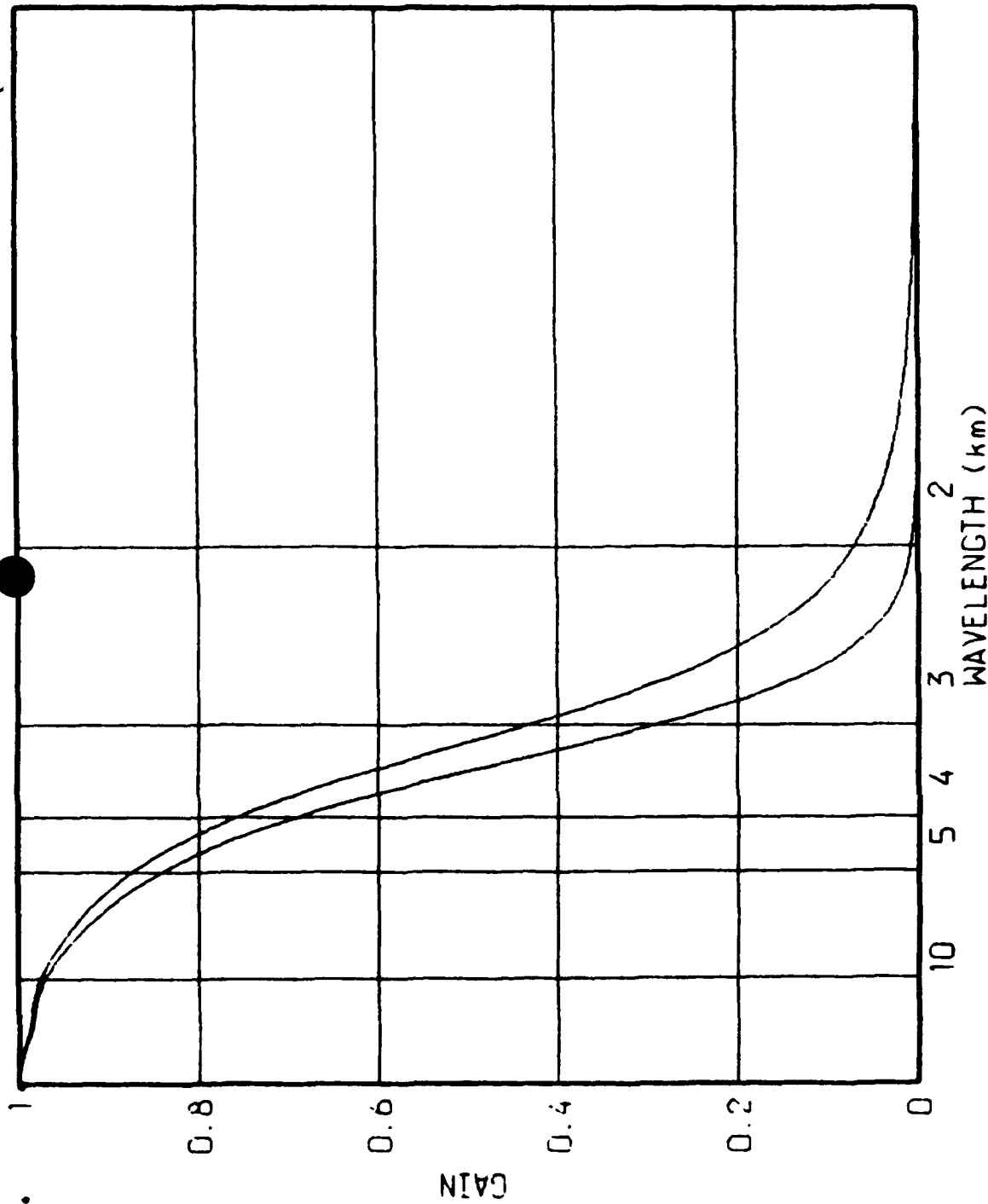
EQUIVALENT MODELS OF OPTIMAL GRADIOMETER SYSTEM

DETAILED MODEL OF GRADIOMETER SYSTEMS

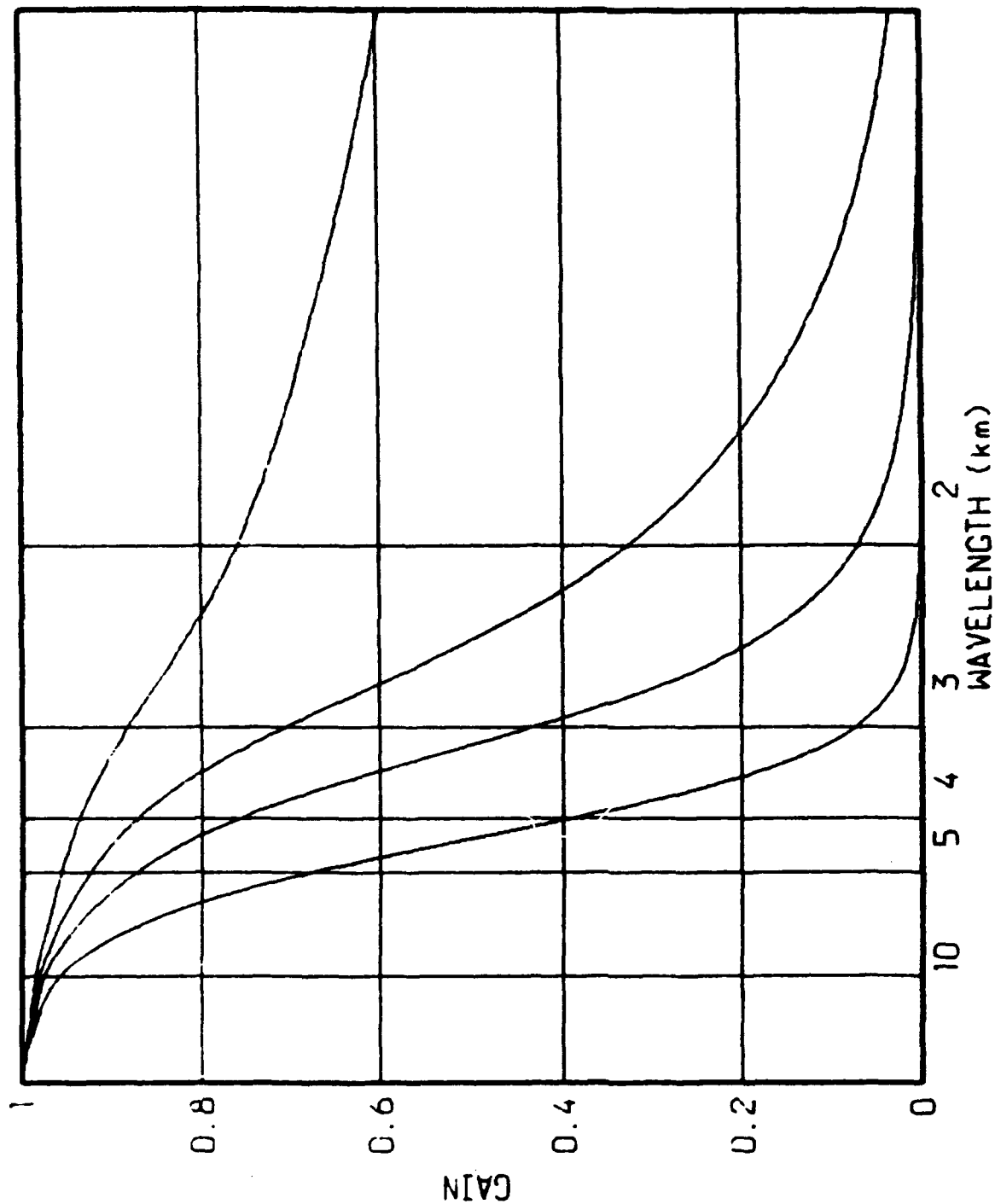


EQUIVALENT LINER MODEL





GAIN FROM SIGNAL TO ~~ESTIMATE~~ ESTIMATE
 SURVEY AT 600 m WITH 600 E*2/hz WHITE NOISE
 7-SHELL Awn MODEL WITHOUT AND WITH TERRAIN SIGNAL MODEL



GAIN FROM SIGNAL TO [REDACTED] ESTIMATE.
 SURVEY AT 1200, 600, 300 & 0 m WITH 600 E*2/hz WHITE NOISE

GAIN

0.8

0.6

0.4

0.2

0

WAVELENGTH (km)

10

5

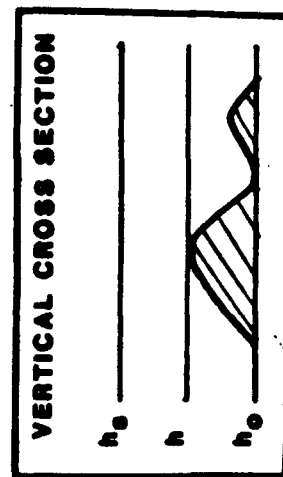
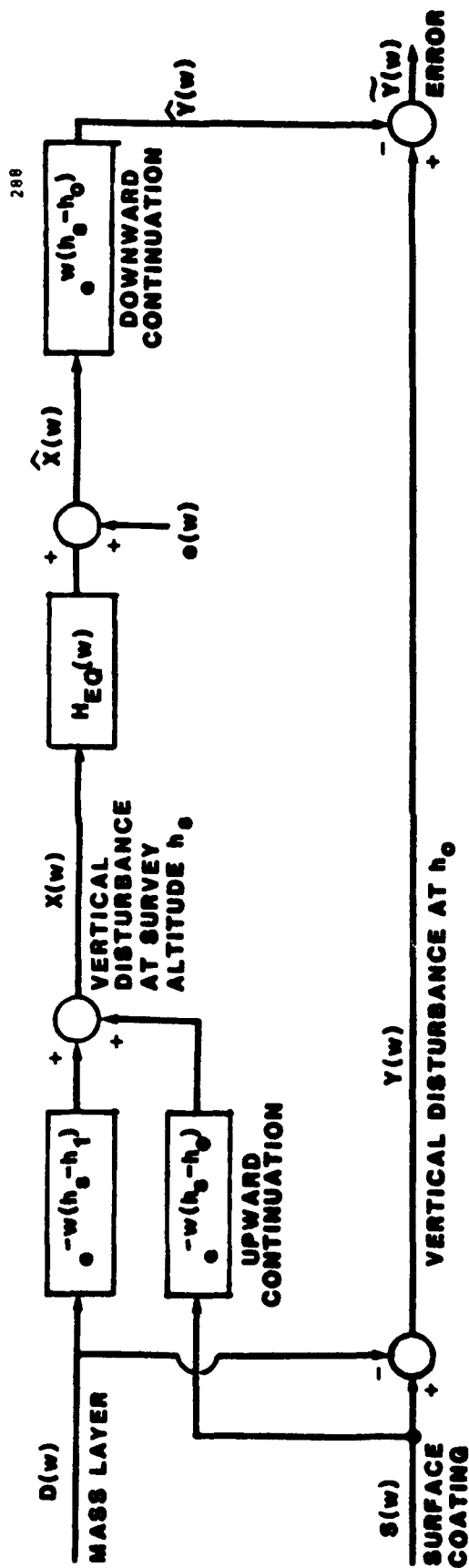
4

3

2

GAIN FROM SIGNAL TO ~~ESTIMATE~~ ESTIMATE
SURVEY AT 600 m WITH 600, 200 & 60 E*2/hz WHITE NOISE

SURVEY ERROR ANALYSIS FLOW



PAPER TITLE: USE OF TERRAIN ELEVATION DATA IN AIRBORNE GRADIOMETRY

SPEAKERS NAME: Julian Center

Questions and Comments:

Dan DeBra : Is a single site an adequate basis for verifying a GGSS and data reduction systems given the disagreement based on simulation?

Terry Fundak: The site chosen, Bakers' Peak, has a variety of terrain- some with lots of topographic relief and relatively little gravity structure and some with flat terrain which is geologically active. White Sands or another site is possibility.

Chris Jekeli: How do you know how much terrain correction to subtract from the data without compromising the instrument test in terms of what it will sense.

SPEAKERS RESPONSE: There should be no problem. If you subtract out a major portion of the signal and you have no problems in data reduction you know the instrument works (has sensed the field you subtracted).

THE GRAVITY GRADIOMETER SURVEY SYSTEM

T. J. Fundak

Air Force Geophysics Laboratory

Earth Sciences Division

Hanscom AFB, MA 01731

ABSTRACT

The Gravity Gradiometer Survey System (GGSS) is now entering its first phase of testing as a system. Over the next year a series of tests will be conducted to understand the limits and characteristics of the instrument and the gradient environment in which it operates. This presentation will outline the status of the GGSS development program and highlight the events to take place over the next year in the GGSS Test Program.

The Gravity Gradiometer Survey System (GGSS) is a self-contained gravity measuring system designed to provide gravity gradients from a moving vehicle. The GGSS combines state of the art inertial technology and satellite based navigation to produce a system with the capability to provide gravity data in all types of environments throughout the world. The GGSS is being developed to perform gravity surveys from an airborne platform or in a land vehicle with a recovery of the gravity vector to an accuracy of better than 1.0 milligals magnitude and .18 arcsecs in each deflection component. For more details about the GGSS specifications see Table 1.

A gravity gradiometer works by differencing the applied forces (both inertial and gravitational) across the distance between two acceleration measurements. Most of the linear inertial acceleration environment is naturally rejected by this method, leaving only the difference in gravitational force across that distance: the gravity gradient (Figure 1). By properly integrating the gravity gradient along a survey track, the relative value of gravity between two points can be found. In contrast to a gravimeter, however, all three components of the gravity vector can be found with a tensor gradiometer, such as the GGSS.

Like all geophysical quantities, a measurement is only valuable when the location of the measurement is known. In the case of a gravimeter, the estimate of gravity at the 1 milligal accuracy level is only valid and useful if the location of the measurement is known to about a meter in vertical and about a hundred meters in horizontal position. However, in contrast to gravimeter measurements, in order to produce similar accuracy in the recovery of gravity the gravity gradients are needed to only one part in 3000. In an airborne environment, this means that the need for positioning a measurement of gravity gradients in space is not nearly as stringent as for a conventional gravimeter survey. One hundred meters of absolute position error is acceptable to recover gravity to better than one milligal in accuracy. A satellite based navigation system, such as Global Positioning System (GPS), can routinely provide position information with this level of accuracy.

Near the surface of the earth, however, positioning becomes more critical. While the gravity field is relatively well characterized even at the high frequencies, the high frequency variations of the gradient field at the 1 Eotvos* level are not well characterized to date. Figure 2 indicates that many common objects produce significant signals that can normally be ignored in measuring the gravity field. It is expected, however, that the power spectrum of the horizontal components of the gradient field will not have significant power at wavelengths of tens of meters. To provide the meter level navigation accuracy that may be needed will require a supplement to the GPS system.

HARDWARE

The heart of the GGSS system consists of a gyro-stabilized platform with the three orthogonal gravity gradient instruments mounted in an umbrella configuration. Six electronics racks containing an airborne computer, a GPS Navigation System, power supplies, control electronics, a vehicle interface buffer, and data recording equipment service the gradiometer and platform, and record data for post mission reduction.

* 1 Eotvos = ten to the minus nine per second squared
= 0.1 milligal over 1 kilometer.

The Gravity Gradiometer Instrument and the Platform

The basic gravity gradiometer instrument consists of 2 pairs of specially selected accelerometers (figure 3). A pair of accelerometers provides a measurement of the average gravity gradient field across the distance that separates them. In a dynamic environment, it is necessary to use a slow rotation to modulate the gravity gradient signal. This technique allows the use of frequency domain signal extraction techniques, so that the signal to noise ratio can be improved. In this way, gradient signals many millions of times smaller than the acceleration which produce them can be extracted. This method has proven very effective in the Navy's Gravity Sensing System (GSS) program where the Bell Aerospace gradiometer is being used to correct ship inertial navigation systems for gravity anomaly induced errors.

Two sets of accelerometer pairs are mounted as orthogonal pairs at the edge of a rotating disk (figure 4). These, plus control electronics, are then mounted in two half spherical shells. This makes up one Gravity Gradiometer Instrument (GGI) (figure 5). A set of three GGIs is mounted on the gyro-stabilized platform mechanized to provide a north, east, down (NED) or "Local Level" environment. The platform maintains the local level attitude with the aid of position information from the GPS receiver for the airborne survey and a "fifth wheel"/inertial mechanization for the land survey. The stabilized platform itself acts as a short term navigation system in a free inertial mode, if the GPS signal is lost for a short period of time. With this mechanization, the long term navigation error (drift) is handled by the GPS system and the short term high accuracy navigation is handled by the inertial platform (two two-degree-of-freedom gyros and a triad of accelerometers).

Electronics & Interfaces

While the heart of the GGSS is mechanical, the brains are in the electronics. Figure 6 shows a block diagram of the major components of the system and the signal flow. At the center of all the electronics is the ROLM MSE-14 airborne computer. This computer is used for everything from platform control and aircraft survey mission control to data recording and system health and control functions monitoring.

A majority of the GGSS electronics is housed in five electronics racks. Rack 1 takes care of the GGI's needs. Rack 2 monitors and controls platform parameters, takes care of housekeeping and serves as an interface between the platform, the GGIs and the computer. The other three racks of electronics contain the computer, a GPS receiver, an atomic clock, data recording equipment, and interfaces to the various aircraft sensors and systems.

All of the various interfaces necessary to monitor the aircraft sensors and systems, and to feed control signals to the autopilot and to receive power for the GGSS are funnelled through a vehicle interface buffer (VIB). The antenna lead for the GPS receiver, for example, is interfaced through the VIB to the Texas Instruments GPS receiver which in turn is interfaced with the computer. The GPS system consists of a TI-4100 GPS Navigator and a CHU aircraft antenna.

Another peripheral, but significant, component is the Uninterruptable Power Supply (UPS) and battery backup which provides power conditioning and emergency power for the GGSS. (The aircraft power environment is very noisy and the GGSS is very unforgiving when it comes to power surges, transients, drop outs, etc.)

Land Vehicle and Aircraft

The GGSS will be installed in a modified motorhome to perform the land test and in a commercial C-130 Hercules aircraft for the airborne survey. The choice of aircraft for the GGSS was made to maximize testing and operational flexibility. The C-130 aircraft is also well suited for low level airborne surveys that will be required of the GGSS and will require little modification. Aircraft modification can be a very long and costly process due to the complex nature of the aircraft environment - safety is always the first priority. With the GGSS program, an air transportable land vehicle will be loaded into the C-130 aircraft, strapped down, connected to the various interface cabling, and be flown on the day's mission. This arrangement should help minimize "down time" of the GGSS due to aircraft related maintenance and repair. A back up aircraft can easily be substituted, if extended maintenance time is required. This is in contrast to a system that is "hardwired" to an aircraft.

SOFTWARE

The GGSS contains three levels of software: 1) real-time, and two stages of post mission software, 2) Stage 1 - time domain processing, and 3) Stage 2- space domain processing. A functional block diagram of the software is shown in figure 7. All data reduction is accomplished off-line with the aid of two stages of reduction software. Stage 1 Processing is common to both the land and airborne tests, whereas Stage 2 Processing is tailored to the particular survey vehicle and conditions.

Real Time Software

The real time software is run on imbedded microprocessors and a ROLM MSE-14 airborne computer. During the survey the MSE-14 monitors system performance, controls the vehicle and platform, and records the system outputs. GGI and other instrument outputs are corrected for environmental sensitivities, such as pressure and temperature, and are compensated for instrument bias and drift, in real time. The GGSS instrument outputs are then stored on magnetic tape for post mission analysis and reduction. The outputs of the real time software are modulated gradients, accelerometer outputs, platform angles and rates, GGI wheel angles, position information (latitude, longitude, and altitude), time, and other sampled instrument outputs from various aircraft and GGSS sensors.

Stage 1 Data Processing

Stage 1 software takes the modulated gradiometer outputs, platform parameters, and position information and transforms these time domain signals into estimates of the gradient in the instrument coordinates at the location of the measurement in space. During this stage, compensations are made for the self gradient of the platform, static and time varying vehicle induced gradients, angular acceleration sensitivity and other residual instrument sensitivities. The outputs of this stage of processing are estimates of the along track gradients and their location in space.

Stage 2 Data Processing

During Stage 2 Data Processing, the output of Stage 1 is transformed into estimates of gravity. Stage 2 Land software takes the along track gradient

estimates and integrates them from a "truth data point" to the point where a comparison is desired. Stage 2 Airborne software contains a set of routines which takes the gradient estimates at survey altitude, grids them, compensates them for track crossing mismatch, incorporates the long wavelength information contained in the astro-geodetic tie points, and downward continues the data to the surface of the earth. Estimates of the gravity field are then made for the area of overflight. The outputs are an estimates of the gravity vector on the Earth's surface.

TESTING

Testing will be conducted in two geographic areas of the United States. The first site was chosen for its proximity to the Bell Aerospace plant. It will include the areas adjacent to Niagara Falls, New York. The second site was picked for its excellent truth data coverage, limited topographic relief, nearby contrasting areas of active and benign gravity field, and good weather and aviation environment. It is located in the Texas/Oklahoma Panhandle region of the Central United States (see figures 8 thru 10).

The GGSS test program is divided into three parts: Laboratory testing, and two "Phases" of Land and Airborne Testing. As a matter of course, each test will build on the knowledge gained in the previous one. Each will provide a different look at the use of a gradiometer, its capabilities and shortfalls and each will provide unique challenges for testing. For example, the airborne environment provides for an attenuation of the high frequency gravity gradient field, relatively low spacial sampling rates because of the aircraft velocity and a potentially hostile acceleration environment. The signal in the land environment, on the other hand, may be dominated by the high frequency signal. Even at relatively high sampling rates aliasing may occur, thus requiring faster sampling rates, a slow vehicle survey speed and more accurate positioning information.

The way in which the data from each phase of testing is reduced is also significantly different. In the case of the land testing, the gradients are integrated between a start and an end point. Any error between the known relative values and gradiometer measured values, is a direct indication of instrument performance. In the airborne test, a grid of data at flight altitude is used to make estimates of gravity values. Downward continuation and estimation procedure errors may dominate the errors sources here. Spatial aliasing errors will also limit the system's level of performance. The aircraft's relatively high velocity gives a relatively low spatial sampling rate. This, along with the finite spacial sampling of the grid inherently limit the spatial resolution.

The ability to optimally reduce the gradiometer data post-mission, while an important question for comparison to truth data, is not a critical factor when only GGI noise performance is being gauged. Therefore, two types of tests are performed for each of the two testing environments (land and airborne). The first test type, "Phase I testing", gauges the system's sensitivity to various vehicle and environmental conditions, determining the true instrument noise performance. The second test type "Phase II testing" is designed to assess the performance of this survey tool under a nominal set of "operational conditions".

Laboratory Testing

Laboratory Testing consists of a series of tests which are designed to take the individual components of the GGSS through a series of calibration and performance verification runs. Component level testing is followed by the

integration and systems level testing. Static and Dynamic Tests are performed with the aid of a Scorsby Table and various laboratory calibration and checkout equipment. The various operating modes of the system are checked and a set of error coefficients for the platform induced self gradients is produced, in addition to the bias and trend estimates.

Phase I Testing

Phase I is both an instrument performance test and an optimization tool for Phase II testing. It will allow for more effective "survey planning". During this phase of testing, each of the controllable parameters is varied and optimized for use in Phase II testing. Each day's run is used to estimate the system's expected performance and sensitivities so that a simulated Phase II test performance result can be estimated. An understanding of the characteristics of the land and airborne gradient environments will also be gained during this phase of testing. These characteristics are also fed into the simulation to understand how the gradiometer will be affected by differing gravity field power spectrums. The software is then optimized for Phase II testing and operations. In summary, Phase I will evaluate the conditions under which the instrument has ability to give consistent results, i.e. can maintain the noise at the requisite level.

The testing strategy for this phase of testing can be summed up in two words - repeat tracks. To evaluate the instrument noise characteristics, the GGSS is required to traverse a particular track many times. Statistical analysis will then be applied to the data to determine the instrument noise floor, drift patterns and environmental sensitivities.

Phase I land testing will be conducted on a set of roads in the neighborhood of the contractor's plant. The GGSS van will be driven in a test pattern similar to those use to test an inertial positioning system. After the vehicle has completed a number of repeat tracks, a study will be made to determine instrument parameters and sensitivities. Noise sources are then isolated and corrected or compensated for in the software.

Similar repeat tracks are then flown with the van in the aircraft. In each case, parameters such as vehicle velocity, track control mechanisms (autopilot, cruise control, and manual) and road surface or atmospheric turbulence will be varied to test for instrument sensitivity to a particular parameter.

While the statistical characteristics of the gradient field will show up in this test, it is not critical that they be understood exactly at this point in testing. The test method here is repeatability. Therefore, it is only important that the gradient field have no temporal variations, so that the difference between each traverse can be judged as an error.

Phase II Testing

During Phase II testing, each vehicle will "survey" a predetermined set of tracks and be required to produce estimates of gravity at points along the track in the land case, and at selected points beneath the flight grid for the airborne test. During this phase of testing, the system's performance will be evaluated under near "optimum" conditions, subject only to changes in the strength of the gravity field. This will allow an understanding of the gradiometer's ability to recover the gravity field under optimal "operational" conditions. Both a relatively smooth and a relatively rough gravimetric field are found in the Phase II test area (Figure 9).

Phase II Land testing will verify the GGSS's ability to "transfer" gravity and deflection of the vertical between a point with a known gravity vector and a point with unknown values. A series of increasingly longer loops will be traversed starting at the Clinton-Sherman Airfield in Burns Flat, Oklahoma (Figure 10). On each of these loops a number of "truth data" points will be presurveyed. Comparisons will be made at a selected number of these points. The mismatch between "truth" and the measured value will be a direct indication of the error in the GGSS's recovery of the gravity vector.

Phase II Airborne testing will verify the capability of the GGSS to provide survey quality gravity data from an airborne platform. The GGSS van will be loaded onboard the C-130 aircraft and then fly a grid pattern like that of figure 11. An area of approximately three hundred kilometers square will be covered with orthogonal tracks at five kilometer track intervals by the end of the test program.

A day's survey will be controlled by the operator through the airborne computer. Flight planning information will be stored by the operator prior to each day's mission in the form of "waypoints". Once the aircraft is in the survey area, the GGSS computer will fly the aircraft through an autopilot interface. A set of cockpit informational displays and instruments, and control switches will allow the pilot to engage, disengage and monitor the progress of the survey.

A typical flight will last six to eight hours at a constant altitude near six hundred meters above ground level and at a constant ground speed of about four hundred fifty kilometers per hour. Operation of the GGSS requires that at least three GPS satellites are visible while the survey is in progress. Because GPS will only be partially operational during this test program, GGSS testing can only be conducted only in a satellite availability "window". With the present constellation of satellites, approximately six hours of coverage will be available each day. The number of satellites and the times of day they will be visible during October of 86 is shown in figure 12. The general shape of this bar chart does not change from day to day. Each month, the "window" moves about two hours earlier in time.

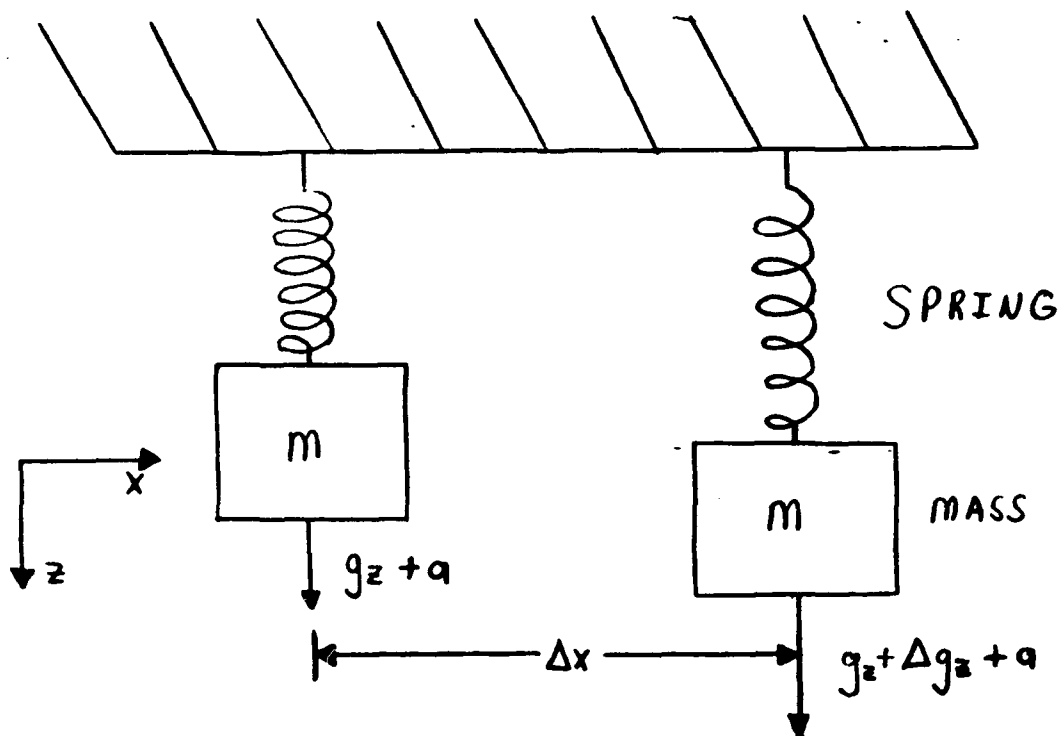
It is the philosophy of this test program to attempt to measure the instruments potential for providing needed gravity survey capability. Phase II testing is specifically designed with as few obscuring variables as is possible. Many factors can and will degrade system performance. The "noisy" aircraft vibration and turbulence environment, poor aircraft control parameters: altitude hold times, poor tracking or airspeed control or uncoordinated flight, and suboptimal data processing are all examples of possible degrading factors. Others will be found in the course of testing. Like other instrument tests, one tries to control as many of the known parameters as possible until they are characterized or their influence mitigated. Compensation for those that cannot be controlled will be accomplished post mission using signal processing.

For the land vehicle, an attempt will be made to maintain an optimum constant speed on relatively "good" roads, free of interfering traffic. Events such as the passing of a large truck will be logged for analysis and, if needed, later compensation.

In the airborne environment, every attempt will be made to minimize interference from other air traffic. The test will be flown under near perfect aviation conditions. Altitude and airspeed will be maintained near constant, and heading will remain constant for long periods of time. The aircraft's airspeed will be maintained so as to minimize vibration and turbulence induced acceleration errors found in Phase I testing. Flights will probably be flown during or at least with prior knowledge of optimal GPS satellite geometry. A grid of evenly spaced tracks will be flown with every attempt to maintain the uniformity of the grid. Attempts have been made to provide a flight environment which minimizes weather induced errors and delays, air traffic conflicts and deviation from the constant set of test conditions. Therefore, the test should conclude with an accurate forecast of the potential value of the GGSS to a survey organization, like DMA.

Laboratory testing will begin in January of 1986 with Phase I and II to follow. Initial testing is expected to be completed in early 1987. A summary of the test program is provided in Table 2. Follow-on tests are anticipated and will evaluate the best way to deal with operational problems such as variable altitudes, airspeeds, topographic relief patterns, weather, and aircraft capabilities.

The development of the GGSS is being managed by the Earth Sciences Division of the Air Force Geophysics Laboratory (AFGL), Hanscom AFB, Massachusetts under funding from the Defense Mapping Agency (DMA), Washington D.C.. The GGSS is a product of Bell Aerospace Textron, Niagara Falls, New York.



$$\Gamma_{zx} = \frac{(g_z + a + \Delta g_z) - (g_z + a)}{\Delta x} = \frac{\Delta g_z}{\Delta x}$$

Figure 1 - This figure shows two accelerometers located side by side and with sensitive axes aligned in the z direction. Each accelerometer is measuring the total force applied to it. Both accelerometers are subject to an inertial acceleration a and gravitational force which differs by Δg over the distance separating them Δx . The difference in applied force divided by the distance separating the accelerometers is the measurement of the z component of the gravity gradient in the x direction. In other words, it is the difference in the z component of gravity over the distance Δx .

GRAVITY GRADIENT DUE TO VARIOUS MASSES

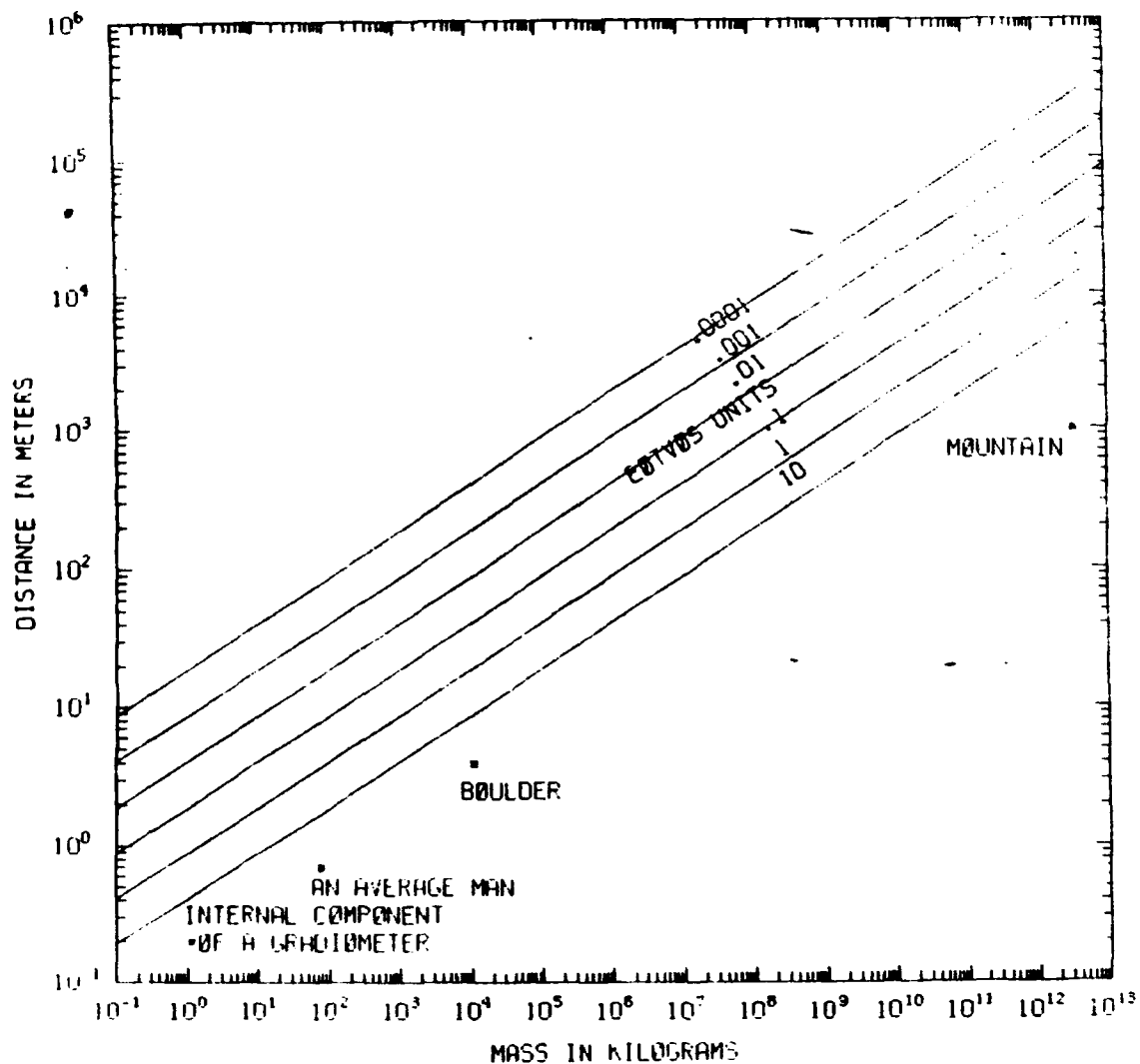


Figure 2 - The gravity gradient produced by a mass located at the given distance from a gradiometer is plotted here. Examples of the gradient produced by masses of interest in the testing of a gravity gradiometer are shown.

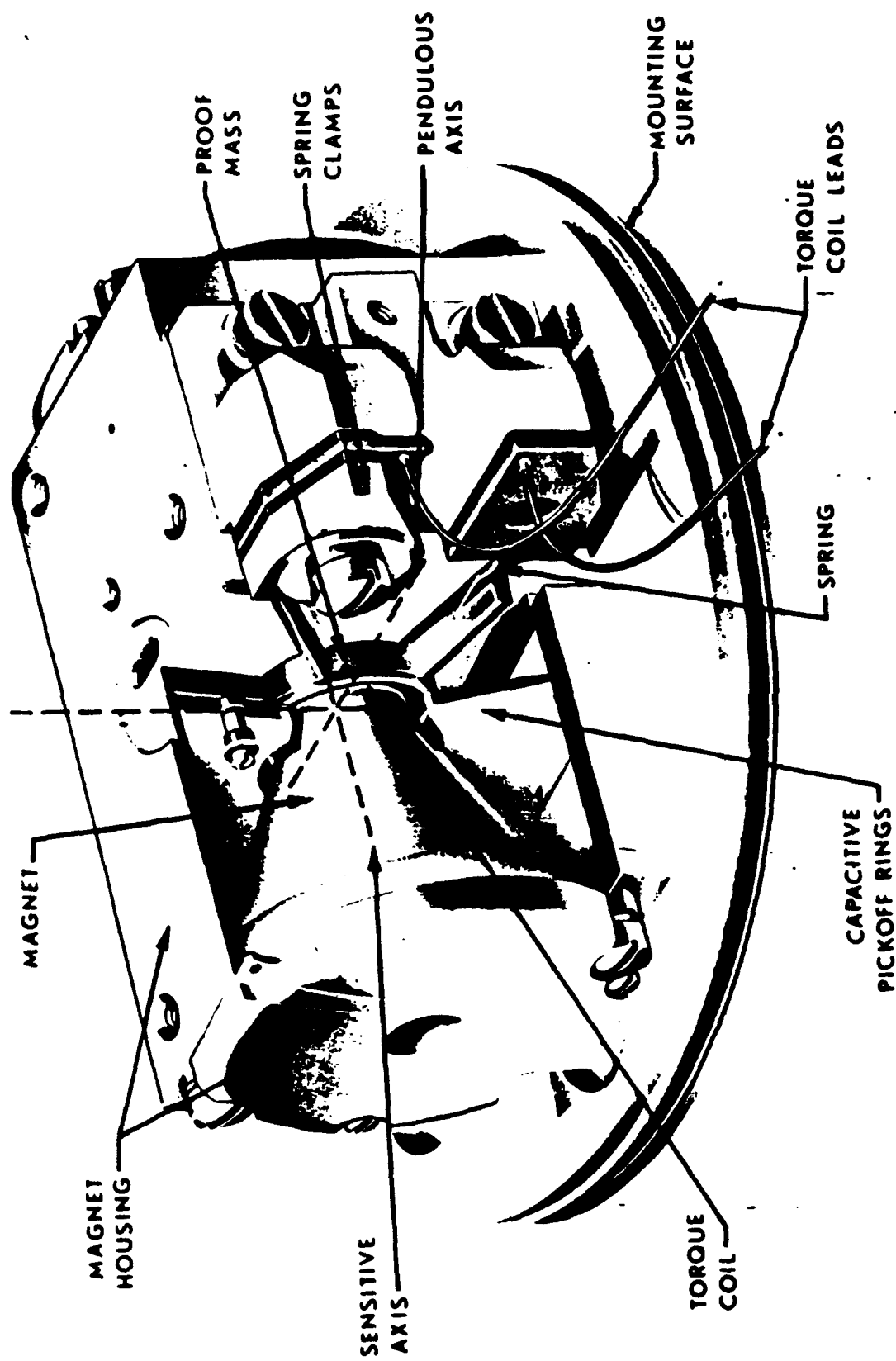


Figure 3 - Bell Model VIIB Accelerometer

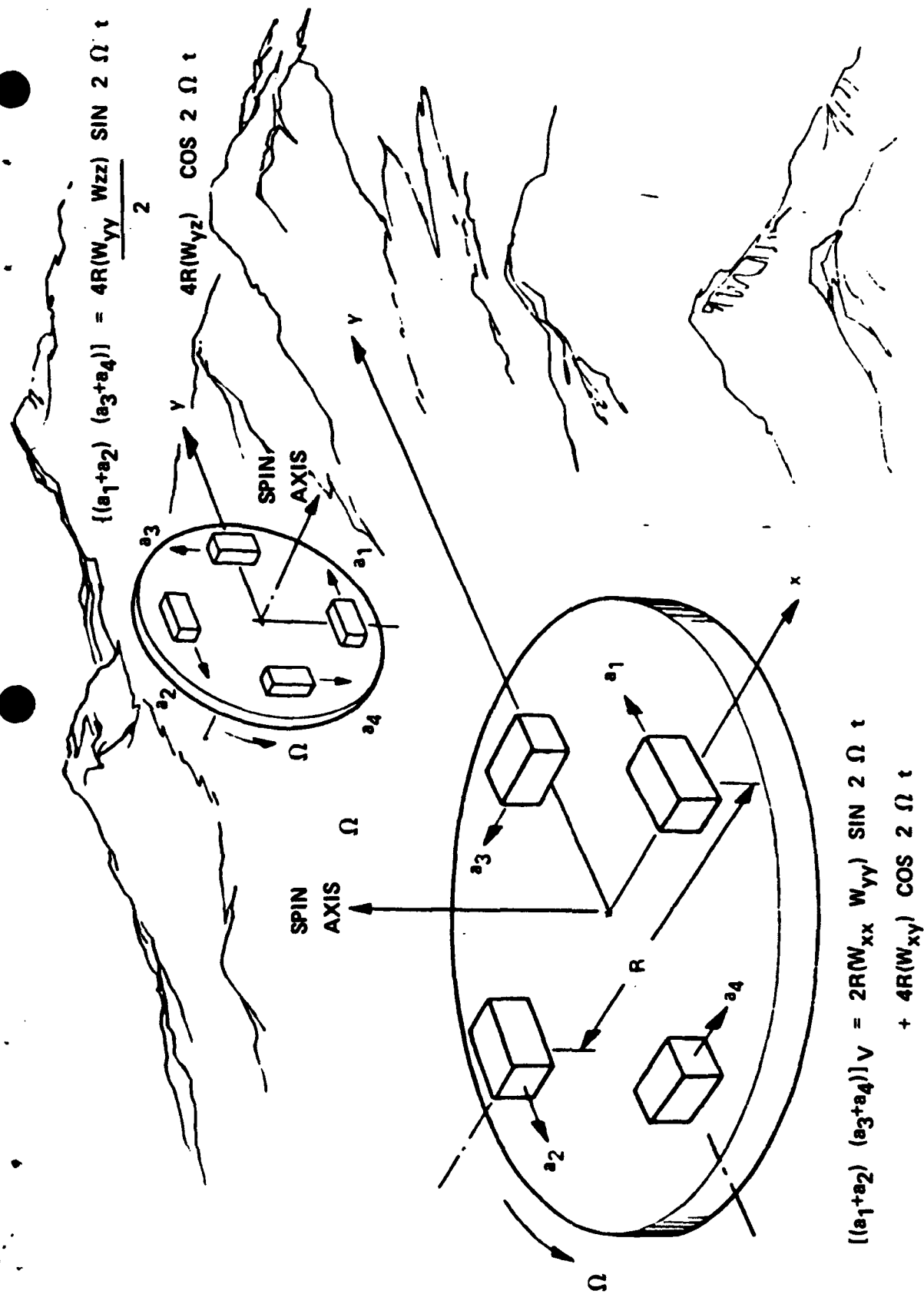


Figure 4 - Schematic Illustration of a Rotating Accelerometer Gravity Gradiometer

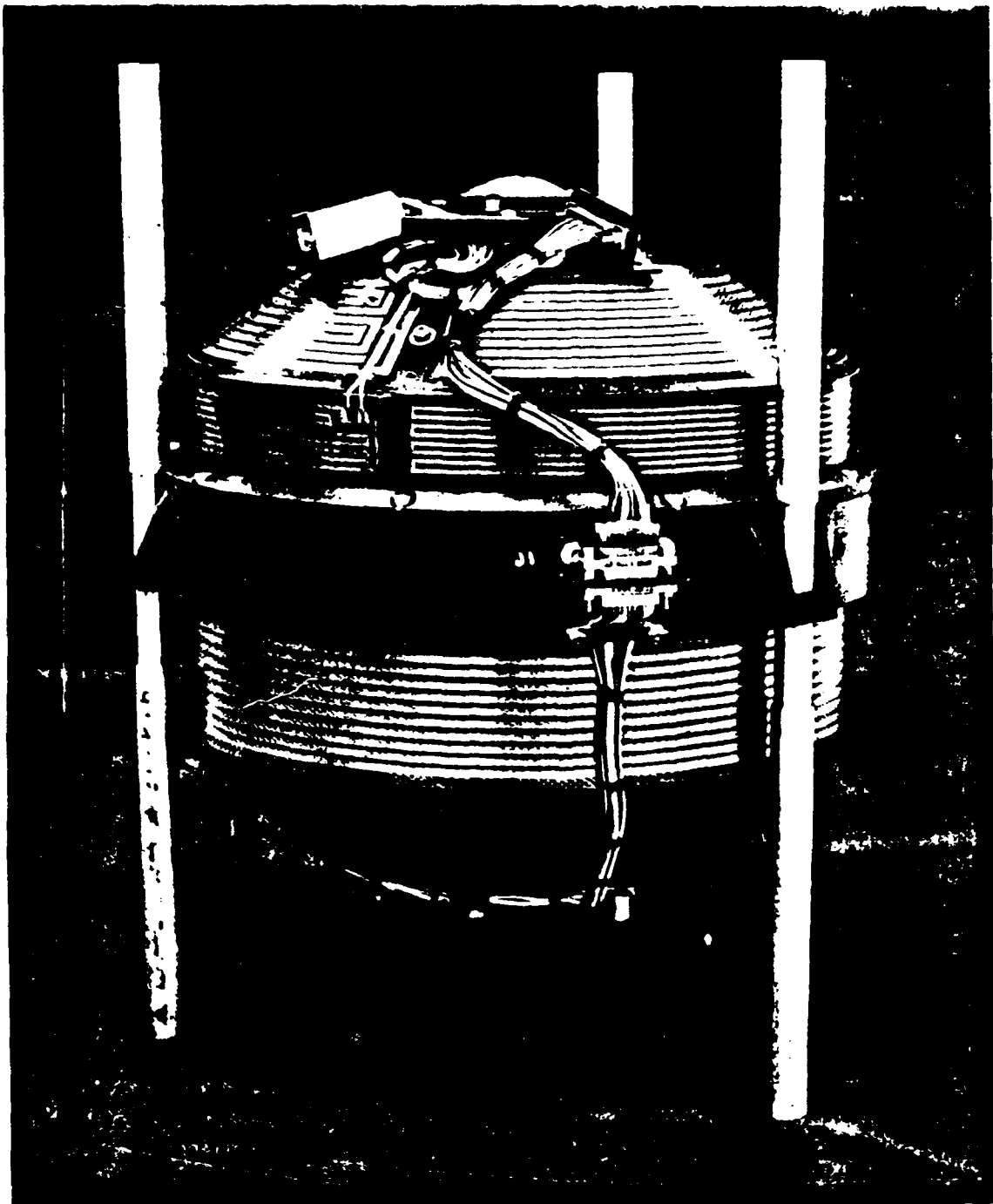


Figure 5-The GGI is the heart of the GGSS system. It contains four of the BELL Model VII accelerometers, mounted tangentially to the edge of a rotating disk, at 90 degree intervals. The sum of the outputs of a set of accelerometers gives the average gradient across the distance of separation. A set of three GGIs are mounted on the gyro stabilized platform shown.

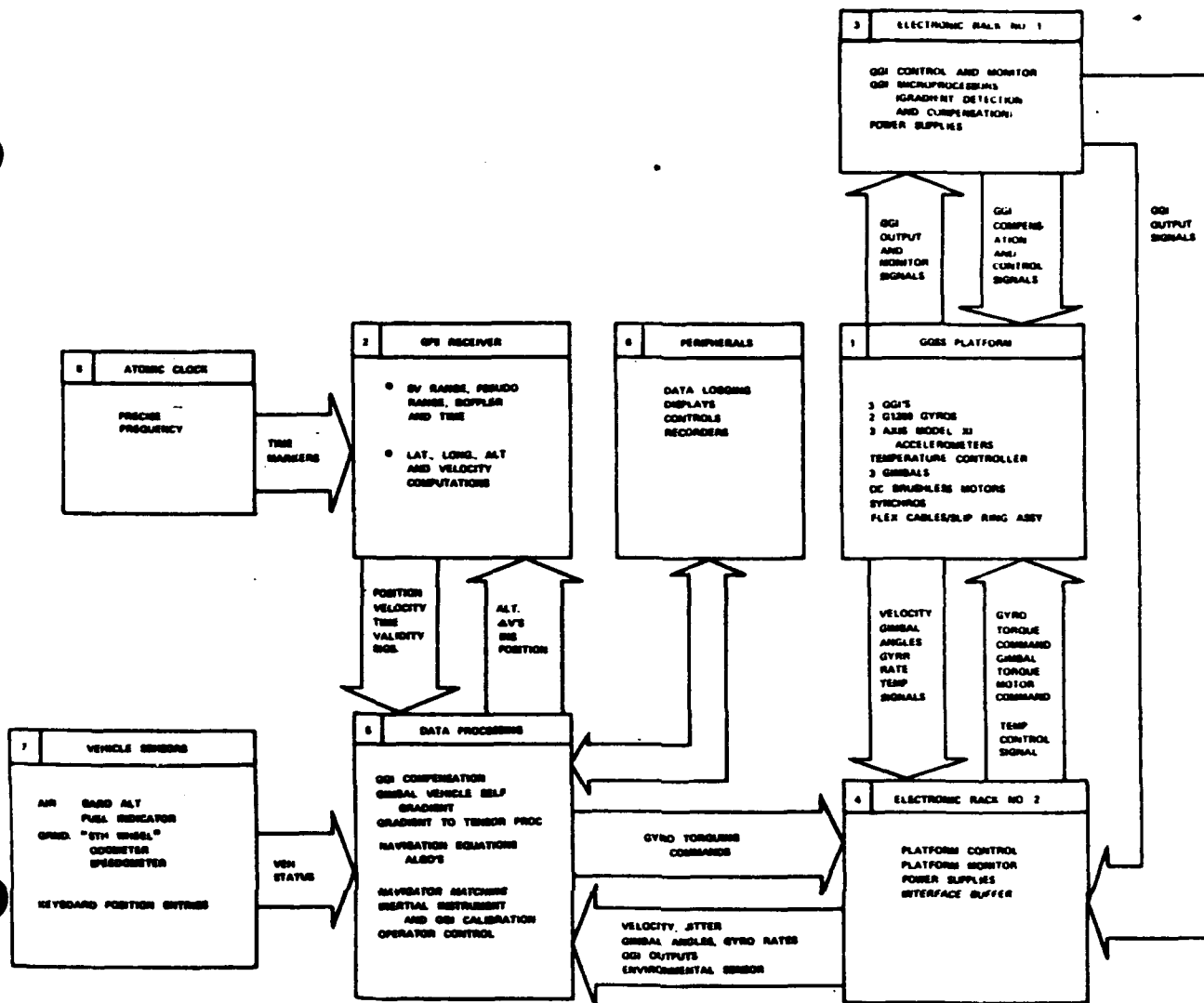


FIGURE 6 - A SIMPLIFIED FUNCTIONAL BLOCK AND SIGNAL FLOW DIAGRAM FOR THE GGSS

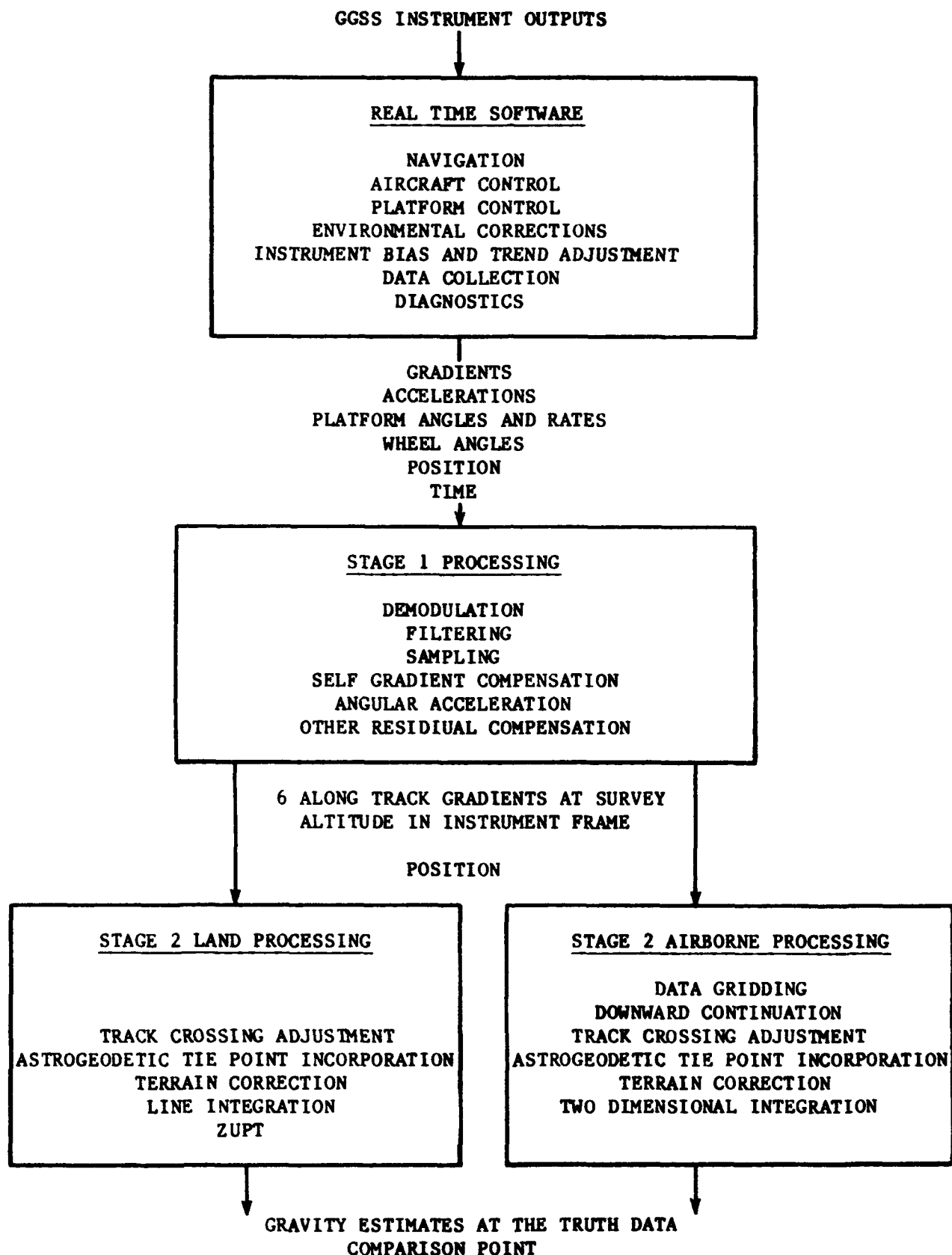


Figure 7-Block Diagram of the Stages of Data Processing

GRAVITY ANOMALY MAP OF THE UNITED STATES

Continued from Page 1

1962

NAVY & AIR FORCE COMMISSIONERS

UNITED STATES GEOGRAPHIC SURVEY

DEFENSE MAPPING AGENCY

NATIONAL OCEANIC AND ATMOSPHERIC ADMINISTRATION

NIAGARA, NEW YORK

PHASE I TEST AREA

Figure 8 - Phase I CGSS Test Area



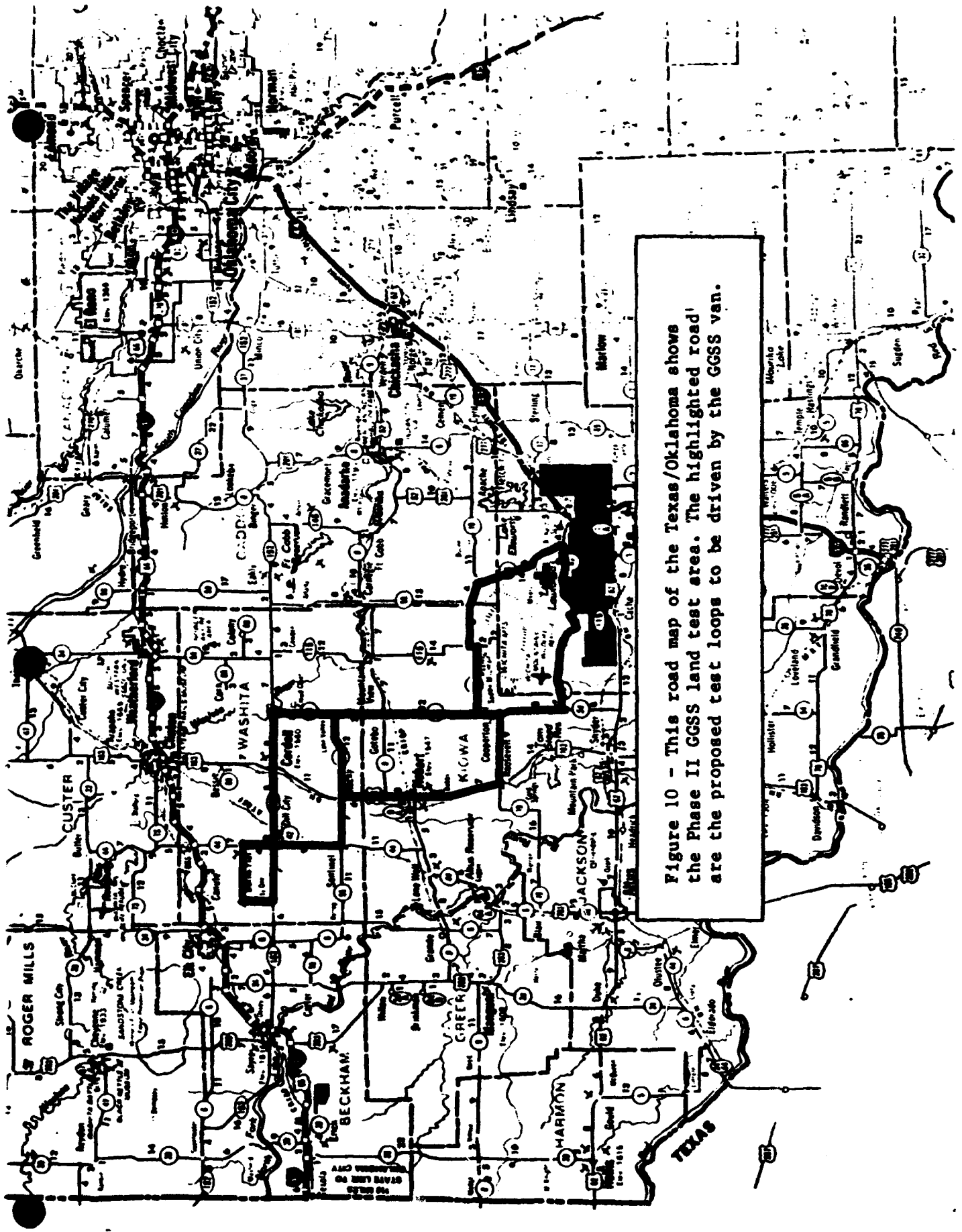


Figure 10 - This road map of the Texas/Oklahoma shows the Phase II GGSS land test area. The highlighted road are the proposed test loops to be driven by the GGSS van.

AIRBORNE GRAVITY GRADIOMETRY

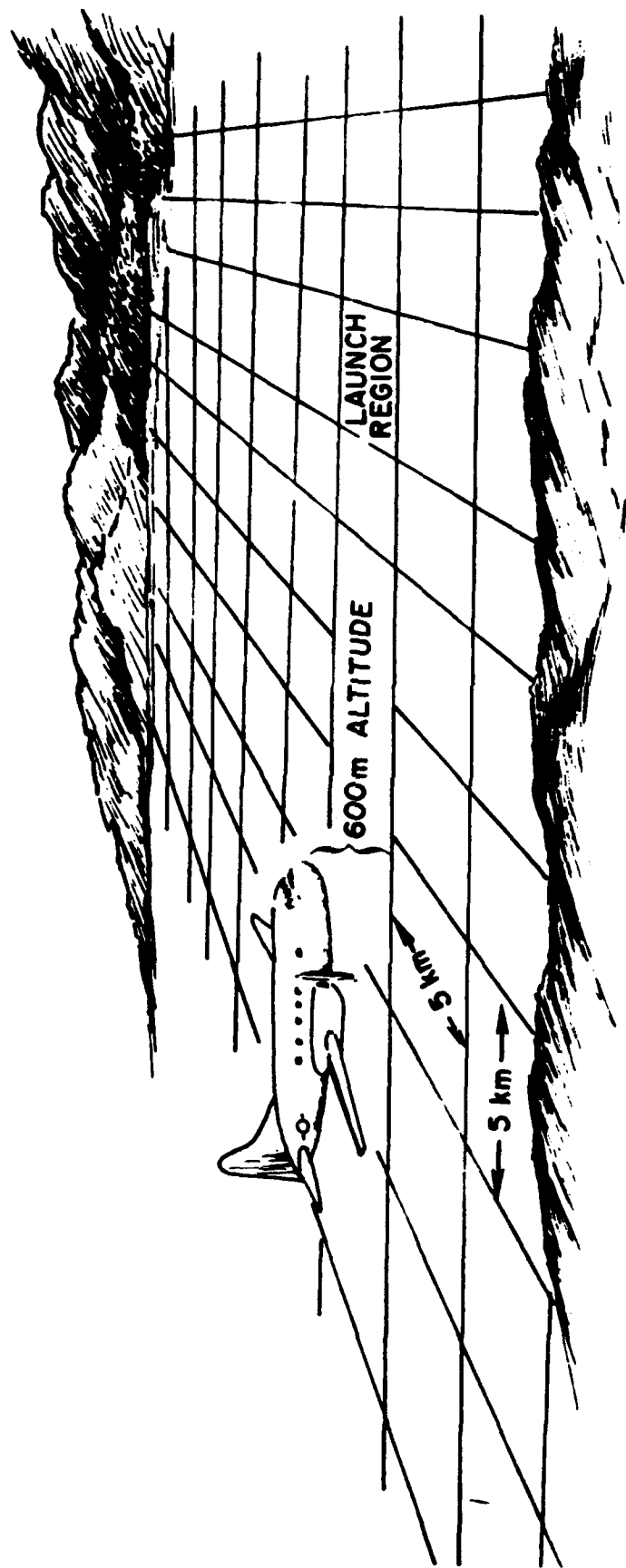


Figure 11 - Schematic of Phase II Aircraft Testing.

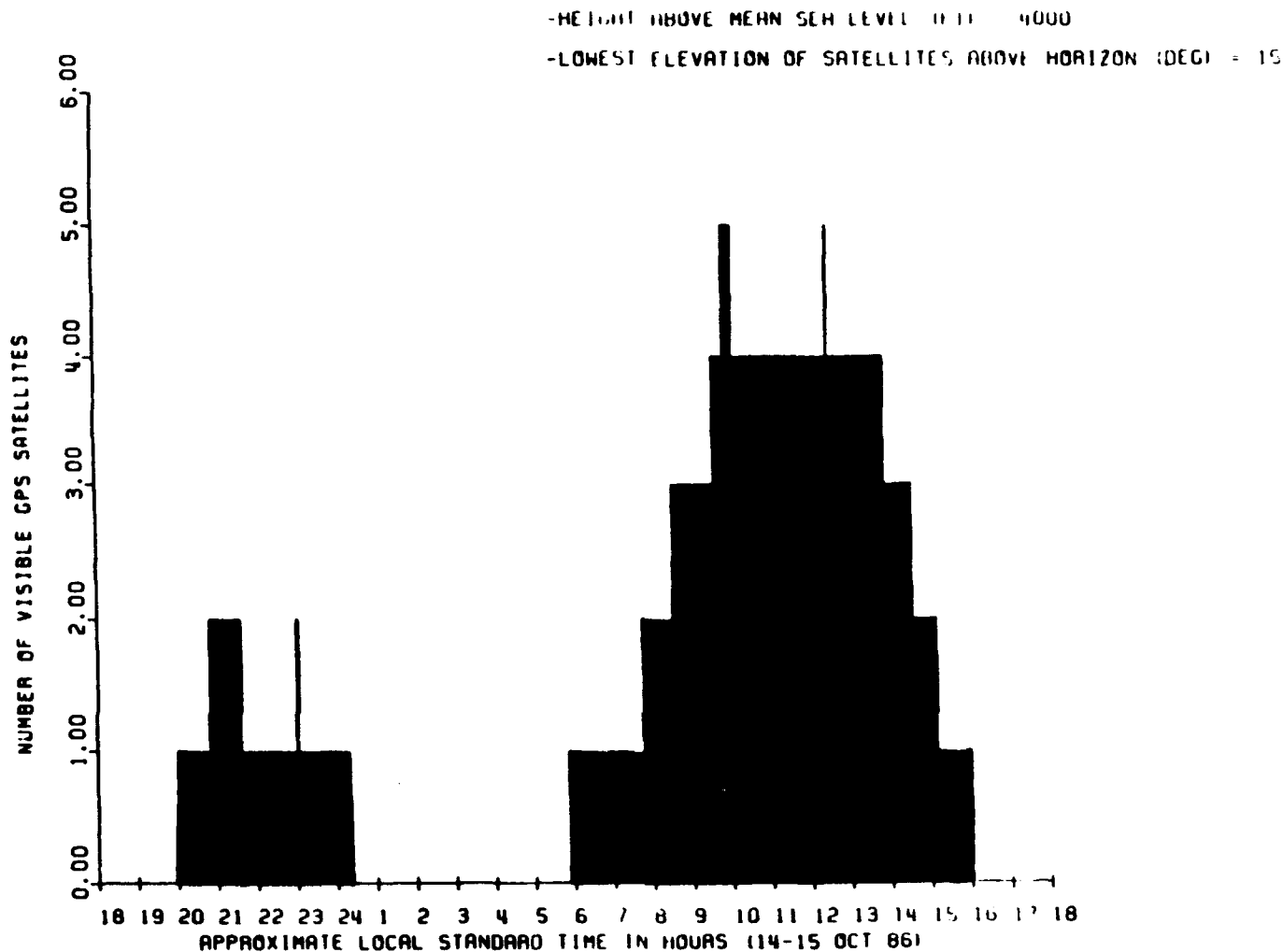


Figure 12 - The Global Positioning System (GPS) will be the primary navigation tool used during this test program. Four visible satellites are required to obtain a three dimensional position without other aids such as an atomic clock or barometric altimeter. GPS will provide worldwide navigation capability in the near future. The present constellation of satellites provides four satellites visibility only a limited number of hours per day. The projection for an average day in October 1986 is given above. The height of the bar indicates the number of satellites that will be visible at that hour of the day in the Texas/Oklahoma Area.

	<u>SPEC</u>	<u>ANTICIPATED</u>
GRAVITY DISTURBANCE RECOVERY (WAVELENGTHS \leq 500 KM)	.9 mgal	.83 mgal
DEFLECTION OF THE VERTICAL	.18 arcsec	.16 arcsec
POSITION ERROR	100 meter	15 meters
PLATFORM TILT	26 arcsec	15 arcsec
AZIMUTH	66 arcmin	34 arcmin
SYSTEM NOISE (maximum allowable)	$\frac{10^{-3}}{w^{1.6}} + 190 \text{ (E/R/S)}$	

TABLE 1 - AIRBORNE GGSS ACCURACY REQUIREMENTS

<u>Test</u>	<u>Method</u>	<u>Purpose</u>
LABORATORY	LABORATORY METHODS	
	Study instrument outputs produced by various inputs under static and dynamic but controlled conditions.	Calibration and compensation Understand instrument outputs and their sensitivities
PHASE I	REPEATABILITY TEST	
LAND & AIRBORNE	Comparison of the ability of the instrument to give consistent results when the instrument traverses the same test track many times.	Verify instrument noise and sensitivity Characterize the statistical nature of the gradient field
PHASE II	COMPARISON TO "TRUTH" DATA	
LAND	Comparison to "truth" data by along track integration between a "truth" data point and a test point.	
AIRBORNE	Comparison to "truth" data by gathering data in a large area and reducing this data to gravity values at selected point where "truth" data is available.	Verify the system is capable of providing survey quality data

Table 2 - GCSS Testing in Summary

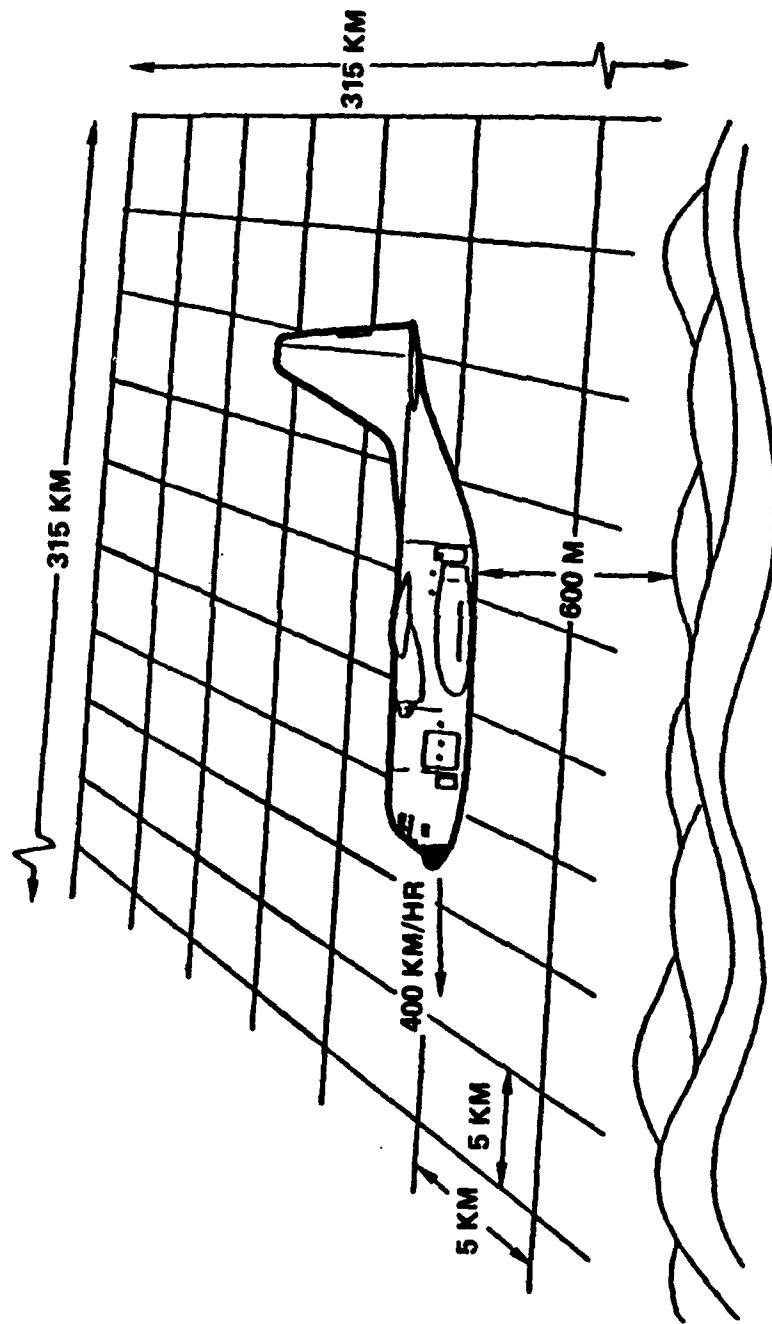
AIRBORNE GRAVITY GRADIENT SURVEY DATA REDUCTION

W. J. Hutcheson
Bell Aerospace Textron
P. O. Box One
Buffalo, NY 14240

ABSTRACT

Algorithms which have been developed at Bell Aerospace Textron for the GGSS Phase II test plan data reduction requirements, will be described in detail. The data reduction stages include track crossing adjustment, optimal spatial integration, gridding, interpolation and smoothing, low frequency adjustment using astrogeodetic data and downward continuation. Simulation results obtained using a synthetic field will be presented to demonstrate the algorithm performance.

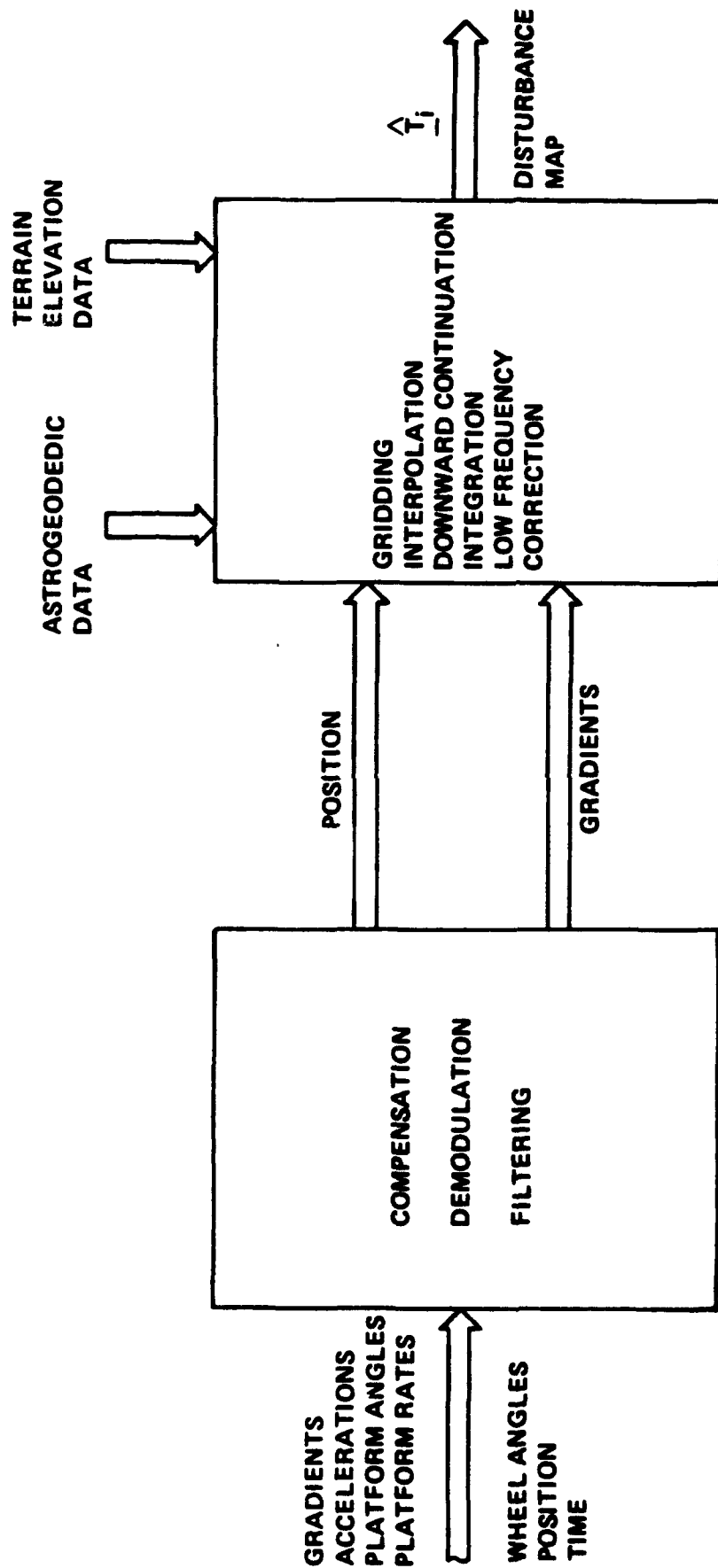
GGSS PHASE 2 TEST SURVEY GEOMETRY



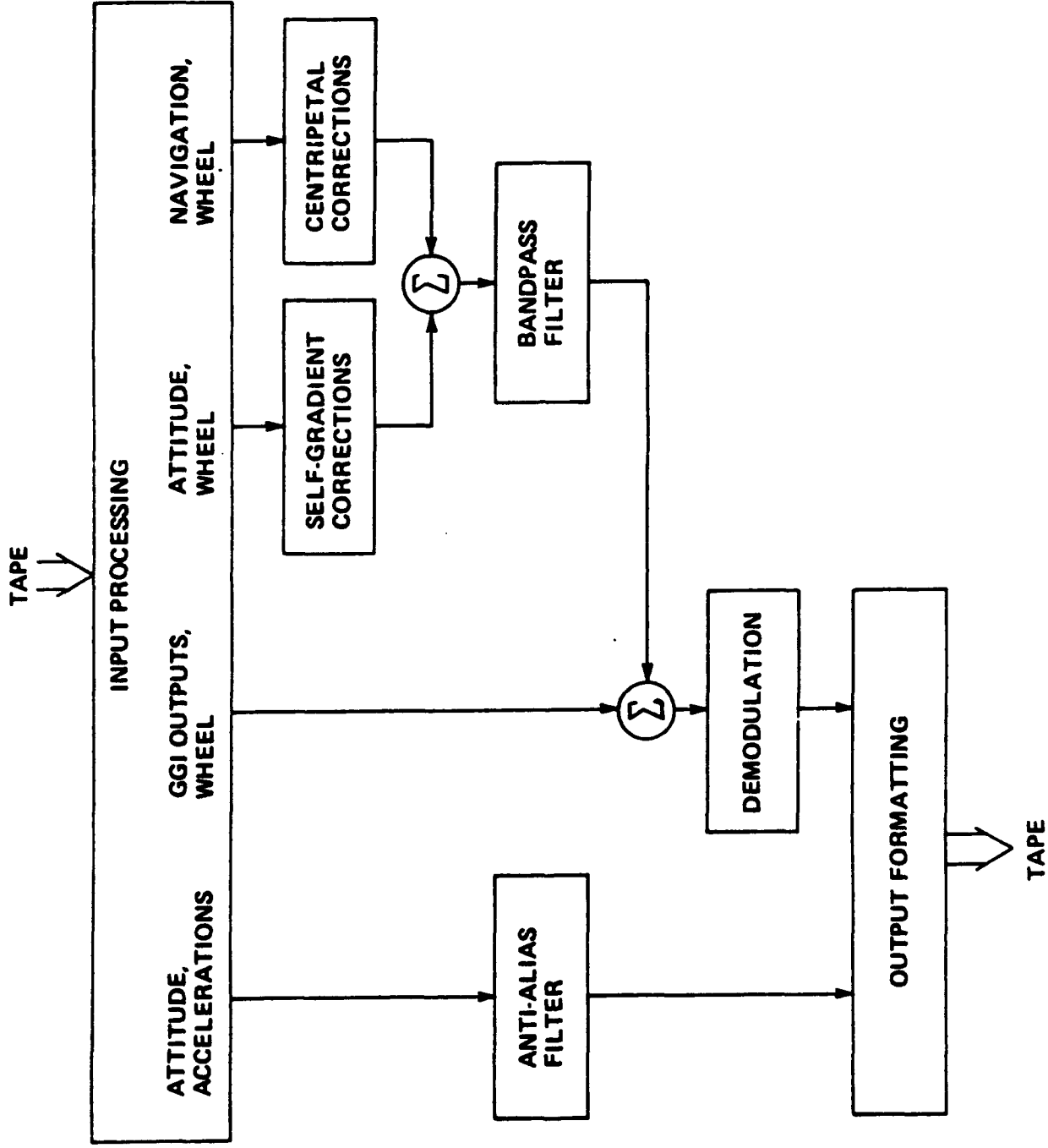
DATA PROCESSING REQUIREMENT: DERIVE HIGH ACCURACY GRAVITY DISTURBANCE MAP FROM GRADIENT DATA AND DOWNWARD CONTINUE TO TEST POINTS WITHIN SURVEY.

Bell Aerospace **TEXTRON**

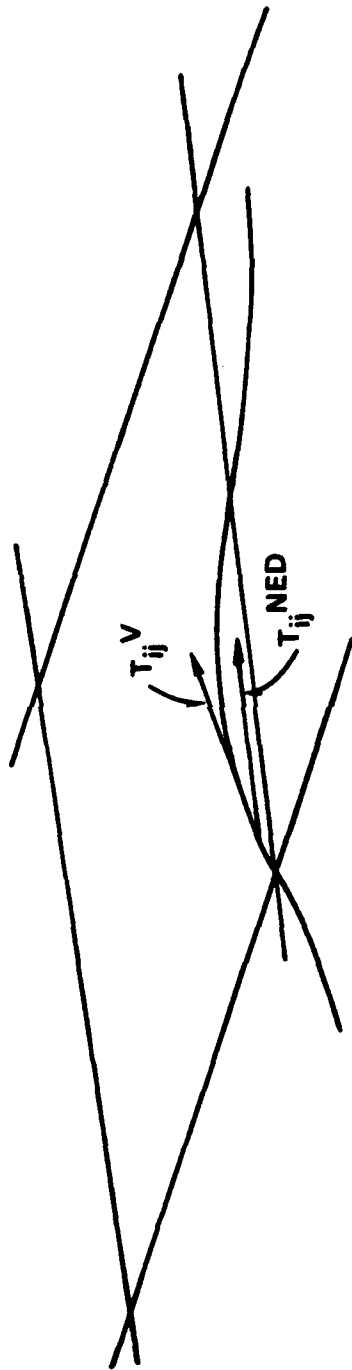
DATA PROCESSING OVERVIEW



GGSS STAGE I DATA PROCESSING



INTEGRATION



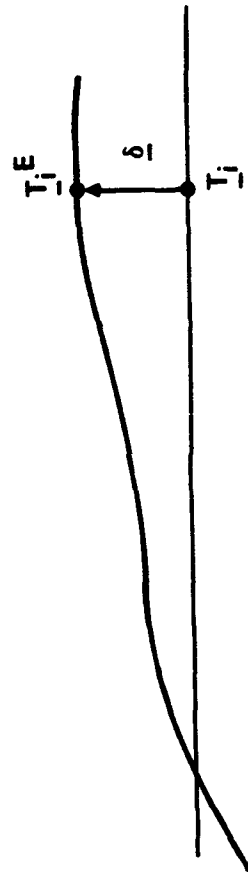
$$T_{ij}^V = C_V^NED T_{ij}^NED C_V^NED$$

EXAMPLE: T_x ALONG N/S TRACK

$$T_x^NED(K) = C_V^NED \sum_{\ell=1}^{315} T_{xx}^V(\ell) \delta K(\ell)$$

$$= \sum_{\ell=1}^{315} T_{xx}^NED(\ell) C_V^NED K \delta(\ell)$$

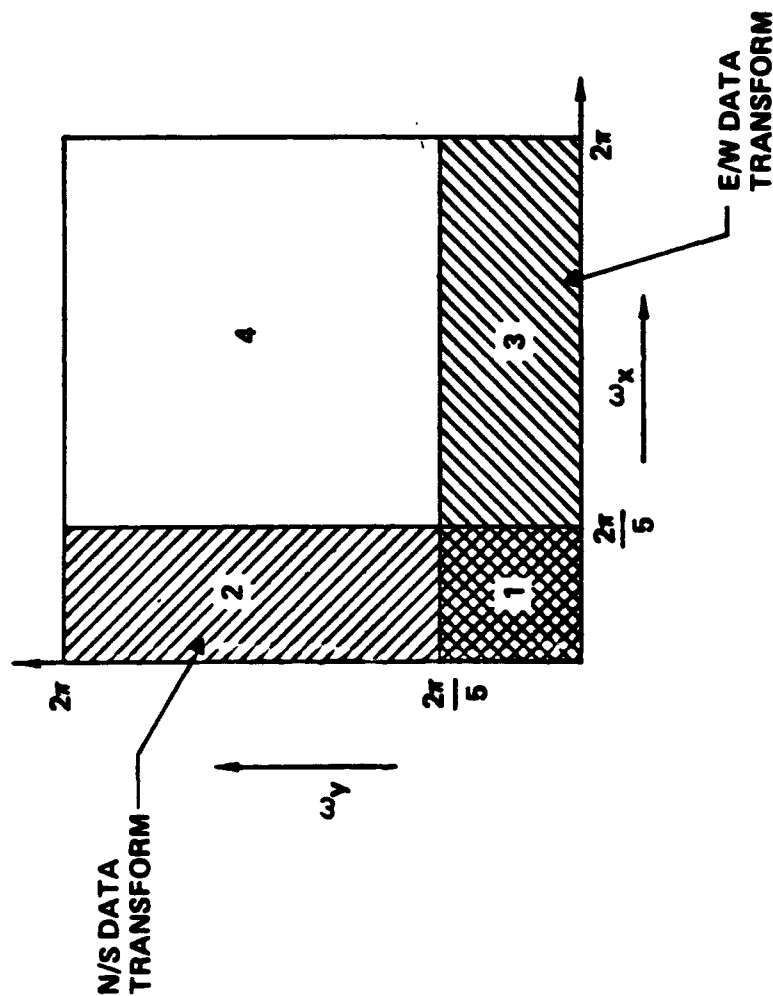
GRIDDING



$$T_{ij} = T_{ij}^t + T_{ij} \cdot \delta$$

INTERPOLATION AND SMOOTHING

APPROACH: EXPLOIT REGULAR GRID AND USE FREQUENCY DOMAIN TECHNIQUES



OPTION 1

FREQUENCY DOMAIN AVERAGING

OPTION 2

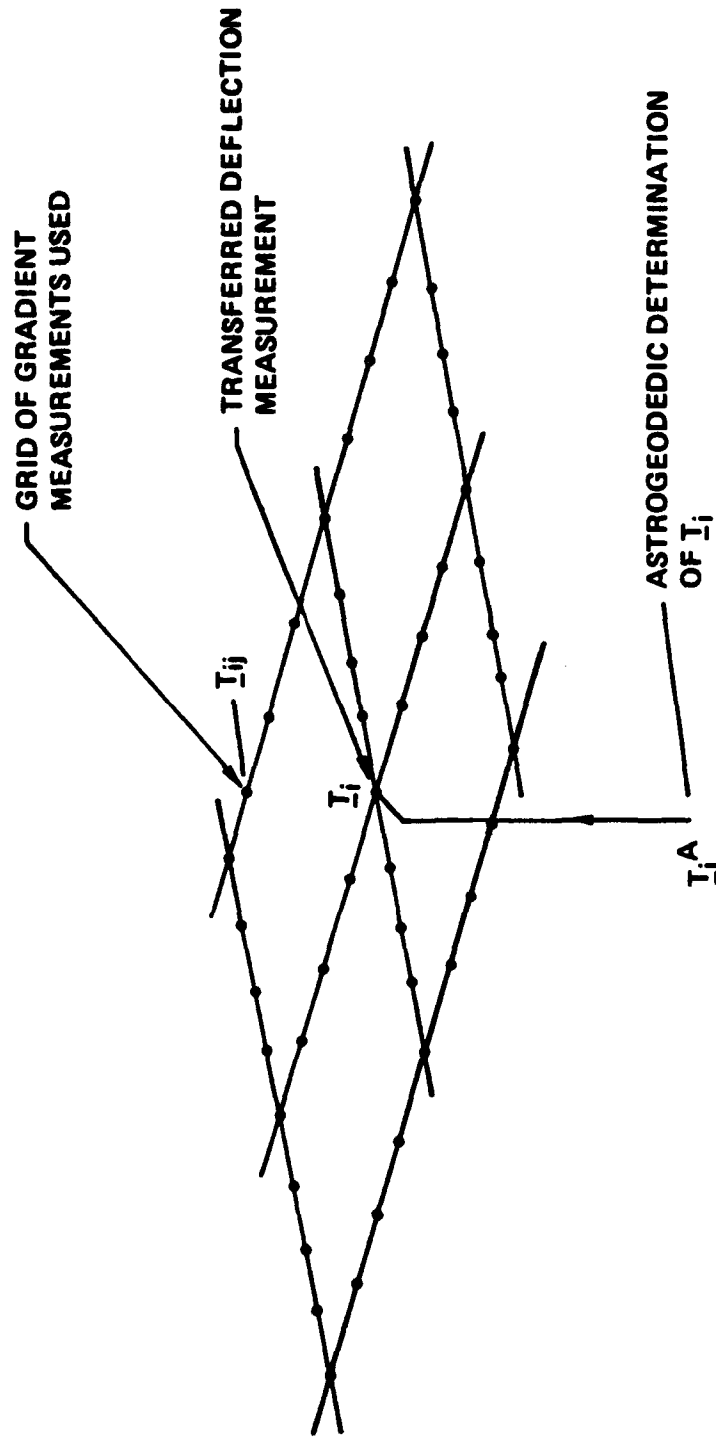
USE OPTIMAL WIENER SMOOTHING GAINS VIZ:

$$\hat{I}_i = S_{T_i}^{-1} T_i(\omega) \left[S_{T_i}^{-1} T_i(\omega) + S_{nn} \right]^{-1} T_i(\bar{\omega})$$

OPTION 3

LOCAL LEAST SQUARES COLLOCATOR

INCORPORATION OF ASTROGEODEDIC DATA



APPROACH: USE LEAST SQUARES COLLOCATION ALGORITHM TO GENERATE OPTIMAL GAINS FOR MEASUREMENT VECTOR CONSISTING OF ASTROGEODEDIC DETERMINATION OF I_i AND GRADIENT MEASUREMENTS OF ALTITUDE.

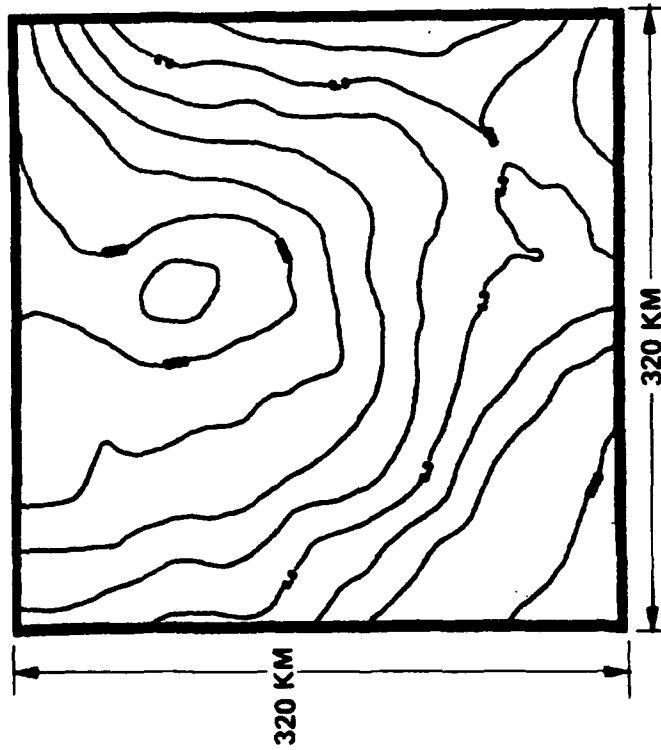
DOWNWARD CONTINUATION

OPTION 1 USE DOWNWARD CONTINUATION OPERATOR

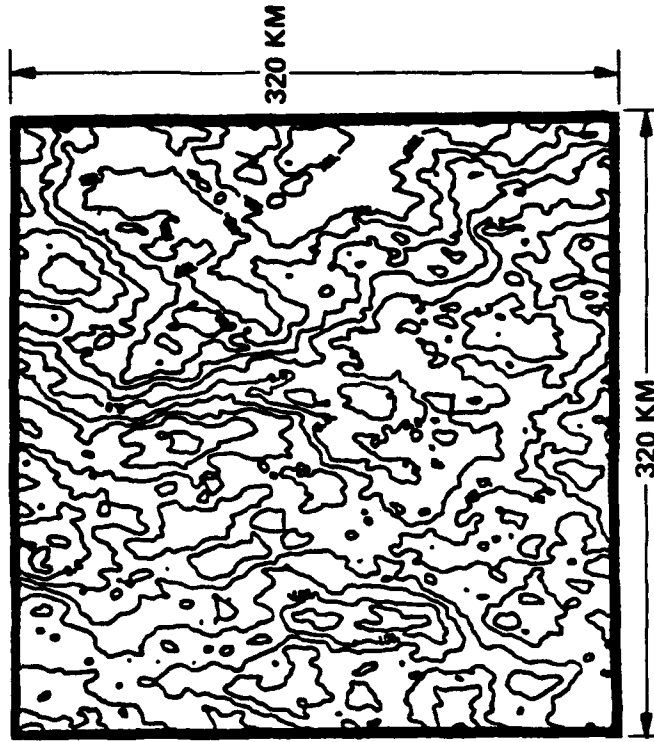
$$\ell \sqrt{\omega_x^2 + \omega_y^2} \text{ ON DATA TRANSFORM}$$

OPTION 2 USE LEAST SQUARES COLLOCATOR ON GRADIENT AND DEFLECTION
MEASUREMENTS AT ALTITUDE

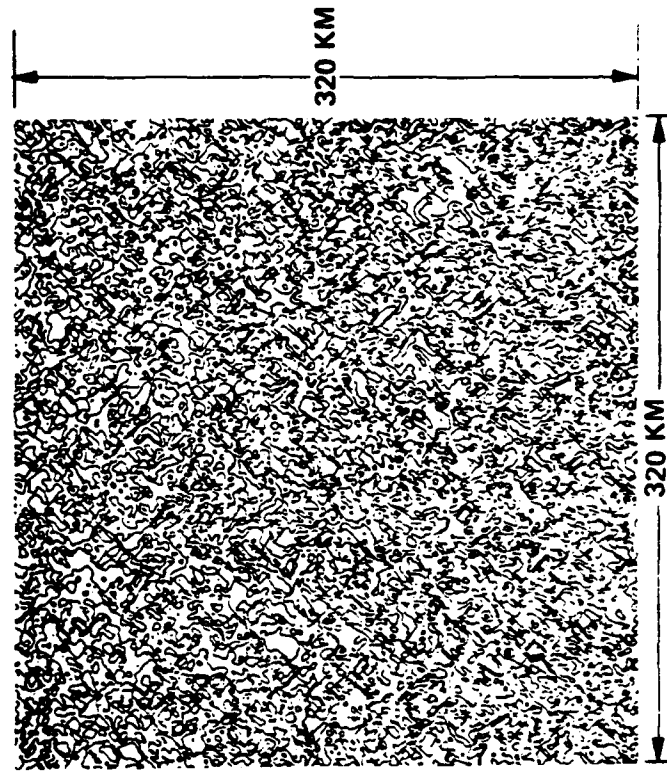
SYNTHETIC FIELD POTENTIAL CONTOUR MAP
CONTOUR INTERVAL 2000 E KM²



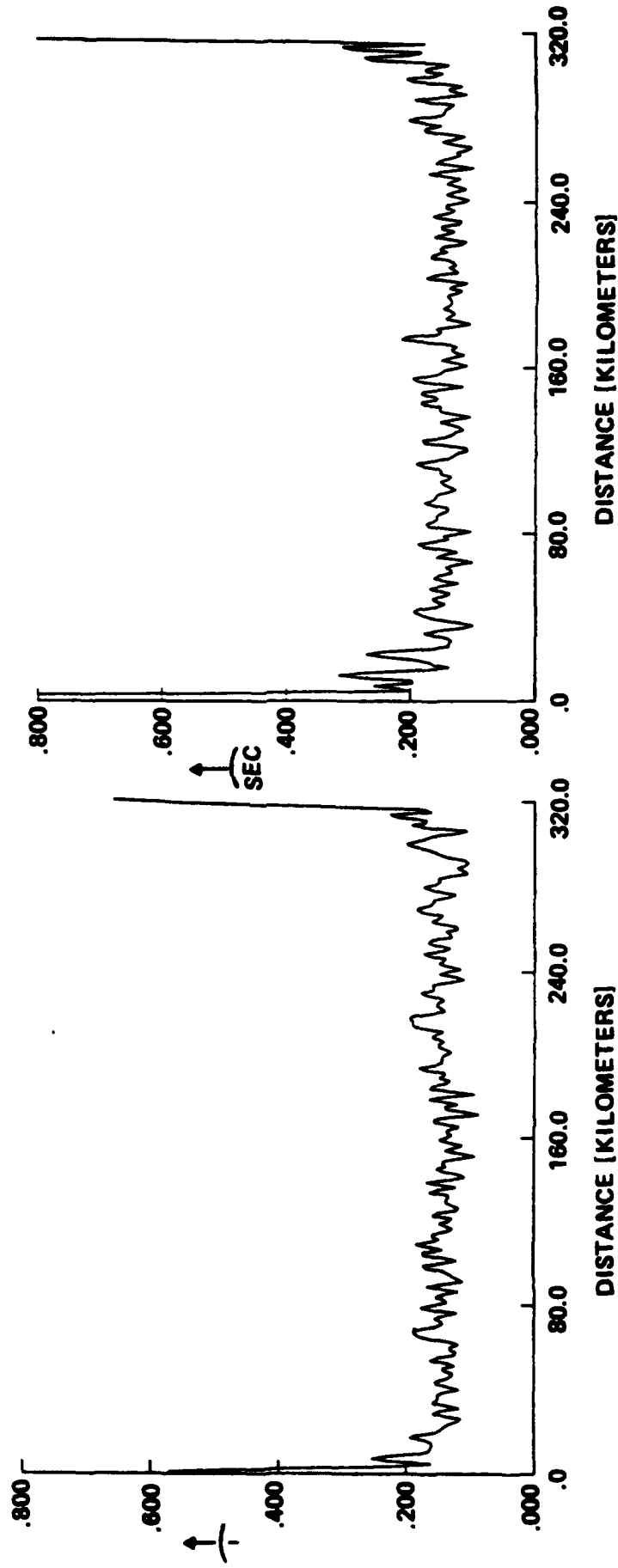
SYNTHETIC FIELD VERTICAL DEFLECTION (T_x) CONTOUR MAP
CONTOUR INTERVAL 1/2 SEC



SYNTHETIC FIELD GRADIENT (T_{xy}) CONTOUR MAP
CONTOUR INTERVAL 2 EOTVOS



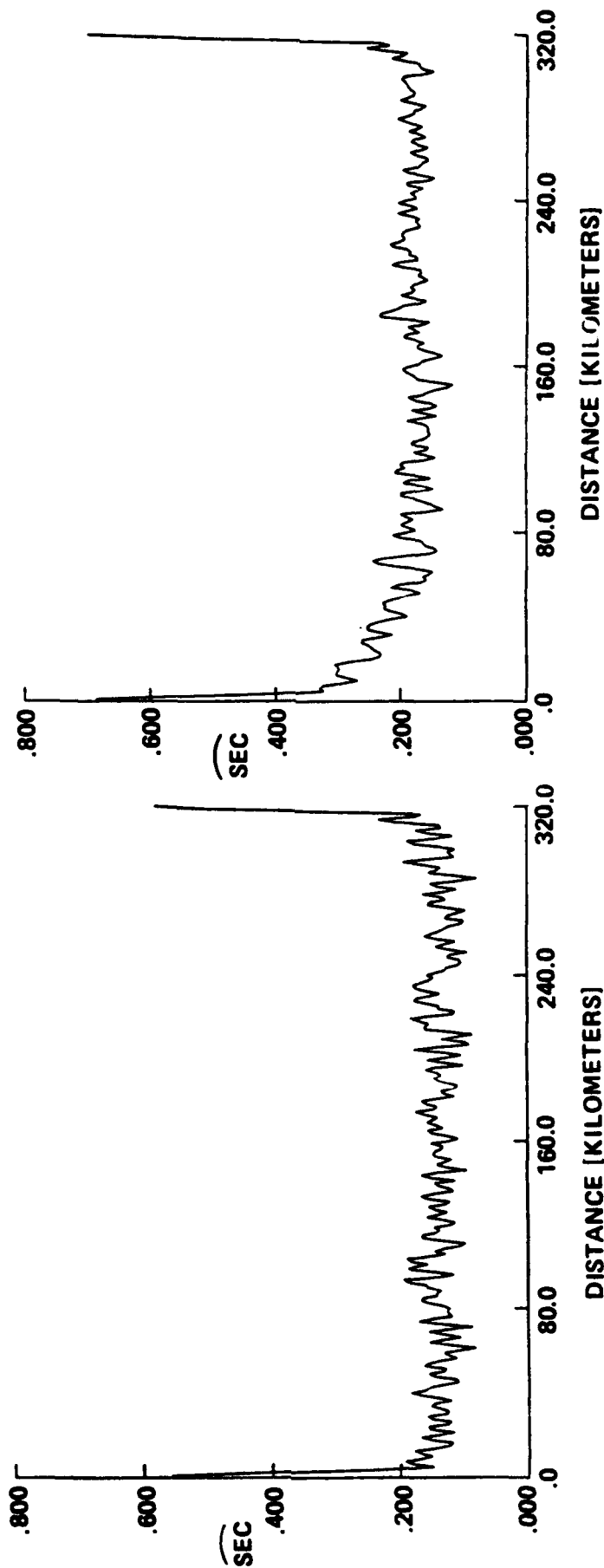
T_x: AVERAGE POSITIVE ERROR OF CENTRAL STRIP PASSING THROUGH FIELD



LOW FREQUENCY ESTIMATED USING TRUTH DATA FIELD.

LOW FREQUENCY ERROR ESTIMATED USING 9 ASTROS

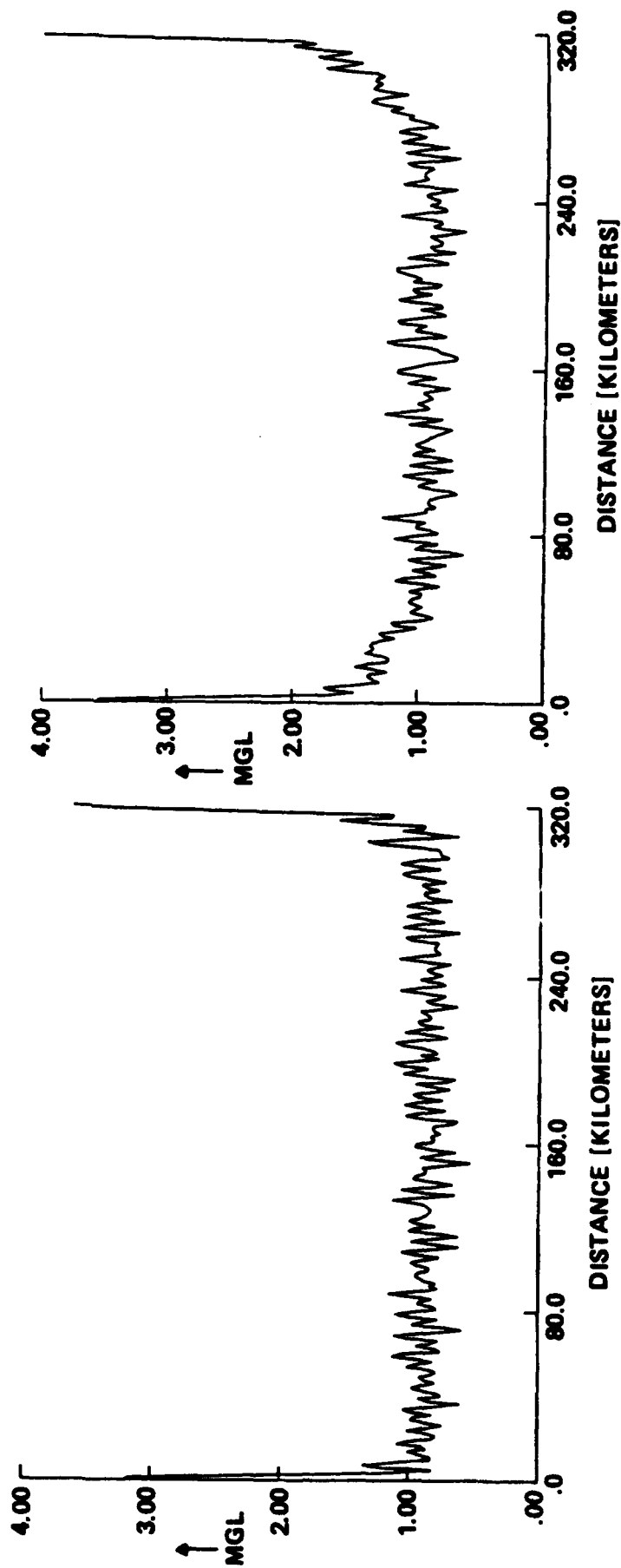
T_y: AVERAGE POSITIVE ERROR OF CENTRAL STRIP PASSING THROUGH FIELD



LOW FREQUENCY ERROR ESTIMATED USING TRUTH DATA FIELD

LOW FREQUENCY ERROR ESTIMATED USING 9 ASTROS

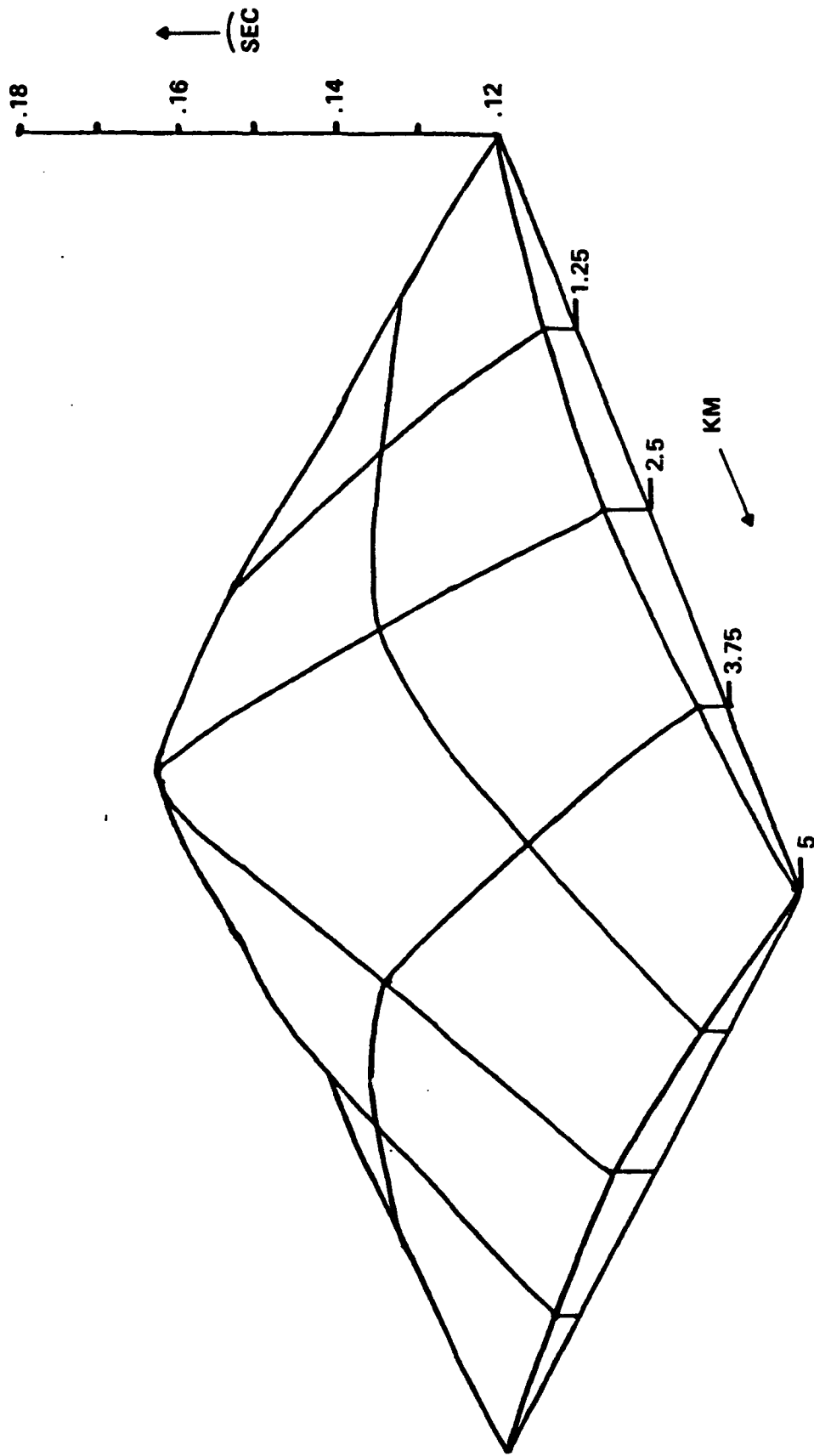
T₂: AVERAGE POSITIVE ERROR OF CENTRAL STRIP PASSING THROUGH FIELD



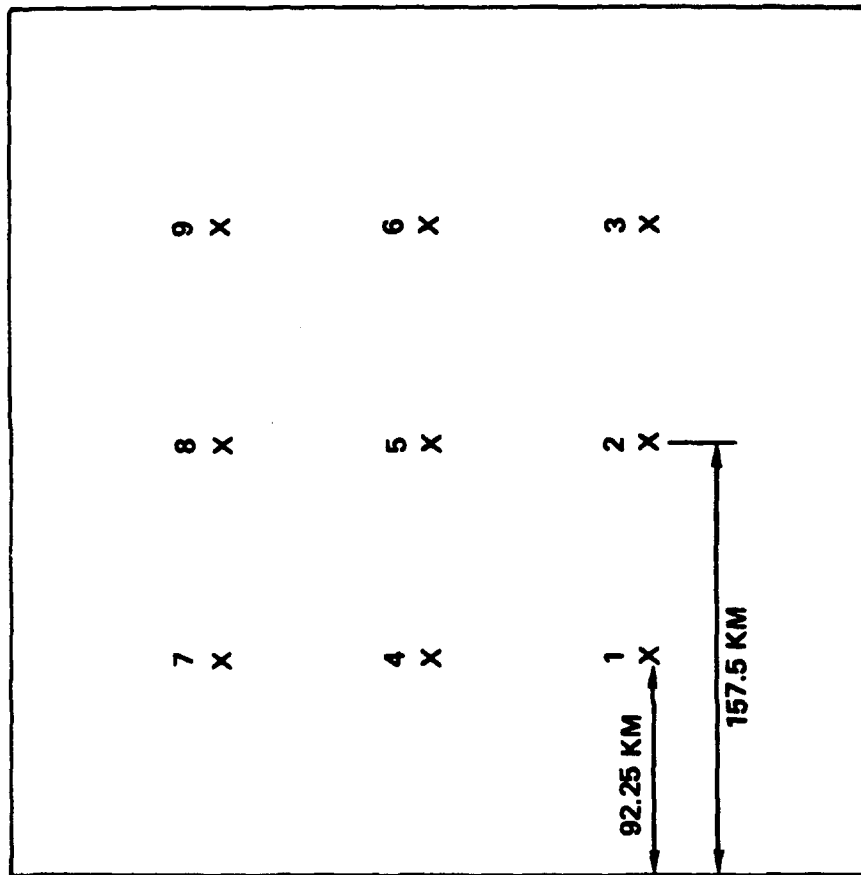
LOW FREQUENCY ERROR ESTIMATED USING TRUTH DATA FIELD

LOW FREQUENCY DATA ESTIMATED USING 9 ASTROS

HORIZONTAL DISTURBANCE AVERAGE ERROR OVER GRID SQUARE



TRUTH DATA/ESTIMATE COMPARISON



	T_x (SEC)	T_y (SEC)	T_z (MGAL)
MEAN	0.0304	0.108	0.197
S.D.	0.108	0.113	0.724
RMS	0.112	0.157	0.75

PAPER TITLE: AIRBORNE GRAVITY GRADIENT SURVEY DATA REDUCTION

SPEAKERS NAME: John Hutcheson

Questions and Comments:

- Julian Center: What statistical model do you use for least squares collocation to incorporate tie points?

SPEAKERS RESPONSE: The STAG (or reciprocal distance) 7-term gravity model is used in the LSC algorithm to upward continue the astro tie point to a node on the derived map.

ISOMORPHIC GEODETIC AND ELECTRICAL NETWORKS: AN APPLICATION TO
THE ANALYSIS OF AIRBORNE GRAVITY GRADIOMETER SURVEY DATA

RRH: GRAVITY GRADIOMETER SURVEY ANALYSIS

D. H. Eckhardt

Air Force Geophysics Laboratory

Earth Sciences Division

Hanscom AFB, MA 01731-5000

ABSTRACT

Late in 1986, the Bell Aerospace/Textron Gravity Gradiometer Survey System (GGSS) will be tested by the Air Force Geophysics Laboratory in an airborne survey of a 300 km x 300 km region of Oklahoma and Texas. The survey pattern will be a grid with a 5 km separation between adjacent tracks, north-south and east-west. One way to process the GGSS survey data is to analyze an electrical network that is isomorphic to the survey network. The integrated gradients between the survey crossing nodes correspond to the applied voltages between the nodes of the electrical network; the gradient variances correspond to the inter-nodal resistances; the elements of the adjusted gravity vector correspond to the nodal voltages; and the solution variances correspond to the resistances to ground. The survey error analysis is performed by calculating the resistance to ground of the electrical network; a technique for making the calculations in large networks is explored in detail. For a sample survey scenarios with one ground truth control point near each corner of the survey square and with realistic values for the survey parameters, the gravity disturbance standard deviation is less than 0.25 at all nodes. With no ground truth, but with a gravimeter on the aircraft that can independently determine gravity to 10 mGal at all nodes, the adjusted gravity disturbance standard deviation is less than 1 mGal.

(For more detailed information see Geophysics Vol 51 #11 November 86)

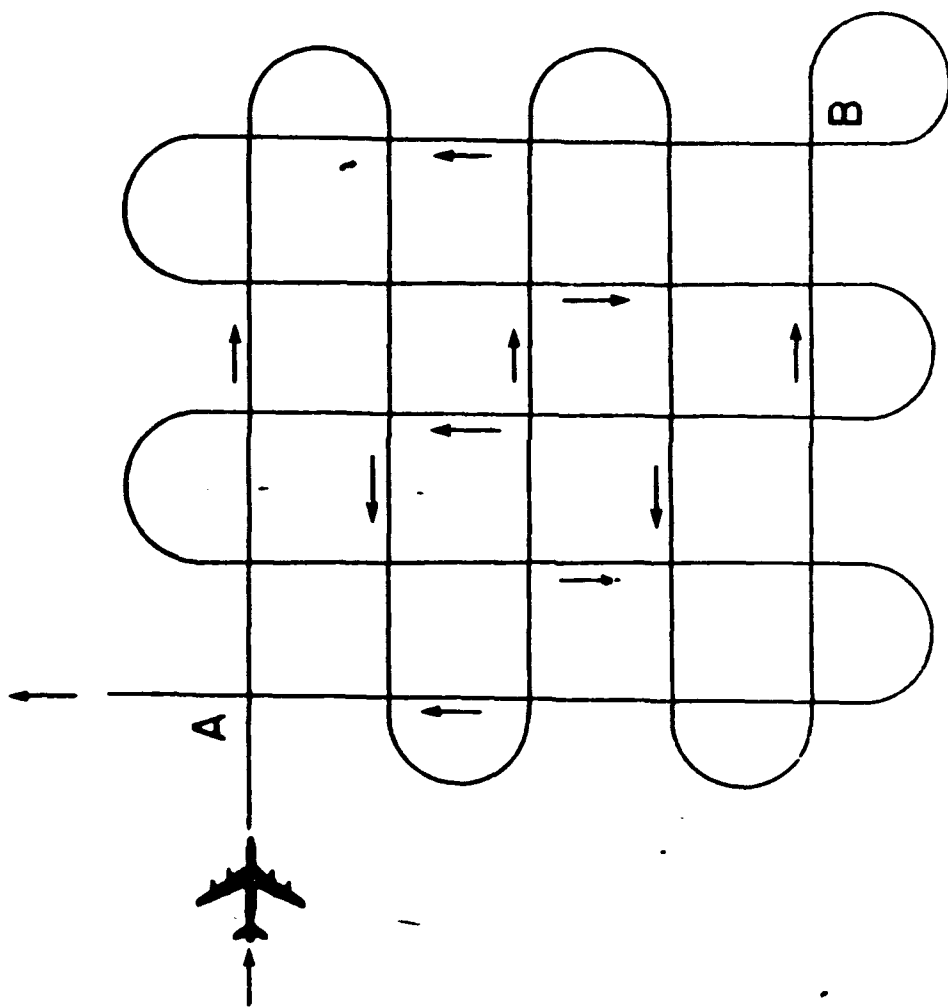


FIG. 1. 4 x 6 flight grid for the Airborne MSS.

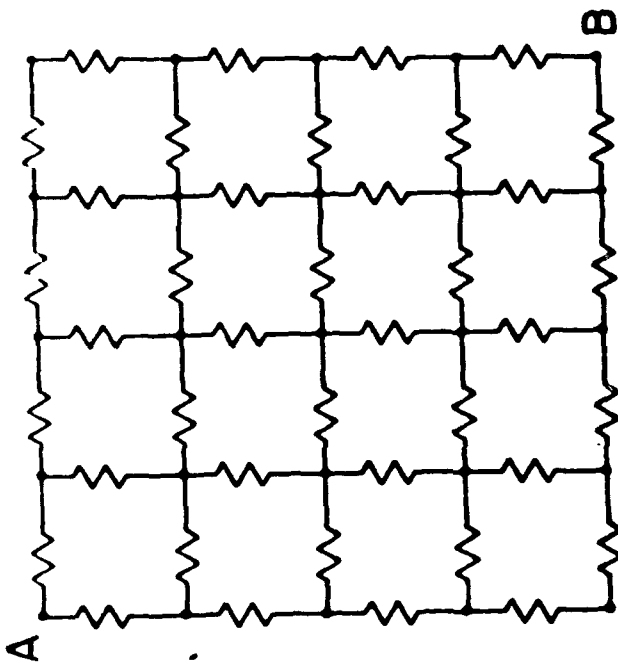


FIG. 2a. Electrical network isomorphic to the survey network of Figure 1. If all resistors have unit resistance, the resistance between A and B is $47/22$.

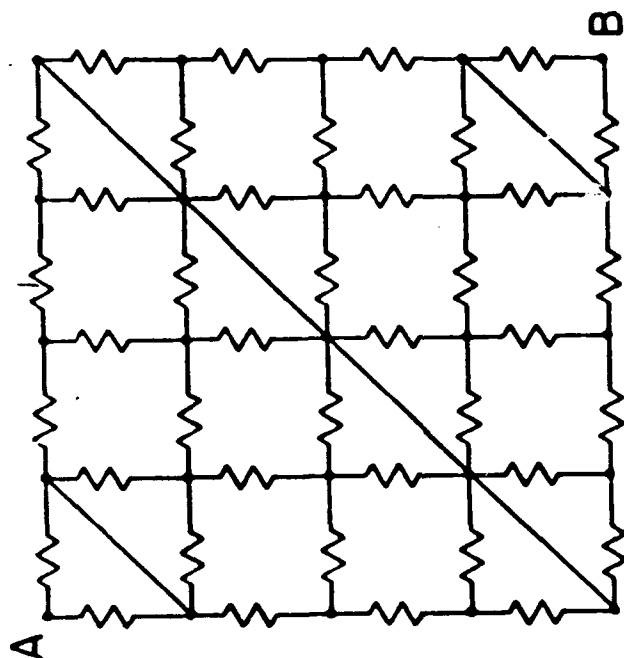


FIG. 2b. Adding these shunts, the resistance between A and B remains
47/22.

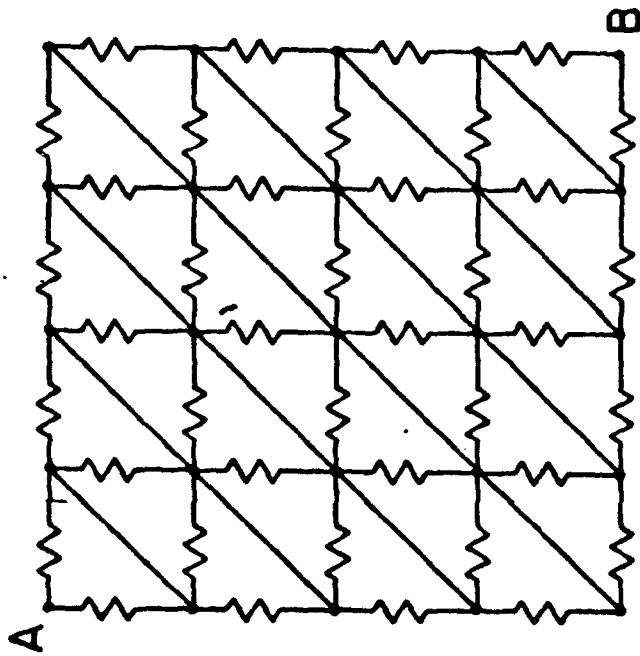


FIG. 2c. Adding these shunts, the resistance between A and B drops $7/132$ to $25/12$.

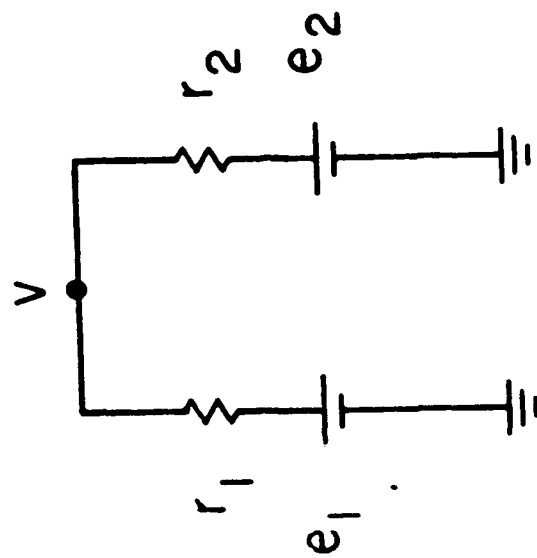


FIG. 3a. Elementary parallel connection.

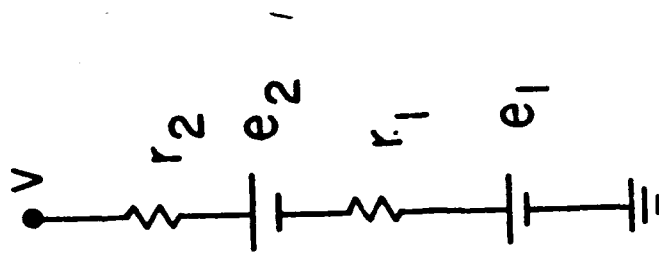


FIG. 3b. Elementary series connection.

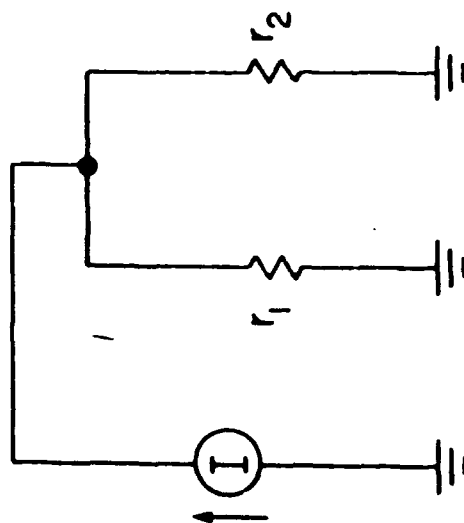


FIG. 4a. Elementary parallel circuit.

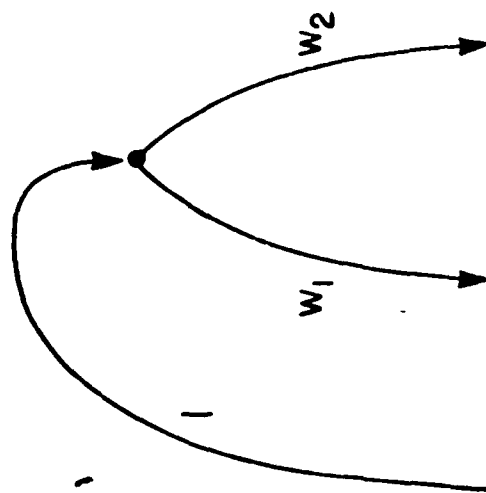


FIG. 4b. Gains of Figure 4a.

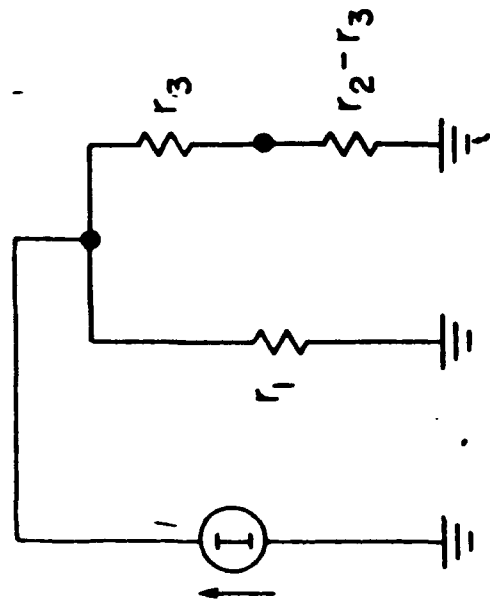


FIG. 5a. Elementary circuit with series-parallel connection.

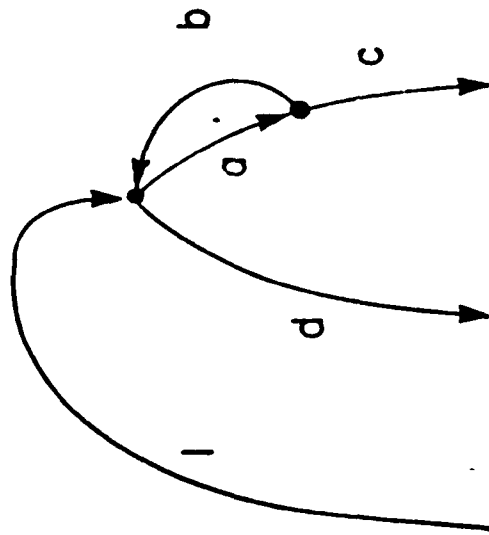


FIG. 5b. Gains of Figure 5a.

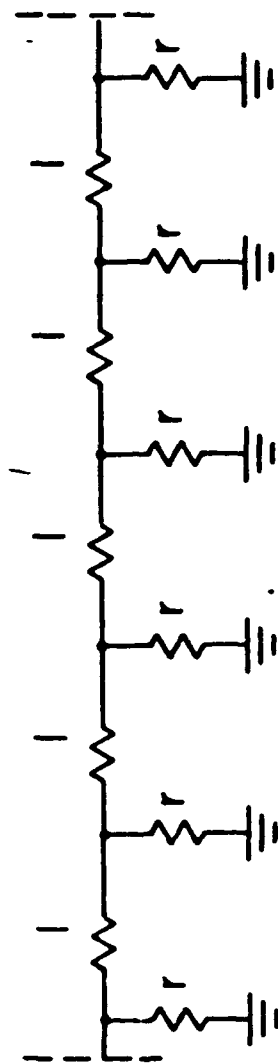


FIG. 6. This infinite ladder of resistors is a pantopod network.

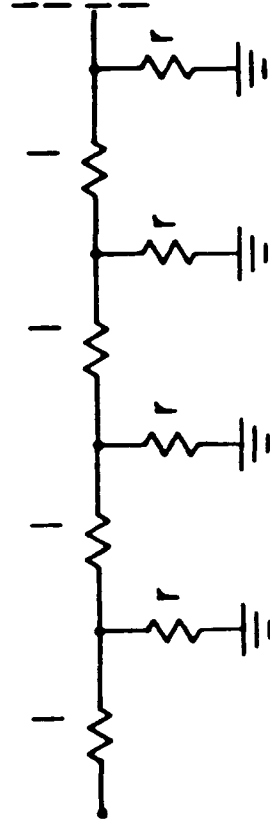


FIG. 7. Semiinfinite ladder of resistors.

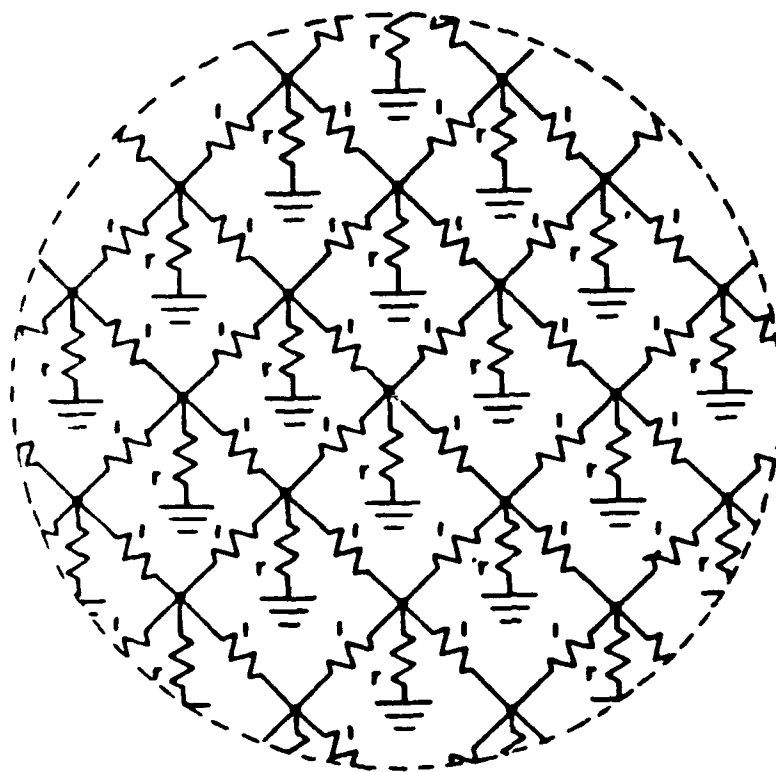
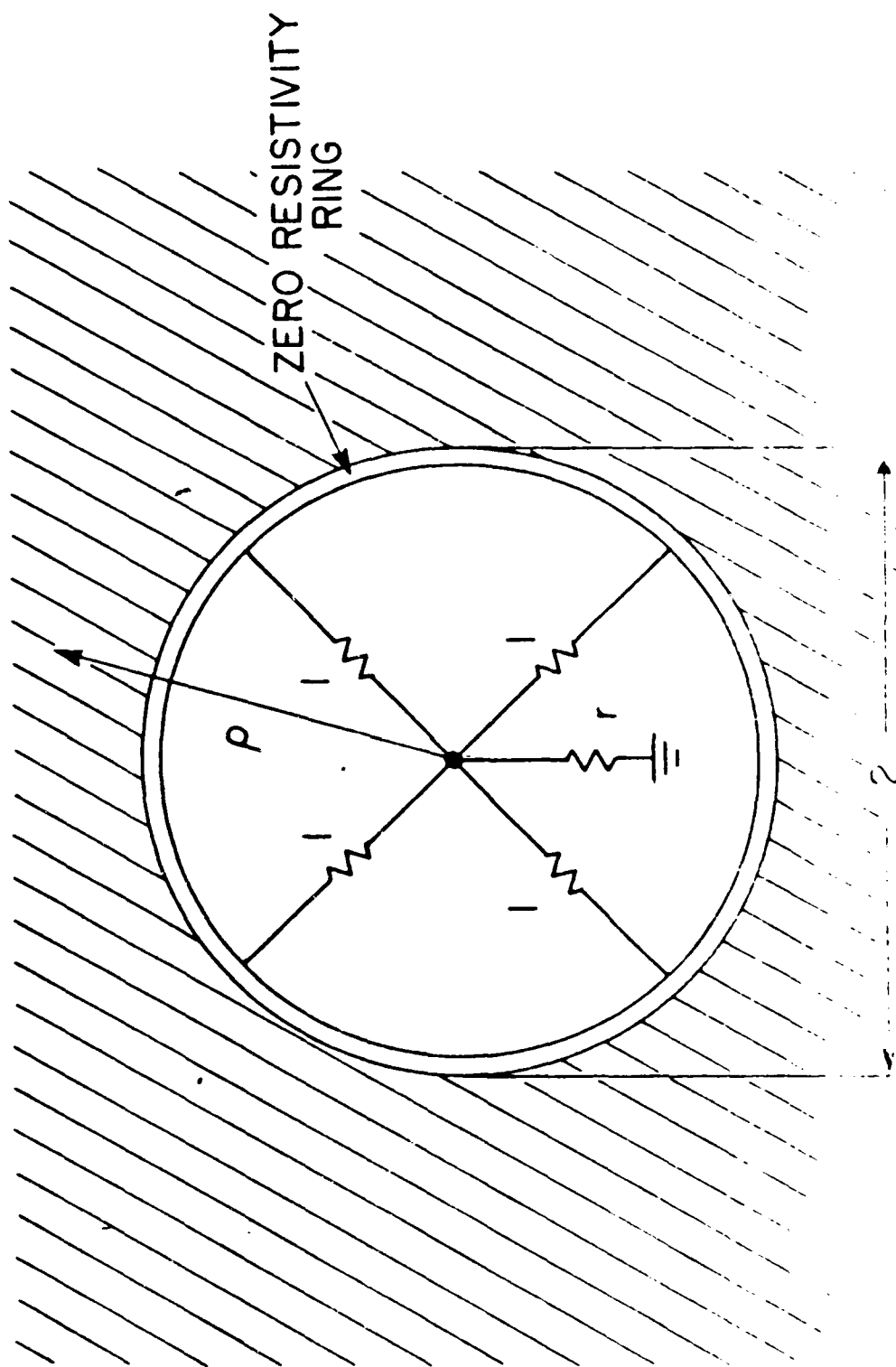


FIG. 8. This infinite lattice of resistors is a pantopod network.



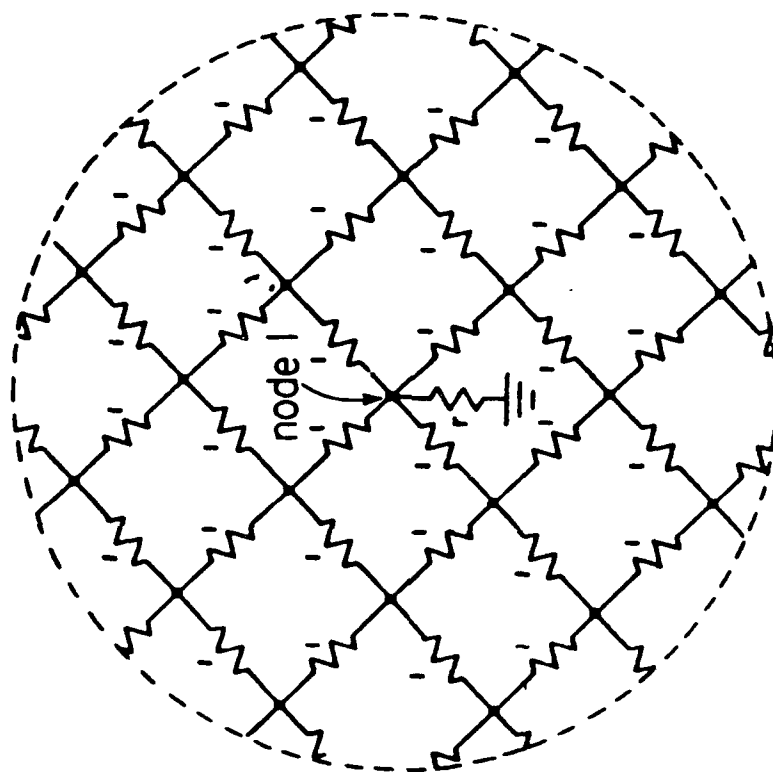


FIG. 10. This infinite lattice of resistors is a monopode network.

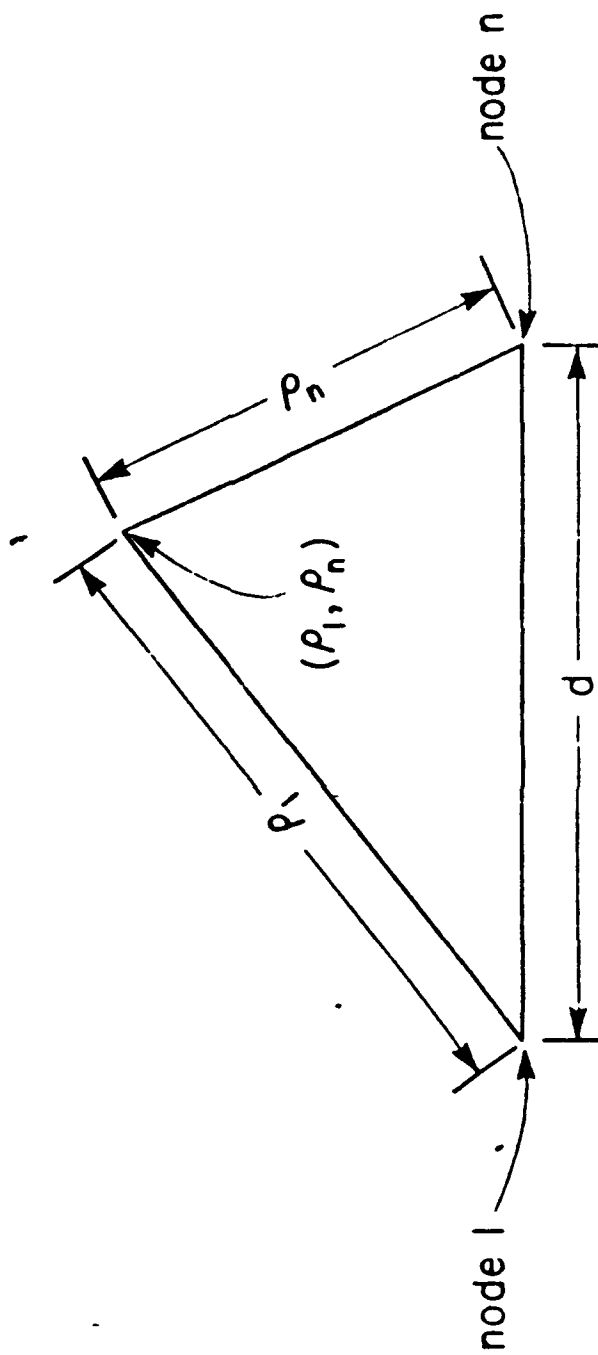


FIG. 11. The voltage is a function of ρ_1 and ρ_n , the distances from nodes 1 and n.

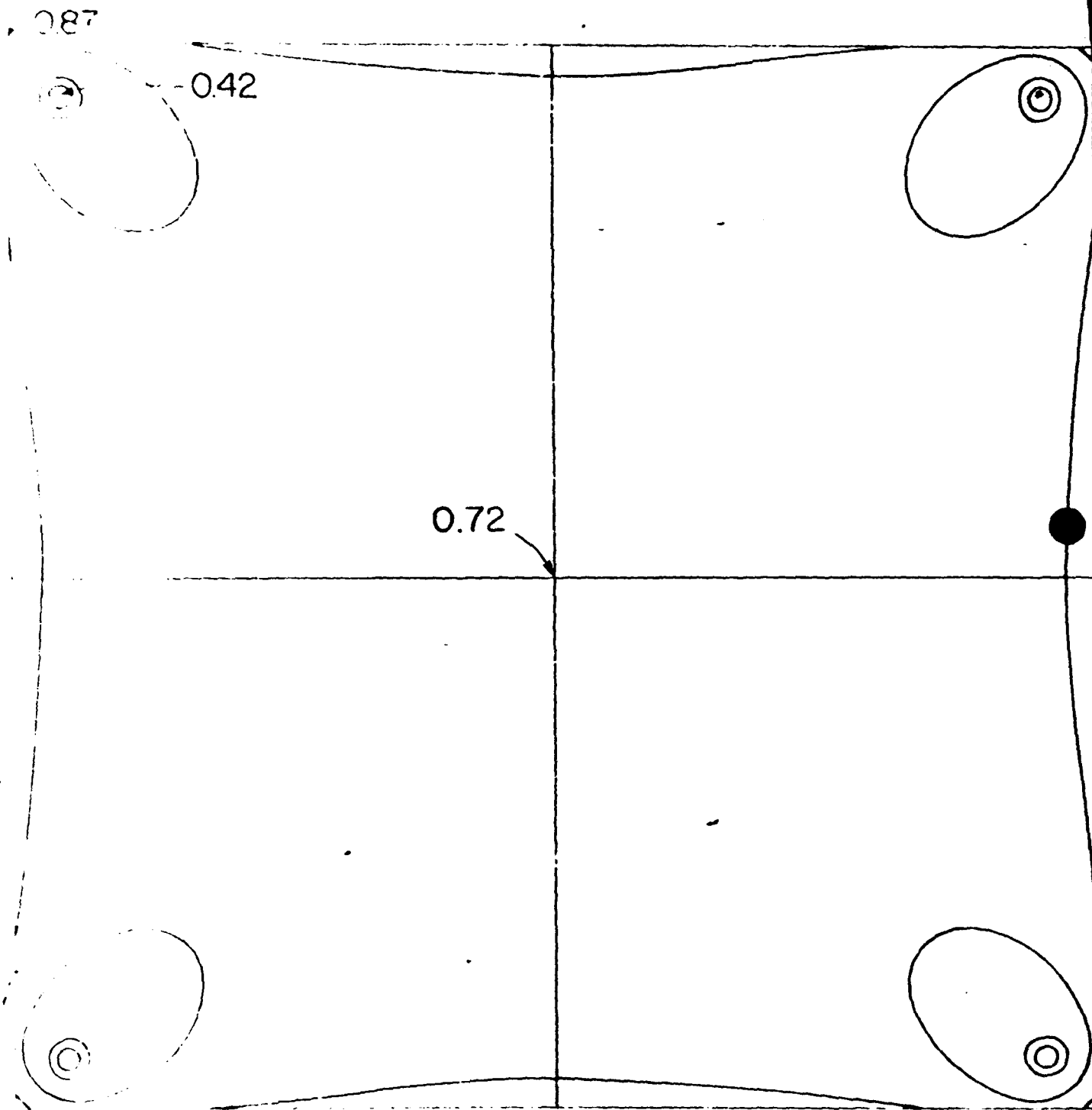


FIG. 12. Map (0.10 mGal contour interval) of gravity disturbance standard deviation in test survey area; at the four tie points near the corners the standard deviations are 0.46 mGal a priori, and 0.42 mGal a posteriori.

091

0.55

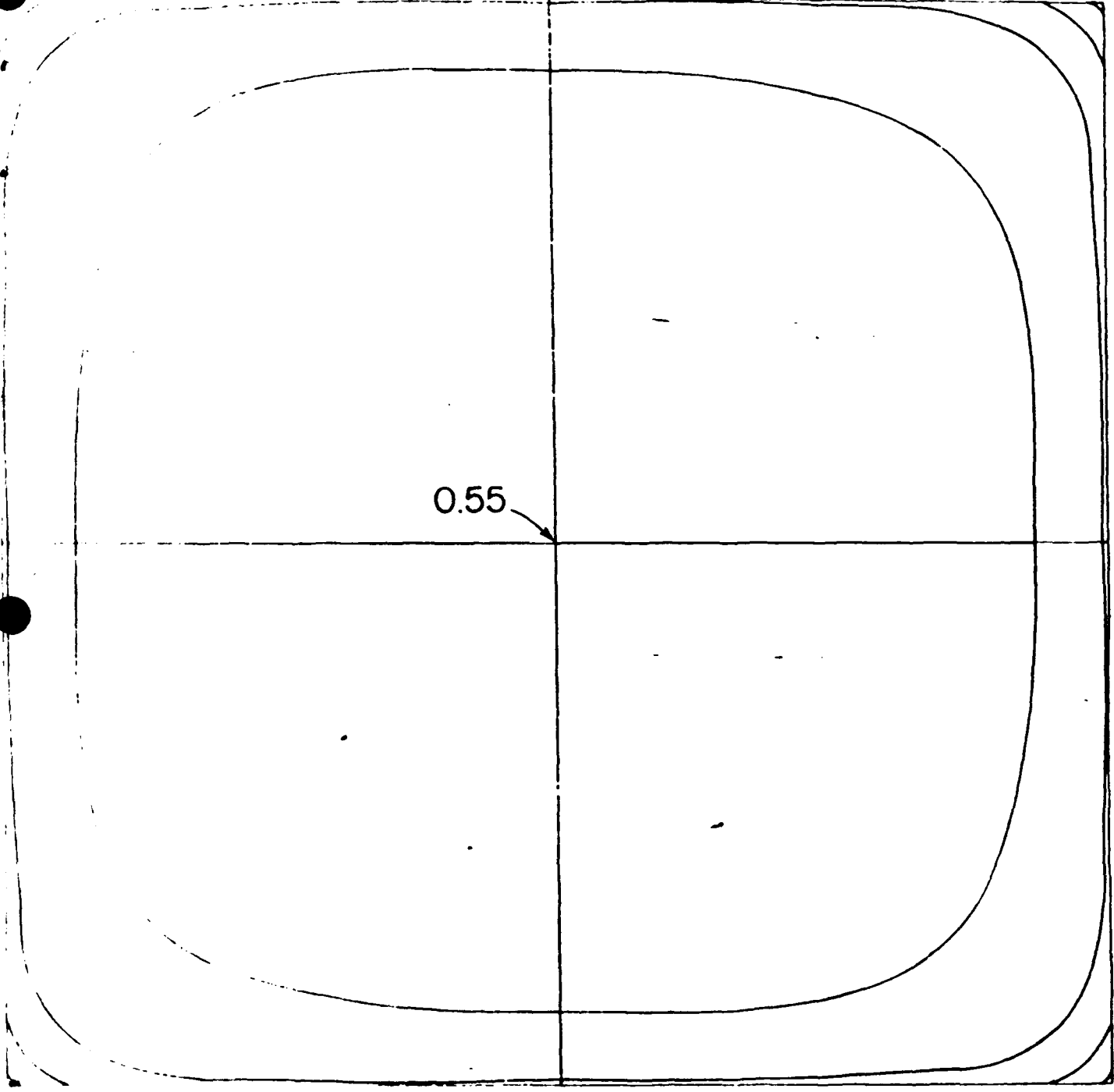


FIG. 13. Map (0.10 mGal contour interval) of gravity disturbance standard deviation in test survey area; 10 mGal gravimeter system aboard aircraft.

STAGE II PROCESSING OF AIRBORNE GRAVITY GRADIOMETER
DATA USING FREQUENCY DOMAIN TECHNIQUES

A. A. Vassiliou

The University of Calgary
Division of Surveying Engineering
2500 University Drive N.W.
Calgary, Alberta, T2N 1N4
Canada

ABSTRACT

A set of frequency response functions between the first-order and the second-order gravity gradients is developed in this paper using flat-earth approximation. In this way the spectrum of each first-order gradient is related to the spectra of one or more second-order gravity gradients. Assuming noise-free second-order gradient measurements, these equations are transformed back into the space domain as integral equations relating each first-order gradient to all of its second-order gradients (e.g. T_z to T_{xz} , T_{yz} , T_{zz}). The frequency domain relations are used to estimate the first-order gradients employing FFT. A set of simulated data is used to test these relationships. Results from these tests and computer time requirements are finally discussed in this paper.

STAGE II PROCESSING OF AIRBORNE GRAVITY
GRADIOMETER DATA USING FREQUENCY DOMAIN TECHNIQUES

Anthony A. Vassiliou

The University of Calgary
Division of Surveying Engineering
2500 University Drive N.W.
Calgary, Alberta T2N 1N4
CANADA

Presented at the 14th Annual Gravity Gradiometer Conference

Colorado Springs, Colorado
February 11-12, 1986

OBJECTIVES:

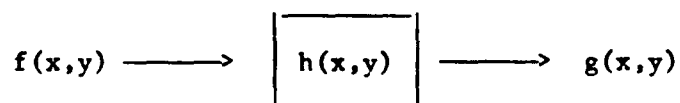
1. Develop a fast computational method in the frequency domain for the estimation of the first-order anomalous gravity gradients from gravity gradiometer data. Take advantage of the efficiency of FFT.
2. Use as many second-order gravity gradients as possible for the estimation of any single first-order gradient. Take the gradiometer self-noise explicitly into account.

DATA USED:

A set of about 250 000 simulated airborne gradient measurements on a 2.31×2.44 km grid, over a 472 (north) \times 496 (east) km area, is used.

2. INPUT - OUTPUT FILTERING EQUATIONS

2.1 Single Input - Single Output Equations



$$G(u,v) = H(u,v) F(u,v) \quad (1)$$

$$S_{gg}(u,v) = |H(u,v)|^2 S_{ff}(u,v) \quad (2)$$

$$S_{fg}(u,v) = H(u,v) S_{ff}(u,v) \quad (3)$$

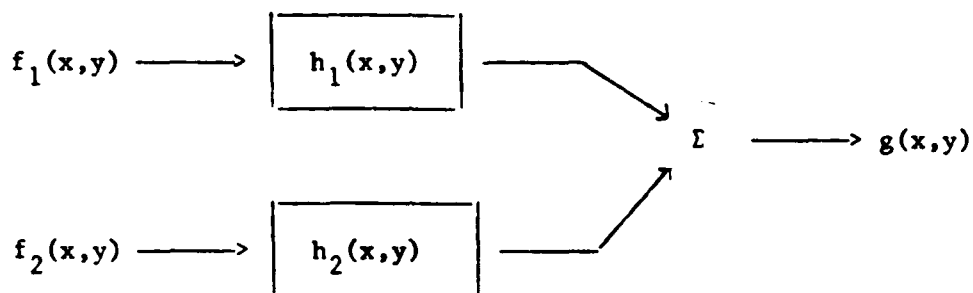
For extraneous noise $n(x,y)$ present

$$S_{gg}(u,v) = |H(u,v)|^2 \{S_{ff}(u,v) + S_{nn}(u,v)\} \quad (4)$$

$$S_{fg}(u,v) = H(u,v) \{S_{ff}(u,v) + S_{nn}(u,v)\} \quad (5)$$

2.2 Multiple Input - Single Output Filtering Equations

For simplicity reasons, discuss only two input - single output systems



- The two inputs and output related in the frequency domain by

$$G(u,v) = H_1(u,v) F_1(u,v) + H_2(u,v) F_2(u,v) \quad (6)$$

- For partially correlated inputs $f_1(x,y)$, $f_2(x,y)$, the transfer functions are given by

$$H_1(u,v) = \frac{S_{f_2, f_2}(u,v) S_{f_1, g}(u,v) - S_{f_1, f_2}(u,v) S_{f_2, g}(u,v)}{S_{f_1, f_1}(u,v) S_{f_2, f_2}(u,v) - |S_{f_1, f_2}(u,v)|^2} \quad (7)$$

$$H_2(u,v) = \frac{S_{f_1, f_1}(u,v) S_{f_2, g}(u,v) - S_{f_2, f_1}(u,v) S_{f_1, g}(u,v)}{S_{f_1, f_1}(u,v) S_{f_2, f_2}(u,v) - |S_{f_1, f_2}(u,v)|^2} \quad (8)$$

- For fully correlated inputs f_1, f_2 , the transfer functions H_1, H_2 take the form

$$H_1(u,v) = \frac{S_{f_1, g}(u,v)}{S_{f_1, f_1}(u,v) + S_{f_2, f_2}(u,v)} \quad (9)$$

$$H_2(u,v) = \frac{S_{f_2, g}(u,v)}{S_{f_1, f_1}(u,v) + S_{f_2, f_2}(u,v)} \quad (10)$$

- For input noise uncorrelated to both fully correlated input signals, the transfer functions are modified

$$H_1(u,v) = \frac{S_{f_1,g}(u,v)}{S_{f_1,f_1}(u,v) + S_{f_2,f_2}(u,v) + S_{n,n}(u,v)} \quad (11)$$

$$H_2(u,v) = \frac{S_{f_2,g}(u,v)}{S_{f_1,f_1}(u,v) + S_{f_2,f_2}(u,v) + S_{n,n}(u,v)} \quad (12)$$

- Similar expressions to (9), (10), (11), (12) can be derived for a case of more than two fully correlated input signals.
- Multi-input - Single output filtering equations very useful for airborne gravity gradiometer where all input signals T_{xx} , T_{xy} , T_{xz} , T_{yy} , T_{zz} , T_{yz} are fully correlated.

3. APPLICATION OF MULTIPLE INPUT - SINGLE OUTPUT SYSTEMS TO THE ESTIMATION OF FIRST-ORDER GRADIENTS FROM SECOND-ORDER GRADIENT DATA

Statement of the problem: Estimate T_z from T_{xz} , T_{yz} , T_{zz} , T_{xx} , T_{yy}
Flat earth approximation is assumed.

3a. Estimation of T_z from T_{zz} gradient measurements

- To estimate $T_z(x,y)$ from measurements of $T_{zz}(x,y, z=h)$, is necessary to derive the transfer function between them

$$H(u,v) = \frac{S_{T_{zz}, T_z}(u,v)}{S_{T_{zz}, T_{zz}}(u,v) + S_{n,n}(u,v)} = - \frac{8\pi^3 q^3 e^{-2\pi h q} S_{T,T}(u,v)}{16\pi^4 q^4 e^{-4\pi h q} S_{T,T}(u,v) + S_{n,n}(u,v)} \quad (13)$$

$$\text{where } q = (u^2 + v^2)^{\frac{1}{2}} \quad (14)$$

- For simplicity reasons assume noise-free measurements

$$H(u,v) = - \frac{e^{2\pi h q}}{q} \quad (15)$$

$T_z(x,y)$ cannot be computed at the (0,0) point. The mean of T_z has to be evaluated from other sources.

- Equations (13), (14) incorporate plane integration and downward continuation.

Pure plane integration corresponds to Stokes formula

$$T_z(x,y) = - \frac{1}{2\pi} \int_{-\infty}^{\infty} \int_{-\infty}^{\infty} \frac{T_{zz}(x_1, y_1)}{[(x-x_1)^2 + (y-y_1)^2]^{\frac{3}{2}}} dx_1 dy_1 \quad (16)$$

3b. Estimation of T_z from $T_{xz} - T_{yz}$

- Necessary to determine the transfer functions between $T_{xz} - T_{yz}$ and T_z (noise-free measurements assumed)

$$H_1(u,v) = - \frac{1}{2\pi q^2} u e^{2\pi h q} \quad (17)$$

$$H_2(u,v) = - \frac{1}{2\pi q^2} v e^{2\pi h q} \quad (18)$$

$$\mathcal{F}\{T_z(x,y)\} = H_1(u,v) \mathcal{F}\{T_{xz}(x,y,z=h)\} + H_2(u,v) \mathcal{F}\{T_{yz}(x,y,z=h)\} \quad (19)$$

where \mathcal{F} denotes the Fourier transform.

- Pure plane integration transformed in the space domain yields

$$T_z(x,y) = - \frac{1}{2\pi} \int_{-\infty}^{\infty} \int_{-\infty}^{\infty} \frac{T_{xz}(x_1,y_1) \sin a}{[(x-x_1)^2 + (y-y_1)^2]^{\frac{3}{2}}} dx_1 dy_1 - \frac{1}{2\pi} \int_{-\infty}^{\infty} \int_{-\infty}^{\infty} \frac{T_{yz}(x_1,y_1) \cos a}{[(x-x_1)^2 + (y-y_1)^2]^{\frac{3}{2}}} dx_1 dy_1 \quad (20)$$

where

$$\sin a = \frac{(x-x_1)}{[(x-x_1)^2 + (y-y_1)^2]^{\frac{3}{2}}}, \quad \cos a = \frac{(y-y_1)}{[(x-x_1)^2 + (y-y_1)^2]^{\frac{3}{2}}} \quad (21)$$

- Equation (20) is important, providing T_z directly in terms of T_{xz} , T_{yz} . A similar equation can be derived for the anomalous potential

$$T(x,y) = - \frac{1}{2\pi} \int_{-\infty}^{\infty} \int_{-\infty}^{\infty} \frac{T_x(x_1,y_1) \sin a}{[(x-x_1)^2 + (y-y_1)^2]^{\frac{3}{2}}} dx_1 dy_1 - \frac{1}{2\pi} \int_{-\infty}^{\infty} \int_{-\infty}^{\infty} \frac{T_y(x_1,y_1) \cos a}{[(x-x_1)^2 + (y-y_1)^2]^{\frac{3}{2}}} dx_1 dy_1 \quad (22)$$

- According to (22), geoidal undulations can be computed in a local area from gridded 2-D deflections of the vertical (ideal case).

3c. Estimation of T_z from $T_{xz} - T_{yz} - T_{zz}$

- Determine transfer functions between $T_{xz} - T_{yz} - T_{zz}$ and T_z for noise free measurements

$$H_1(u, v) = - \frac{j u \cdot e^{2\pi h q}}{2\pi q^2} \quad (23)$$

$$H_2(u, v) = - \frac{j u \cdot e^{2\pi h q}}{2\pi q^2} \quad (24)$$

$$H_3(u, v) = - \frac{e^{2\pi h q}}{4\pi q} \quad (25)$$

$$F\{T_z(x, y)\} = H_1(u, v)F\{T_{xz}(x, y, z=h)\} + H_2(u, v)F\{T_{yz}(x, y, z=h)\} + H_3(u, v)F\{T_{zz}(x, y, z=h)\} \quad (26)$$

- Pure plane integration transformed in the space domain results in

$$T_z(x, y) = - \frac{1}{4\pi} \iint_{-\infty}^{\infty} \frac{T_{xz}(x_1, y_1) \sin a}{[(x-x_1)^2 + (y-y_1)^2]^{\frac{3}{2}}} dx_1 dy_1 - \frac{1}{4\pi} \iint_{-\infty}^{\infty} \frac{T_{yz}(x_1, y_1) \cos a}{[(x-x_1)^2 + (y-y_1)^2]^{\frac{3}{2}}} dx_1 dy_1 - \frac{1}{4\pi} \iint_{-\infty}^{\infty} \frac{T_{zz}(x_1, y_1)}{[(x-x_1)^2 + (y-y_1)^2]^{\frac{3}{2}}} dx_1 dy_1 \quad (27)$$

T_z related directly to T_{xz} , T_{yz} , T_{zz} by an integral formula.

- A similar formula can be developed for the anomalous potential T

$$T(x, y) = - \frac{1}{4\pi} \iint_{-\infty}^{\infty} \frac{T_x(x_1, y_1) \sin a}{[(x-x_1)^2 + (y-y_1)^2]^{\frac{3}{2}}} dx_1 dy_1 - \frac{1}{4\pi} \iint_{-\infty}^{\infty} \frac{T_y(x_1, y_1) \cos a}{[(x-x_1)^2 + (y-y_1)^2]^{\frac{3}{2}}} dx_1 dy_1 - \frac{1}{4\pi} \iint_{-\infty}^{\infty} \frac{T_z(x_1, y_1)}{[(x-x_1)^2 + (y-y_1)^2]^{\frac{3}{2}}} dx_1 dy_1 \quad (28)$$

- Formula (28) provides the anomalous potential (geoidal undulations) in terms of all of its first-order gradients. For local gravity approximation though, this formula is not applicable due to the unavailability of T_x, T_y (deflection data) in 2-D grids. Nevertheless equation (28) is very useful because all second-order gradients T_{xz}, T_{yz}, T_{zz} are available from a gravity gradiometer system.

Notes:

1. In sections 3a, 3b, 3c, the second-order gradient T_{zz} can be substituted by the sum $-(T_{xx} + T_{yy})$. So equation (15) takes the form

$$F\{T_z(x,y)\} = \frac{1}{2\pi} \frac{e^{2\pi hq}}{q} F\{T_{xx}(x,y,z=h) + T_{yy}(x,y,z=h)\} \quad (29)$$

2. All the multiple input - single output equations are equivalent to the ones derived from a multidimensional Wiener filtering with linearly correlated inputs. Wiener filtering (in a planar approximation) can be formulated as the 2-D Fourier transform of a least-squares collocation estimate. However, Wiener-filtering is much faster computationally to least-squares collocation. For instance assuming a 2-D grid with 50 points in each direction and three gradient measurements per point, least-squares collocation has to invert a 22500×22500 matrix. This takes more than 15 CPU hours on the Supercomputer Cyber 205. On the other hand application of multi-dimensional Wiener filtering or multiple input-output filtering equations, leads to an inversion of a 3×3 matrix for each pair of frequencies (u,v). For linearly related inputs this inversion reduces down to an inversion of a 1×1 matrix.

3. So far the effect of topography on the gradients has been neglected. However it can be explicitly computed from the spectra

$$F\{T_{xx}\} = -2\pi Ge^{-2\pi qz_0} \sum_{n=1}^{\infty} \frac{(2\pi q)^{n-1}}{n!} \frac{2\pi u^2}{q} F\{\rho(x,y) h^n(x,y)\} \quad (30)$$

$$F\{T_{yy}\} = -2\pi Ge^{-2\pi qz_0} \sum_{n=1}^{\infty} \frac{(2\pi q)^{n-1}}{n!} \frac{2\pi v^2}{q} F\{\rho(x,y) h^n(x,y)\} \quad (31)$$

$$F\{T_{zz}\} = -2\pi Ge^{-2\pi qz_0} \sum_{n=1}^{\infty} \frac{(2\pi q)^n}{n!} F\{\rho(x,y) h^n(x,y)\} \quad (32)$$

$$F\{T_{xy}\} = -2\pi Ge^{-2\pi qz_0} \sum_{n=1}^{\infty} \frac{(2\pi q)^{n-1}}{n!} \frac{2\pi uv}{q} F\{\rho(x,y) h^n(x,y)\} \quad (33)$$

$$F\{T_{xz}\} = -2\pi Ge^{-2\pi qz_0} \sum_{n=1}^{\infty} \frac{(2\pi q)^{n-1}}{n!} j 2\pi u F\{\rho(x,y) h^n(x,y)\} \quad (34)$$

$$F\{T_{yz}\} = -2\pi Ge^{-2\pi qz_0} \sum_{n=1}^{\infty} \frac{(2\pi q)^{n-1}}{n!} j 2\pi v F\{\rho(x,y) h^n(x,y)\} \quad (35)$$

Note 3. (continued)

where in equations (30) to (35) $F\{T_{ij}\}$ represent the spectrum of the effect of topography on the second-order gradient T_{ij} ;

z_0 is the flying altitude

$h(x,y)$ is the gridded height

$\rho(x,y)$ is the gridded density (it can be taken as constant =
2.67 gr/m³)

4. DATA, TESTS AND RESULTS

4a Simulated data

- Airborne and earth's surface first-order and second-order gravity gradients are simulated on a 2.31 km (north) × 2.44 km (east) grid. For the simulation 9.26 km (north) × 9.74 km (east) (i.e. 5' × 10') gravity anomaly data are used. The gravity anomaly data are given on a grid in Northern Saskatchewan, Canada. Extent of the grid is 472 × 496 km.

- Flat-earth approximation is used under the transformation

$$dx = R \cos\phi \, d\lambda$$

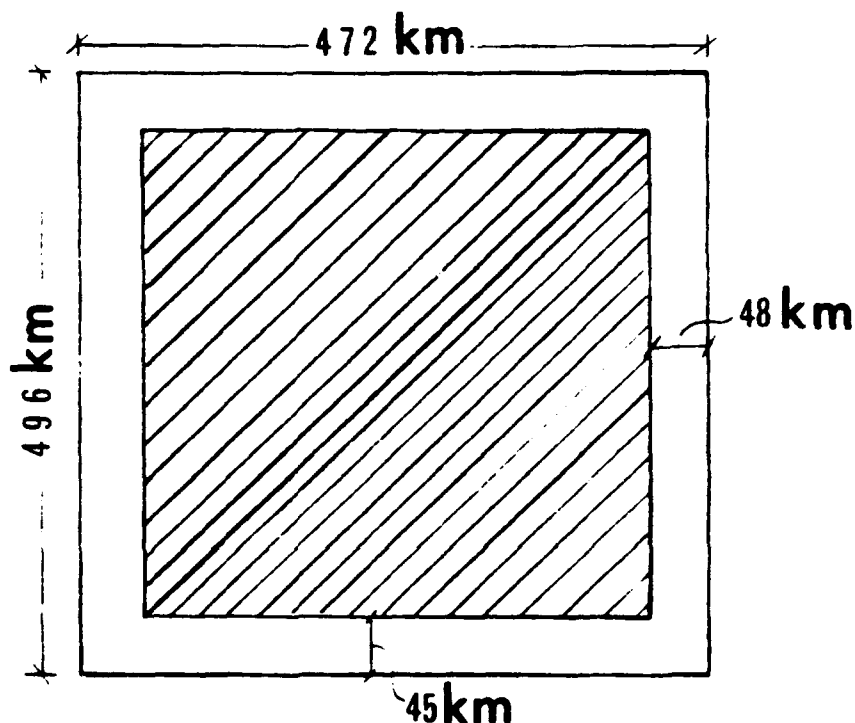
$$R = 6371 \text{ km}$$

$$dy = R d\phi$$

- Long-wavelengths are eliminated by subtracting the spherical harmonic expansion up to degree and order 36 of Rapp 1978 model, from the original free-air gravity anomalies.
- The modelling of the gravity data is made by a two-layer point mass model (depths at 15.5 km and 5 km respectively). For high frequency information a third layer is added buried at depth of 1 km, with white-noise point mass distribution on it.
- The second-order gradients are simulated at a flying altitude of 600 m. They were corrupted by gradiometer noise (following the model published by White (1980)).

4b. Results from the estimation of T_z from T_{xz} , T_{yz} , T_{zz}

The mean of T_z over the whole area is assumed known from other sources. Results are given on the inner area bounded 45 km from the north and the south borders and 48 km inside the east and west borders.



1st Case : No noise is taken into account.

T_z is estimated directly below measurement grid points

Measurements

	T_{zz}	$T_{xz} - T_{yz}$	$T_{xz} - T_{yz} - T_{zz}$
RMS error of T_z	0.70 mgals	0.46 mgals	0.41 mgals
CPU time (on a Honeywell Multic DPS 68 computer)	545 CPU seconds	560 CPU seconds	578 CPU seconds (124848 measurements)

2nd case : The gradiometer self-noise is taken into account.
The PSD of the anomalous potential T is modelled by

$$S_{T,T}(u,v) = \frac{A_1}{q^{1.6}},$$

where A_1 has been determined from data of all the Saskatchewan province.

Measurements

	T_{zz}	$T_{xz} - T_{yz}$	$T_{xz} - T_{yz} - T_{zz}$
RMS error of T_z	0.63 mgals	0.44 mgals	0.37 mgals
CPU time	622 CPU seconds	640 CPU seconds	660 CPU seconds

1st case : The gradiometer self-noise isn't taken into account.

T_z is estimated by FFT interpolation at all the points on
 1.155×1.22 km (north-east) grid.

Measurements

	T_{zz}	$T_{xz} - T_{yz}$	$T_{xz} - T_{yz} - T_{zz}$
RMS error of T_z	0.50 mgals	0.38 mgals	0.32 mgals
CPU time			(estimation at 499 392 points) 1 680 CPU seconds

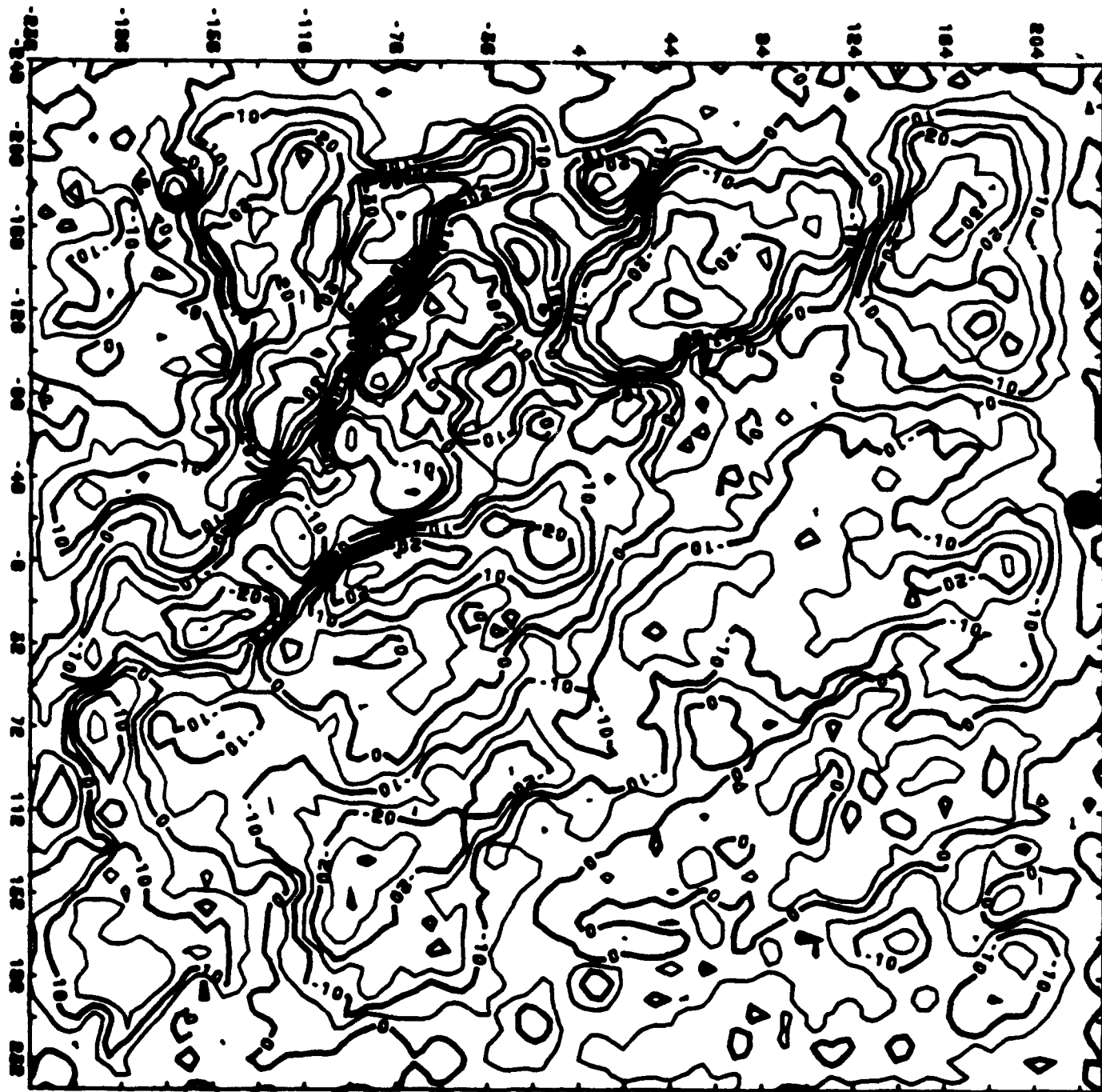


CONT. MAP OF GRADIENTS TZ

PLOT NO. 1

DATE 12/19/85

TIME 09.55.3





BLOCK DIAGRAM OF TZ GRADIENTS

PLOT NO. 1

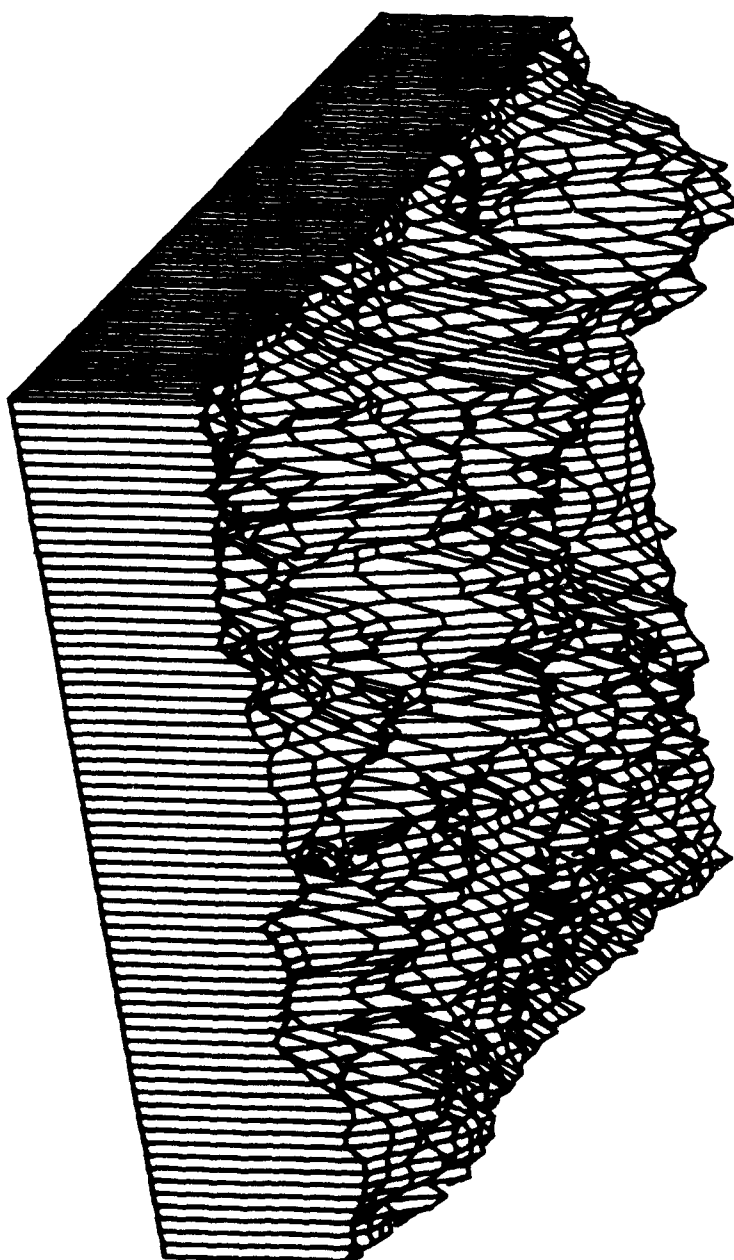
DATE 12/19/85

TIME 19.11.5

AZIM = -25.0

ELEV = 25.0

DIST = 10000





BLOCK DIAGRAM OF TZ ER. FROM TZZ

PLOT NO. 1

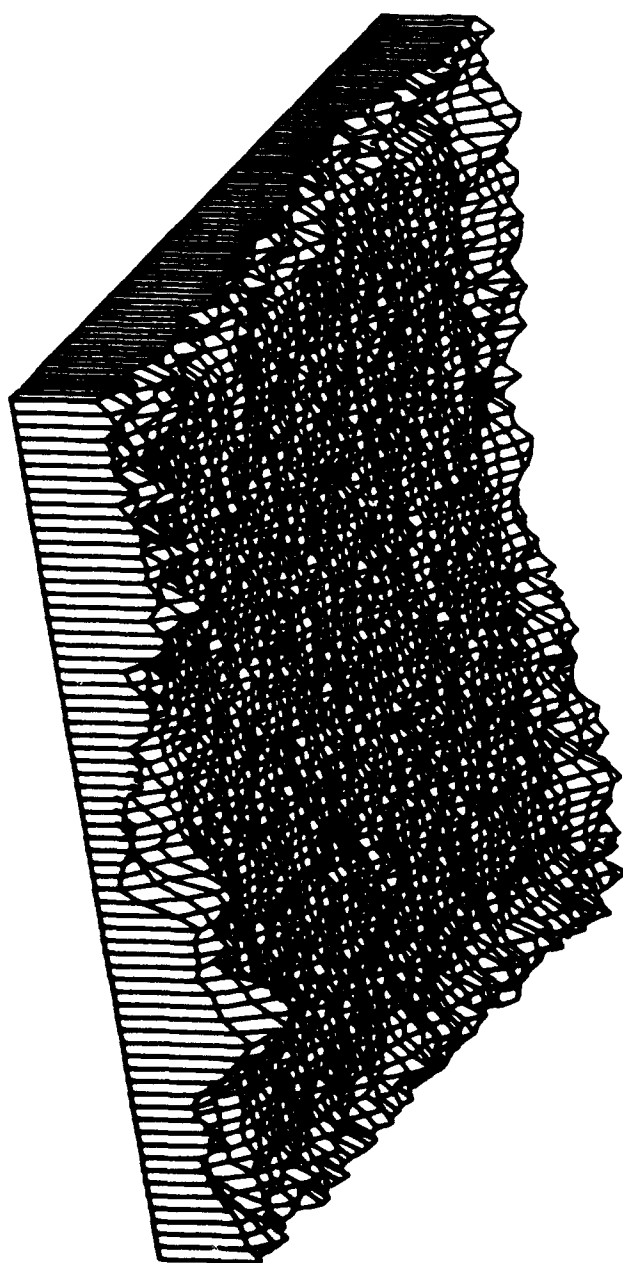
DATE 12/23/85

TIME 19.09.3

AZIM = -25.0

ELEV = 25.0

DIST = 10000





BLOCK DIAGRAM OF TZ ER. FROM TXZ - TYZ

PLOT NO. 1

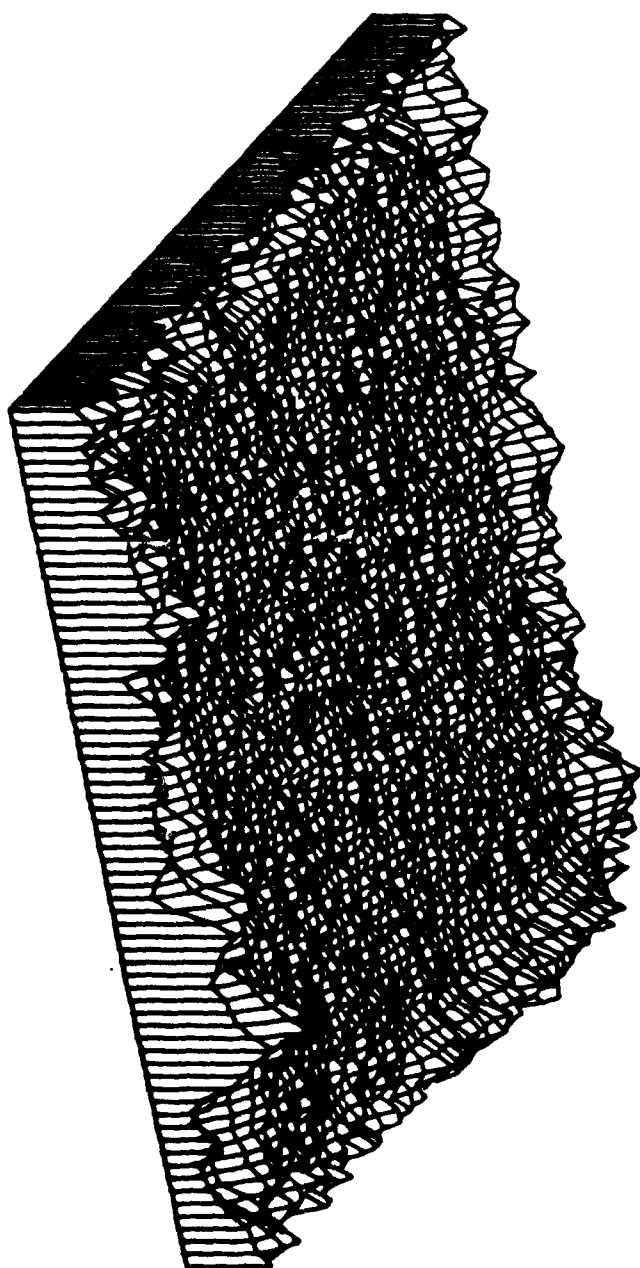
DATE 12/23/85

TIME 19.16.3

AZIM = -25.0

ELEV = 25.0

DIST = 10000





BLOCK DIAGRAM OF TZ ER. FROM TXZ - TYZ - TZZ

PLOT NO. 1

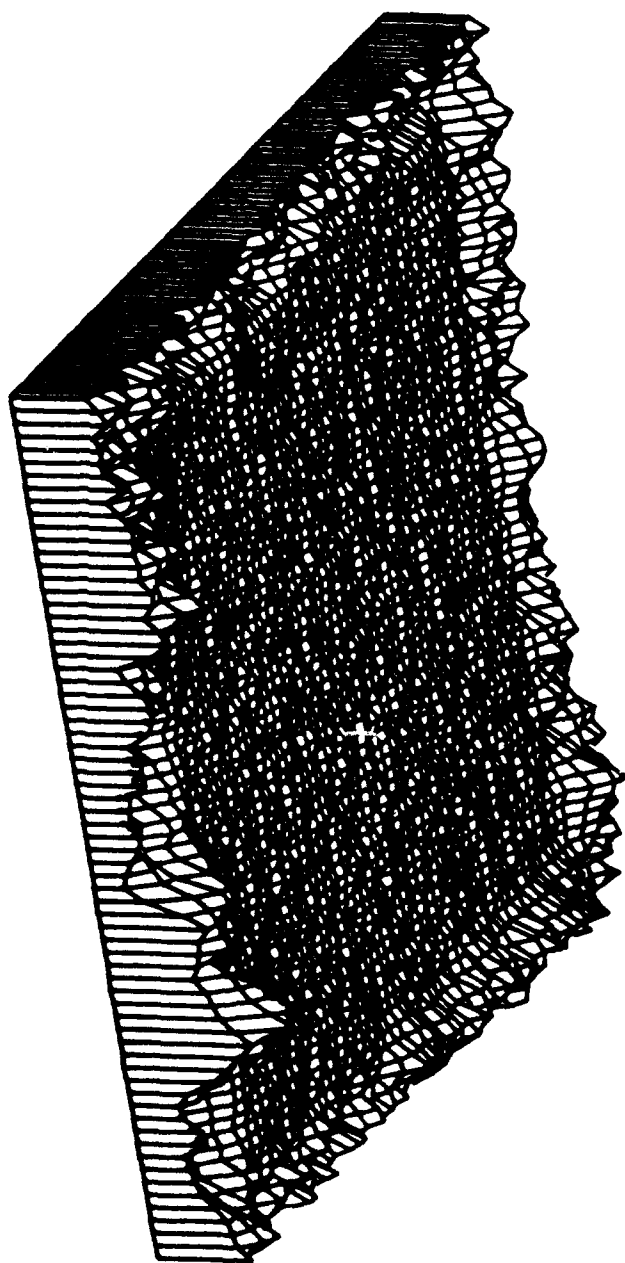
DATE 12/23/85

TIME 19.22.1

AZIM = -25.0

ELEV = 25.0

DIST = 10000



CONCLUSIONS

- A fast computational method, employing FFT, is developed for the estimation of first-order gradients from second-order gradients. The method is based on the application of the multiple input - single output filtering equations.
- The method handles all possible combinations of gradiometer data. For the estimation of T_z uses T_{zz} , $T_{xz} - T_{yz}$, $T_{xz} - T_{yz} - T_{zz}$. Furthermore takes the noise explicitly into account.
- Results from test runs with simulated data show that T_z can be estimated, directly below the gradiometer points with an RMS error of less than 0.70 mgals. The points at the middle of the gradiometer points, can be interpolated with an RMS error of less than 0.5 mgals.

KARHUNEN-LOEVE GRAVITY GRADIOMETER DATA PROCESSING

S. Bose

Applied Science Analytics, Inc.

7041 Owensmouth Ave.

Suite 206

Canoga Park, CA 91303

ABSTRACT

The Karhunen-Loeve data processing technique for gravity gradiometry is reviewed. The method is based on the White Noise Layer (WNL) model which replaces the unknown mass distribution below the survey region as multiple two-dimensional white noise layers representing the vertical derivative of the disturbance potential to any order. Such a gravity signal model is derived from the physical theory of geodesy and is particularly suited for modeling high frequency phenomena. Of particular interest is that such a model results in a nonstationary nonisotropic representation of the disturbance potential. A two-dimensional signal processing algorithm to process all the gradiometer data simultaneously is presented. The estimation algorithm can handle multiple layers of different inline or crossline data given in two dimensional grids at the same or different altitudes on or above the surface of the earth. Different grid patterns of the same inline or crossline measurements at the same or different altitudes are also accommodated by the algorithm without resorting to any pre-processor averaging techniques. The method is such that at any given spatial point the gravity field's correlation in

any direction is not ignored and the estimation algorithm does not enforce any unnecessary limitation of causality on the data inasmuch as no one-dimensional scanning is performed. The problem of simultaneous smoothing of all the gradiometer measurements from all survey traverses in the region is solved by representing the disturbance potential solution as a Karhunen-Loeve (KL) expansion. Estimating the gravity field or any of its derivatives simply reduces to estimating the KL coefficients and performing the appropriate transformations involving sine and cosine functions. Neither the estimation of the KL coefficients nor the implementation of these transformations requires any matrix inversions. Downward continuation as well as interpolation of estimates between grid measurements are performed automatically. Thus large amounts of moving base gravity gradiometry data can be handled by this technique in a computationally efficient manner.

KARHUNEN-LOEVE

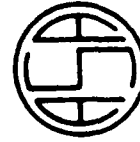
GRAVITY GRADIOMETER DATA PROCESSING

by

Dr. Sam C. Bose

Fourteenth Moving Base
Gravity Gradiometer Conference
United States Air Force Academy
Colorado Springs, Colorado

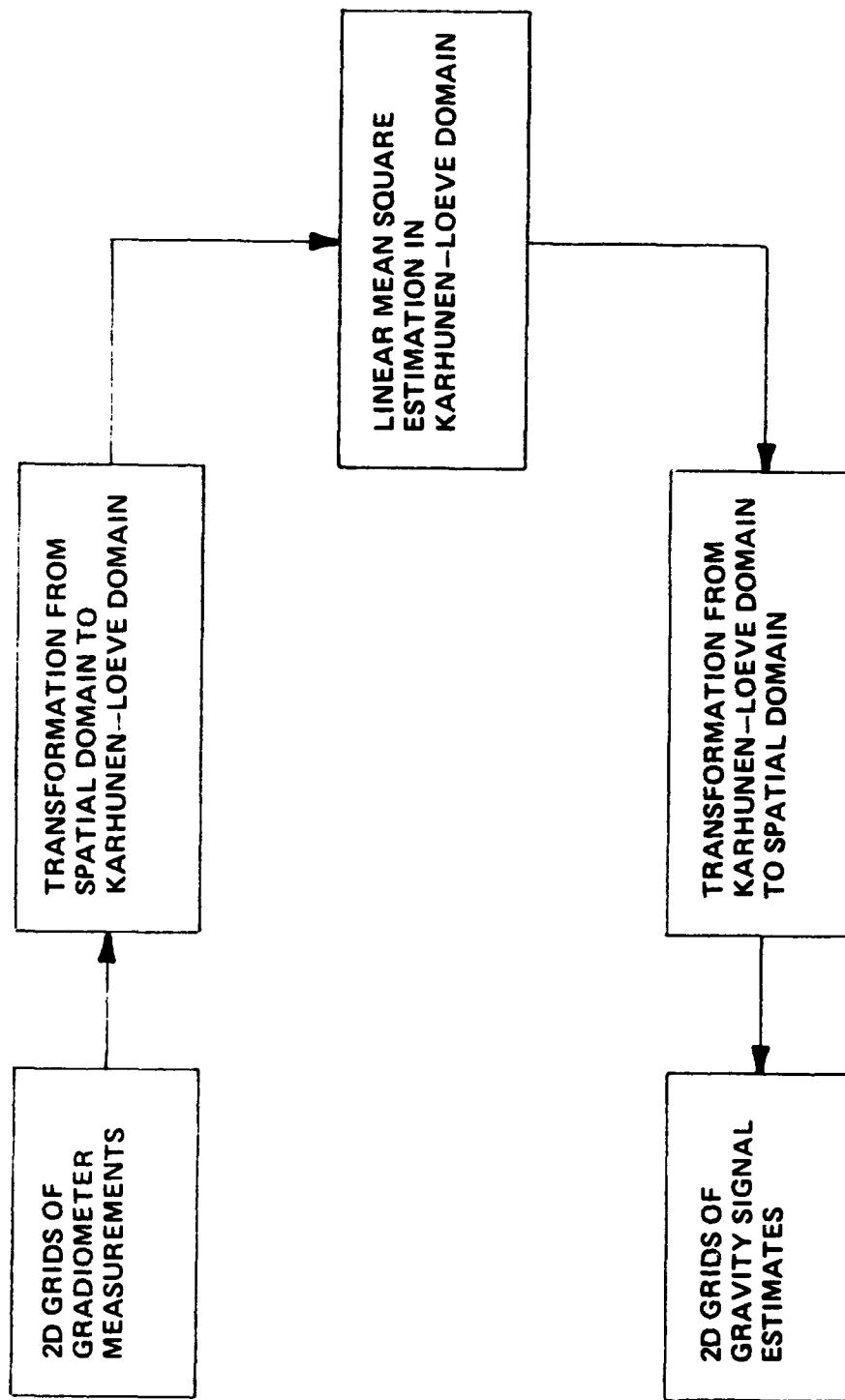
11-12 FEBRUARY 1986



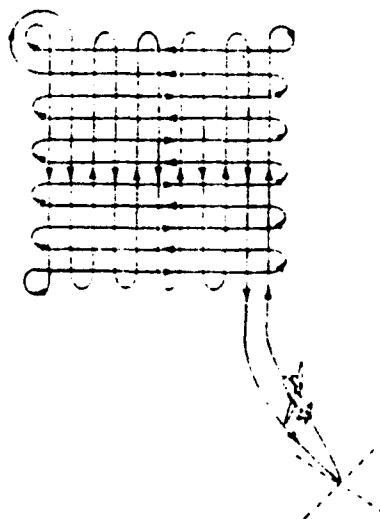
APPLIED SCIENCE ANALYTICS, INC.

7049 OWENSMOUTH AVENUE, CANOGA PARK, CALIFORNIA 91303 • (818) 716-1237

OVERALL DATA PROCESSING SCHEME



DATA COLLECTION DUAL GRID



$\Delta Y_1 = 5 \text{ Km}$

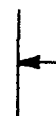


$\Delta X_2 = 1 \text{ Km}$



$\Delta X_1 = 1 \text{ Km}$

$\Delta X_2 = 5 \text{ Km}$



$A = \Delta X_1 (K_1 + 1)$
 $B = \Delta Y_1 (L_1 + 1)$

$A = \Delta X_2 (K_2 + 1)$
 $B = \Delta Y_2 (L_2 + 1)$

APPLIED SCIENCE ANALYTICS, INC.



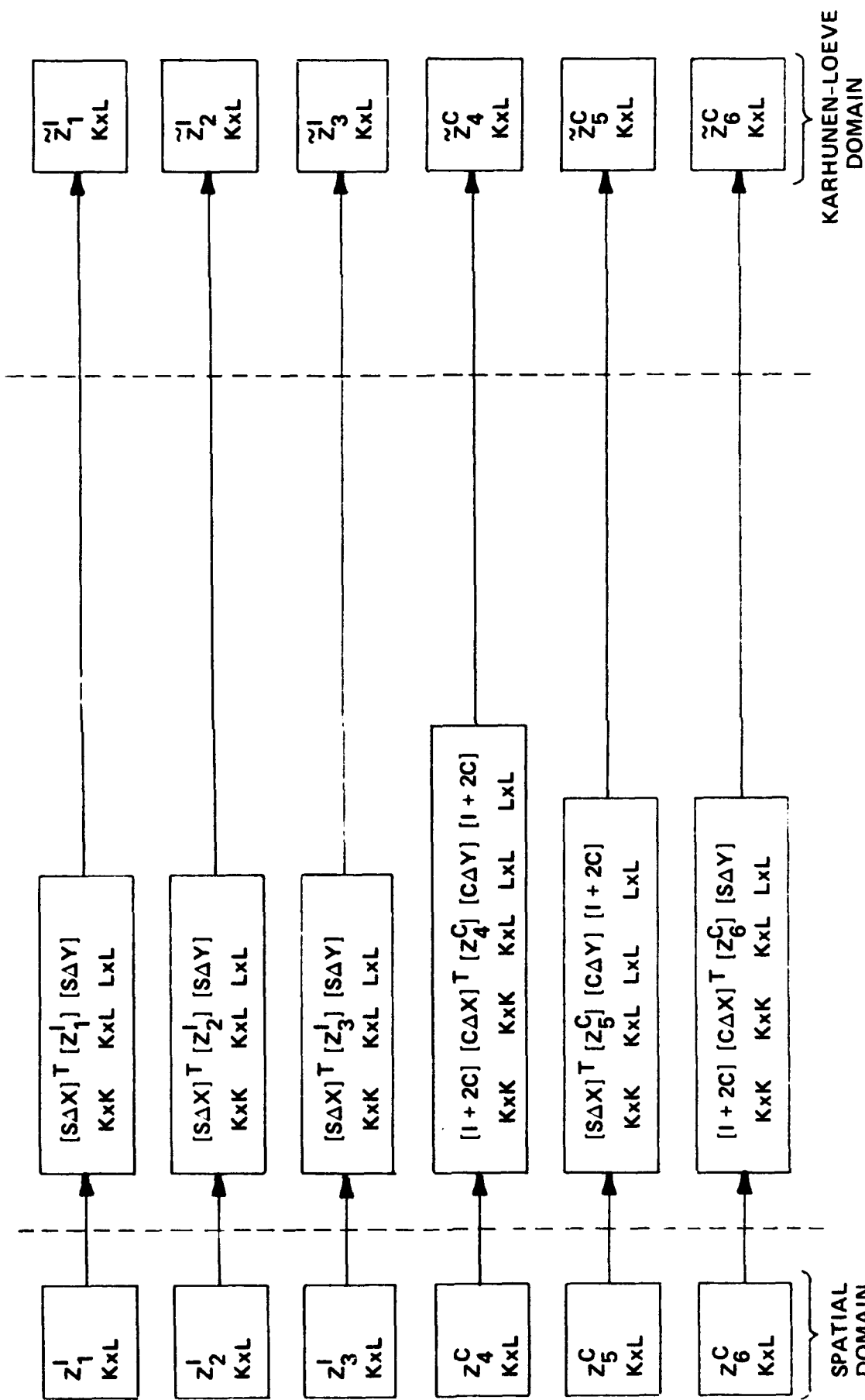
GRADIOMETER INLINE AND CROSSLINE MEASUREMENTS

$$\begin{bmatrix} z_1^I \\ z_2^I \\ z_3^I \\ z_4^C \\ z_5^C \\ z_6^C \end{bmatrix} = \begin{bmatrix} \frac{1}{2} \left(\frac{\partial^2 T}{\partial x^2} - \frac{\partial^2 T}{\partial y^2} \right) \\ \frac{1}{2} \left(\frac{\partial^2 T}{\partial y^2} - \frac{\partial^2 T}{\partial z^2} \right) \\ \frac{1}{2} \left(\frac{\partial^2 T}{\partial z^2} - \frac{\partial^2 T}{\partial x^2} \right) \\ \frac{\partial^2 T}{\partial x \partial y} \\ \frac{\partial^2 T}{\partial y \partial z} \\ \frac{\partial^2 T}{\partial z \partial x} \end{bmatrix} + \begin{bmatrix} \nu_1 \\ \nu_2 \\ \nu_3 \\ \nu_4 \\ \nu_5 \\ \nu_6 \end{bmatrix}$$

MEASUREMENT
SIGNAL
NOISE



TRANSFORMATION FROM SPATIAL DOMAIN TO KARHUNEN-LOEVE DOMAIN



APPLIED SCIENCE ANALYTICS, INC.



DEFINITION OF TRANSFORMATION MATRICES

$$[S\Delta X] = \begin{bmatrix} \sin \pi (1x1) \frac{\Delta X}{A} & \sin \pi (1x2) \frac{\Delta X}{A} & \dots\dots\dots \sin \pi (1xK) \frac{\Delta X}{A} \\ \sin \pi (2x1) \frac{\Delta X}{A} & \sin \pi (2x2) \frac{\Delta X}{A} & \dots\dots\dots \sin \pi (2xK) \frac{\Delta X}{A} \\ \vdots & \vdots & \vdots \\ \sin \pi (Kx1) \frac{\Delta X}{A} & \sin \pi (Kx2) \frac{\Delta X}{A} & \dots\dots\dots \sin \pi (KxK) \frac{\Delta X}{A} \end{bmatrix}$$

$$[S\Delta X(i,j)] = \sin \pi (ixj) \frac{\Delta X}{A} ; [C\Delta X(i,j)] = \cos \pi (ixj) \frac{\Delta X}{A}$$

$$[S\Delta Y(i,j)] = \sin \pi (ixj) \frac{\Delta Y}{B} ; [C\Delta Y(i,j)] = \cos \pi (ixj) \frac{\Delta Y}{B}$$



UTILIZATION OF SPECIAL PROPERTIES OF A TOEPLITZ CIRCULANT MATRIX

$$\begin{bmatrix} [S\Delta X] \\ K \times K \end{bmatrix}^T \begin{bmatrix} [S\Delta X] \\ K \times K \end{bmatrix} = \frac{K+1}{2} [I] \quad K \times K$$

$$\begin{bmatrix} [C\Delta X] \\ K \times K \end{bmatrix}^T \begin{bmatrix} [C\Delta X] \\ K \times K \end{bmatrix} = \frac{K+1}{2} [I] - [C] \quad K \times K \quad K \times K$$

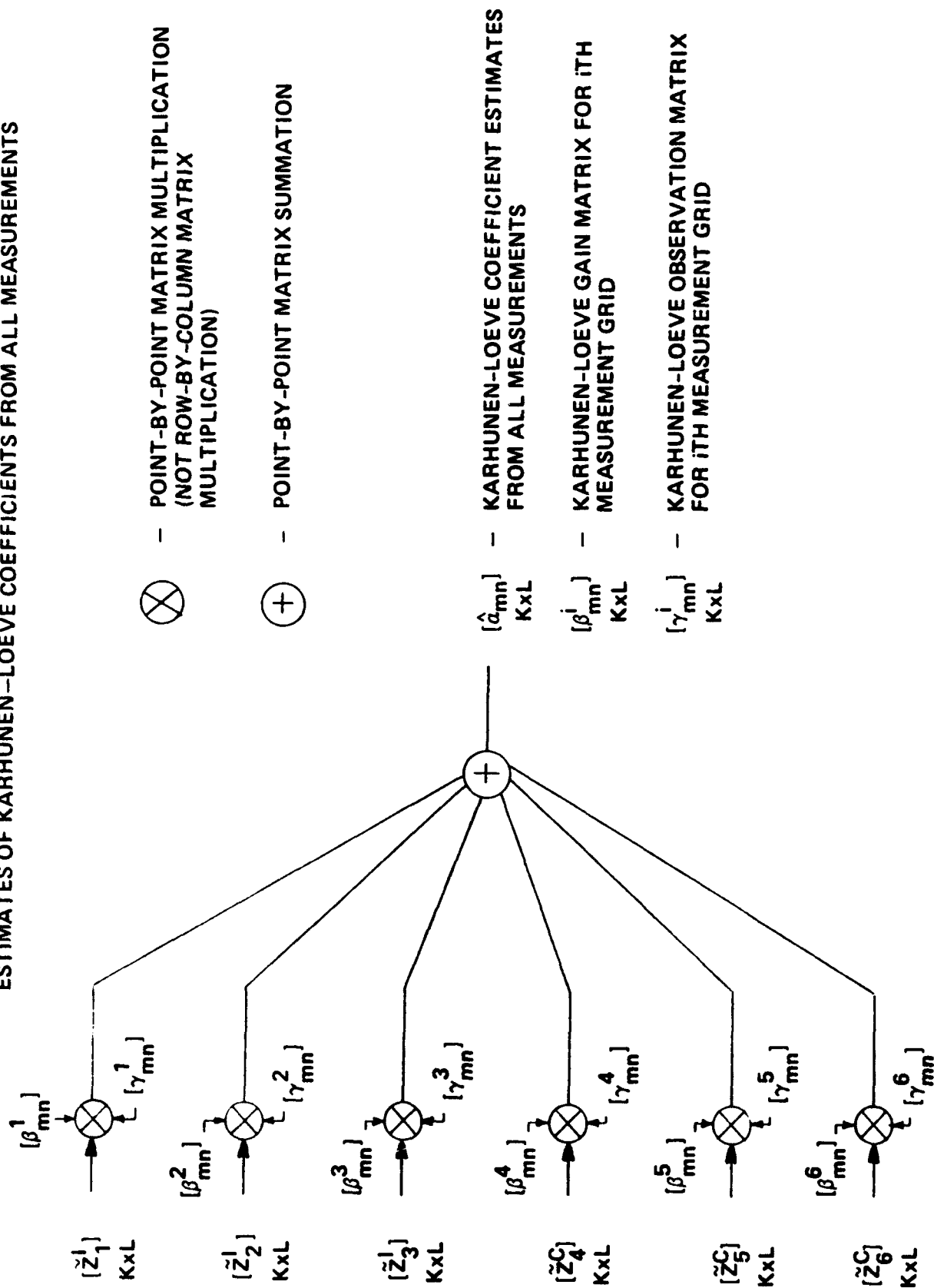
$$\left(\frac{K+1}{2} [I] - [C] \right)^{-1} = \frac{2}{K+1} ([I] + 2 [C]) \quad ; \quad K - \text{even}$$

$$([S\Delta X]^T [S\Delta X])^{-1} = \frac{2}{K+1} [I]$$

$$([C\Delta X]^T [C\Delta X])^{-1} = \frac{2}{K+1} ([I] + 2 [C])$$

$$[I] = \begin{bmatrix} 1 & 0 & 0 & 0 \\ 0 & 1 & 0 & 0 \\ 0 & 0 & 1 & 0 \\ 0 & 0 & 0 & 1 \end{bmatrix} \quad ; \quad [C] = \begin{bmatrix} 1 & 0 & 1 & 0 \\ 0 & 1 & 0 & 1 \\ 1 & 0 & 1 & 0 \\ 0 & 1 & 0 & 1 \end{bmatrix}$$

ESTIMATES OF KARHUNEN-LOEVE COEFFICIENTS FROM ALL MEASUREMENTS

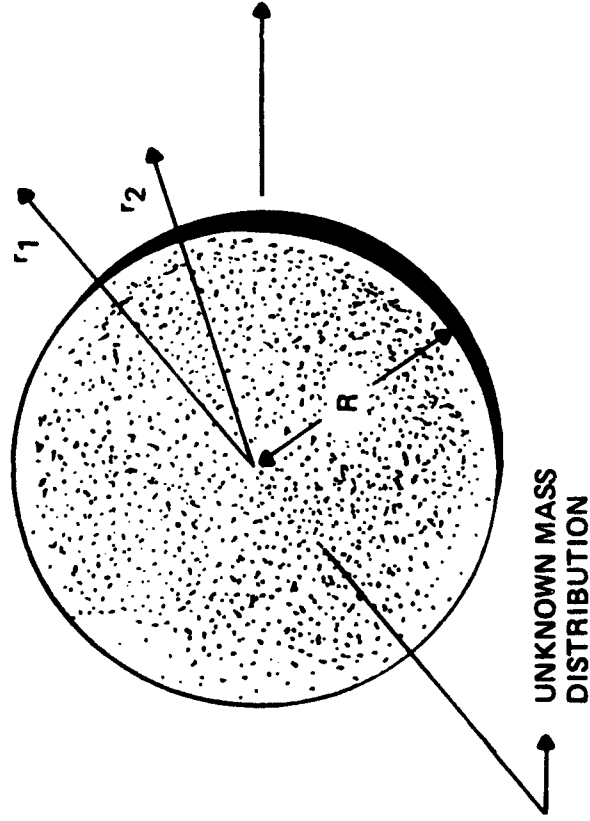


APPLIED SCIENCE ANALYTICS, INC.

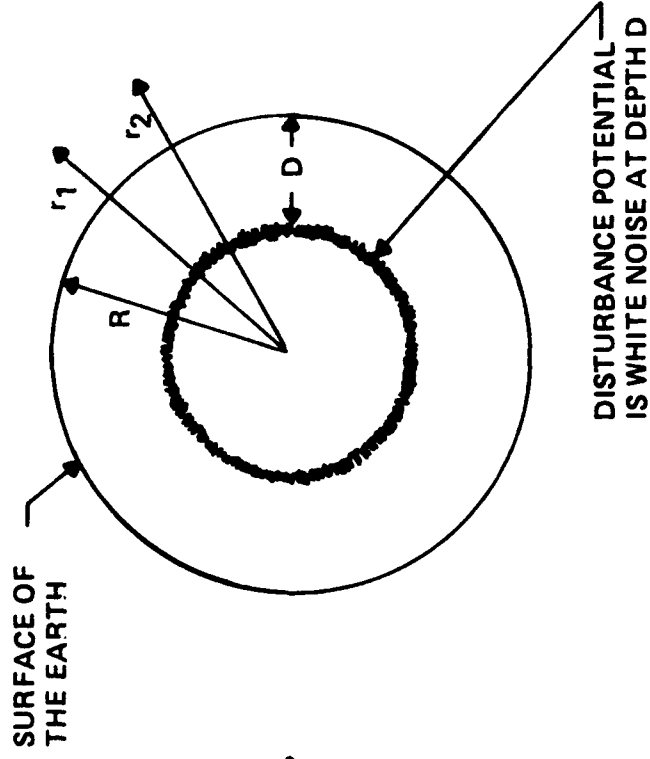


ATTENUATED WHITE NOISE MODEL

PHYSICAL PHENOMENA



MATHEMATICAL MODEL



$$\nabla^2 T = 0 \quad ; \quad r > R$$

$$\nabla^2 T = \rho \quad ; \quad r < R$$

$$T \rightarrow 0 \quad ; \quad r \rightarrow +\infty$$

$$\nabla^2 T = 0 \quad ; \quad r > 0$$

$$E \left\{ T(r, \theta_1, \phi_1) T(r, \theta_2, \phi_2) \right\} = \sigma^2 \delta(\theta_1 - \theta_2) \delta(\phi_1 - \phi_2) \quad ; \quad r = D$$

$$@ r = D \quad @ r = D$$

$$T \rightarrow 0 \quad ; \quad r \rightarrow \infty$$

LINEAR SUPERPOSITION SOLUTION OF DISTURBANCE POTENTIAL

$$T = T_p + T_c$$

- PARTICULAR SOLUTION - T_p

- LAPLACE'S EQUATION

$$\nabla^2 T_p = 0$$

- NON-ZERO SOURCES

$$E \left\{ \frac{\partial^k T_p}{\partial z^k} (x_1, y_1, z) \right\} \times \frac{\partial^k T_p}{\partial z^k} (x_2, y_2, z) \Bigg|_{@ z=-D}^{@ z=-D} = \sigma_0^2 \delta(x_1-x_2) \delta(y_1-y_2)$$

$$0 < x_1, x_2 < A$$

$$0 < y_1, y_2 < B$$

$$z = -D$$

- ZERO BOUNDARY CONDITIONS

$$T(x=0, y, z) = 0$$

$$T(x=A, y, z) = 0$$

$$T(x, y=0, z) = 0$$

$$T(x, y=B, z) = 0$$

$$T(x, y, z = \pm \infty) = 0$$

- COMPLEMENTARY SOLUTION - T_c

- LAPLACE'S EQUATION

$$\nabla^2 T_c = 0$$

- ZERO SOURCES

$$T_c = 0$$

$$0 < x < A$$

$$0 < y < B$$

$$-\infty < z < +\infty$$

- NON-ZERO BOUNDARY CONDITIONS

$$T(x, y=0, z) = f_1(x)$$

$$T(x, y=B, z) = f_2(x)$$

$$T(x=0, y, z) = g_1(y)$$

$$T(x=A, y, z) = g_2(y)$$

$$T(x, y, z = \pm \infty) = 0$$



APPLIED SCIENCE ANALYTICS, INC.

KARHUNEN-LOEVE SERIES REPRESENTATION FOR THE DISTURBANCE POTENTIAL PARTICULAR SOLUTION

- ORTHONORMAL SERIES SOLUTION OF DISTURBANCE POTENTIAL

$$T(x,y,z) = \frac{2}{\sqrt{AB}} \sum_{m=1}^{\infty} \sum_{n=1}^{\infty} a_{mn} \sin(a_m x) \sin(b_n y) e^{-c_{mn}} e^{-D} |z-D|$$

$$a_m = \frac{m\pi}{A} ; b_n = \frac{n\pi}{B} ; c_{mn} = (a_m^2 + b_n^2)^{1/2}$$

- UNCORRELATEDNESS OF EXPANSION COEFFICIENTS

$$E \left\{ a_{mn} a_{m'n'} \right\} = \lambda_{mn} \delta_{mm'} \delta_{nn'}$$

- 2D WHITE NOISE MODEL FOR kth VERTICAL DERIVATIVE OF DISTURBANCE POTENTIAL

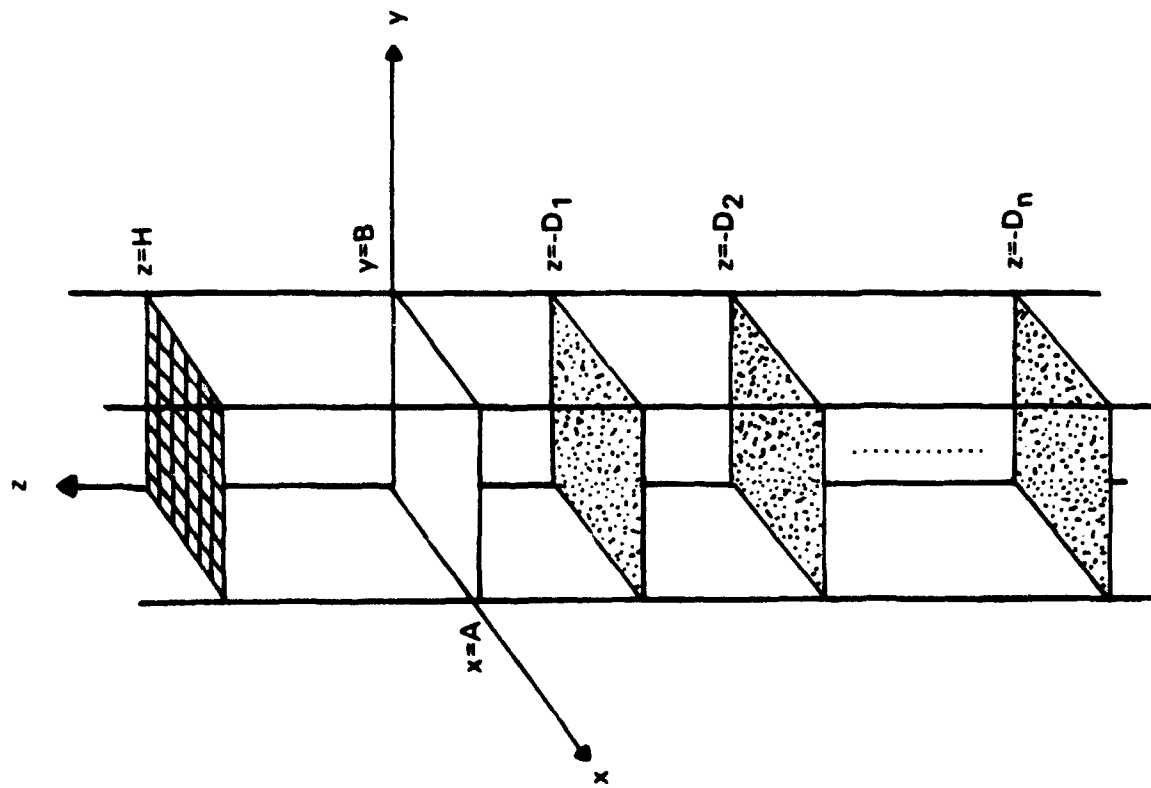
$$\lambda_{mn} = \frac{\sigma_0^2 e^{4D c_{mn}}}{2k c_{mn}}$$

- A - LENGTH OF SURVEY REGION
- B - WIDTH OF SURVEY REGION
- D - DEPTH OF WHITE NOISE LAYER
- σ_0^2 - VARIANCE OF WHITE NOISE
- k - ORDER OF VERTICAL DERIVATIVE OF T
- H - HEIGHT OF SURVEY ABOVE EARTH'S SURFACE



APPLIED SCIENCE ANALYTICS, INC.

EXTENSION TO MULTIPLE LAYERS



- MODEL CAN ACCOMMODATE MULTIPLE LAYERS OF 2D WHITE NOISE LAYERS
- EACH LAYER CAN MODEL THE VERTICAL DERIVATIVE OF THE DISTURBANCE POTENTIAL TO ANY ORDER

NON-ISOTROPIC, NON-STATIONARY DISTURBANCE POTENTIAL COVARIANCE

$$\begin{aligned}
 R_{TT}(x_1, y_1, z_1; x_2, y_2, z_2) &= E \left\{ T(x_1, y_1, z_1) T(x_2, y_2, z_2) \right\} \\
 &= \frac{4}{AB} \sum_{m=1}^{\infty} \sum_{n=1}^{\infty} \lambda_{mn} \sin(a_m x_1) \sin(b_n y_1) \sin(a_m x_2) \sin(b_n y_2) \times \\
 &\quad \exp \left[-c_{mn}(z_1 + z_2 - 2D) \right] \quad ; \quad \begin{aligned} &0 < x_1, x_2 < A \\ &0 < y_1, y_2 < B \\ &D < z_1, z_2 < +\infty \end{aligned}
 \end{aligned}$$

DEFINITION OF BASIS FUNCTIONS

$$\begin{aligned}
 & \left[\begin{array}{c} z_1^I \\ z_2^I \\ z_3^I \\ z_3^C \\ z_b^C \\ z_b^C \end{array} \right] = \sum_{m=1}^{\infty} \sum_{n=1}^{\infty} a_{mn} \left[\begin{array}{c} \frac{1}{2} \left(\frac{\partial^2 T}{\partial x^2} - \frac{\partial^2 T}{\partial y^2} \right) \\ \frac{1}{2} \left(\frac{\partial^2 T}{\partial y^2} - \frac{\partial^2 T}{\partial z^2} \right) \\ \frac{1}{2} \left(\frac{\partial^2 T}{\partial z^2} - \frac{\partial^2 T}{\partial x^2} \right) \\ \frac{\partial^2 T}{\partial x \partial y} \\ \frac{\partial^2 T}{\partial y \partial z} \\ \frac{\partial^2 T}{\partial z \partial x} \end{array} \right] \\
 & = \sum_{m=1}^{\infty} \sum_{n=1}^{\infty} a_{mn} \left[\begin{array}{c} \sin a_m x \sin b_n y \left\{ \frac{-1}{AB} (a_m^2 - b_n^2) e^{-c_{mn}} |H-D| \right\} \gamma_{mn}^{m1} \\ \sin a_m x \sin b_n y \left\{ \frac{-1}{AB} (c_{mn}^2 + b_n^2) e^{-c_{mn}} |H-D| \right\} \gamma_{mn}^{m2} \\ \sin a_m x \sin b_n y \left\{ \frac{-1}{AB} (c_{mn}^2 + a_m^2) e^{-c_{mn}} |H-D| \right\} \gamma_{mn}^{m3} \\ \cos a_m x \cos b_n y \left\{ \frac{2}{AB} a_m b_n e^{-c_{mn}} |H-D| \right\} \gamma_{mn}^{m4} \\ \sin a_m x \cos b_n y \left\{ \frac{-2 \operatorname{sgn}(H-D)}{AB} b_n c_{mn} e^{-c_{mn}} |H-D| \right\} \gamma_{mn}^{m5} \\ \cos a_m x \sin b_n y \left\{ \frac{-2 \operatorname{sgn}(H-D)}{AB} a_m c_{mn} e^{-c_{mn}} |H-D| \right\} \gamma_{mn}^{m6} \end{array} \right]
 \end{aligned}$$

$$\sum_{m=1}^{\infty} \sum_{n=1}^6 \sum_{i=1}^{\infty} a_{mn} \psi_{mn}^i = \sum_{m=1}^{\infty} \sum_{n=1}^{\infty} a_{mn} \psi_{mn}$$

APPLIED SCIENCE ANALYTICS, INC.



ORTHOGONALITY OF BASIS FUNCTIONS

$$\int_{x=0}^{x=A} \int_{y=0}^{y=B} \psi_{mn}^T(x,y,z) \psi_{m'n'}(x,y,z) dx dy = \frac{AB}{4} \sum_{i=1}^6 \gamma_{mn}^i \gamma_{m'n'}^i \delta_{mm'} \delta_{nn'}$$

$$\psi_{mn}(x,y,z) = \sum_{i=1}^6 \psi_{mni}(x,y,z)$$

$$\int_{x=0}^{x=A} \int_{y=0}^{y=B} \psi_{mni}^T(x,y,z) \psi_{m'n'}(x,y,z) dx dy = \frac{AB}{4} \gamma_{mn}^i \gamma_{m'n'}^i \delta_{mm'} \delta_{nn'} \delta_{ij}$$

THE TWO-DIMENSIONAL SMOOTHING ALGORITHM

- LINEAR MEAN SQUARE ESTIMATION CRITERION

$$J = E \left\{ \left| a_{mn} - \hat{a}_{mn} \right|^2 \right\}$$

- OPTIMAL ESTIMATE USING ALL MEASUREMENTS

$$\hat{a}_{mn} = E \left\{ a_{mn} / Z(x, y, z) \right\} ; \quad 0 < x < A, 0 < y < B, z = H \}$$

- LINEAR ESTIMATOR FOR KARHUNEN-LOEVE COEFFICIENTS

$$\hat{a}_{mn} = \int_{x=0}^{x=A} \int_{y=0}^{y=B} Z^T(x, y, H) K_{mn}(x, y, H) dx dy$$

- ORTHOGONAL BASIS FUNCTION REPRESENTATION OF GAINS

$$K_{mn}(x, y, H) = \sum_{m'=1}^{\infty} \sum_{n'=1}^5 \beta_{m'n'}^{mi} \psi_{m'n'}^i(x, y, H)$$



APPLIED SCIENCE ANALYTICS, INC.

DERIVATION OF ESTIMATOR GAINS

- MEASUREMENT NOISE AND SIGNAL UNCORRELATED

$$E \left\{ V(x_1, y_1, z_1) S^T(x_2, y_2, z_2) \right\} = 0 \Rightarrow E \left\{ V(x_1, y_1, z_1) a_{mn} \right\} = 0$$

- ORTHOGONALITY PRINCIPLE OF LINEAR MEAN SQUARE ESTIMATION

$$E \left\{ Z(x_1, y_1, H) a_{mn} \right\} = E \left\{ Z(x_1, y_1, H) \hat{a}_{mn} \right\}$$

- INTEGRAL EQUATION FOR ESTIMATOR GAINS

$$\int_{x_2=0}^{x_2=A} \int_{y_2=0}^{y_2=B} [R_{SS}(x_1, y_1, H; x_2, y_2, H) + R_{VV}(x_1, y_1, H; x_2, y_2, H)] K_{mn}(x_2, y_2, H) dx_2 dy_2 = \lambda_{mn} \psi_{mn}(x_1, y_1, H)$$

- UNIQUE SOLUTION FOR ESTIMATOR GAINS

$$\beta_{mn}^{m'n'i} = \beta_{mn}^i \delta_{mm'} \delta_{nn'}$$

$$K_{mn}(x, y, H) = \sum_{i=1}^6 \beta_{mn}^i \psi_{mn}^i(x, y, H)$$



ESTIMATOR GAINS

- GENERALIZED FORM OF KARHUNEN-LOEVE GAINS

$$\beta_{mn}^i = \frac{\left(\frac{AB}{4}\right) \lambda_{mn} \prod_{\substack{j=1 \\ j \neq i}}^6 \sigma_j^2}{\prod_{i=1}^6 \sigma_i^2 + \left(\frac{AB}{4}\right) \lambda_{mn} \left(\sum_{j=1}^6 \gamma_{mn}^i \prod_{\substack{k=1 \\ k \neq j}}^6 \sigma_k^2 \right)}$$

σ_i — MEASUREMENT NOISE VARIANCE FOR ITH MEASUREMENT GRID

- GAINS FOR EXAMPLE OF TWO (2) MEASUREMENTS, ONE PERFECT ($\sigma_1 = 0, \sigma_2 \neq 0$)

$$\beta_{mn}^1 = \frac{\left(\frac{AB}{4}\right) \lambda_{mn} \sigma_2^2}{\sigma_1^2 \sigma_2^2 + \left(\frac{AB}{4}\right) \lambda_{mn} (\gamma_{mn}^1 \sigma_2^2 + \gamma_{mn}^2 \sigma_1^2)} = \frac{1}{\gamma_{mn}^1} \Rightarrow \text{ACCEPTS PERFECT MEASUREMENT WITH PROPER GAIN TO REPRODUCE SIGNAL}$$

$$\beta_{mn}^2 = \frac{\left(\frac{AB}{4}\right) \lambda_{mn} \sigma_1^2}{\sigma_1^2 \sigma_2^2 + \left(\frac{AB}{4}\right) \lambda_{mn} (\gamma_{mn}^1 \sigma_2^2 + \gamma_{mn}^2 \sigma_1^2)} = 0 \Rightarrow \text{REJECTS IMPERFECT MEASUREMENT}$$



APPLIED SCIENCE ANALYTICS, INC.

FORMULATION OF MEASUREMENT INTEGRALS

$$\hat{a}_{mn} = \gamma_{mn}^1 \beta_{mn}^1 \tilde{Z}_1 + \gamma_{mn}^2 \beta_{mn}^2 \tilde{Z}_2 + \gamma_{mn}^3 \beta_{mn}^3 \tilde{Z}_3 + \gamma_{mn}^4 \beta_{mn}^4 \tilde{Z}_4 + \gamma_{mn}^5 \beta_{mn}^5 \tilde{Z}_5 + \gamma_{mn}^6 \beta_{mn}^6 \tilde{Z}_6$$

$$\tilde{Z}_1 = \int_{x=0}^{x=A} \int_{y=0}^{y=B} Z_1(x,y) \sin(a_m x) \sin(b_n y) dx dy$$

$$\tilde{Z}_2 = \int_{x=0}^{x=A} \int_{y=0}^{y=B} Z_2(x,y) \sin(a_m x) \sin(b_n y) dx dy$$

$$\tilde{Z}_3 = \int_{x=0}^{x=A} \int_{y=0}^{y=B} Z_3(x,y) \sin(a_m x) \sin(b_n y) dx dy$$

$$\tilde{Z}_4 = \int_{x=0}^{x=A} \int_{y=B}^{y=B} Z_4(x,y) \cos(a_m x) \cos(b_n y) dx dy$$

$$\tilde{Z}_5 = \int_{x=0}^{x=A} \int_{y=0}^{y=B} Z_5(x,y) \sin(a_m x) \cos(b_n y) dx dy$$

$$\tilde{Z}_6 = \int_{x=0}^{x=A} \int_{y=0}^{y=B} Z_6(x,y) \cos(a_m x) \sin(b_n y) dx dy$$



APPLICATION OF FOURIER TRANSFORMS

$$Z_1(x,y) = \frac{4}{AB} \sum_{m=1}^{\infty} \sum_{n=1}^{\infty} \tilde{Z}_1(m,n) \sin(a_m x) \sin(b_n y)$$

$$Z_2(x,y) = \frac{4}{AB} \sum_{m=1}^{\infty} \sum_{n=1}^{\infty} \tilde{Z}_2(m,n) \sin(a_m x) \sin(b_n y)$$

$$Z_3(x,y) = \frac{4}{AB} \sum_{m=1}^{\infty} \sum_{n=1}^{\infty} \tilde{Z}_3(m,n) \sin(a_m x) \sin(b_n y)$$

$$Z_4(x,y) = \frac{4}{AB} \sum_{m=1}^{\infty} \sum_{n=1}^{\infty} \tilde{Z}_4(m,n) \cos(a_m x) \cos(b_n y)$$

$$Z_5(x,y) = \frac{4}{AB} \sum_{m=1}^{\infty} \sum_{n=1}^{\infty} \tilde{Z}_5(m,n) \sin(a_m x) \cos(b_n y)$$

$$Z_6(x,y) = \frac{4}{AB} \sum_{m=1}^{\infty} \sum_{n=1}^{\infty} \tilde{Z}_6(m,n) \cos(a_m x) \sin(b_n y)$$



APPLIED SCIENCE ANALYTICS, INC.

MATRIX FORMULATION FOR 2D DISCRETE MEASUREMENTS

$$\begin{matrix} [Z_1^1] \\ K \times L \end{matrix} = \frac{4}{AB} \begin{matrix} [S \Delta X] & [\tilde{Z}_1^1] & [S \Delta Y]^T \\ K \times M & M \times N & N \times L \end{matrix}$$

$$\begin{matrix} [Z_2^1] \\ K \times L \end{matrix} = \frac{4}{AB} \begin{matrix} [S \Delta X] & [\tilde{Z}_2^1] & [S \Delta Y]^T \\ K \times M & M \times N & N \times L \end{matrix}$$

$$\begin{matrix} [Z_3^1] \\ K \times L \end{matrix} = \frac{4}{AB} \begin{matrix} [S \Delta X] & [\tilde{Z}_3^1] & [S \Delta Y]^T \\ K \times M & M \times N & N \times L \end{matrix}$$

$$\begin{matrix} [Z_4^C] \\ K \times L \end{matrix} = \frac{4}{AB} \begin{matrix} [C \Delta X] & [\tilde{Z}_4^C] & [C \Delta Y]^T \\ K \times M & M \times N & N \times L \end{matrix}$$

$$\begin{matrix} [Z_5^C] \\ K \times L \end{matrix} = \frac{4}{AB} \begin{matrix} [S \Delta X] & [\tilde{Z}_5^C] & [C \Delta Y]^T \\ K \times M & M \times N & N \times L \end{matrix}$$

$$\begin{matrix} [Z_6^C] \\ K \times L \end{matrix} = \frac{4}{AB} \begin{matrix} [C \Delta X] & [\tilde{Z}_6^C] & [S \Delta Y]^T \\ K \times M & M \times N & N \times L \end{matrix}$$

- K, L – NO. OF MEASUREMENTS IN x,y PLANE
- M, N – NO. OF COEFFICIENTS IN K-L SPACE
- M = K, N = L FOR SQUARE MATRIX



BRUTE FORCE APPROACH USING MATRIX INVERSIONS

$$[\tilde{Z}_1^I] = \frac{AB}{4} [S_{\Delta X}]^{-1} [Z_1^I] [S_{\Delta Y}]^{-1}$$

$$[\tilde{Z}_2^I] = \frac{AB}{4} [S_{\Delta X}]^{-1} [Z_2^I] [S_{\Delta Y}]^{-1}$$

$$[\tilde{Z}_3^I] = \frac{AB}{4} [S_{\Delta X}]^{-1} [Z_3^I] [S_{\Delta Y}]^{-1}$$

$$[\tilde{Z}_4^C] = \frac{AB}{4} [C_{\Delta X}]^{-1} [Z_4^C] [C_{\Delta Y}]^{-1}$$

$$[\tilde{Z}_5^C] = \frac{AB}{4} [S_{\Delta X}]^{-1} [Z_5^C] [C_{\Delta Y}]^{-1}$$

$$[\tilde{Z}_6^C] = \frac{AB}{4} [C_{\Delta X}]^{-1} [Z_6^C] [S_{\Delta Y}]^{-1}$$



APPLIED SCIENCE ANALYTICS, INC.

GRAVITY VECTOR EXPRESSED IN TERMS OF K-L COEFFICIENT ESTIMATES

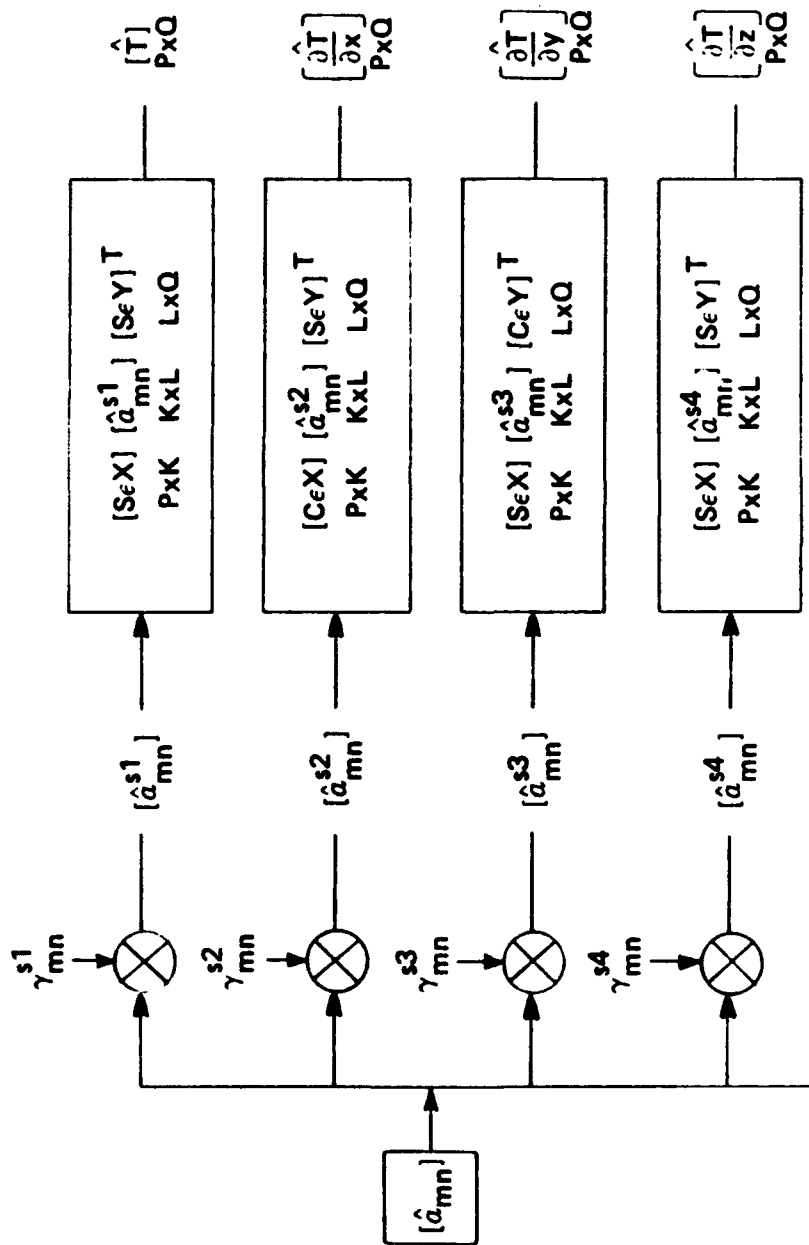
$$\begin{aligned}
 & \begin{bmatrix} \hat{T}(x,y,h) \\ \frac{\partial \hat{T}}{\partial x}(x,y,h) \\ \frac{\partial \hat{T}}{\partial y}(x,y,h) \\ \frac{\partial \hat{T}}{\partial z}(x,y,h) \end{bmatrix} \\
 &= \sum_{m=1}^{\infty} \sum_{n=1}^{\infty} \hat{a}_{mn} \\
 & \begin{bmatrix} \sin a_m x \sin b_n y \left\{ \frac{2}{\sqrt{AB}} e^{-c_{mn}} |h-D| \right\} \gamma_{mn}^{s1} \\ \cos a_m x \sin b_n y \left\{ \frac{2}{\sqrt{AB}} a_m e^{-c_{mn}} |h-D| \right\} \gamma_{mn}^{s2} \\ \sin a_m x \cos b_n y \left\{ \frac{2}{\sqrt{AB}} b_n e^{-c_{mn}} |h-D| \right\} \gamma_{mn}^{s3} \\ \sin a_m x \sin b_n y \left\{ \frac{-2 \operatorname{sgn}(h-D)}{\sqrt{AB}} c_{mn} e^{-c_{mn}} |h-D| \right\} \gamma_{mn}^{s4} \end{bmatrix}
 \end{aligned}$$



GRAVITY GRADIENTS EXPRESSED IN TERMS OF K-L COEFFICIENT ESTIMATES

$$\begin{aligned}
 & \left[\begin{array}{l} \frac{\partial^2 T}{\partial x^2}(x,y,h) \\ \frac{\partial^2 T}{\partial y^2}(x,y,h) \\ \frac{\partial^2 T}{\partial z^2}(x,y,h) \\ \frac{\partial^2 T}{\partial x \partial y}(x,y,h) \\ \frac{\partial^2 T}{\partial y \partial z}(x,y,h) \\ \frac{\partial^2 T}{\partial z \partial x}(x,y,h) \end{array} \right] \\
 &= \sum_{m=1}^{\infty} \sum_{n=1}^{\infty} \hat{a}_{mn} \left[\begin{array}{l} \sin a_m x \sin b_n y \left\{ \frac{-2}{\sqrt{AB}} a_m^2 e^{-c_{mn}} |h-D| \right\} s5 \\ \sin a_m x \sin b_n y \left\{ \frac{-2}{\sqrt{AB}} b_n^2 e^{-c_{mn}} |h-D| \right\} s6 \\ \sin a_m x \sin b_n y \left\{ \frac{2}{\sqrt{AB}} c_{mn}^2 e^{-c_{mn}} |h-D| \right\} s7 \\ \cos a_m x \cos b_n y \left\{ \frac{2}{\sqrt{AB}} a_m b_n e^{-c_{mn}} |h-D| \right\} s8 \\ \sin a_m x \cos b_n y \left\{ \frac{-2 \operatorname{sgn}(h-D)}{\sqrt{AB}} b_n c_{mn} e^{-c_{mn}} |h-D| \right\} s9 \\ \cos a_m x \sin b_n y \left\{ \frac{-2 \operatorname{sgn}(h-D)}{\sqrt{AB}} a_m c_{mn} e^{-c_{mn}} |h-D| \right\} s10 \end{array} \right] \gamma_{mn}
 \end{aligned}$$

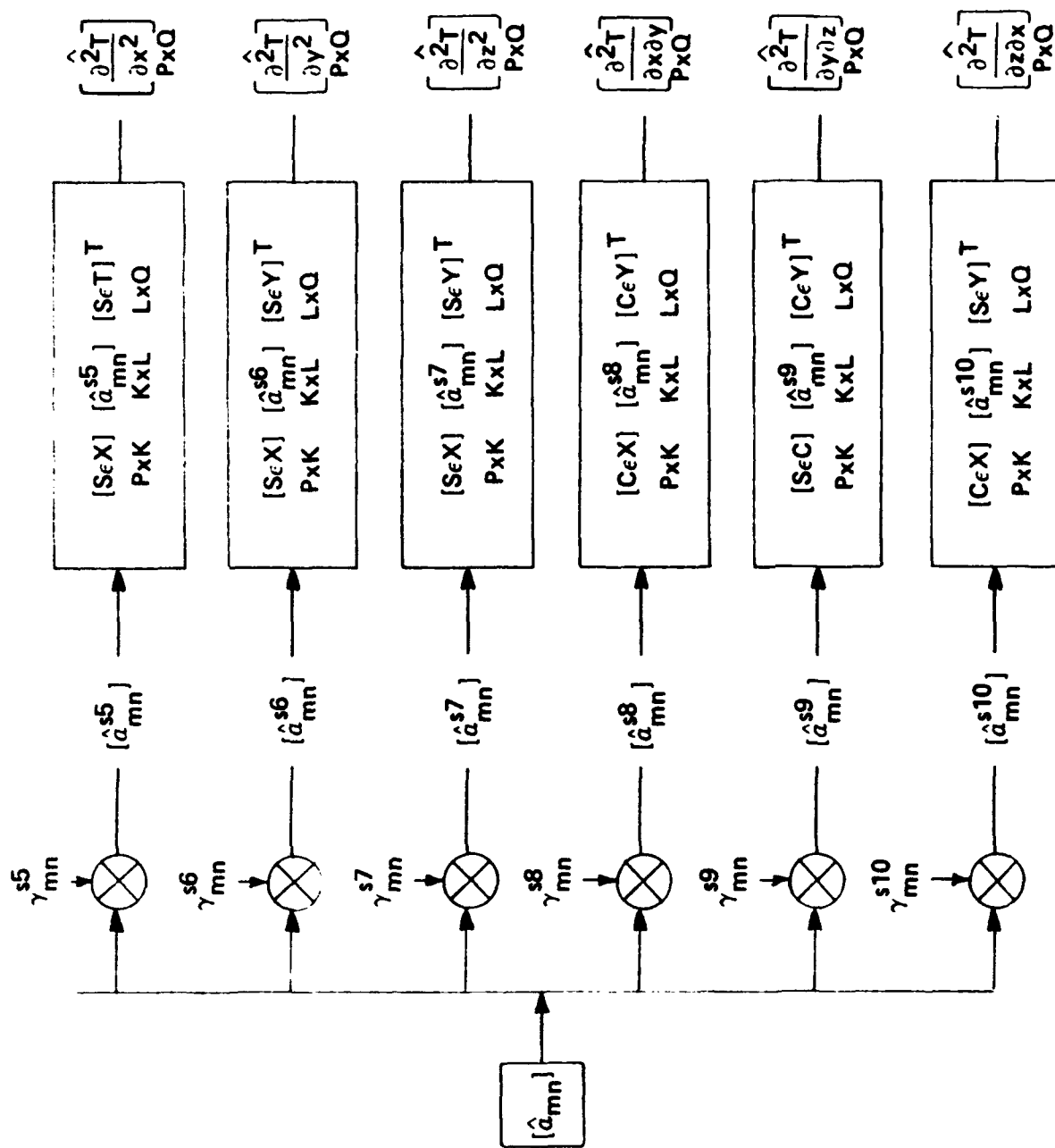
INTERPOLATED AND DOWNWARD CONTINUED 2D GRID ESTIMATES OF GRAVITY VECTOR



$$A = \epsilon X(P+1), B = \epsilon Y(Q+1)$$

$$\epsilon X < \Delta X \quad \epsilon Y < \Delta Y$$

INTERPOLATED AND DOWNWARD CONTINUED 2D GRID ESTIMATES OF GRAVITY GRADIENTS



SUMMARY

- THE MODEL IS DERIVED FROM THE PHYSICAL THEORY OF GEODESY AND IS NOT BASED UPON EMPIRICAL ASSUMPTIONS OF CORRELATION FUNCTIONS OR POWER SPECTRAL DENSITIES
- MODEL CAN ACCOMMODATE MULTIPLE TWO-DIMENSIONAL WHITE NOISE LAYERS BELOW THE SURFACE OF THE EARTH
- EACH LAYER CAN MODEL THE VERTICAL DERIVATIVE OF THE DISTURBANCE POTENTIAL TO ANY ORDER
- NON-ZERO BOUNDARY VALUES FOR THE DISTURBANCE POTENTIAL ON THE EXTERIOR OF THE SURVEY REGION PERMITTED
- THE MODEL IS SUCH THAT AT ANY GIVEN SPATIAL POINT THE GRAVITY FIELD'S CORRELATION WITH NEIGHBORING POINTS IS PRESERVED AND CORRELATION IN ANY DIRECTION IS NOT IGNORED
- THE ESTIMATION ALGORITHM DOES NOT ENFORCE ANY UNNECESSARY LIMITATION OF CAUSALITY ON THE DATA INASMUCH AS NO ONE-DIMENSIONAL SCANNING IS PERFORMED
- EACH COEFFICIENT IN THE SERIES EXPANSION FOR THE GRAVITY FIELD IS ESTIMATED USING ALL THE MULTI-SENSOR DATA SIMULTANEOUSLY
- THE ESTIMATION ALGORITHM CAN HANDLE MULTISENSOR DATA GIVEN IN TWO-DIMENSIONAL GRIDS AT THE SAME OR DIFFERENT ALTITUDES ON OR ABOVE THE SURFACE OF THE EARTH
- DOWNWARD CONTINUATION OF THE GRAVITY FIELD FROM MEASUREMENTS ABOVE THE SURFACE OF THE EARTH IS AUTOMATICALLY DONE WITHOUT ANY LOSS OF ACCURACY
- INTERPOLATION OF ESTIMATES BETWEEN GRID MEASUREMENTS PERFORMED AUTOMATICALLY
- DIFFERENT APRIORI ACCURACIES CAN BE ASSIGNED TO MEASUREMENTS FROM DIFFERENT SENSORS
- CORRELATED NOISE SOURCES CAN BE ACCOMMODATED TO THE EXTENT THAT THEY CAN BE REPRESENTED BY THE BASIS FUNCTIONS
- ESTIMATION ALGORITHM REQUIRES NO MATRIX INVERSIONS
- MEASUREMENT DATA MUST BE IN PLANAR GRIDDED FORM

PAPER TITLE: KARHUNEN-LOEVE GRAVITY GRADIOMETER DATA PROCESSING

SPEAKERS NAME: Sam Bose

Questions and Comments:

John V. Breakwell: Aren't you, in effect, assuming that your finite gravitational ground pattern is repeated (to infinity in all 4 directions)?

SPEAKERS RESPONSE: No

Julian Center: 1. Why are there only sine terms in the K-H expansion for the potential?
2. How does your method differ from the Fourier-Transform/ Wiener Smoother Method?

SPEAKERS RESPONSE: 1. Only sine terms in representation of T because the solution of T was with zero boundary conditions; contributions from non-zero boundary conditions can be linearly superimposed.

2. The method is general such that any choice of basis functions can be used. Also the Karhunen-Loeve condition is imposed. There are also no matrix inversions. Fourier transform techniques deal with stationary processes whereas this method results in non-stationary nonisotropic covariance of the gravity field.

GRAVITY GRADIOMETER (GGSS) TEST PLANNING AND
TEST DATA TREATMENT

W. G. Heller

The Analytic Sciences Corporation

One Jacob Way

Reading, MA 01867

ABSTRACT

Data reduction from an airborne gravity gradiometer survey system (GGSS) has been long recognized as a challenging problem. The difficulty arises because of the large amount of gradient data required to estimate gravity disturbances at the surface. The work reported here decomposes the airborne survey data reduction problem into a track-by-track treatment which is both optimal in a least squares sense and utilizes surface gravity vector tie-point data. For low altitude GGSS surveys (circa 600m), it is shown that the upward and downward continuation portions of the reduction process can be effectively accomplished with few data points (e.g. less than 10) and that track-by-track processing in a template zone format is near optimal. In this case, near-optimal indicates that processing algorithm-induced errors are less than 0.2 mgal/0.04 arcsec. Synthetic airborne GGSS data from a gravity field realization typical of the Clinton-Sherman test area is reduced. Gravity vector estimation results indicate that surface recovery at an accuracy near 1.0 mgal/0.2 arcsecond can be expected from a $100 \text{ E}^2/\text{Hz}$ ($30 \text{ E}^2/\text{r}/\text{sec}$) GGSS. Quantification of the relative information contents of each track of gradiometer data, as determined by the gradiometer noise, vs the predictability of the gravity field along a track, based on its correlation characteristics only (i.e. in the absence of gradient data), leads to further simplification in the data reduction process. In particular, for a gravity field typical of the Clinton-Sherman test area, a statistical gravity model can be dropped from the GGSS data reduction process without penalty if the GGSS errors are less than about $300 \text{ E}^2/\text{Hz}$.

SP-4423-29

**GRAVITY GRADIOMETER
(GGSS) TEST PLANNING
AND TEST DATA TREATMENT**

11-12 February 1986

Prepared for:

FOURTEENTH MOVING BASE GRAVITY GRADIOMETER REVIEW
United State Air Force Academy
Colorado

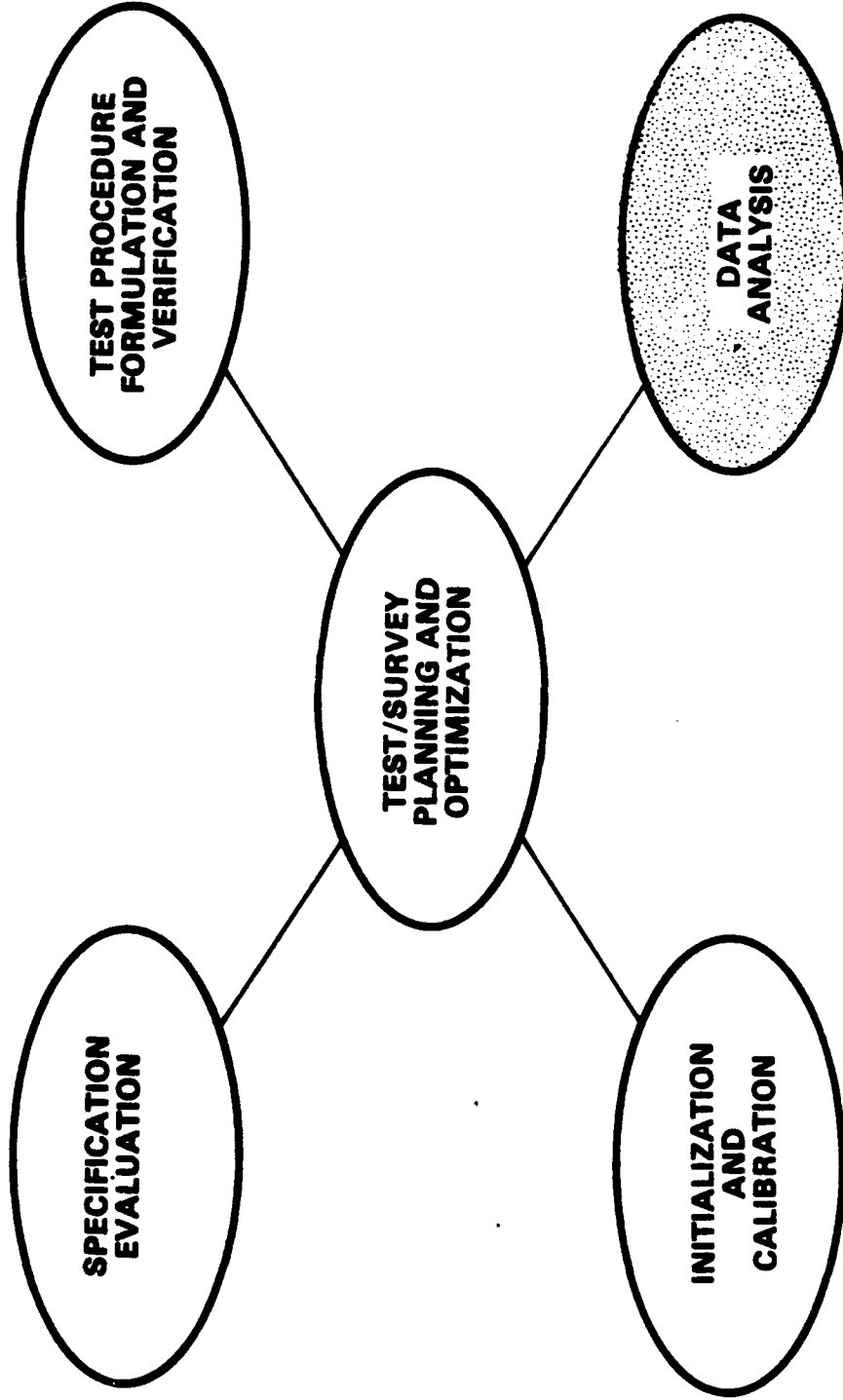
Prepared by:

W.G. Heller

THE ANALYTIC SCIENCES CORPORATION
One Jacob Way
Reading, Massachusetts 01867

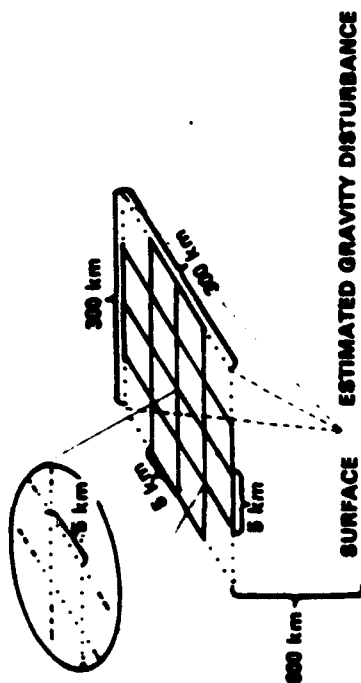
TASC'S ACTIVITIES IN THE GGSS DEVELOPMENT PROGRAM

A-34425

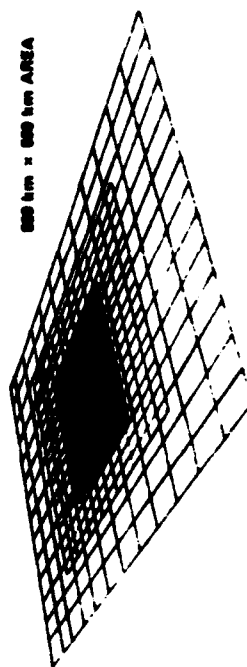


AIRBORNE GGSS DATA REDUCTION — AS OF FEBRUARY 1985

KNOWN

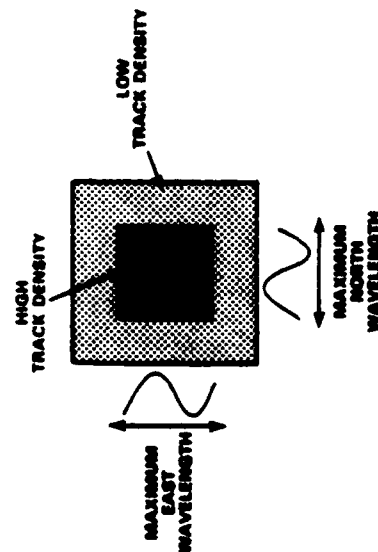


- PROBLEMS ASSOCIATED WITH VERY LARGE DATA RETURNS ($\sim 5 \times 10^5$ GRADIENT VALUES PER 300 km \times 300 km SQUARE)
- STAGE I (PREFILTERING) AND STAGE II (DOWNWARD CONTINUATION) PROCESS
- FEASIBILITY OF TEMPLATE ALGORITHM TO PROVIDE STAGE II REDUCTION
- USE OF GRADIENT DATA ALONE NECESSITATES LARGE "APRON" OF DATA BEYOND THE TEST/SURVEY REGION

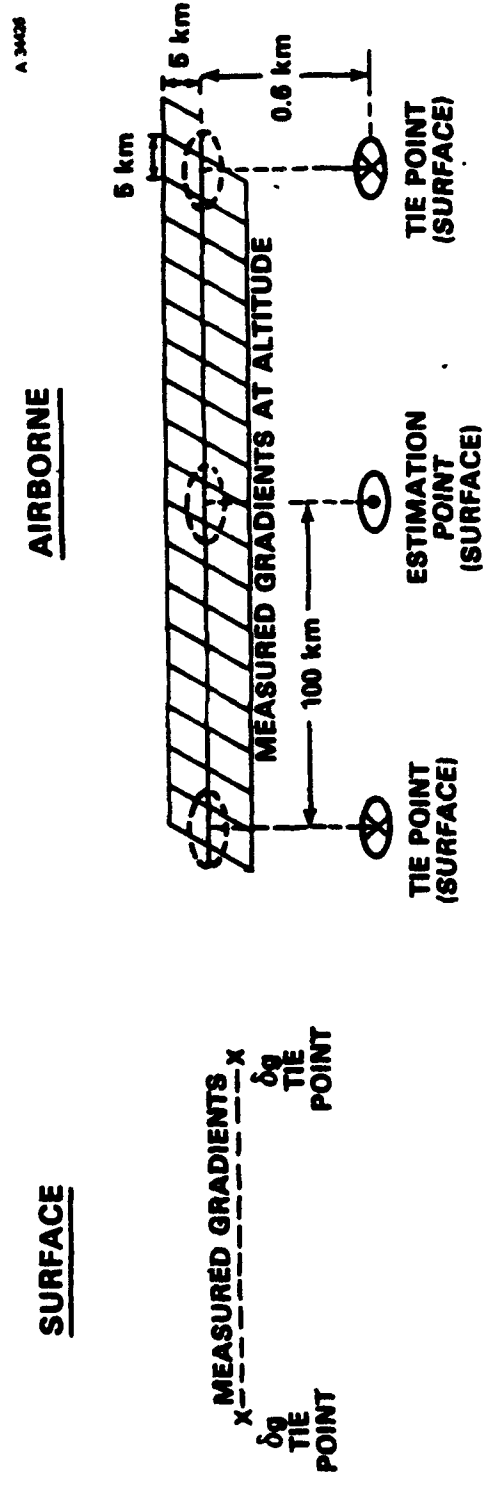


UNKNOWN (THEN)

- OPTIMAL TEMPLATE CONFIGURATION
- APPROPRIATE TREATMENT (UNDERSTANDING) OF SURFACE GRAVITY DISTURBANCE TIE POINT DATA
- STRONG ABILITY OF TIE POINT DATA TO MITIGATE NEED FOR DATA IN DISTANT ZONES



SURFACE VS AIRBORNE GGSS DATA REDUCTION

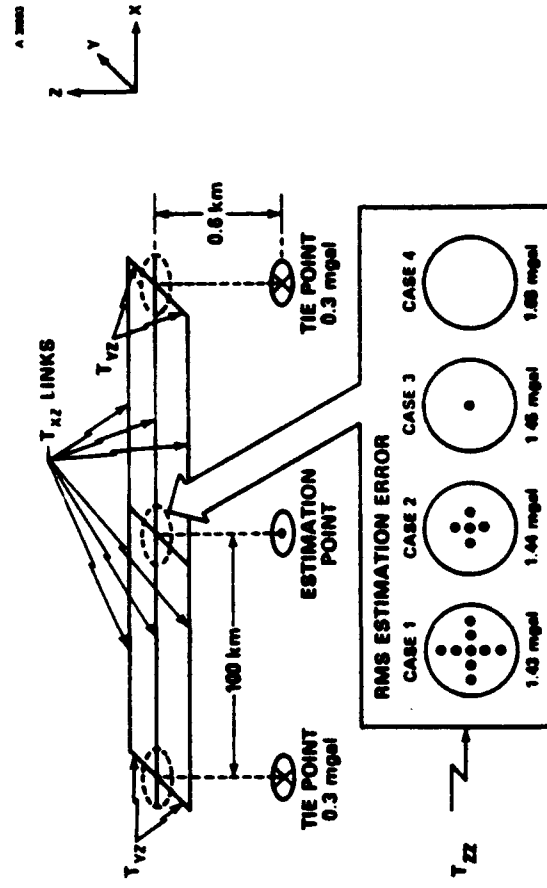


- OPTIMAL DATA REDUCTION IS BAND-LIMITED INTEGRATION OF GRADIENTS ALONG VEHICLE PATH
- FIRST TIE POINT PROVIDES INTEGRATION CONSTANT
- SECOND TIE POINT CALIBRATES GRAVITY DISTURBANCE RAMP ERROR CAUSED BY RESIDUAL BIAS GRADIOMETER ERROR (1.0E over 10 km \rightarrow 1.0 mgal)
- DOWNWARD CONTINUATION REQUIRED
- MULTIPLE INTEGRATION PATHS
- KEY OBSERVATION:

ALTITUDE	<<	TRACK SPACING	<<	GRADIENT CORRELATION DISTANCE
----------	----	---------------	----	-------------------------------
- DOWNWARD CONTINUATION CAN BE PERFORMED USING ONLY LOCAL DATA
- MULTIPLE INTEGRATION PATHS PROVIDE MECHANISM TO MINIMIZE EFFECTS OF SYSTEM NOISE

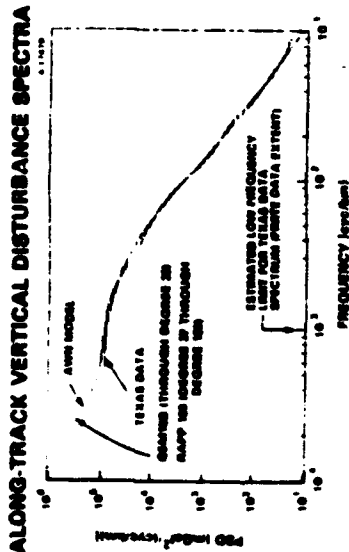
ILLUSTRATION OF AIRBORNE GGSS DATA REDUCTION

OPTIMAL ESTIMATION OF T_z (COVARIANCE ANALYSIS)

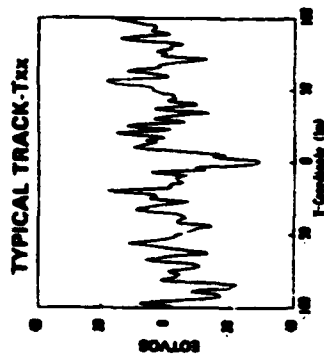
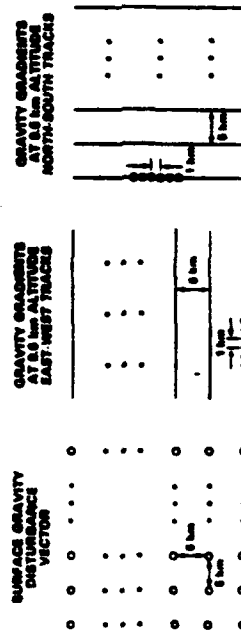


- GRADIOMETER NOISE = $100 \text{ E}^2/\text{Hz}$, SURVEY SPEED = 400 km/hr
- TOTAL NUMBER OF TEMPLATE ZONES IN CASES 1 THROUGH 4 ARE 74, 50, 26, 20
- GRADIENT DATA IMMEDIATELY ABOVE TIE POINT/ESTIMATION POINT ARE SUFFICIENT FOR UPWARD/DOWNWARD CONTINUATION
- SIMILAR RESULTS OBTAINED FOR VERTICAL DEFLECTIONS (0.29 arcsec in CASE 1)

SYNTHETIC GRAVITY MEASUREMENTS USED TO DEMONSTRATE AIRBORNE GGSS DATA REDUCTION



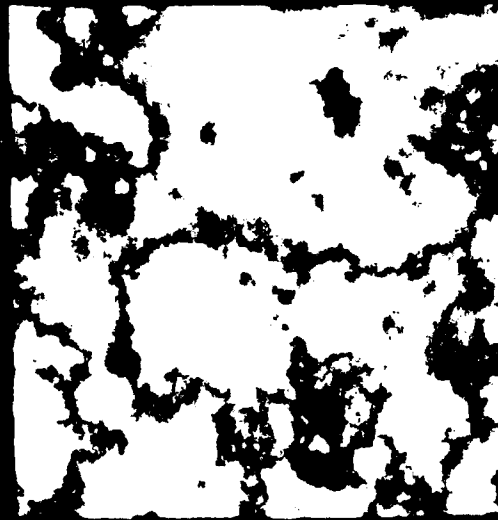
SYNTHETIC DATA SET



*NORTH TEXAS AND OKLAHOMA
 33° 23.0'N < ϕ < 36° 13.3'N
 97° 06.0'W < λ < 100° 29.7'W

- DMAAC-SUPPLIED GRAVITY DATA FROM CLINTON-SHERMAN TEST AREA* AUGMENTED WITH GEM10B AND RAPP 180 DEGREE VARIANCES
- RESULTANT GLOBAL PSD FITTED BY 7-SHELL ATTENUATED WHITE NOISE (AWN) MODEL
- DISCRETE REALIZATION OF AWN MODEL DEVELOPED (FINITE DIPOLE LAYERS)
- SYNTHETIC DATA FOR THE CLINTON-SHERMAN TEST AREA GENERATED FROM THE MODEL BY NSWC-DL (500 km x 500 km OF COVERAGE)
- REALIZATION CONSISTS OF ENTIRE GRADIENT TENSOR AT ALTITUDE AND GRAVITY DISTURBANCE VECTOR AT THE SURFACE
- DATA SET IS COMPLETELY CONSISTENT WITH ITS COVARIANCE MODEL
- FIGURE WHICH FOLLOWS SHOWS 500 km x 500 km AREA OF THE FIELD

SYNTHETIC GRAVITY FIELD



NSWC IL generated field is statistically consistent with North Te-as attenuated White Noise Model (7 shells)



-64 0 64
Data Key (Millibals)

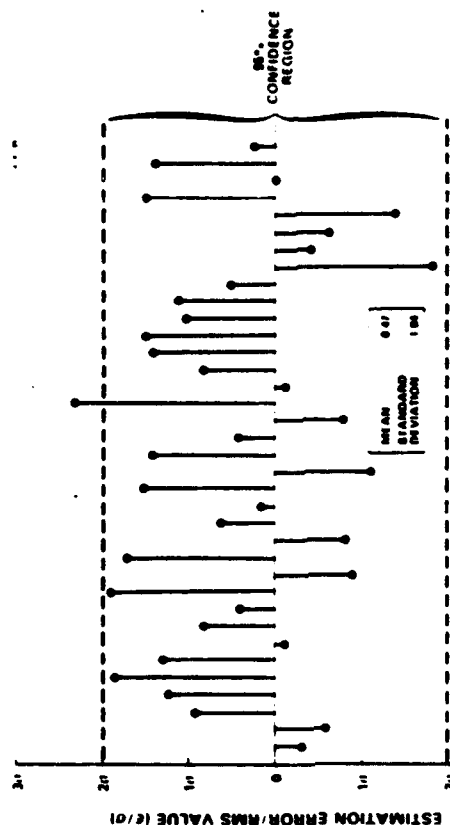
ESTIMATION RESULTS

A 34428

TWO NOISE RELIZATIONS

GRAVITY DISTURBANCE VECTOR COMPONENT	WHITE NOISE LEVEL (10^{-7} Hz)	ESTIMATION ERROR (ϵ)	RMS ACCURACY (σ)	ϵ/σ
X (arcsec)	100 600	0.27 0.27	0.25 0.25	1.1 0.6
Y (arcsec)	100 600	-0.15 -0.76	0.24 0.64	0.6 1.4
Z (mgal)	100 600	1.64 0.88	1.28 2.72	1.4 0.2

SUMMARY -- ALL NOISE RELIZATIONS



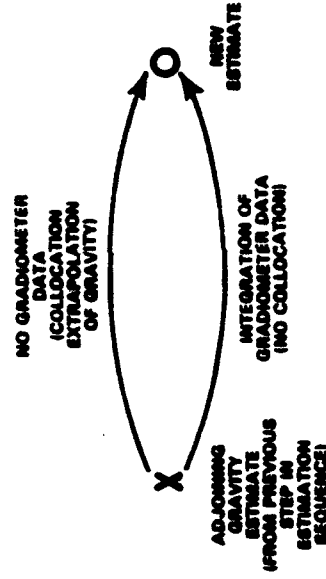
- DATA REDUCTION USED 5 N-S AND 5 E-W DATA TRACKS, EACH 200 km LONG
- FOUR TIE POINTS (ONE PER CARDINAL DIRECTION), EACH 200 km FROM ESTIMATION POINT
- TIE POINT ACCURACY -- VERTICAL DISTURBANCE, 0.3 mgal; DEFLECTIONS, 0.1 arc sec
- AIRCRAFT VELOCITY WAS 400 km/hr; EACH NOISE REALIZATION REPRESENTS A DIFFERENT SURVEY SORTIE
- ERROR (ϵ) DEFINED AS (TRUE SURFACE GRAVITY DISTURBANCE) - (ESTIMATED SURFACE GRAVITY DISTURBANCE)

TASC
THE ANALYTICAL SCIENCE CORPORATION

CONCLUSIONS AND OBSERVATIONS

- GRADIOMETRICALLY-RECOVERED GRAVITY AND DEFLECTIONS CAN ECONOMICALLY REACH GOAL ACCURACIES (1.0 mgal; 0.2 arcsec) AT REASONABLE TIE POINT SPACINGS (200 km)
- DETAILED UNDERSTANDING OF HOW SURFACE TIE POINTS AND EACH GRADIENT ELEMENT CONTRIBUTES INFORMATION AT EACH ALONG-TRACK SURVEY POINT PROVIDES CAPABILITY TO SIMPLIFY THE DATA REDUCTION (AND SURVEY DESIGN) PROCESS
- FOR EXAMPLE, TWO TYPES OF INFORMATION DRIVE THE ESTIMATION PROCESS IN AN INCREMENTAL WAY

A 24027



- IF GRADIOMETER SYSTEM NOISE IS LOW ENOUGH SO THAT THE GRAVITY FIELD DECORRELATES FASTER WITH DISTANCE THAN GRADIOMETER NOISE ACCUMULATES, THEN STATISTICAL GRAVITY MODEL "DROPS OUT" OF ESTIMATE -- CRITICAL NOISE LEVEL IS $\sim 300 \text{ E}^2/\text{Hz}$ IN CLINTON-SHERMAN TEST AREA
- STRONG ADVANTAGES OF THE "NETWORK IMPLEMENTATION" OF THE TEMPLATE ALGORITHM (IN WHICH EACH ZONE DEGENERATES INTO A LINK) INCREASES MOTIVATION TO MINIMIZE GGSS ERRORS

PAPER TITLE: GRAVITY GRADIOMETER (GGSS) TEST PLANNING AND TEST DATA TREATMENT

SPEAKERS NAME: Warren G. Heller

Questions and Comments:

Stan Jordan: You have presented a simplistic and optimistic view of how tie points are used. I feel that the use of tie points should be approached cautiously; local geologic features may have significant (one milligal) effects on the tie points but are unobserved by the gradiometer at aircraft altitude. If such aliasing effects arise at the tie points, they cannot be used to improve estimation of low-frequency gravity disturbances in the region. These difficulties are not revealed by your analysis because the 7-shell AWN model is not valid at wavelengths shorter than 3.5 km. To avoid aliasing effects at tie points, mini-surveys should be conducted in the vicinity of each tie point. These mini-surveys can be done with the (land-based) gradiometer van.

Julian Center: To do upward and downward continuation you need to know the vertical gradients all along the path. This may not be achievable with high accuracy if there is high-frequency activity of the gravity field around the tie point or estimation point.

SPEAKERS RESPONSE: For sufficiently short upward continuation distance (e.g. 600 meters), local gradient data (measured by the gradiometer) at altitude suffices. In an extreme case, say in which the tie points were chosen injudiciously, such that the gravity field curved significantly (perhaps, 50E or more) then surface gradient measurements near the tie point could be appropriate. The practicalities of continuous use of gradient data along the entire upward continuation path preclude "continuous upward continuation". Fortunately it is not necessary.

GRADIENT INTEGRATION PROCEDURE FOR
PATH ERROR REDUCTION

A. E. Rufty

Naval Surface Weapons Center

Dahlgren, Virginia 22448-5000

ABSTRACT

A procedure to integrate gravity gradients aloft to obtain gravity disturbance values (aloft) will be presented. The algorithm simultaneously weights all possible path integrals of the gradient to yield an optimal estimate of the disturbance.

**GRADIENT INTEGRATION PROCEDURE
FOR
PATH ERROR REDUCTION**

BY

ALAN E. RUFTY

NSWC

11 FEB 1986

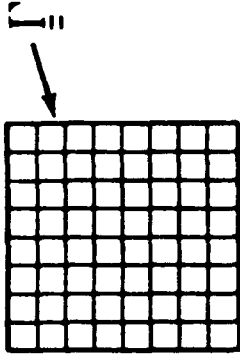
PREVIOUS TALKS ON THE SAME TOPIC

**AUGUST 1985 DAWG: DIRECT ESTIMATION OF GRAVITY TRACK DATA AT
ALTITUDE FROM GRADIENT TRACK DATA AT ALTITUDE**

**OCTOBER 1985 DAWG: FILTERING ASPECTS FOR "DIRECT ESTIMATION OF
GRAVITY TRACK DATA AT ALTITUDE FROM GRADIENT
TRACK DATA AT ALTITUDE"**

OUTLINE

- BASICS



$$\vec{G} \approx \int \vec{\Gamma} \cdot d\vec{x}$$

- TECHNIQUE

- CONDITIONS ON GRAVITY GRADIENT
- PATH DEPENDENT GRAVITY ESTIMATES
- PATH SEGMENTS \longleftrightarrow SURVEY GRID SEGMENTS
- SEGMENT INTEGRALS
- SURVEY GRID SEGMENT WEIGHTING SCHEMES
- OPTIMIZED WEIGHTING SCHEME (MINIMUM VARIANCE OF GRAVITY ERRORS)

- RESULTS

GRADIENT INTEGRABILITY CONDITIONS

- $\Gamma_{ij} = \Gamma_{ji} ; i, j = 1, 2, 3 \quad \Gamma_{11} + \Gamma_{22} + \Gamma_{33} = 0$

- LET $\bar{\gamma}_{\mu} \equiv (\Gamma_{\mu 1}, \Gamma_{\mu 2}, \Gamma_{\mu 3})^T, \mu = 1, 2, 3$

A FUNCTION G_{μ} EXISTS SUCH THAT

$$\bar{\gamma}_{\mu} = \bar{\nabla} G_{\mu} \quad \text{IF AND ONLY IF } \bar{\nabla} \times \bar{\gamma}_{\mu} \equiv 0$$

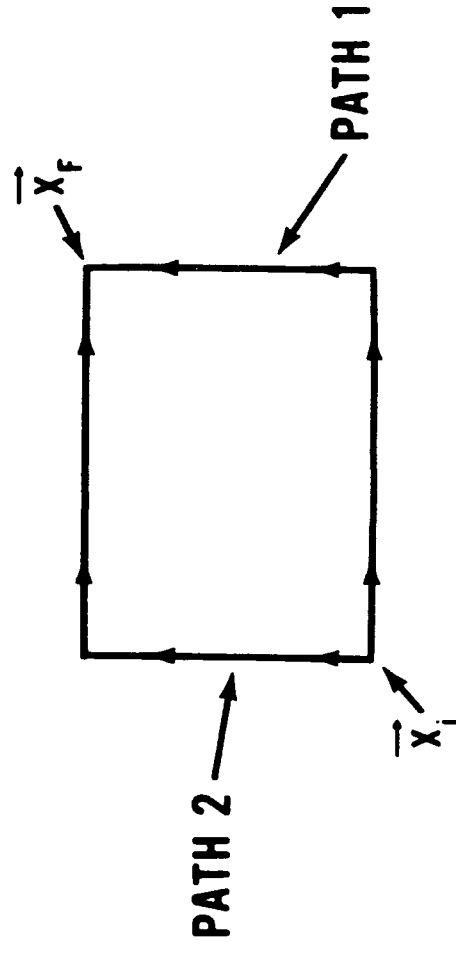
- LET $\Gamma_{ij, \kappa} \equiv \frac{\partial \Gamma_{ij}}{\partial x_{\kappa}}$ THEN $\Gamma_{ij, \kappa}$ MUST BE

SYMMETRIC IN ALL INDICES $\left[\Gamma_{ij, \kappa} \equiv \frac{\partial}{\partial x_{\kappa}} \frac{\partial}{\partial x_i} \frac{\partial}{\partial x_j} v(\bar{x}) \right]$

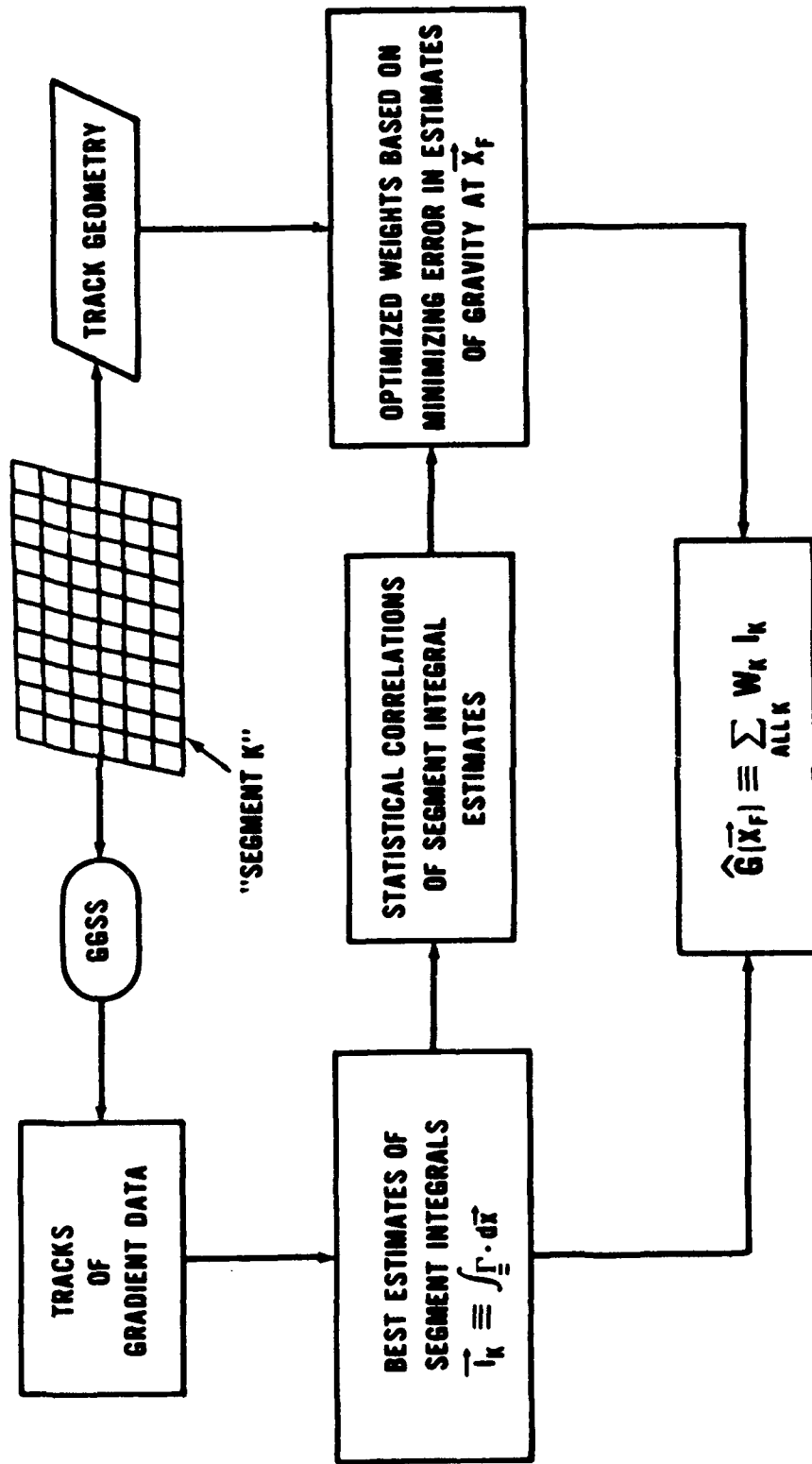
PATH DEPENDENCE OF GRADIENT INTEGRALS

- BECAUSE OF NOISE $\vec{\nabla} \times \vec{\gamma}_\mu \neq 0$ HENCE

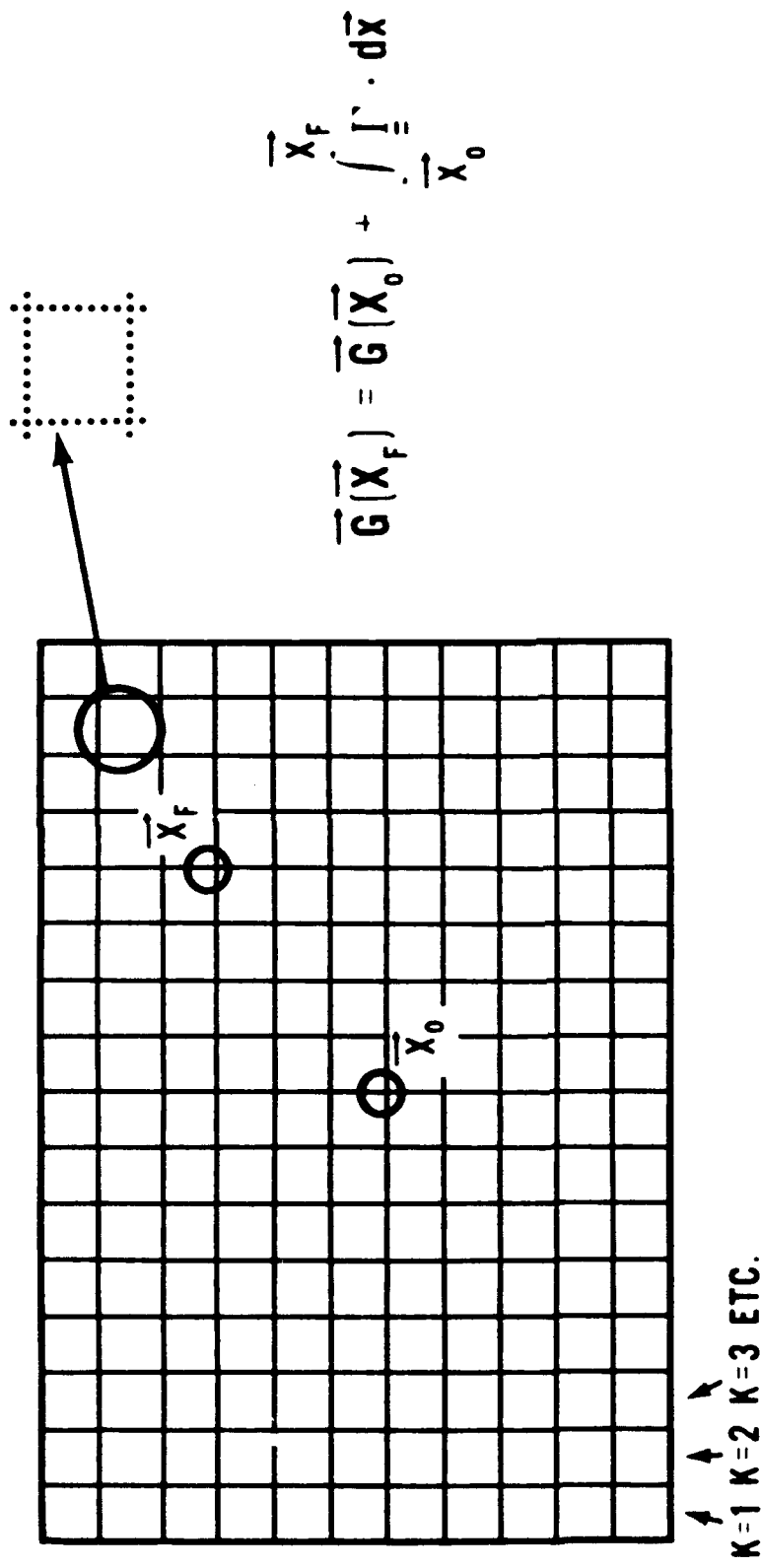
$$\vec{G}(\vec{X}_F) - \vec{G}(\vec{X}_i) \equiv \int_{\vec{X}_i}^{\vec{X}_F} \vec{\Gamma} \cdot d\vec{x} \text{ IS PATH DEPENDENT}$$



GIPPER OVERVIEW



TRACK GEOMETRY



- LABEL SEGMENTS (K)
 - COMPUTE "BEST ESTIMATES" OF SEGMENT INTEGRALS
- $$\vec{I}_K \equiv \int_{\text{SEGMENT K}} \vec{I} \cdot d\vec{x}$$
- BY CONVENTION (IF NO "TIE POINTS" ARE USED) $\vec{G}(\vec{X}_0) \equiv 0$

SEGMENT WEIGHTING FUNCTION

- LET $\bar{W} \equiv (W_1, W_2, W_3, \dots, W_K, \dots)^T$ BE GIVEN

THEN

$$\bar{L}(\bar{W}) \equiv \sum_K W_K \bar{I}_K$$

- LET P BE A PARTICULAR PATH AND LET

$$\begin{cases} W_K \equiv 1 & \text{IF SEGMENT K IS PART OF PATH P} \\ W_K \equiv 0 & \text{OTHERWISE} \end{cases}$$

THEN

$$\bar{L}(\bar{W}(P)) \equiv \int_{\bar{X}_i}^{\bar{X}_F} \bar{I} \cdot d\bar{x} \equiv \hat{G}_P(\bar{X}_F) \approx \bar{G}(\bar{X}_F)$$

NEW GRAVITY ESTIMATES FROM OLD

- ESTIMATES FROM VARIOUS PATHS CAN BE COMBINED:

$$\hat{G}(\bar{X}_f) \equiv \sum_p \lambda_p \hat{G}_p(\bar{X}_f) \text{ WHERE } \sum_p \lambda_p \equiv 1$$

OR EQUIVALENTLY

$$\hat{G}(\bar{X}_f) \equiv \sum_k W_k \bar{I}_k \text{ WHERE } W_k \equiv \sum_p \lambda_p W_k(p)$$

- "ALL CHOICES OF λ_p AND ALL CHOICES OF PATH"
IS EQUIVALENT TO
"ANY CHOICE OF \bar{W} SUBJECT TO 'PATH LIKE' CONDITIONS OF CONSTRAINT"
- WHAT IS THE OPTIMUM CHOICE OF \bar{W} ?
(SUBJECT TO THESE CONSTRAINTS)

OPTIMUM CHOICE OF WEIGHTS

- LET \bar{t}_k^j BE THE ERROR IN j^{th} COMPONENT OF \bar{t}_k

THE ERROR IN THE GRAVITY ESTIMATE IS

$$G_j(\bar{X}_F) - \hat{G}_j(\bar{X}_F) = \sum_k W_k \bar{t}_k^j$$

- THE VARIANCE OF THIS ERROR IS

$$\sigma_G^2 \equiv \sum_k \sum_{k'} W_k W_{k'} E[\bar{t}_k^j \bar{t}_{k'}^j]$$

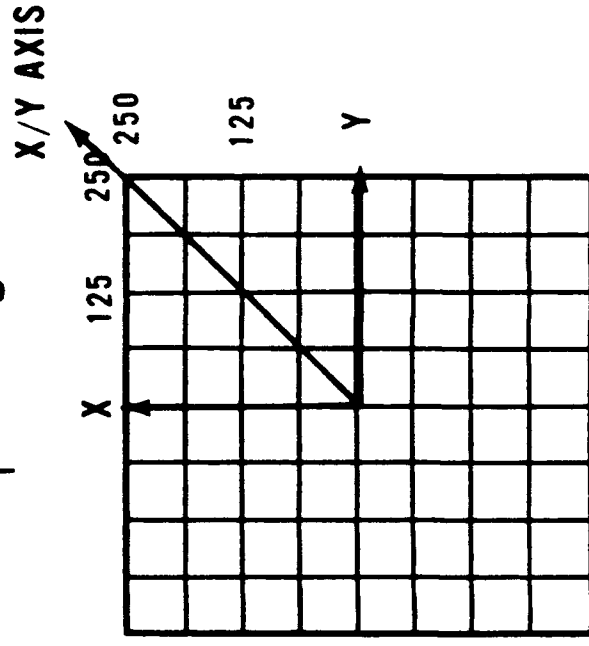
- THE VALUE OF \bar{W} IS DETERMINED BY MINIMIZING σ_G^2 SUBJECT TO THE (PATH) CONSTRAINT CONDITIONS

ASSUMPTIONS

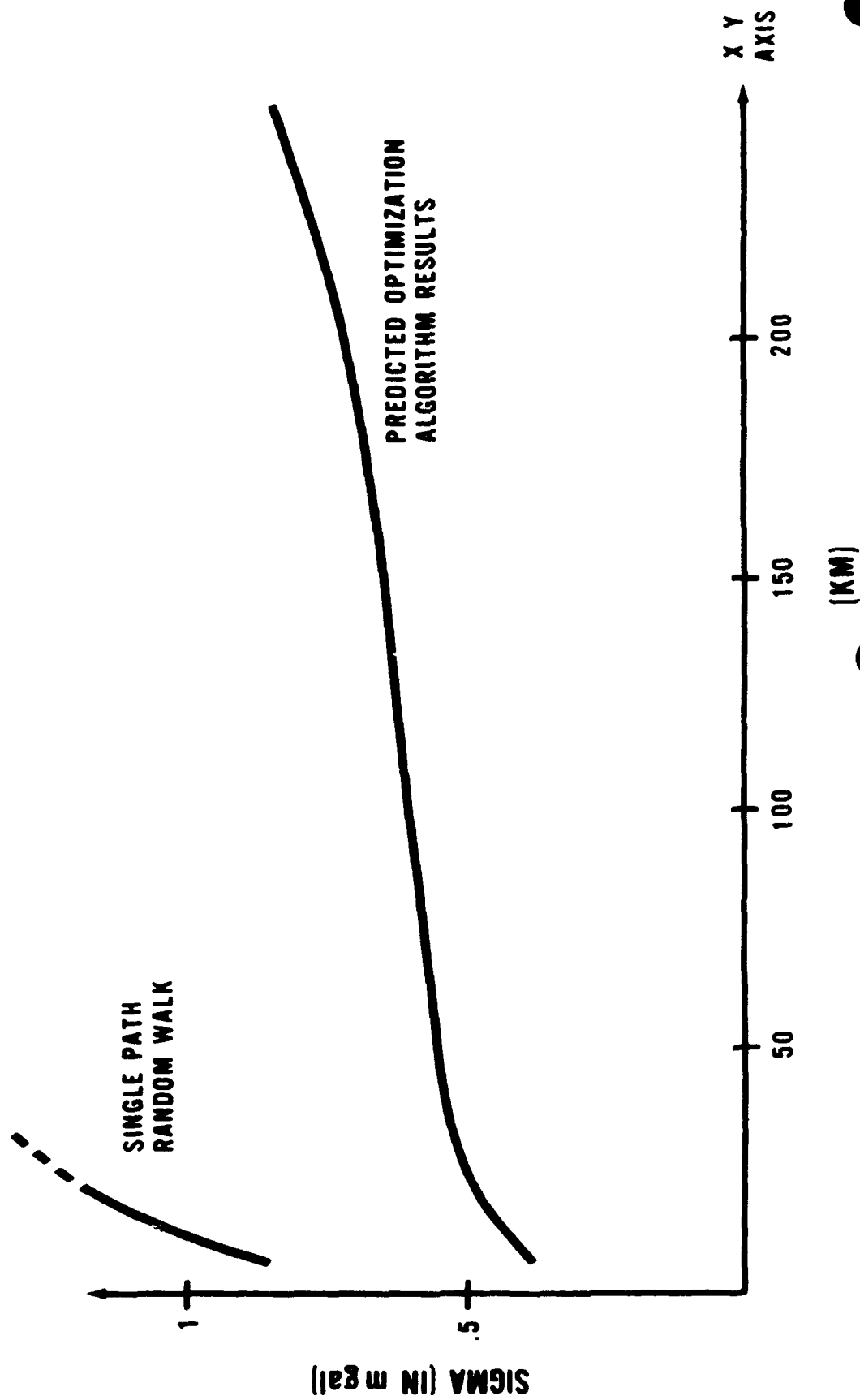
- NO TIE POINTS USED
- UNCORRELATED SEGMENT INTEGRALS:

$$E \left[I_K^j I_{K'}^j \right] = \delta_{KK'} \sigma_I^2$$

WHERE $\sigma_I = .5 \text{ mgal}$



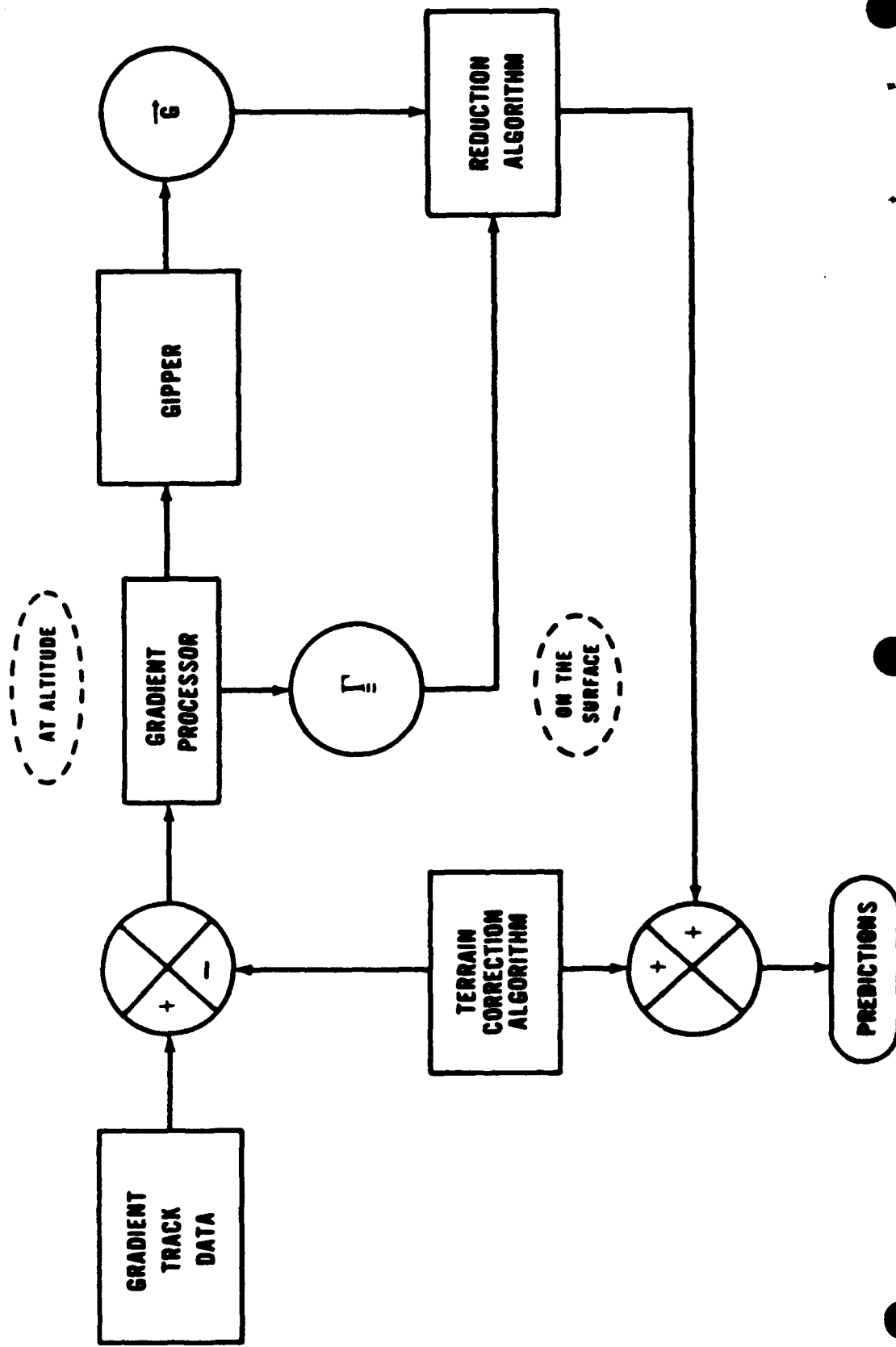
RESULTS ($\sigma_1 = .5 \text{ mgal}$)



SUMMARY

- **CONSIDER ALL PATHS SIMULTANEOUSLY**
- **(LARGELY) INDEPENDENT OF STATISTICS OF FIELD AND SURVEY GRIDDING**
- **CAN BE EASILY MODIFIED TO INCLUDE TIE POINT DATA**
- **CAN BE EASILY MODIFIED TO INCLUDE CORRELATION EFFECTS**

STAGE II PROCESSOR OVERVIEW



PAPER TITLE: GRADIENT INTEGRATION PROCEDURE FOR PATH ERROR REDUCTION

SPEAKERS NAME: Alan E. Rufty

Questions and Comments:

Alan Zorn: Stokes' theorem provides a connection between cross products
• of vector fields and line integrals of gradients: $\oint \nabla \times \underline{f} = \oint \underline{\Gamma} \cdot d\underline{x}$

Thus, the explicit constraint $\underline{\nabla} \times \underline{f} = \underline{0}$ (ie-conservative field)
is equivalent to zero closed line integrals. Is the explicit constraint
• really required for your solution?

SPEAKERS RESPONSE: I use it because it is easy to implement in my algorithm,
and it does reflect the physics of the problem.

NASA REQUIREMENTS FOR A SPACEBORNE GRAVITY GRADIOMETER--AN OVERVIEW

C. J. Finley

Office of Space Science and Applications

NASA Headquarters

Washington, D.C. 20546

D. E. Smith

Space and Earth Science Directorate

NASA/Goddard Space Flight Center

Greenbelt, MD 20771

ABSTRACT

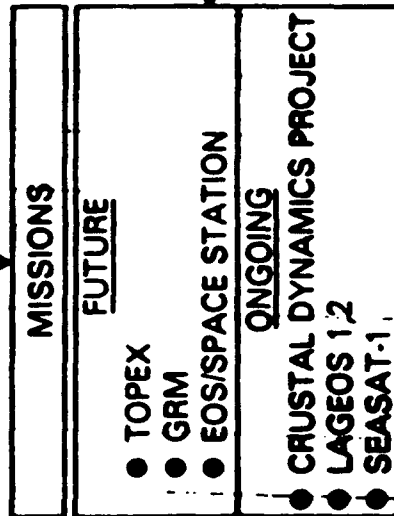
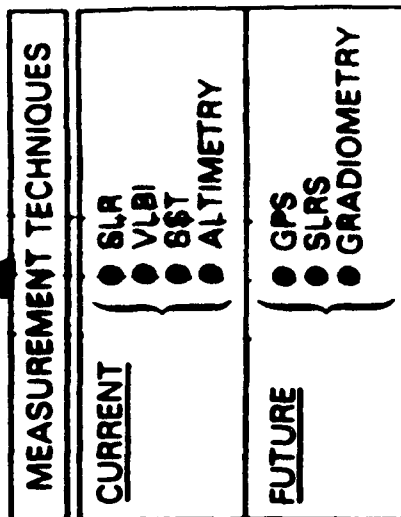
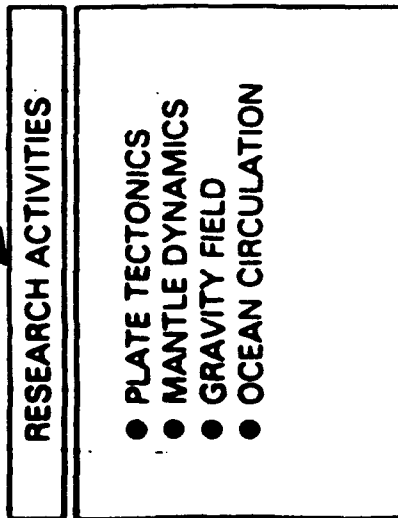
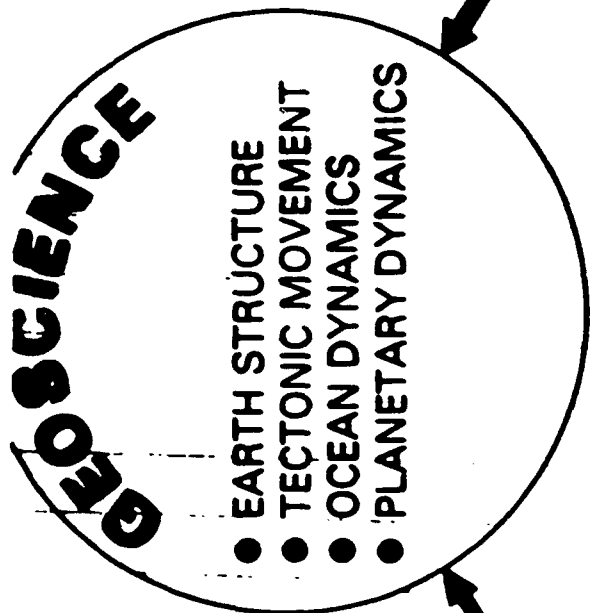
Beginning with Sputnik and Vanguard in 1958, NASA has used artificial satellites and space platforms to measure and map the Earth's gravity. Until now, the gravity field has been derived indirectly by the measurement of satellite perturbations, such as with the Beacon Explorers and Lageos satellites; or by means of satellite altimetry, such as with GEOS-3 and Seasat. Each of these techniques suffer severe limitations, the first in resolution due to the high orbital altitude of anywhere from 500 km to almost 6000 km for Lageos and the second in both resolution and global coverage because of the approximately 800km altitude of the altimetric satellites and being effective only over oceanic areas. Spaceborne gradiometers will for the first time permit direct measurement of the gravity field over the entire surface of the Earth at much improved resolutions and accuracy. The present gravity field with an uncertainty of 5 to 10 mgals at resolutions greater than 500 km is inadequate for NASA's present operational and scientific needs. We need 1 to 2 mgals at 100 km resolution for our solid earth geodynamics studies as well as for improved orbit determination and the derivation of a 10 cm ocean geoid to be used in the Topex satellite ocean circulation studies.

In addition to the Earth, there is equal or greater value in being able to measure the gravity fields of the planets. The same basic geophysical questions about the structural rigidity of the lithosphere and the existence and form of convection in the mantle apply to the moon and the planets as they do the Earth. Further, the engineering difficulties of carrying out a planetary mission compared to an earth mission make it essential that the technology that is used is fully capable of meeting the scientific measurement objectives in both accuracy and resolution; a re-flight may not be a possibility. A space proven gravity gradiometer could be flown on many of the future planetary missions and provide a wealth of new information about the planets and their satellites that cannot be obtained any other way.

NASA REQUIREMENTS FOR A SPACEBORNE GRAVITY GRADIOMETER - AN OVERVIEW

W.D. KAHN

NASA/GSFC



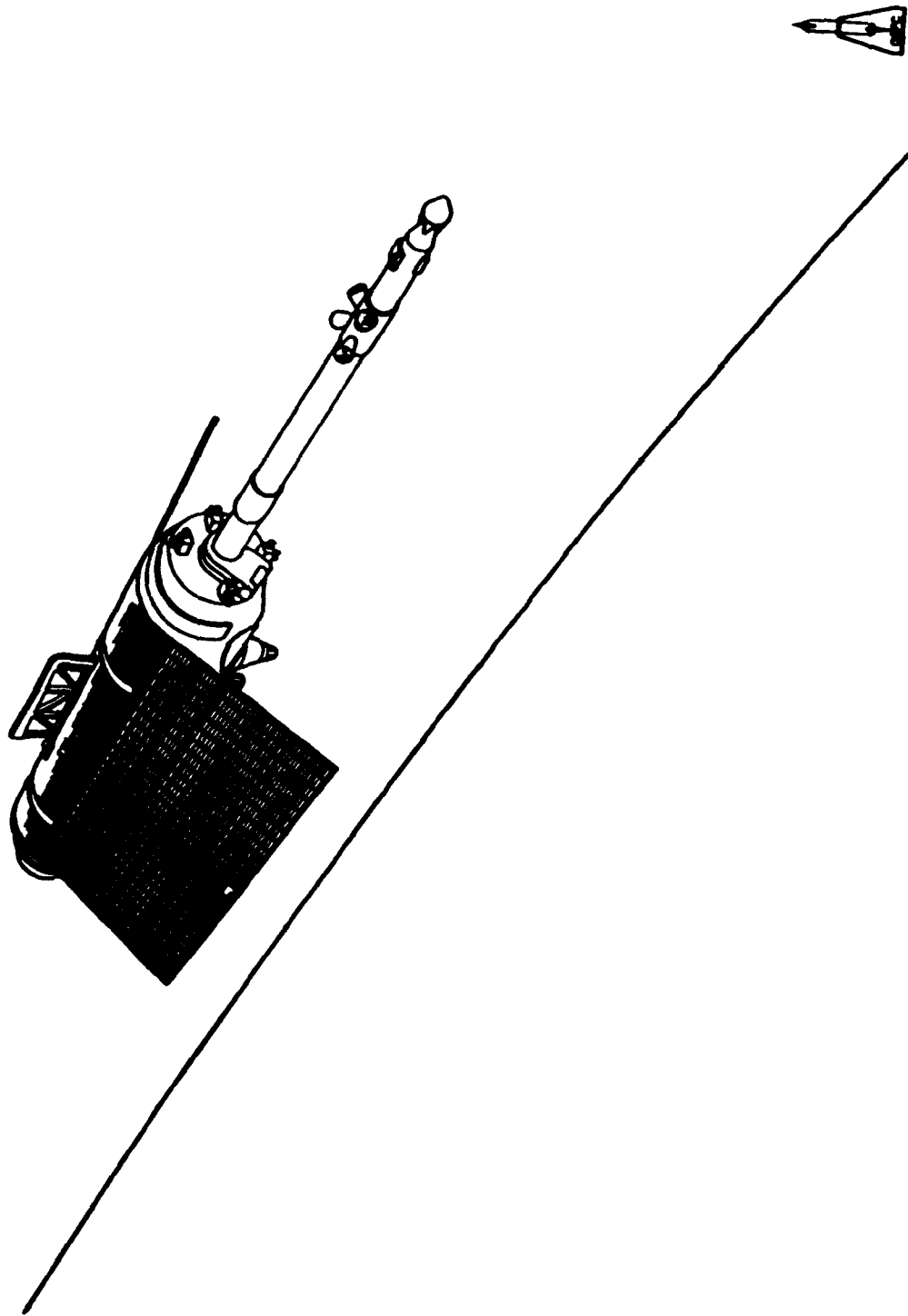
HISTORICAL REVIEW

- **NASA HAS BEEN IN GRAVITY FIELD MODELING SINCE THE EARLY 1960's.**
- **NASA'S GRAVITY MODELS HAVE BEEN USED BY RESEARCHERS THROUGHOUT THE WORLD FOR OVER A DECADE.**
- **DATA USED IN DEVELOPMENT OF GRAVITY MODELS:**
 - 1. SATELLITE TRACKING OF 32 SPACECRAFT**
 - 2. SATELLITE ALTIMETRY (GEOS-3, SEASAT)**
 - 3. SURFACE GRAVIMETRY DATA.**

IMPORTANCE OF THE GRAVITY FIELD OF THE EARTH

THE GRAVITY FIELD OF THE EARTH REFLECTS VARIATIONS IN THE EARTH'S COMPOSITION. THUS, A KNOWLEDGE OF THE EARTH'S GRAVITY FIELD PROVIDES INFORMATION ON THE DENSITY STRUCTURE OF THE EARTH'S INTERIOR AND OUTER LAYERS FROM WHICH WE CAN INCREASE OUR UNDERSTANDING OF THE FORMATION OF GEOLOGICAL FEATURES, SUCH AS MOUNTAINS AND BASINS, AND THE MECHANISMS AND SCALE OF PROCESSES, SUCH AS MANTLE CONVECTION.

GEOPOTENTIAL RESEARCH MISSION



GRM ORBITAL PARAMETERS

NUMBER OF SPACECRAFT
SPACECRAFT ALTITUDE
SPACECRAFT INCLINATION
ECCENTRICITY

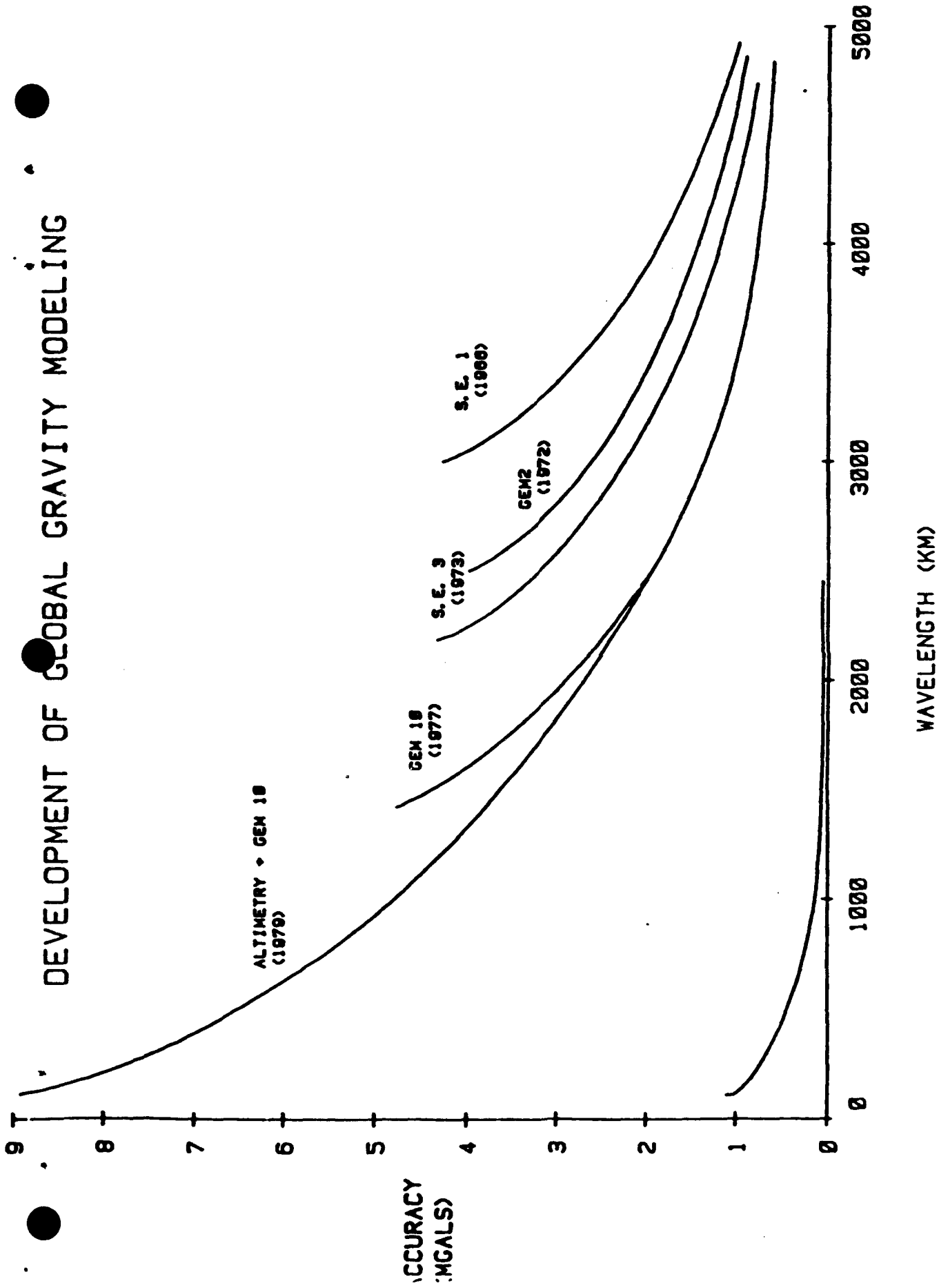
2
160 KM
POLAR
ZERO

SPACIAL SEPARATION OF THE TWO
SPACECRAFT IN MEAN ANOMALY
ORBITAL PERIOD
ORBITS/DAY

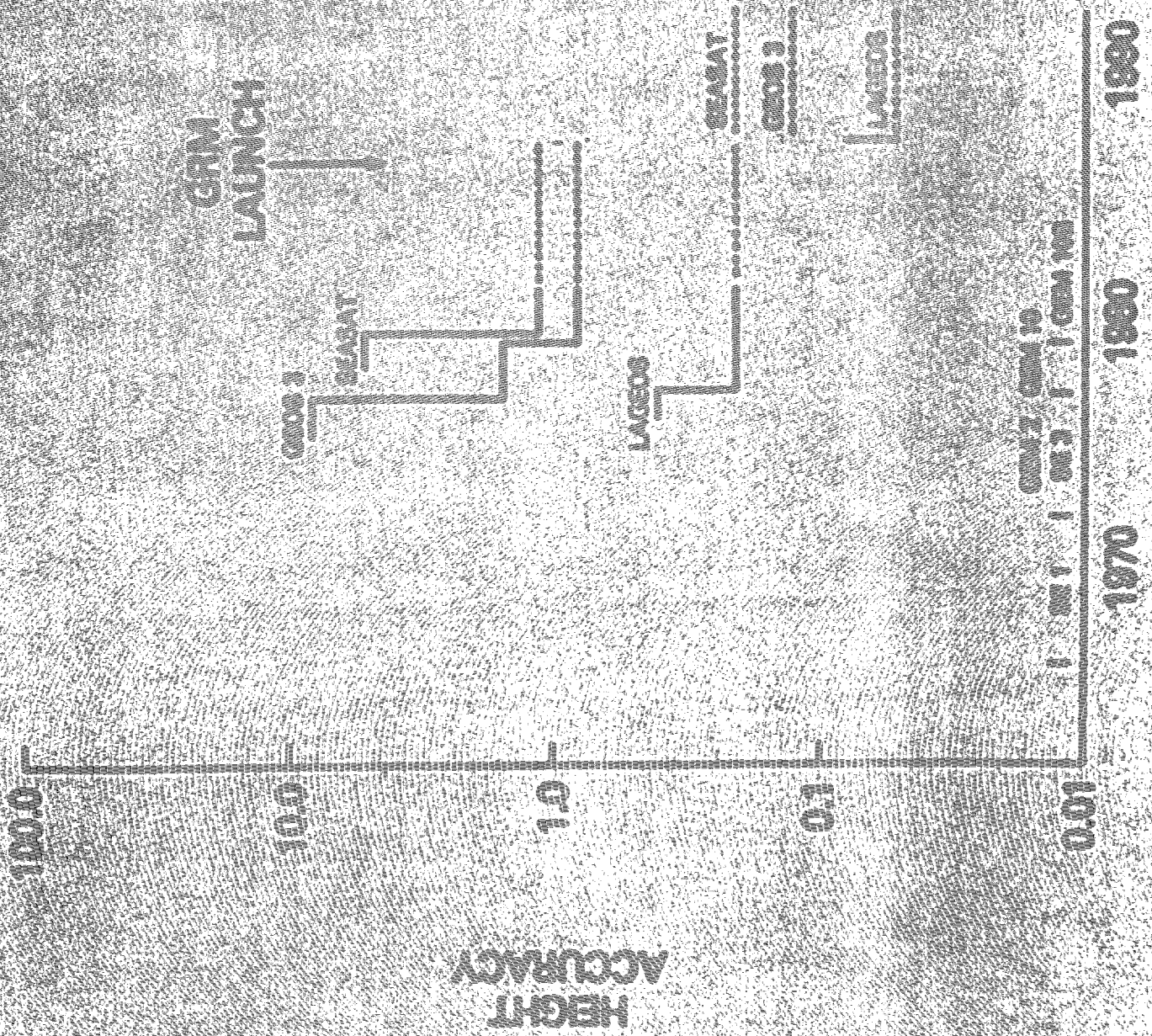
100 TO 600 KM
88.5 MIN.
16.3



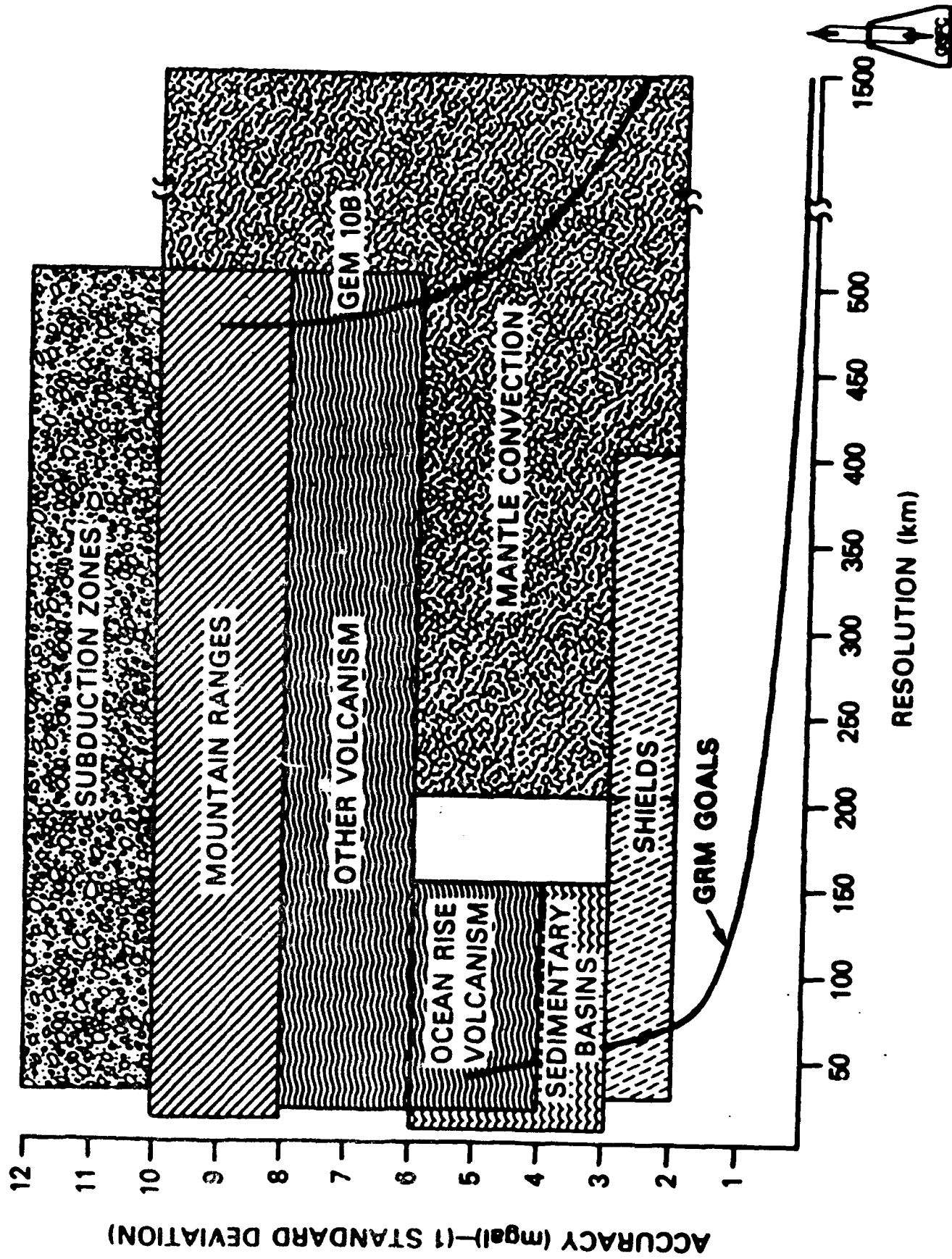
DEVELOPMENT OF GLOBAL GRAVITY MODELING



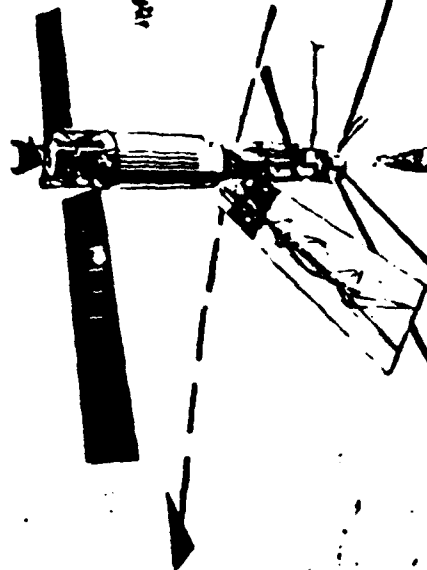
IMPROVEMENT IN ORBIT EPHEMERIDES



GEOPHYSICAL REQUIREMENTS FOR GRAVITY



SATELLITE ALTIMETRY



SEA SURFACE

LASER

LASER

19500
191500



RELATION OF OCEAN HEIGHT TO GEOID AND ELLIPSOID

TERRITORIAL VARIATIONS

HEIGHT

SEA
SURFACE

GEOID

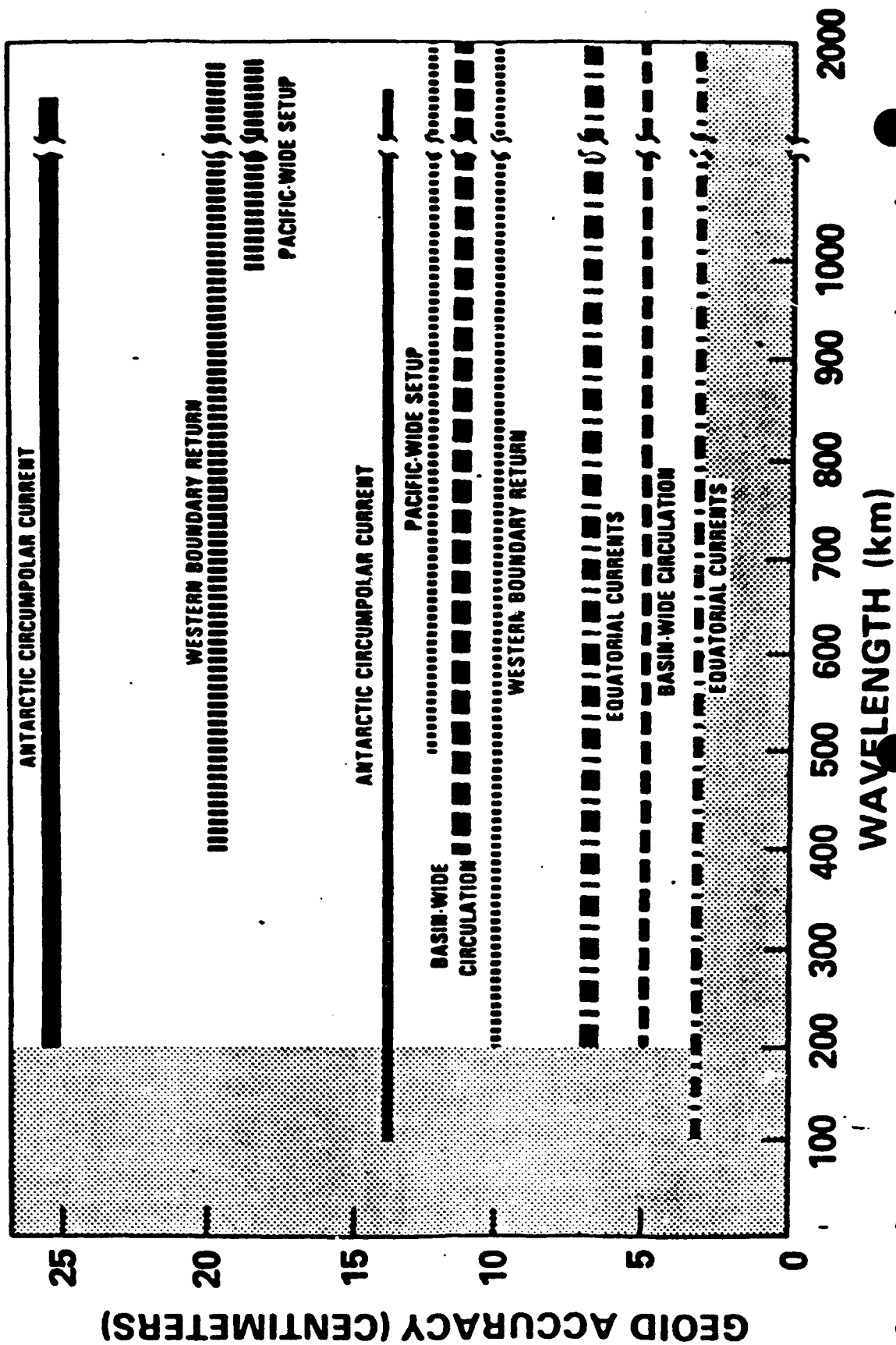
REFERENCE ELLIPSOID

DISTANCE



OCEANOGRAPHIC GEOID REQUIREMENTS

THICK LINES: COARSE RESOLUTION
FINE LINES: FINE RESOLUTION
GRAVSAT CAPABILITY
OUTSIDE STIPPLED REGION



PAPER TITLE: NASA REQUIREMENTS FOR A SPACEBORNE GRAVITY GRADIOMETER-AN OVERVIEW

SPEAKERS NAME: Werner D. Kahn

Questions and Comments:

Jim Faller: Given the time slippage that has occurred with the GRM mission, wouldn't it be appropriate at this time to once again take a hard and contemporary look at the GRM mission, and in particular, to look at what improvements could be effected if a laser tracking system (perhaps using a stabilized laser diode light source) were added and the DISCOS appropriately upgraded. A laser tracking system could result in two orders of magnitude tracking precision improvement which could, for example, be used to fly at a somewhat higher altitude (keeping ground resolution the same) and thereby permit a longer mission and/or a smaller vehicle (which would presumably cost less). Such an optimized mission should then be compared to a single satellite gradiometer system. The fundamental difference between these two approaches is that one is in effect a "point" instrument and as such suffers terribly from local internal-to-the-satellite mass redistributions and their effects in the measured gradient(s). The other, GRM, enjoys the freedom from these critical systematic error sources as a result of its long baseline. (End effects are greatly reduced). One should worry whether or not the single-satellite gradiometer can ever reduce the local mass induced gradient changes much below the 0.01 to 0.1 E region. Certainly to achieve 10^{-3} E is difficult, if not impossible, and to achieve 10^{-2} E on the shuttle is simply out of the question.

Since the science to be learned depends entirely on the achieved resolution on the ground in the presence of any and all systematic biases, it is critical to make realistic estimates of their magnitudes and thereby the useful as opposed to the theoretical sensitivity of both of these systems. It is the achieved rather than the theoretical sensitivity which will dictate the quality of the science. It is my impression that (from a fundamental design point of view) an extended (GRM) instrument (though complicated by requiring two satellites) enjoys a great advantage over the simpler single satellite instrument in regard to this all important and pivotal design question.

Klaus-Peter Schwarz: The question addresses the interpretation of the accuracy curves. You claim an accuracy of better than 1 mgal for gravity anomaly resolution and of better than 1 cm for geoid resolution. On the other hand, you state a wavelength resolution of 50 km. These two sets of numbers are incompatible because the short wavelengths are not resolved, and contain much large RMS errors than the ones you quoted.

SPEAKERS RESPONSE: The numbers refer to one by one degree mean values. Short wavelength variations were not considered. The RMS-values do not therefore represent gravity field or geoid resolution at individual points.

GRAVITY FIELD FINE STRUCTURE MAPPING USING
A SPACEBORNE GRAVITY GRADIOMETER

W. D. Kahn

Goddard Space Flight Center

Mail Code 621

Greenbelt, Maryland 20271

ABSTRACT

Covariance Error Analysis studies have been performed to assess the capabilities of a Spaceborne gravity gradiometer's capability to determine the short wavelength components of the earth's gravity field. For the studies, consideration was given to the effects of gravity signal attenuation due to increase in spacecraft orbit altitude, the effects of orbit errors, altitude rate errors, gradiometer system precision, estimation strategy etc. Typical results obtained are those for a satellite in a 160 km polar-circular orbit, carrying a three-axis gradiometer with a precision of 10^{-3} EOTVOS Units (E)*. The satellite orbit error was assumed to be 5.5 meters, the measurement sampling rate was 1 measurement per 4 seconds. The size of the region surveyed over a 180 day period was $19^\circ \times 19^\circ$ which was traversed by approximately 300 orbit passes of which a maximum of 16 passes traversed each $1^\circ \times 1^\circ$ gravity anomaly block within the region. Results obtained from the simulation indicate that the gravity gradiometer can determine gravity anomalies with a horizontal resolution of 50 km to an accuracy of 0.4 mgals. Slightly improved results say on the order of 10 to 20% can be anticipated if the gradiometer precision is increased to 4×10^{-4} E.

* $1 \text{ E} = 10^{-9} \text{ cm/S/cm}$

**GRAVITY FIELD FINE STRUCTURE MAPPING,
USING A
SPACEBORNE GRAVITY GRADIOMETER**

BY

**WERNER D. KAHN
NASA GODDARD SPACEFLIGHT CENTER/
CODE 621
GREENBELT, MD 20771**

**PRESENTED AT:
THE 14TH GRAVITY GRADIOMETRY CONFERENCE
USAF ACADEMY
COLORADO SPRINGS, CO.
FEB. 11, 12, 1986**

GRAVITY FIELD FINE STRUCTURE MAPPING, USING A SPACEBORNE GRAVITY GRADIOMETER

WILL DISCUSS:

**STUDIES WHICH HAVE BEEN PERFORMED TO
ASSESS A SPACEBORNE GRAVITY GRADIOMETER'S
CAPABILITY TO RECOVER TERRESTRIAL GRAVITY
AND GEOID INFORMATION IN TERMS OF DISCRETE
MEAN FREE AIR GRAVITY ANOMALIES AND GEOID
ANOMALIES**

APPROACH:

COMPUTER SIMULATIONS HAVE BEEN PERFORMED USING COVARIANCE ERROR ANALYSIS METHODS TO:

- DEVELOP ESTIMATION STRATEGIES FOR RECOVERY OF GRAVITY AND GEOID ANOMALIES
- STUDY THE EFFECTS OF ERROR SOURCES SUCH AS:
 - GRADIOMETER MEASUREMENT NOISE
 - SPACECRAFT POSITION ERROR
 - GYRO RATE ERRORS
- STUDY THE EFFECTS OF
 - GRADIOMETER CONFIGURATION
 - SPACECRAFT ALTITUDE
 - MISSION DURATION

MATHEMATICAL MODELS

- TOTAL POTENTIAL

$$V = U + T$$

U = NORMAL POTENTIAL

T = ANOMALOUS POTENTIAL

- ANOMALOUS POTENTIAL IN TERMS OF GRAVITY ANOMALIES

$$T = \frac{R}{4\pi} \sum_i \delta g_i (\phi_i', \lambda_i') S(r, \psi_i) \cos \phi_i' \Delta \phi_i' \Delta \lambda_i'$$

$\delta g_i (\phi_i', \lambda_i')$ = MEAN GRAVITY ANOMALY OVER BLOCK CENTERED AT

LATITUDE ϕ_i' ; LONGITUDE λ_i'

$$\psi_i = \cos^{-1} (\sin \phi \sin \phi_i' + \cos \phi \cos \phi_i' \cos (\lambda_i' - \lambda))$$

- ANOMALOUS POTENTIAL IN TERMS OF GEOID ANOMALIES

$$T = \frac{\gamma R}{4\pi} \sum_i \delta \bar{N}_i (\phi_i, \lambda_i) \frac{(r_i^2 - R^2)}{\rho_i^3} \cos \phi_i' \Delta \phi_i \Delta \lambda_i$$

$\delta \bar{N}_i (\phi_i, \lambda_i')$ = MEAN GEOID ANOMALY OVER BLOCK CENTERED AT

LATITUDE ϕ_i' ; LONGITUDE λ_i'

$$\rho_i^2 = r_i^2 + R^2 - 2Rr_i \cos \psi_i$$

γ \equiv NORMAL GRAVITY (cm/S²)

r \equiv GEOCENTRIC DISTANCE TO SPACECRAFT (cm)

R \equiv RADIUS OF THE EARTH (cm)

- GRAVITY GRADIENT

$$\Gamma = \Gamma_u + \Gamma_T = \vec{\nabla} (\vec{\nabla} V) = \begin{bmatrix} V_{xx} & V_{xy} & V_{xz} \\ V_{xy} & V_{yy} & V_{yz} \\ V_{xz} & V_{yz} & V_{zz} \end{bmatrix}$$

MEASUREMENT MODEL

$$Z = \Gamma_T + v$$

WHERE

Z = VECTOR OF GRADIOMETER OUTPUTS WITH REFERENCE POTENTIAL REMOVED.

Γ_T = GRAVITY GRADIENT ARISING FROM ANOMALOUS POTENTIAL K , T

$$\Gamma_T = A_1 \tilde{g}_1 + A_2 \tilde{g}_2$$

\tilde{g}_1 = VECTOR OF ADJUSTED ANOMALIES

\tilde{g}_2 = VECTOR OF UNADJUSTED ANOMALIES

v = ERROR IN MEASUREMENT WITH THE FOLLOWING SOURCES:

- INSTRUMENT INACCURACIES
- SATELLITE POSITION ERROR
- ATTITUDE RATE ERRORS
- ATTITUDE ERRORS

ESTIMATION ALGORITHM

$$\hat{g}_1 = K A_1^T W^{-1} Z$$

WHERE

$$K = [A_1^T W^{-1} A_1 + P_{g_1}^{-1}]^{-1}$$

W^{-1} = WEIGHTING MATRIX, USUALLY TAKEN TO BE INVERSE OF THE VARIANCE OF THE MEASUREMENT ERROR VECTOR v

TOTAL ERROR COVARIANCE

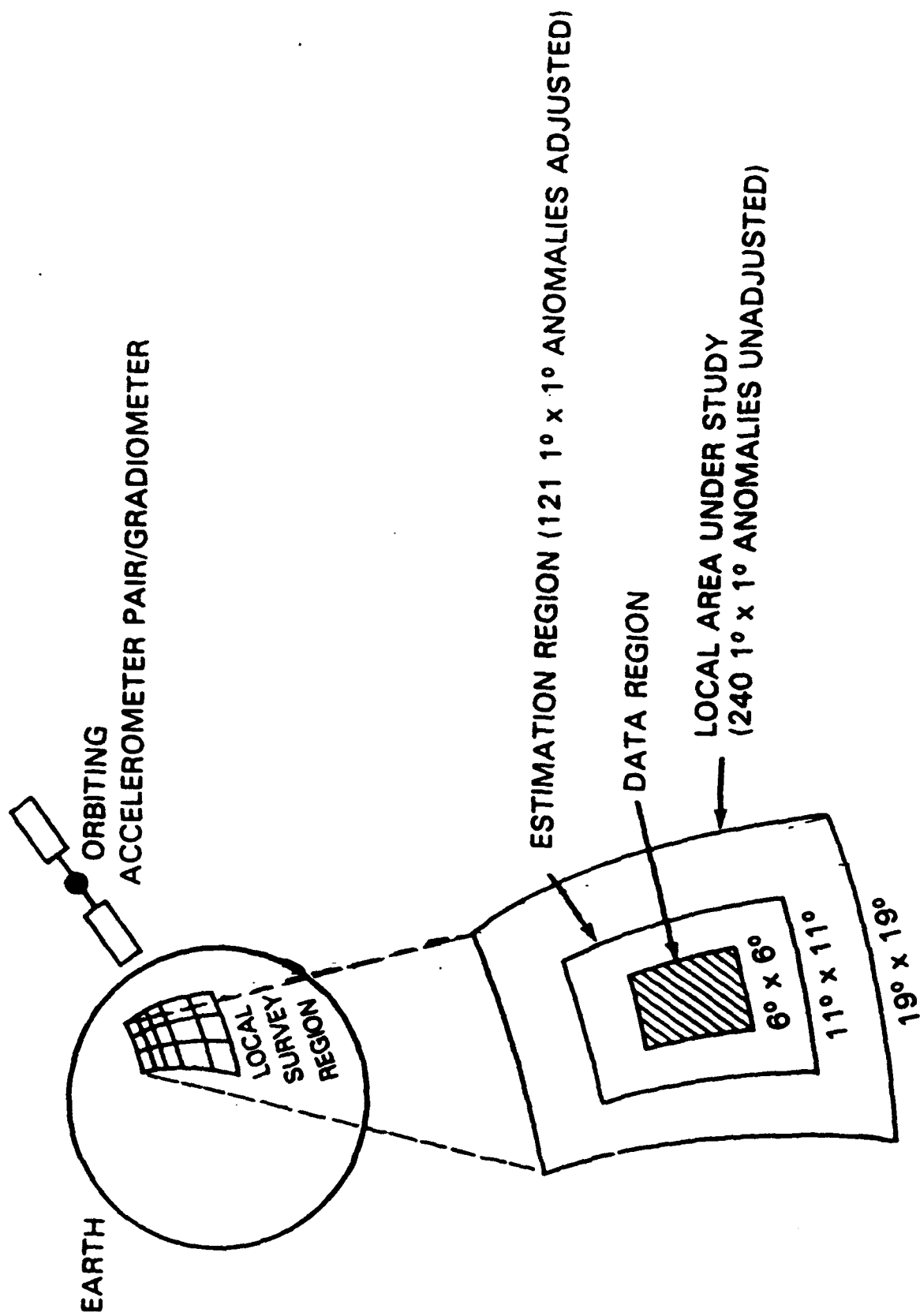
$$\epsilon = \tilde{g}_1 - \hat{g}_1$$

$$E(\epsilon \epsilon^T) = K [P_{g_1}^{-1} + (A_1^T W^{-1} A_2) P_{g_2} (A_2^T W^{-1} A_1) + A_1^T W^{-1} P_v W^{-1} A_1] K$$

IF $P_v = W$ AND $A_2 = 0$ THEN $E(\epsilon \epsilon^T) = K$ AND \hat{g}_1 IS A MINIMUM VARIANCE ESTIMATOR.

STRATEGY

GRADIOMETER/LOCAL SURVEY REGION GEOMETRY FOR $1^\circ \times 1^\circ$ ANOMALIES



GRAVITY AND GEOID ANOMALY UNCERTAINTY FOR A ONE AXIS AND THREE AXIS GRADIOMETER VS RESOLUTION

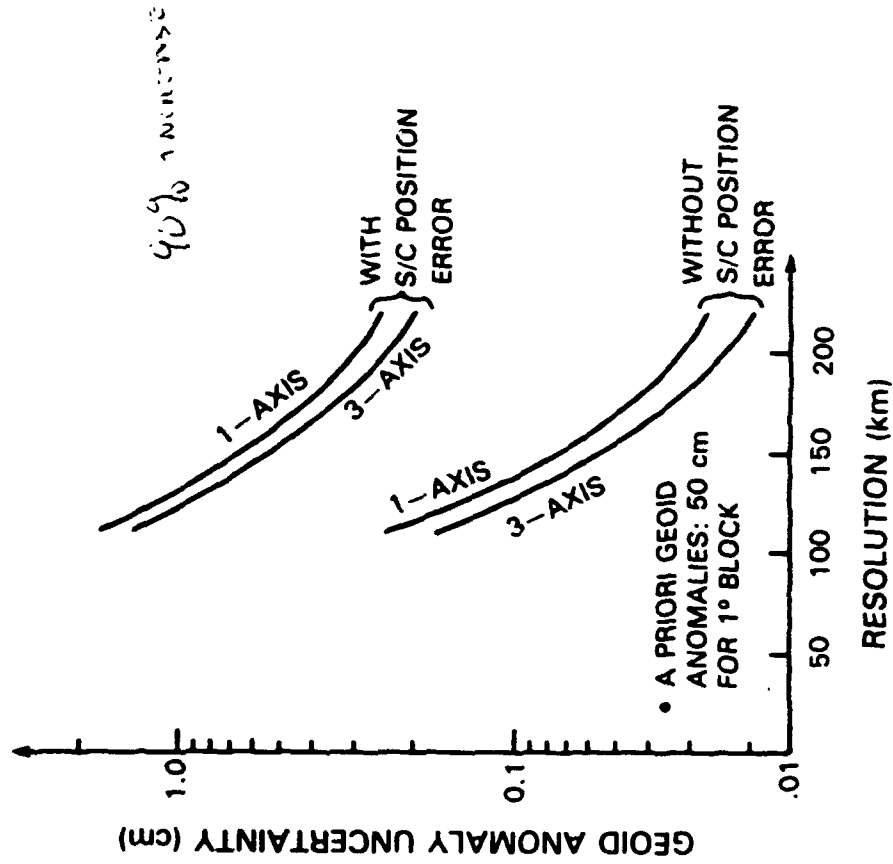
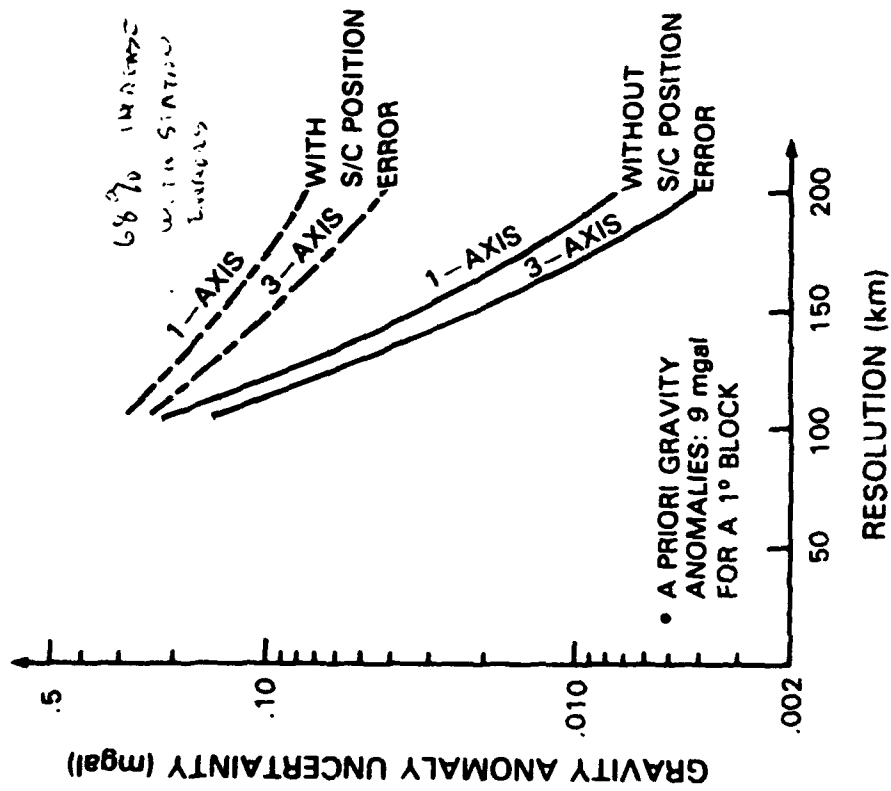
ASSUMPTIONS:

ORBIT

- CIRCULAR/POLAR
- ALTITUDE: 160 km
- MISSION DURATION: 180 DAYS

GRADIOMETER

- PRECISION: $10^{-3}E$
- SAMPLE RATE: 1 MEAS/4S
- SATELLITE POS. ERROR: 5.5 METERS



GRAVITY AND GEOID ANOMALY UNCERTAINTIES FOR A ONE AXIS AND THREE AXIS GRADIOMETER VS RESOLUTION

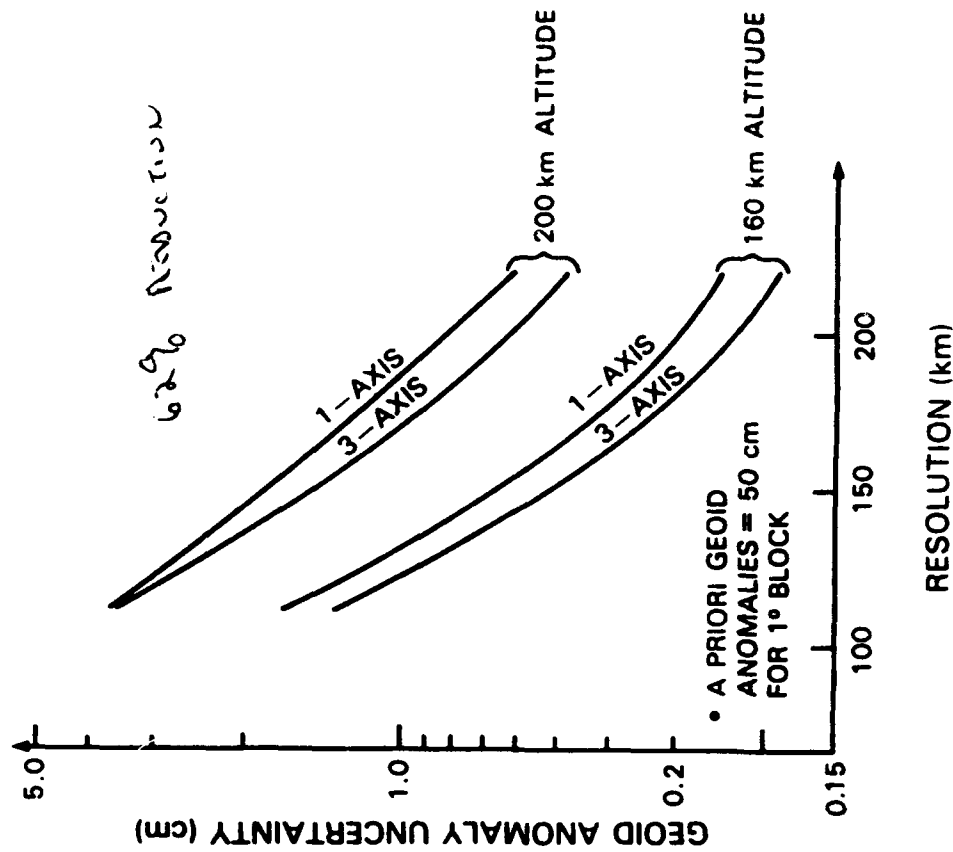
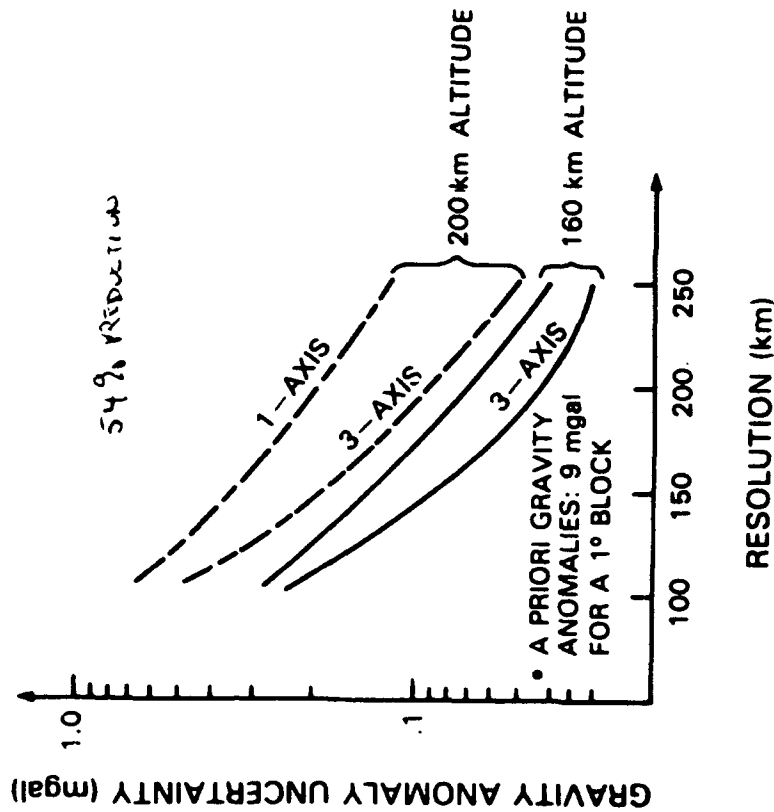
ASSUMPTIONS:

ORBIT

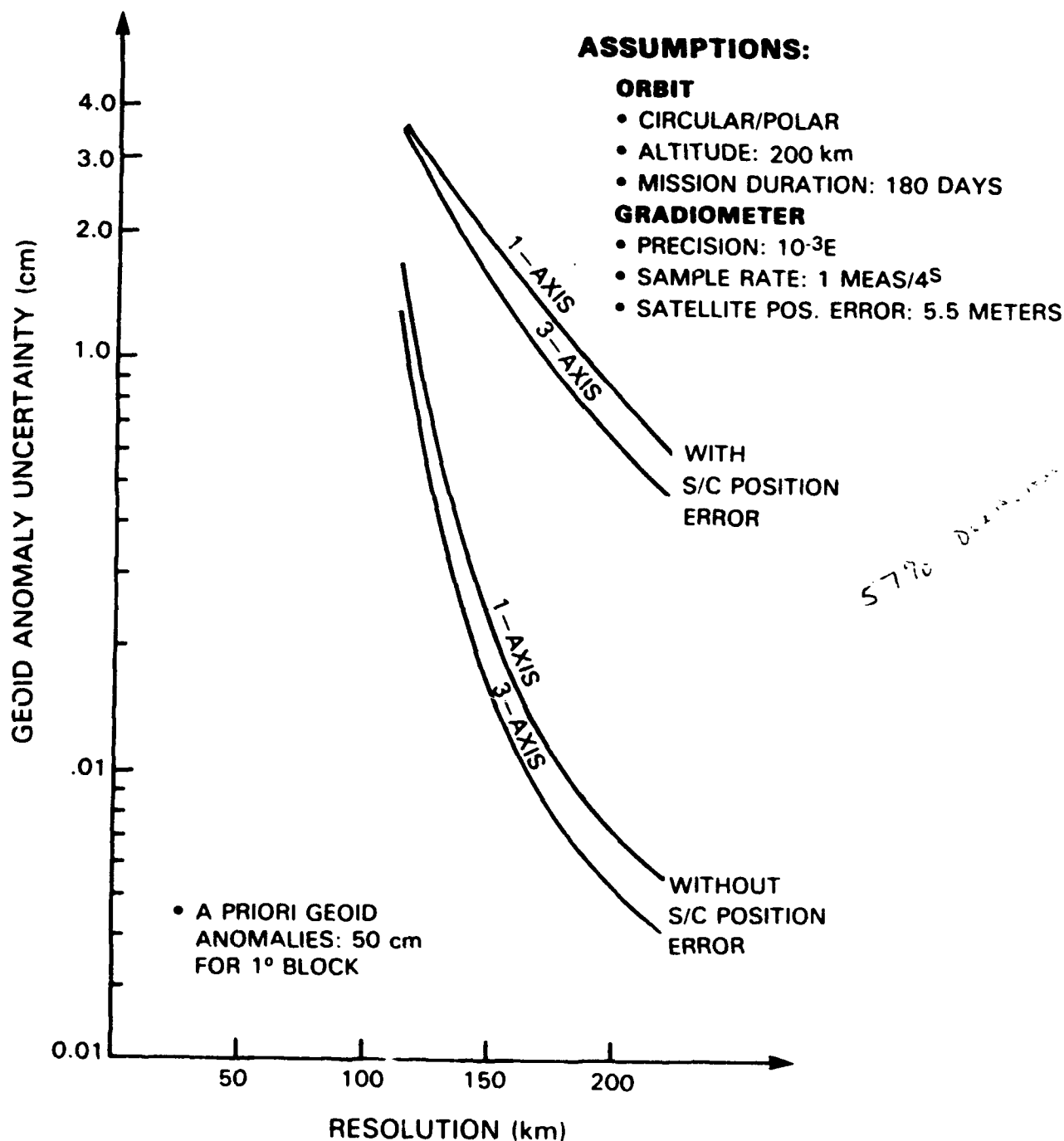
- CIRCULAR/POLAR
- ALTITUDE: 160 km & 200 km
- MISSION DURATION: 180 DAYS

GRADIOMETER

- PRECISION: $10^{-3}E$
- SAMPLE RATE: 1 MEAS/4S
- SATELLITE POS. ERROR: 5.5 METERS



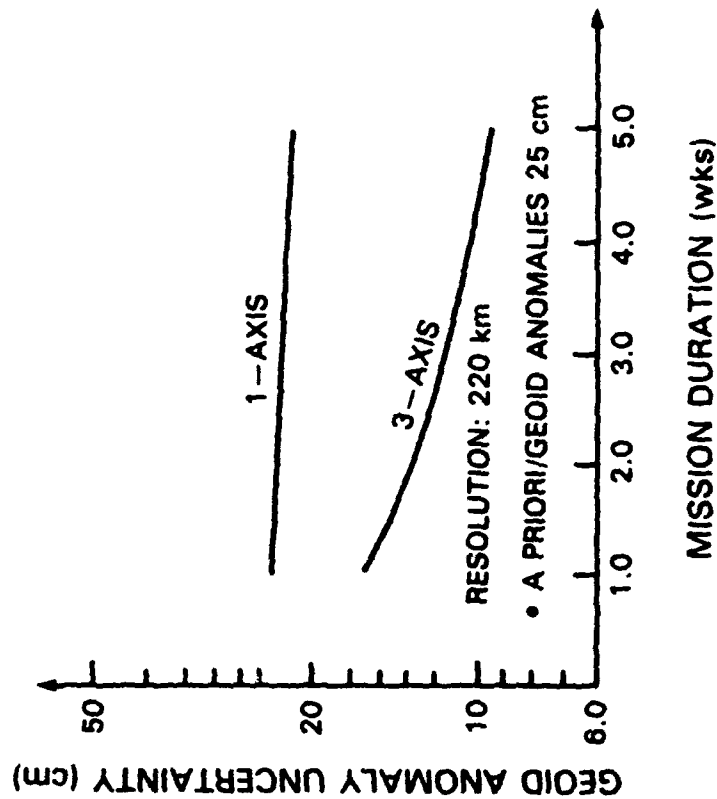
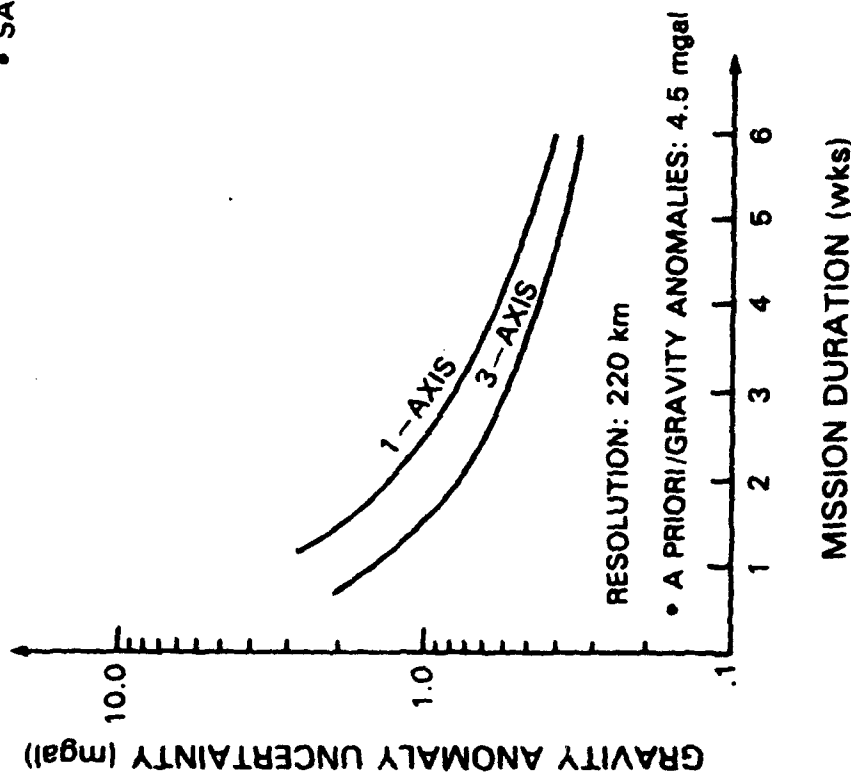
GEOID ANOMALY UNCERTAINTY FOR A ONE AXIS AND THREE AXIS GRAVITY GRADIOMETER VS RESOLUTION



GRAVITY AND GEOID ANOMALY UNCERTAINTY FOR A ONE AXIS AND THREE AXIS GRADIOMETER VS RESOLUTION

ASSUMPTIONS

- ORBIT ALTITUDE: 300km
- INCLINATION: $99^{\circ}.9$
- ECCENTRICITY: 0
- MEASUREMENT PRECISION: $10^{-2}E$
- SAMPLE RATE: 1 MEAS/4S



PAPER TITLE: GRAVITY FIELD FINE STRUCTURE MAPPING USING A SPACEBORNE GRAVITY GRADIOMETER

SPEAKERS NAME: Werner Kahn

Questions and Comments:

Alan Zorn: Have you considered the effects of local or near-field gradients on your 10^{-2} E gradiometer, especially in a shuttle-based experiment?

SPEAKERS RESPONSE: No - but it does need to be considered.

Dave Sonnabend: 1. GRM should be redesigned.

2. Gravity and other problems would drown out shuttle measurements.

A laser would improve GRM range-rate measurement, but other error sources would limit the benefit. Concerns about the shuttle are well founded; but we don't intend to do earth measurements from the shuttle. In a free flyer, we have our work cut out to justify that we can live with these problems.

Stan Jordan: For the GRM and satellite gradiometer missions, what is the track spacing of the orbit at the equator?

SPEAKERS RESPONSE: Speaker did not know off hand.

Lou Decker: What time frame is being considered for the Space Shuttle Gravity Gradiometer Test?

SPEAKERS RESPONSE: The initial flight test of a spaceborne Cryogenic Gravity Gradiometer utilizing the space shuttle is projected for the early 1990's.

SUPERCONDUCTING GRAVITY GRADIOMETER ON THE SPACE SHUTTLE

S. H. Morgan

J. R. Parker

Program Development

NASA, George C. Marshall Space Flight Center

Marshall Space Flight Center, AL 35812

ABSTRACT

NASA is developing a highly precise Superconducting Gravity Gradiometer through the efforts of a research group at the University of Maryland. By providing very precise global mapping of the Earth's gravity field, this gradiometer will be an important element of NASA's Earth Sciences Program of the 1990s. The gradiometer utilizes superconducting technology to measure very small differential gravity signals in the presence of large accelerations and/or disturbances. An engineering group at the Marshall Space Flight Center, in conjunction with a study team composed of other NASA centers, the U.S. Army, the U.S. Air Force, and the University of Maryland, has begun an analysis to define an experiment to be flown aboard the Space Shuttle. The objective of the analysis is to establish the feasibility and to provide data for future detailed design of a Flight Experiment System. This paper contains results to-date of the preliminary design of a Space Shuttle Flight of the Superconducting Gravity Gradiometer.

**A SUPERCONDUCTING GRAVITY GRADIOMETER
FLIGHT DEMONSTRATION ON THE SPACE SHUTTLE**

**JOE R. PARKER
SAMUEL H. MORGAN
PROGRAM DEVELOPMENT
MARSHALL SPACE FLIGHT CENTER
FEBRUARY 12, 1986**

GRAVITY GRADIOMETER TEAM OBJECTIVES

1. TO DEVELOP A TOTAL SYSTEM CONCEPT FOR A SPACE QUALIFIED THREE-AXIS SUPERCONDUCTING GRAVITY GRADIOMETER INTEGRATED WITH A SIX-AXIS SUPERCONDUCTING ACCELEROMETER
2. TO EXAMINE AND RECOMMEND METHODS FOR FLIGHT TEST OF THE GRAVITY GRADIOMETER PACKAGE IN SPACE
3. TO EXAMINE METHODS FOR THE ACQUISITION, PROCESSING AND ANALYSIS OF SPACE DERIVED GRAVITY GRADIOMETER DATA, AND
4. TO PROVIDE A DETAILED PLAN (INCLUDING SCHEDULE AND COSTS) FOR AN INITIAL SPACEBORNE CRYOGENIC GRAVITY GRADIOMETER FLIGHT TEST IN THE EARLY 1990'S

-
5. MAINTAIN COST WITHIN BUDGETARY CONSTRAINTS, I.E. - LOW COST

FLIGHT DEMONSTRATION

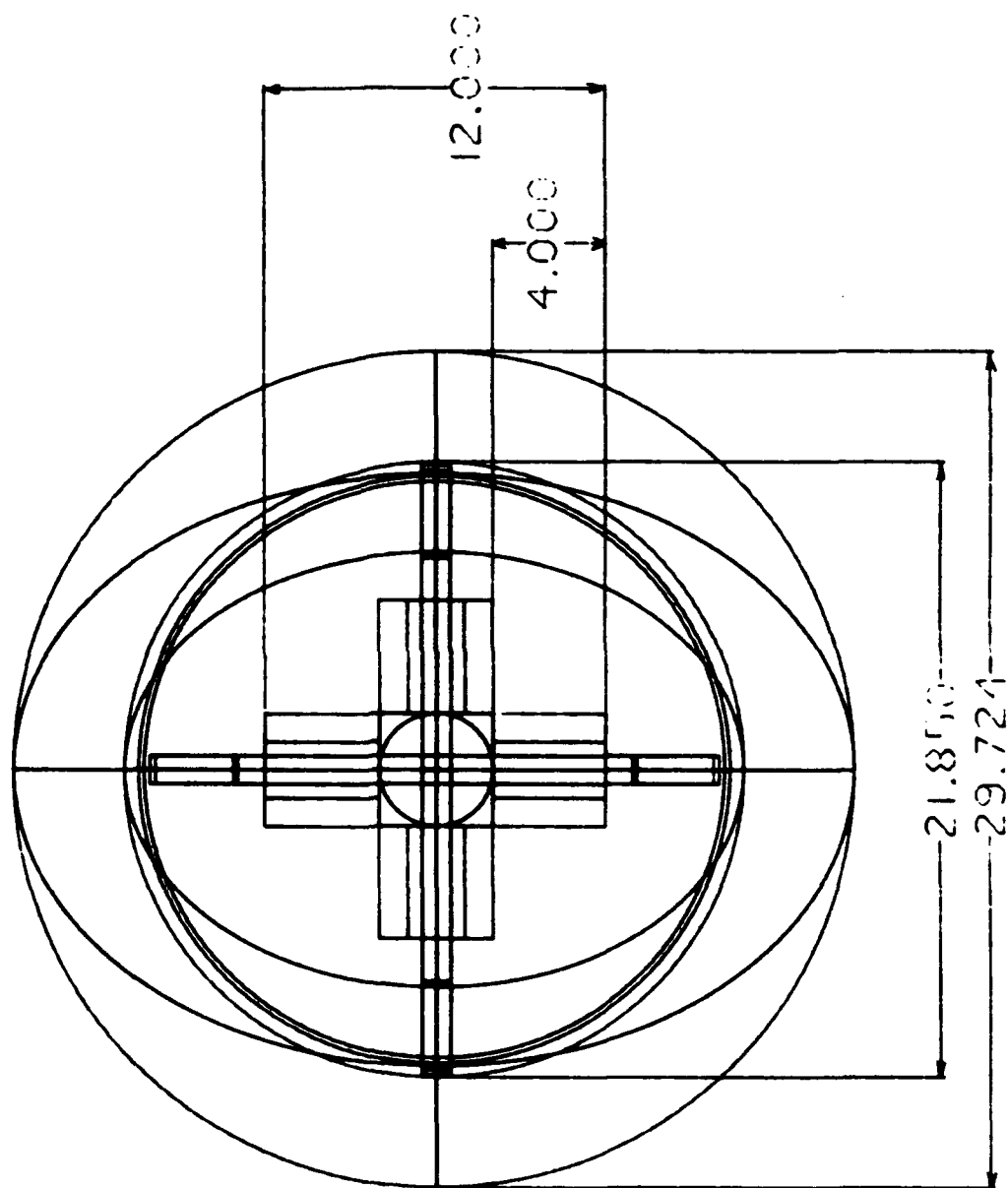
OPTIONS

- 1) INSTRUMENT HARD MOUNTED WITHIN CARGO BAY
- 2) INSTRUMENT ISOLATED (SEMI DRAGFREE) WITHIN
CARGO BAY
- 3) FREE FLYER

OBJECTIVES

- PRECURSOR FLIGHT OF SUPERCONDUCTING GRAVITY GRADIOMETER
IN SPACE IS NECESSARY TO INSURE SUCCESS OF EXPENSIVE LONG-
DURATION MISSION
 - TEST AND CALIBRATE IN ZERO-GRAVITY
- PROMOTE FULL DEVELOPMENT OF TECHNOLOGY

SUPER CONDUCTING GRAVITY GRADIOMETER



INFRARED TELESCOPE (IRT) DEWAR
(FLEW ON SPACELAB 2)

WEIGHT: (LBS)

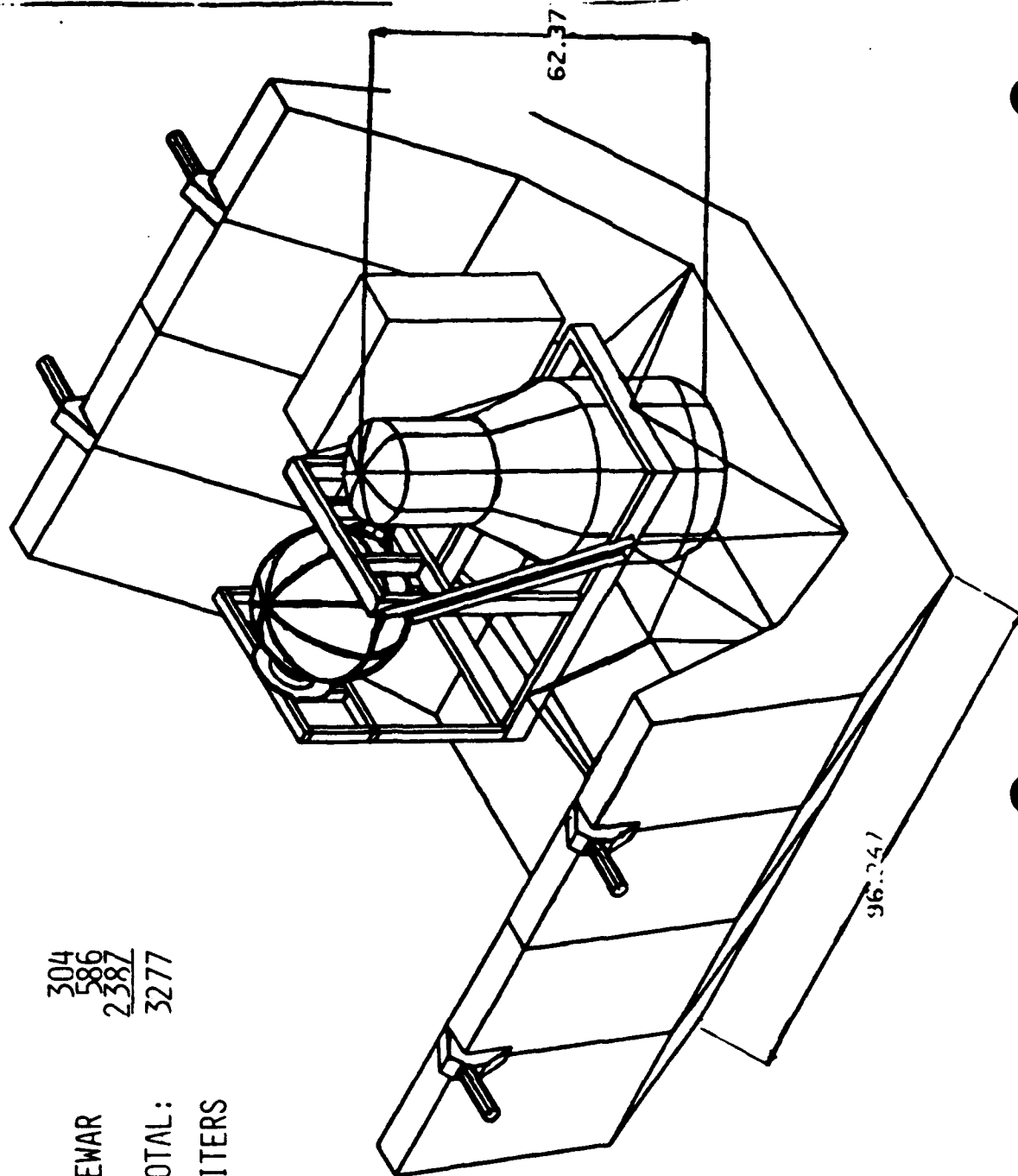
INSTRUMENT
MOUNTING HARDWARE + DEWAR
PALLET + PUMPS

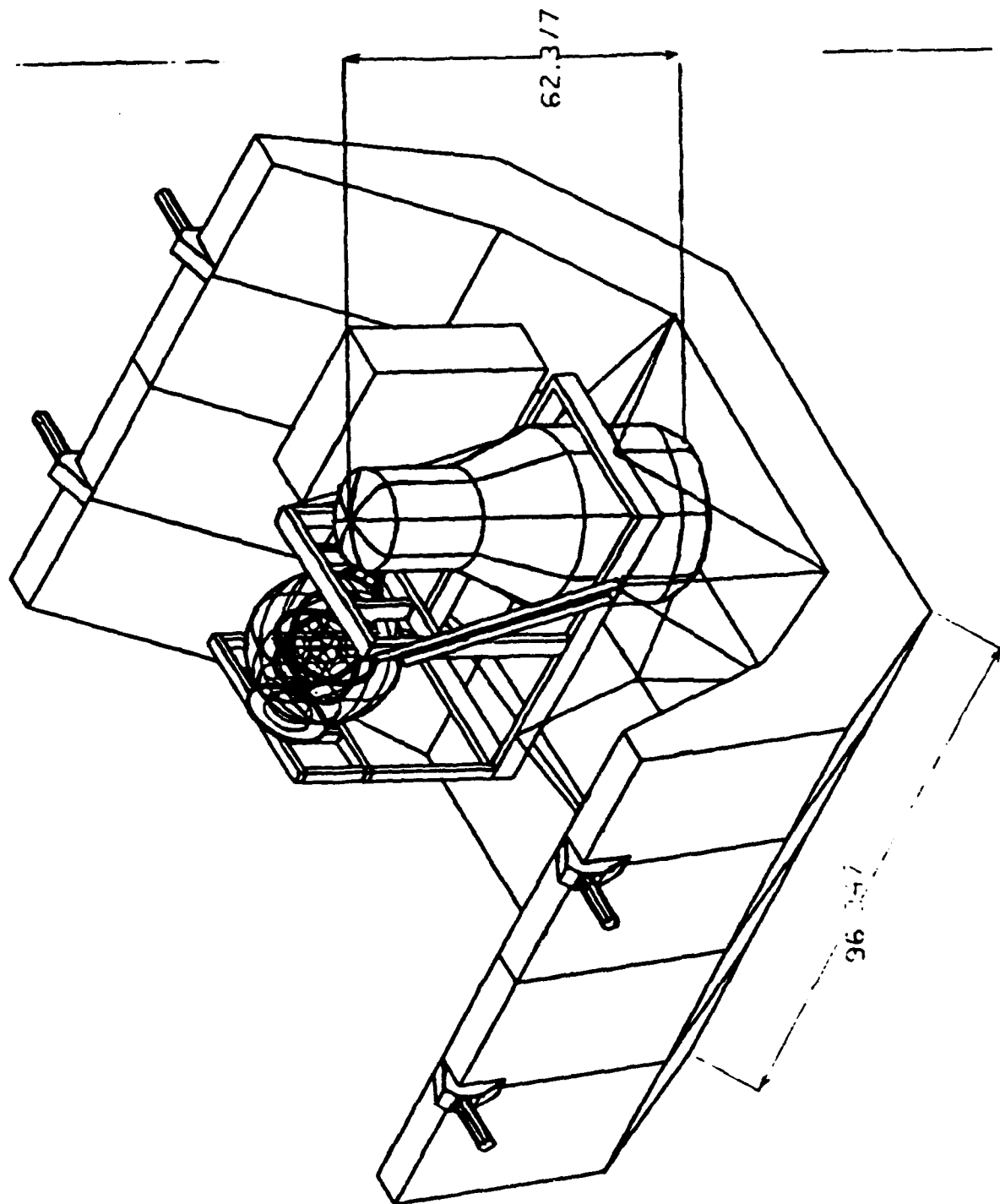
304
586
2387

TOTAL:

3277

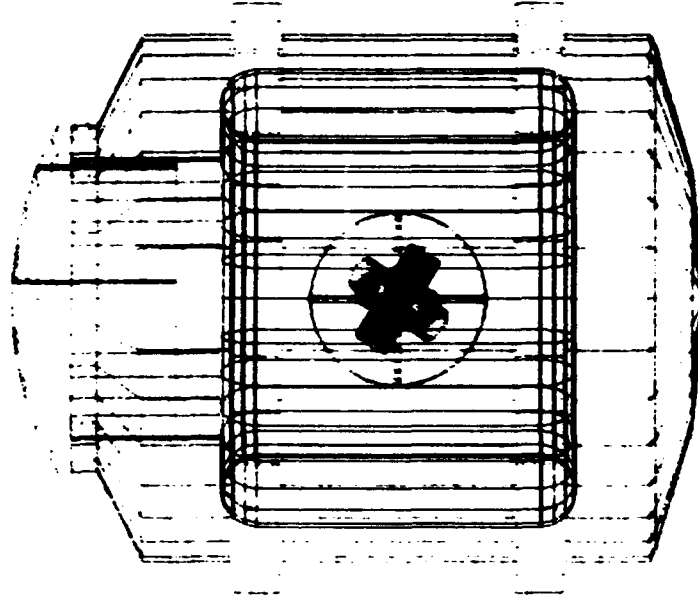
HELIUM CAPACITY: 220 LITERS





11 5

COBE DEWAR WEIGHT:
HELIUM CAPACITY: 660 LITERS



11 5

0 AU:DR

0 COSMIC BACKGROUND EXPLORER (COBE) DEWAR

MSFC/PD23 G. MAJOS

2/12/86

Command:

Logged in as gah.nene.nene Friday, February

SPACELAB I ACCELERATION LEVELS

MDTSCO

TM SEAD-85038A

MAY 1985

	MODULE			PALLET		
	X-DIRECTION	Y-DIRECTION	Z-DIRECTION	X-DIRECTION	Y-DIRECTION	Z-DIRECTION
"QUIET TIME" 11.18-11.23 Hrs. LEVEL (G) FREQUENCY (HZ)	HI - 0.0004 LO - 0.00035 HI - 35 LO - 20	HI - 0.00025 LO - 0.00025 HI - 40 LO - 22	HI - 0.0005 LO - 0.00065 HI - 40 LO - 17	HI - 0.00025 LO - 0.00013 HI - 22 LO - 22	HI - 0.00045 LO - 0.0002 HI - 22 LO - 22	HI - 0.00025 LO - 0.00013 HI - 8 LO - 16
COUGH TEST 11.314-11.315 Hrs. LEVEL (G) FREQUENCY (HZ)	0.001 10	0.001 11	0.0028 9	0.0002 10	0.0003 8	0.0007 10
X-PUSH-OFF 11.340-11.355 Hrs. LEVEL (G) FREQUENCY (HZ)	0.0028 12	0.003 21	0.0025 9	0.0006 12	0.0010 6	0.0012 8
Y PUSH-OFF 11.375-11.385 Hrs. LEVEL (G) FREQUENCY (HZ)	0.0001 16	0.001 21	0.0024 8	0.0003 18	0.0005 15	0.0005 8
Z PUSH-OFF 11.404-11.406 Hrs. LEVEL (G) FREQUENCY (HZ)	0.0011 12	0.001 20	0.0017 16	0.0007 15	0.0011 17	0.0010 9
THRUSTER FIRING 202050-202110 Sec. (25 LB) LEVEL (G) FREQUENCY (HZ)	0.0003-0.0005 17	0.0003-0.0006 25	0.0005-0.0010 18	NOT AVAILABLE	NOT AVAILABLE	NOT AVAILABLE
THRUSTER FIRING 188.870-188.930 Hrs (870 LB) LEVEL (G) FREQUENCY (HZ)	0.025-0.029 9	0.02-0.029 9	0.025-0.029 9	0.01-0.015 8	0.01-0.015 16	0.02-0.029 16
DISTURBANCE 188.431-188.435 Hrs LEVEL (G) FREQUENCY (HZ)	0.012 11	0.006 20	0.009 15	0.0025 12	0.0024 25	0.003 12

Table 3-2. Summary of Orbiter Acceleration Measurement Data

016

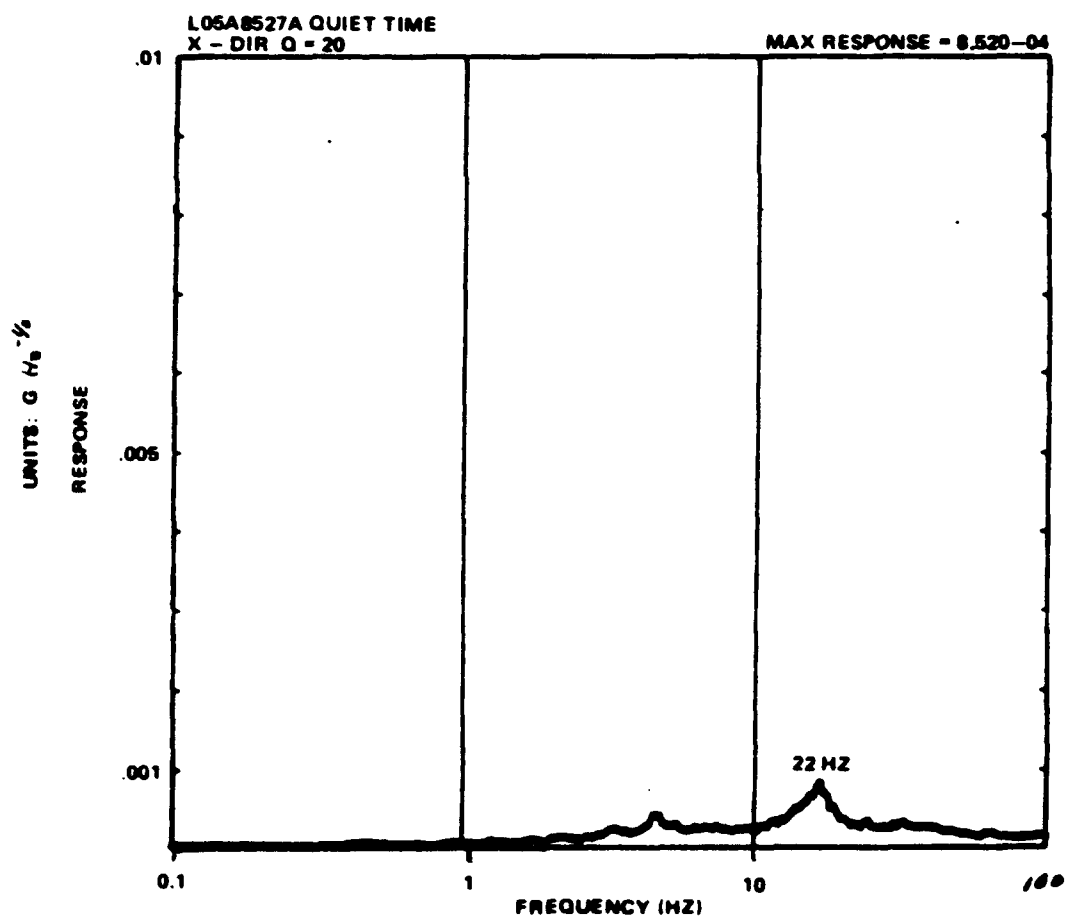
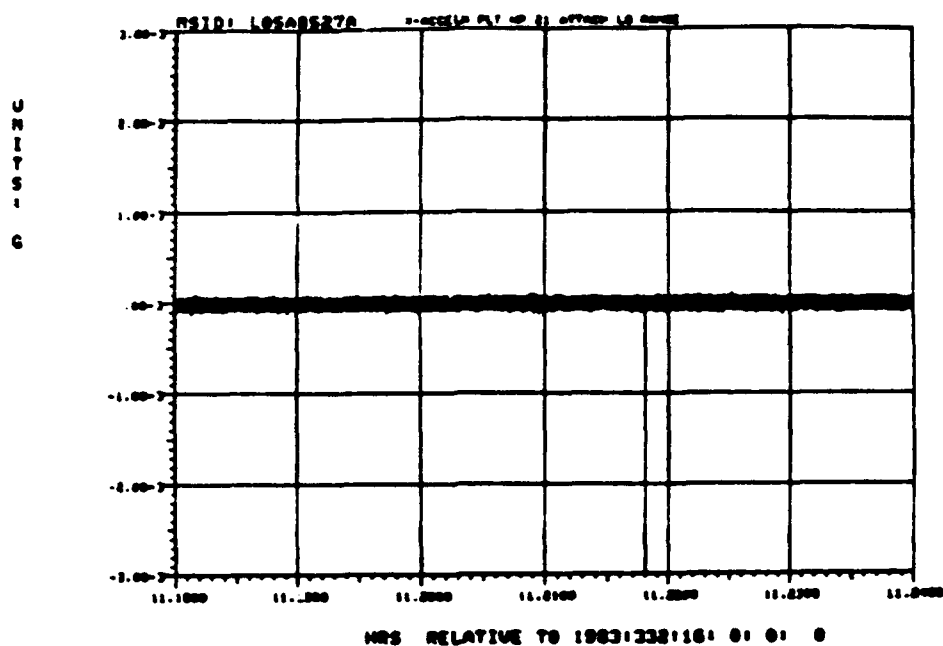


FIGURE B-4 TRANSIENT ACCELERATION AND SHOCK SPECTRUM, HARDPOINT 21, X ACCELERATION (LOWER RANGE) DURING "QUIET TIME"

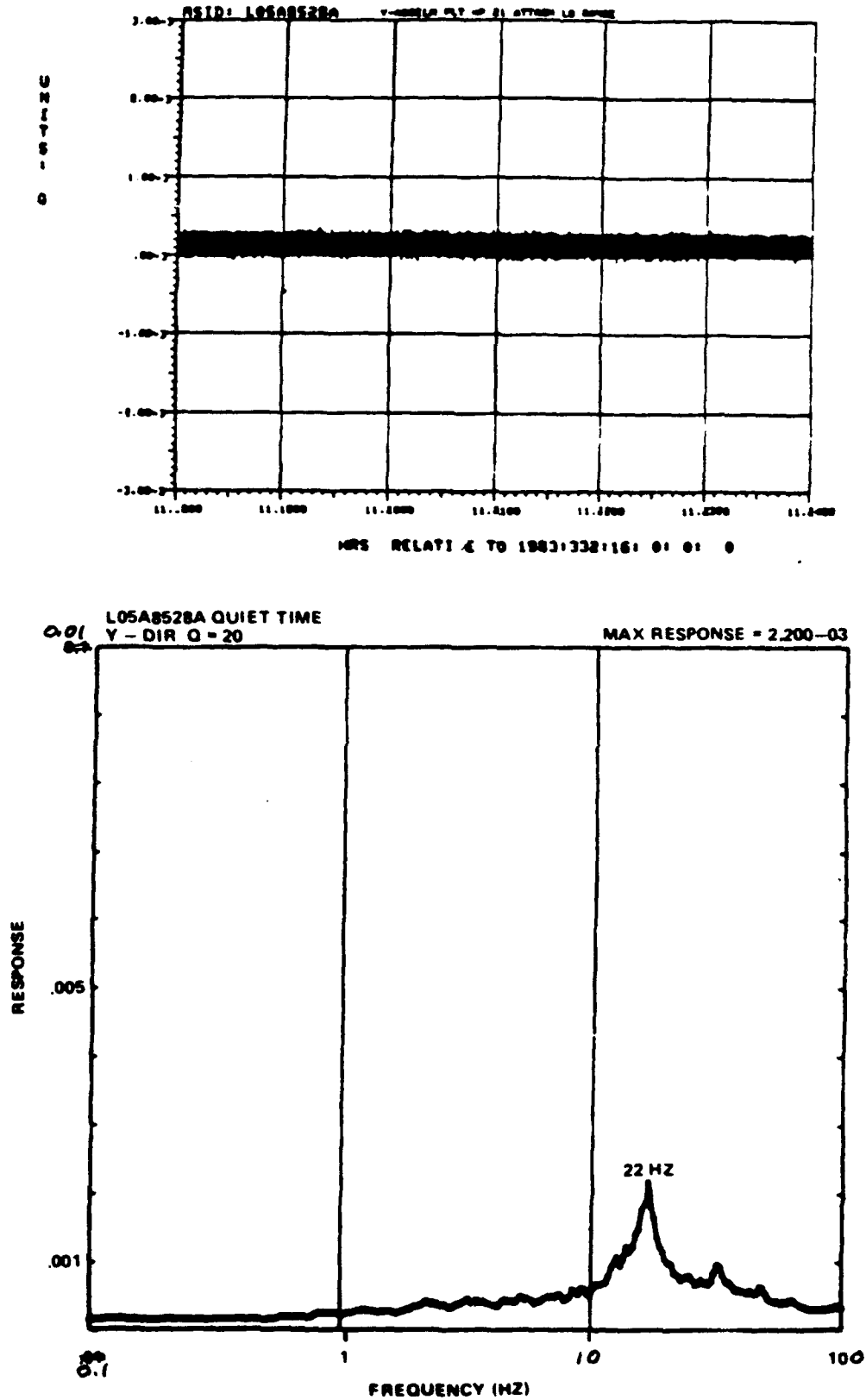


FIGURE B-5 TRANSIENT ACCELERATION AND SHOCK SPECTRUM, HARDPOINT 21, Y ACCELERATION (LOWER RANGE) DURING "QUIET TIME"

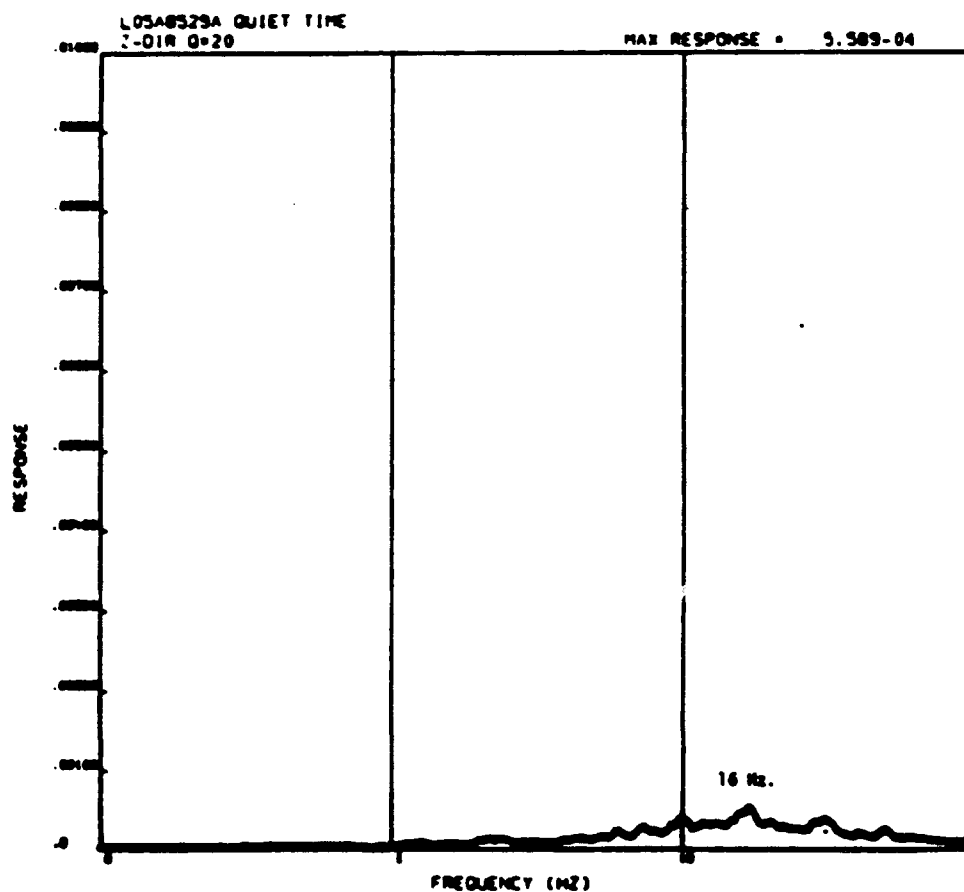
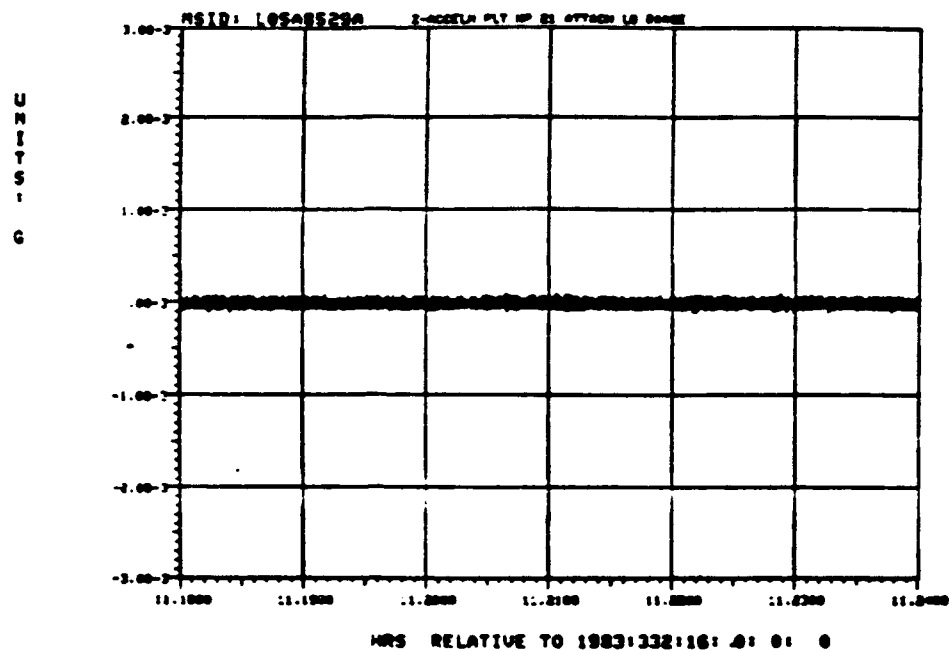


Figure B-6 Transient Acceleration and Shock Spectrum, Hardpoint 21,
Z Acceleration (LOWER RANGE) During "Quiet Time"

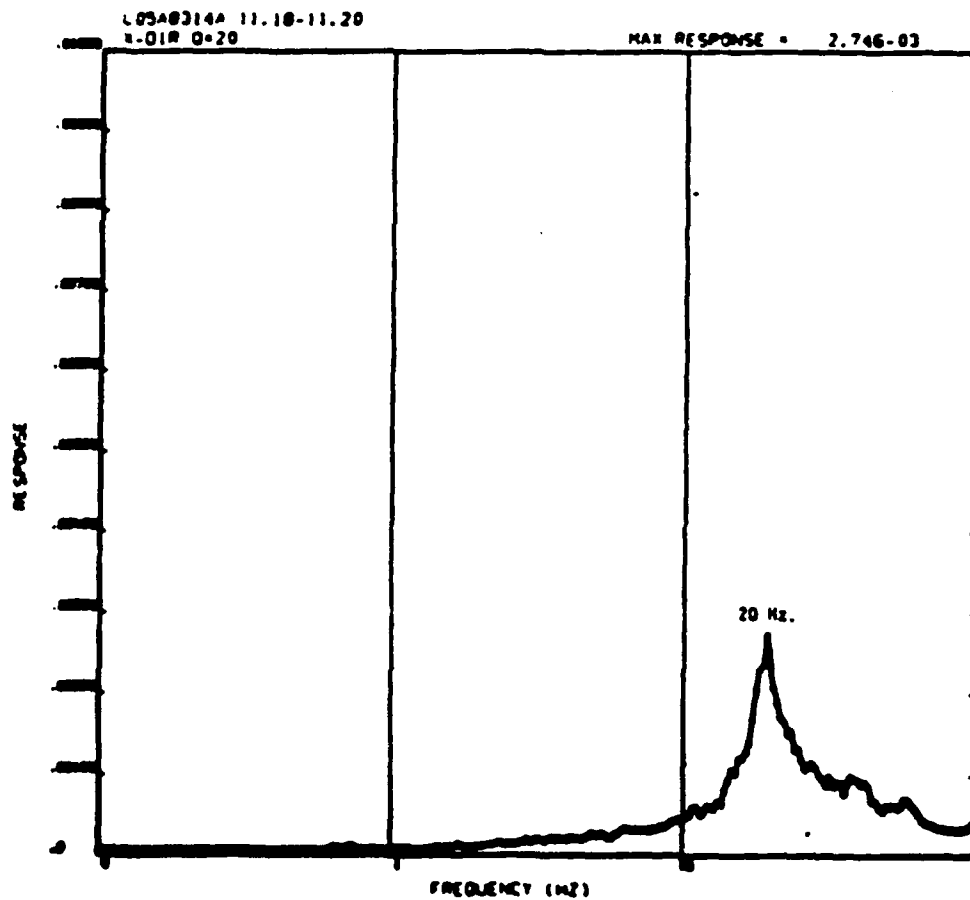
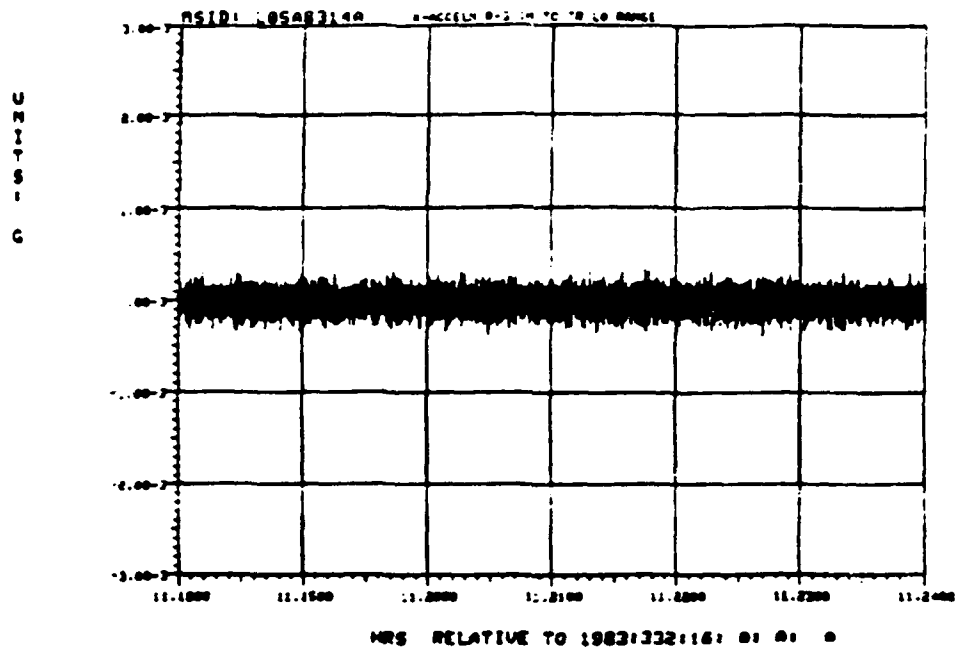


Figure B-1 Transient Acceleration and Shock Spectrum, Rack 3,
X Acceleration (LOWER RANGE) During "Quiet Time"

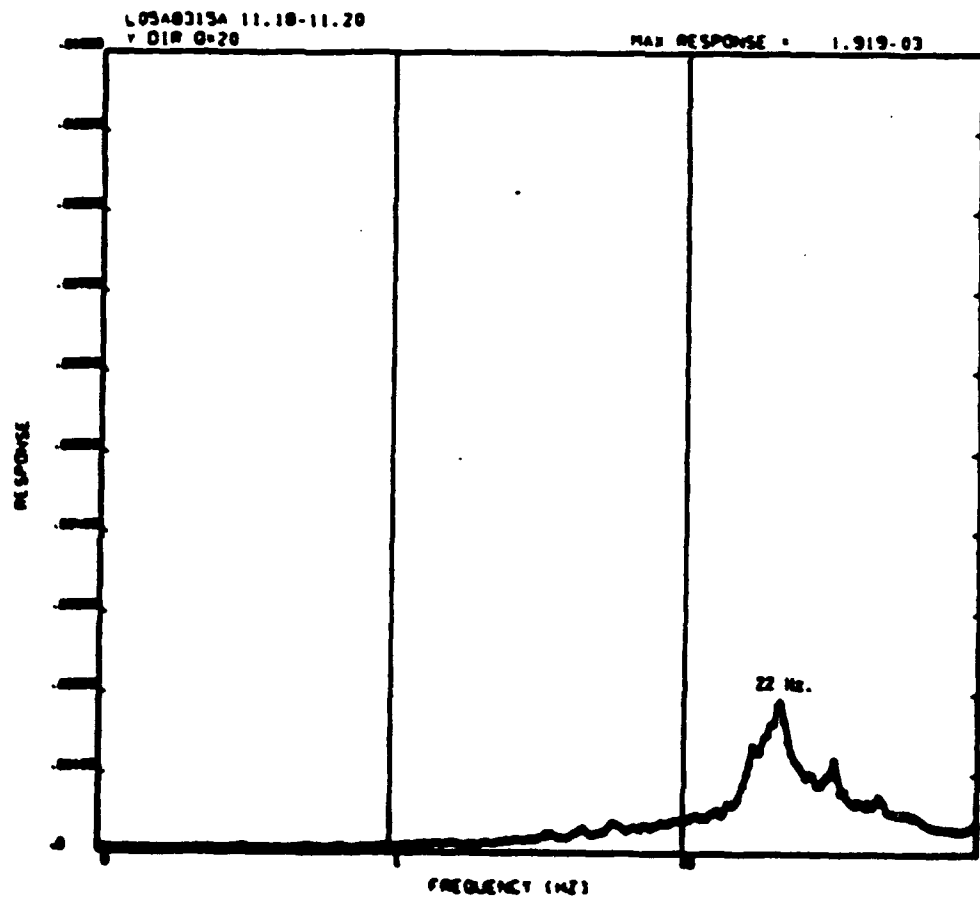
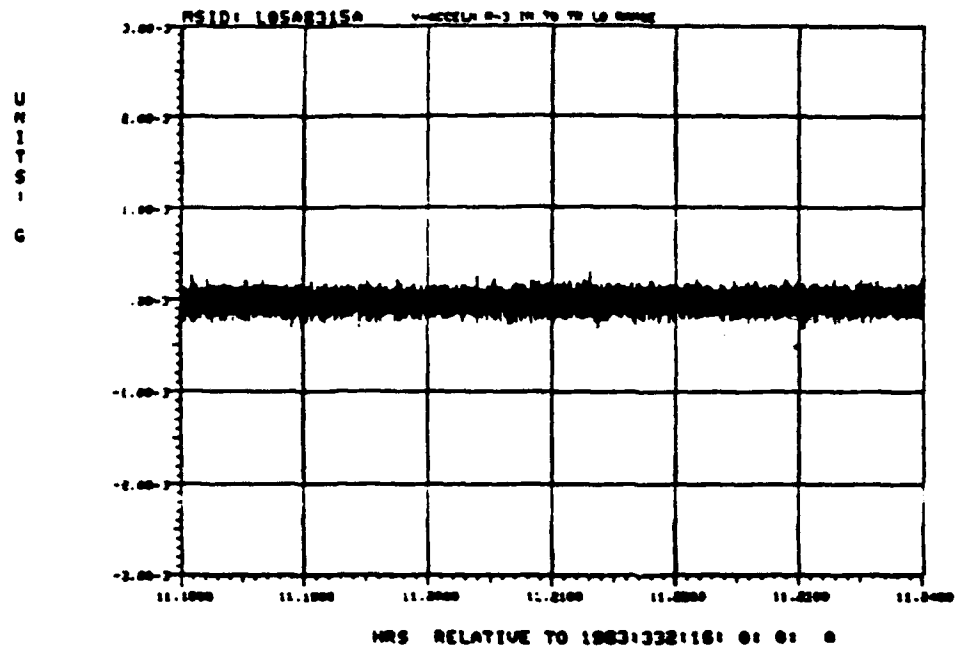


Figure B-2 Transient Acceleration and Shock Spectrum, Rack 3,
Y Acceleration (LOWER RANGE) During "Quiet Time"

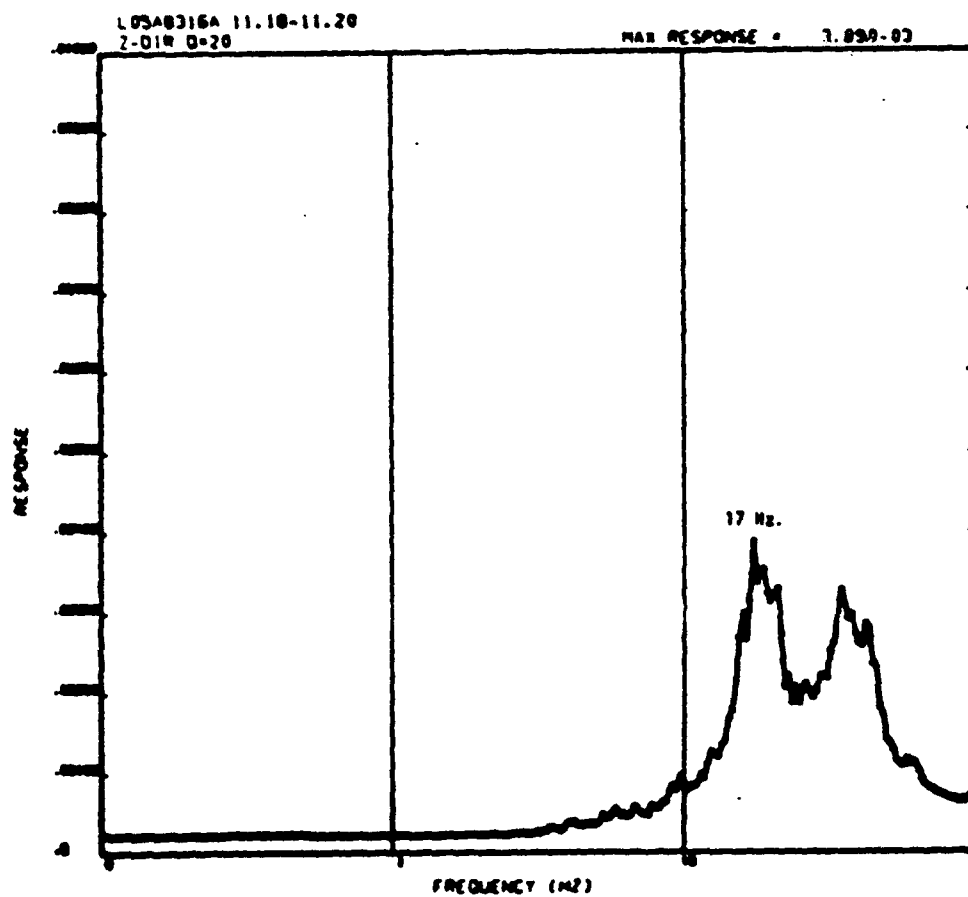
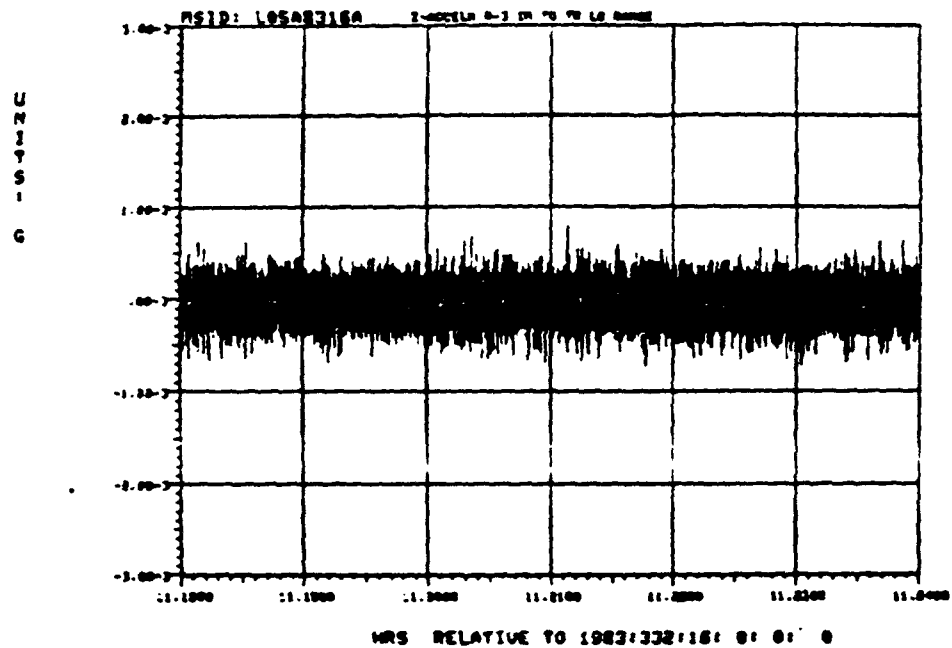


Figure B-3 Transient Acceleration and Shock Spectrum, Rack 3,
Z Acceleration (LOWER RANGE) During "Quiet Time"

DEVELOPMENT OF SUPERCONDUCTING GRAVITY GRADIOMETER
FOR SPACE APPLICATIONS

H. A. Chan

M. V. Moody

H. J. Paik

Dept of Physics and Astronomy

University of Maryland

College Park, Maryland 20742

ABSTRACT

Principles and Design of the Three-Axis Superconducting Gravity Gradiometer
will be discussed. Status of construction and test will be reported.

*Development of a Superconducting Gravity
Gradiometer for Space Applications*

H. A. Chan , M. V. Moody , and H. J. Paik

Superconducting Accelerometer

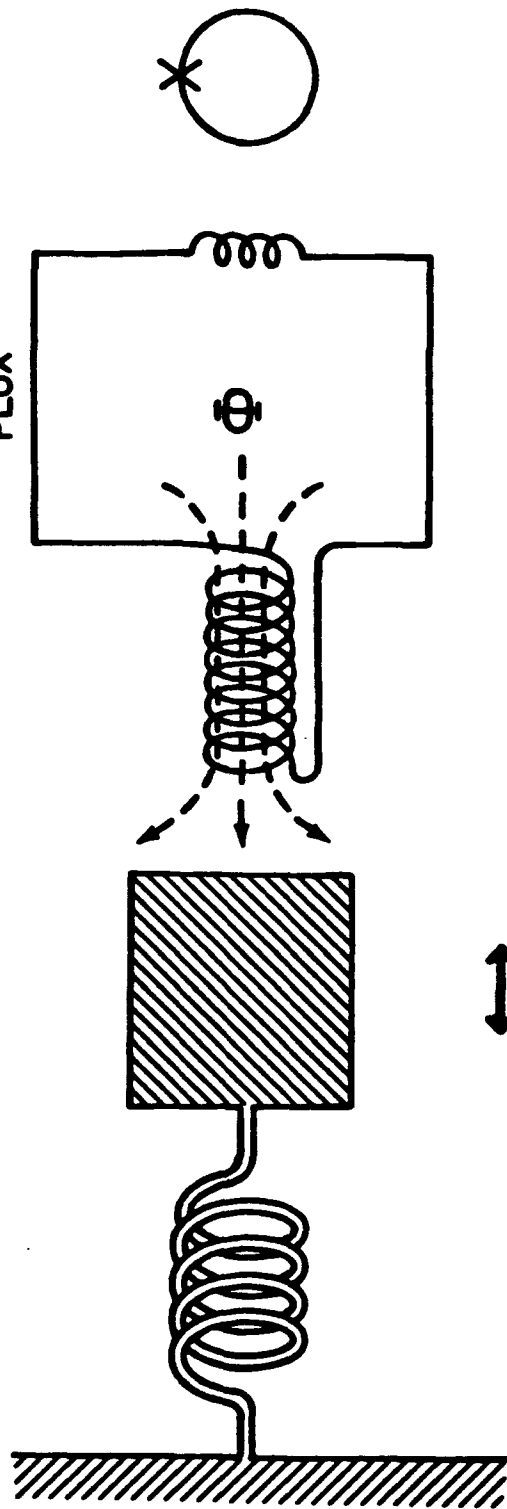
WEAK
SPRING

SUPERCONDUCTING
PROOF MASS

SENSING
COIL

QUANTIZED
MAGNETIC
FLUX

SQUID
AMPLIFIER



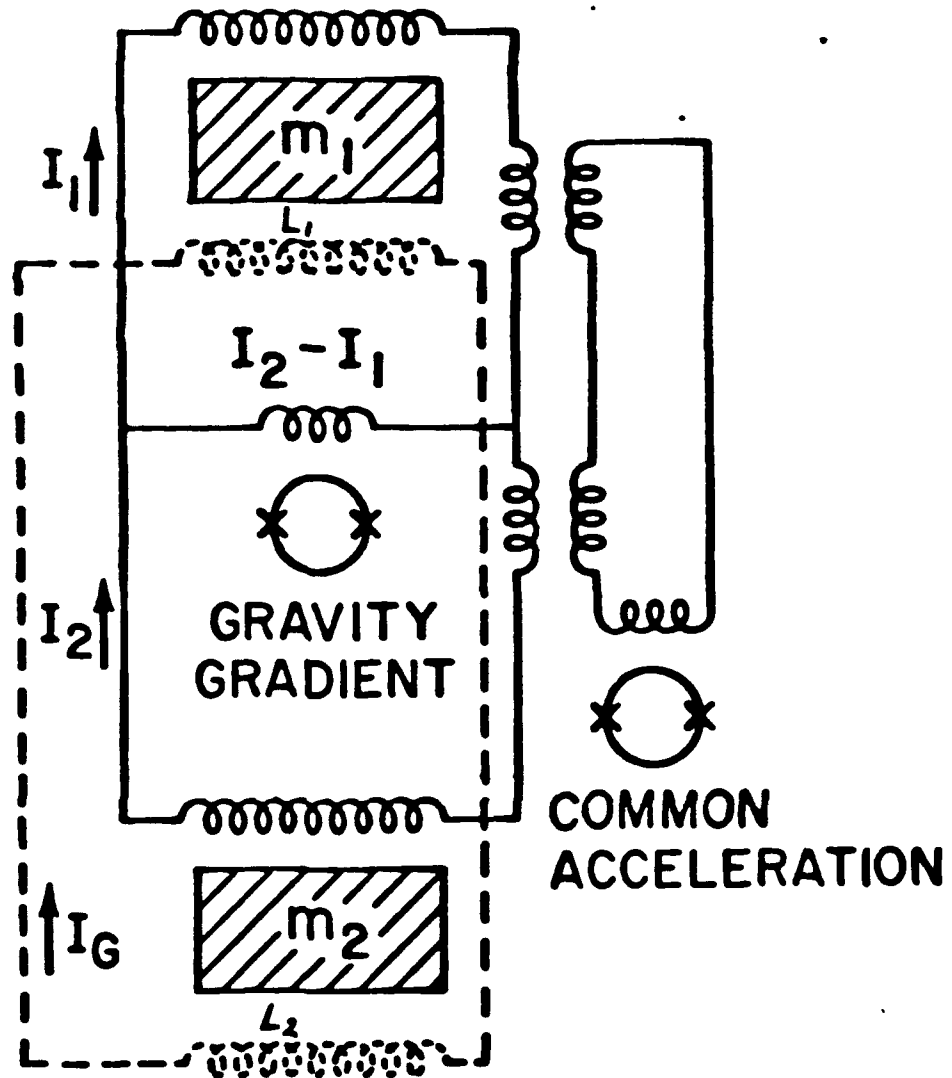
ACCELERATION

DISPLACEMENT

INDUCTANCE
MODULATION

CURRENT
RESPONSE

VOLTAGE
OUTPUT



Sensing circuit —

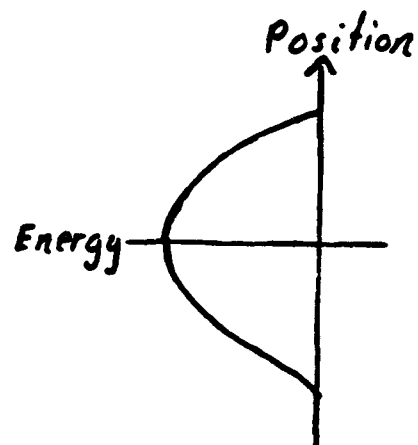
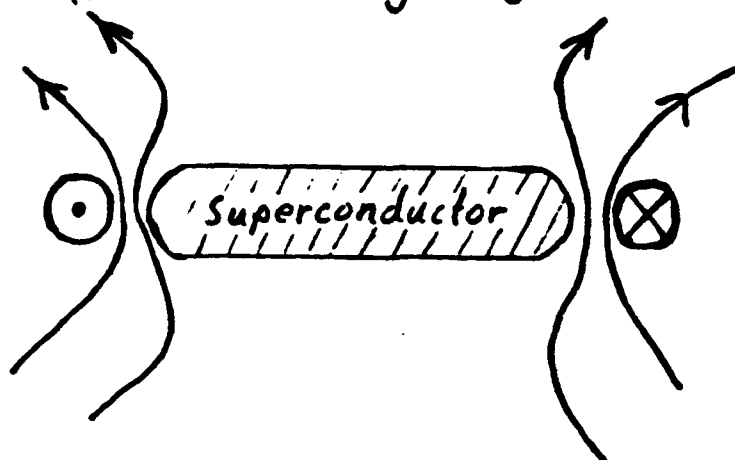
adjust ratio of I_1 to I_2 to balance out common mode accelerations.

Levitation circuit ----

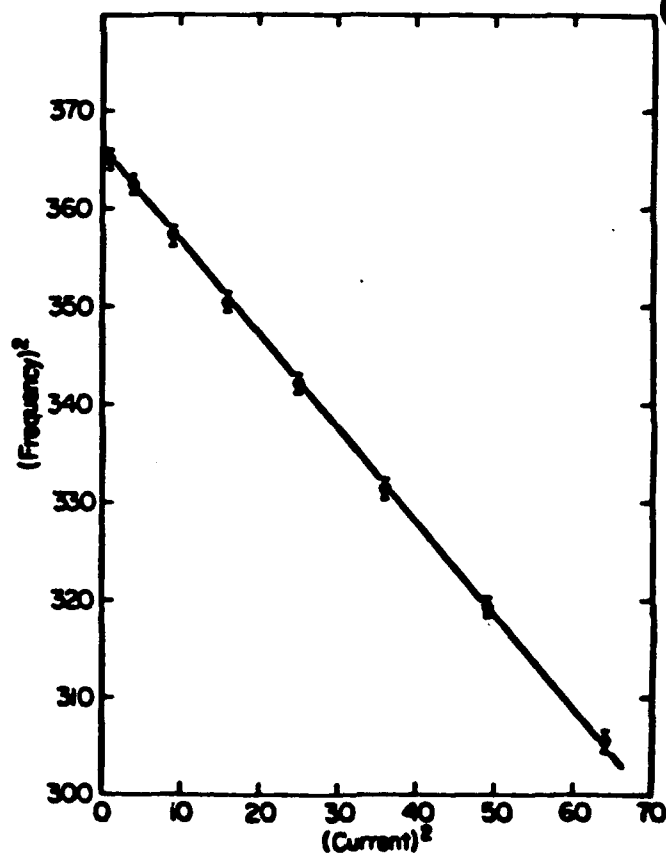
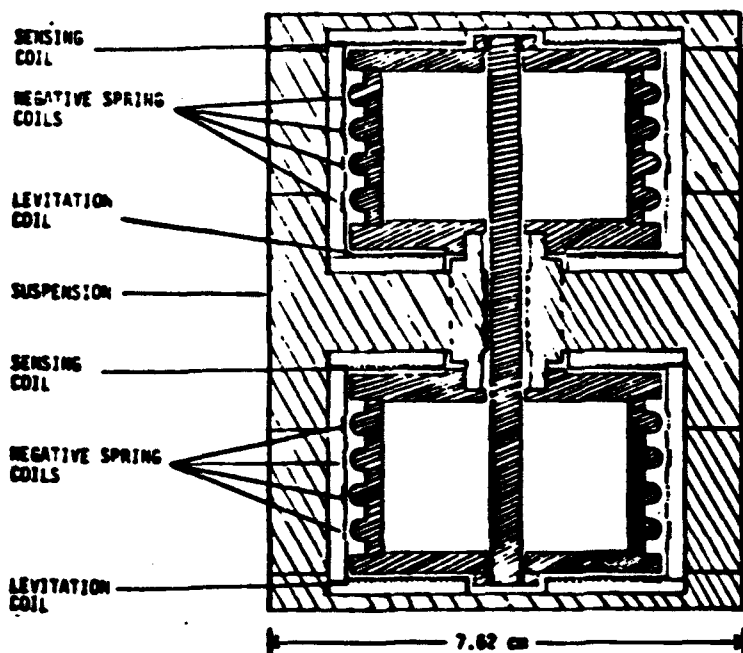
$$(L_1 + L_2) I_G = \Phi \approx \text{constant}$$

increases only differential mode resonance frequency

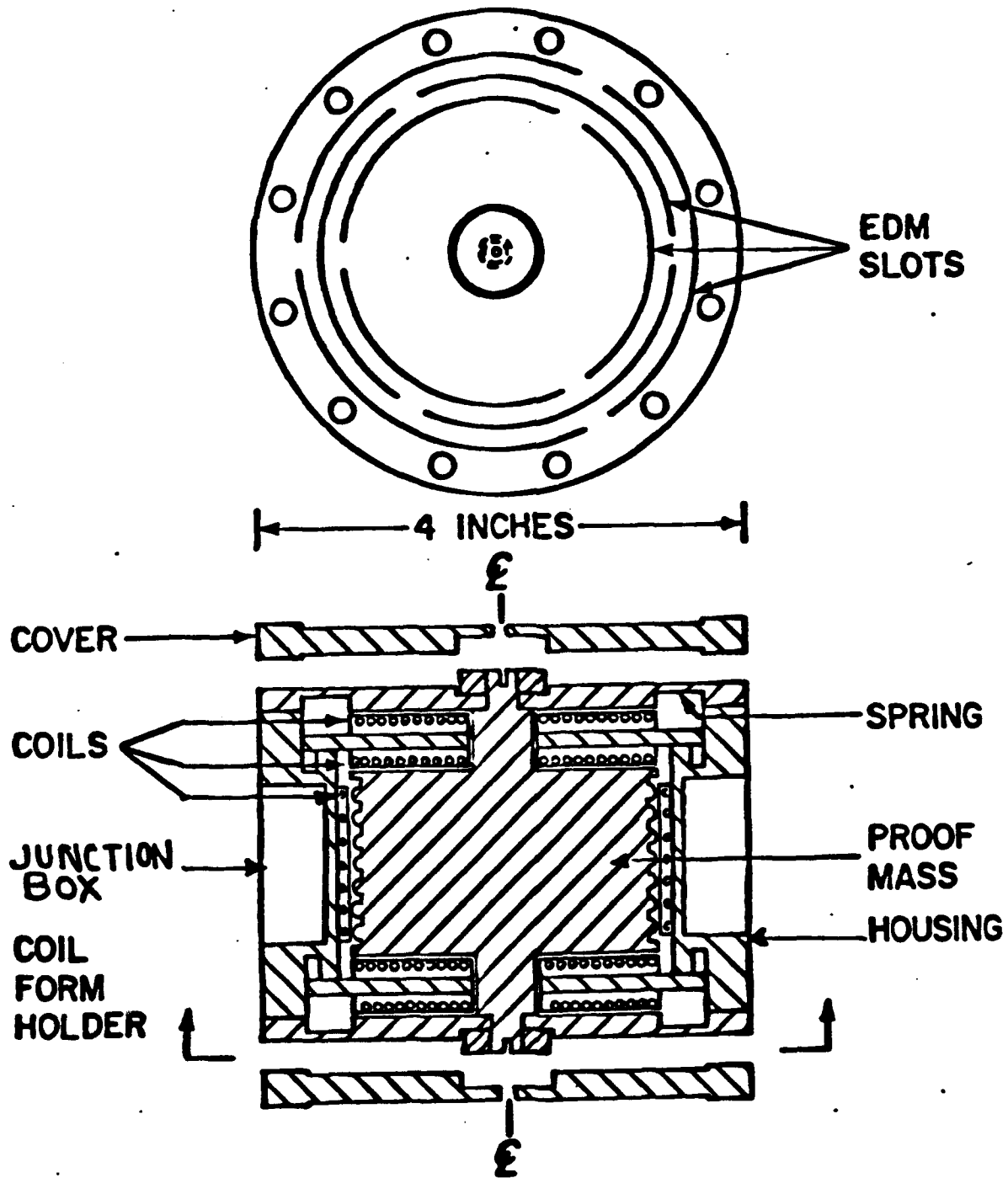
Superconducting Negative Spring



$$\text{Energy} = -\frac{1}{2} kx^2 + cx^4 + \dots$$



**3-AXIS SUPERCONDUCTING GRAVITY GRADIOMETER
DESIGN FOR ONE OF SIX IDENTICAL UNITS**



Intrinsic Spectral Noise

$$S_r(f) = \frac{8}{m l^2} \left[K_B T \frac{2\pi f}{Q(f)} + \frac{(2\pi f_0)^2}{2\beta\eta} E_A(f) \right]$$

Design parameters

proof mass	m	1.3 kg
base line	l	0.19 m
resonance frequency	f_0	1 Hz
temperature	T	1.5 K
quality factor	Q	$\geq 10^5$
amplifier noise (SHE dc SQUID)	E_A	$3 \times 10^{-30} \text{ J Hz}^{-1}$
energy coupling factor	$\beta\eta$	~ 0.5

Gravity Gradient Noise

$$S_r^g(f) = 3 \times 10^{-4} \text{ E Hz}^{-1/2} \quad \text{at } 0.1 \text{ Hz}$$

Feedback Functions

Force rebalance

Maintains null position of proof masses.

Reduces nonlinearities.

Increases dynamic range.

Reduces cross coupling

Cold damping

Reduces amplitude of high Q resonance peak.

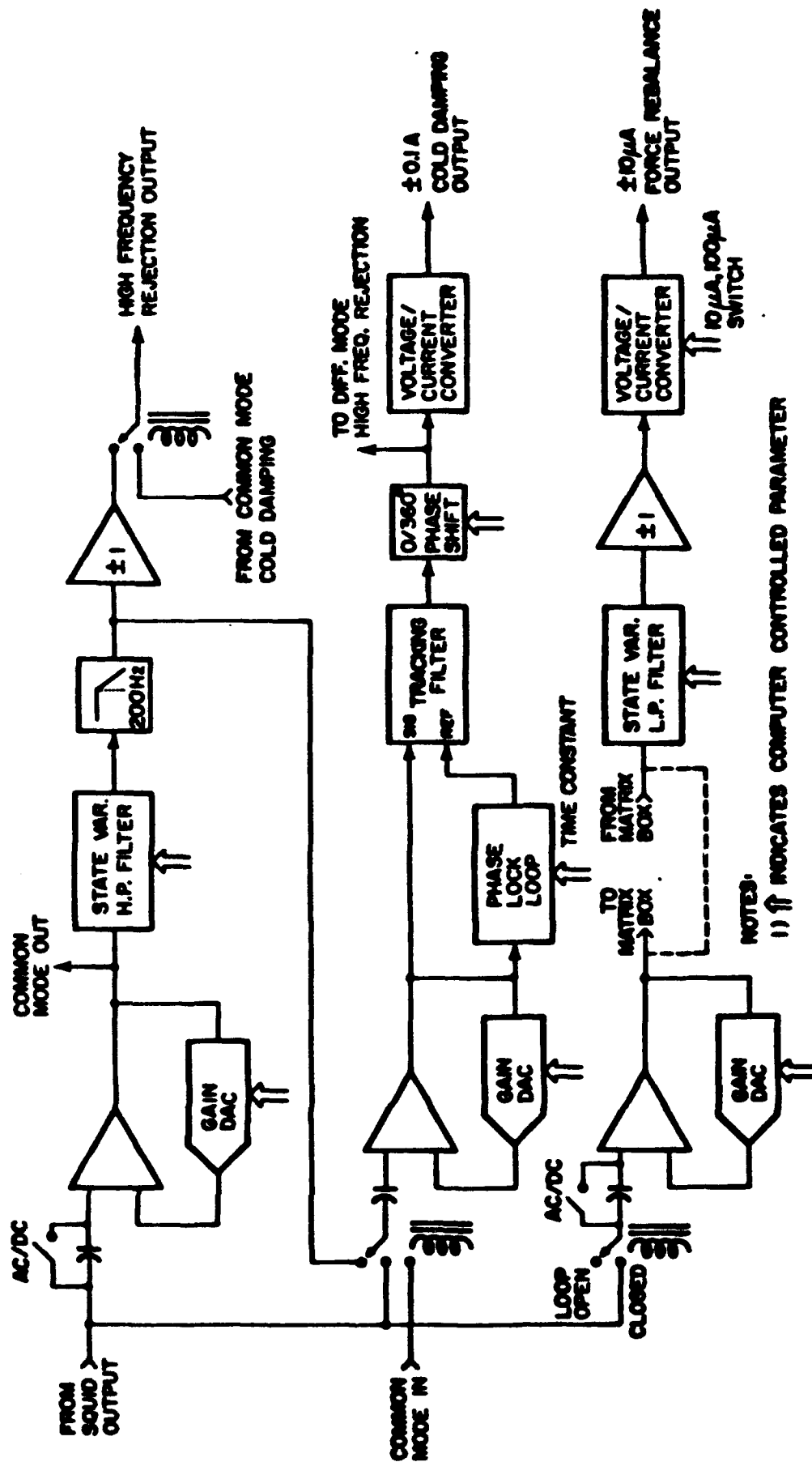
Prevents amplifier overload.

Increases signal to noise ratio by permitting high coupling.

High frequency rejection

Reduces amplitude of peaks above resonance frequency.

Feedback Circuits (one of six)



Primary Error Sources

Temperature sensitivity (penetration depth)

Partially cancelled by common mode balance.

Temperature stability of liquid helium.
(lambda point operation)

Passive rejection by penetration depth thermometer.

Sensitive Axis Misalignment

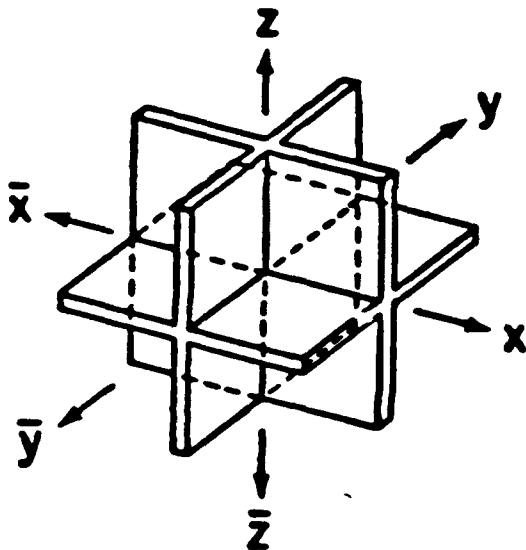
Linear motion \rightarrow three dimensional balance

Angular motion \rightarrow interface with six-axis accelerometer.

Centrifugal acceleration

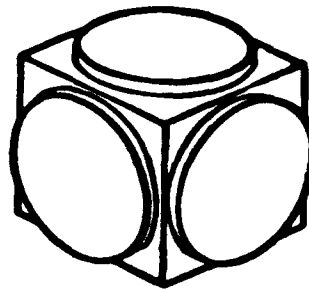
Interface with six-axis accelerometer.

Superconducting Six-axis Accelerometer



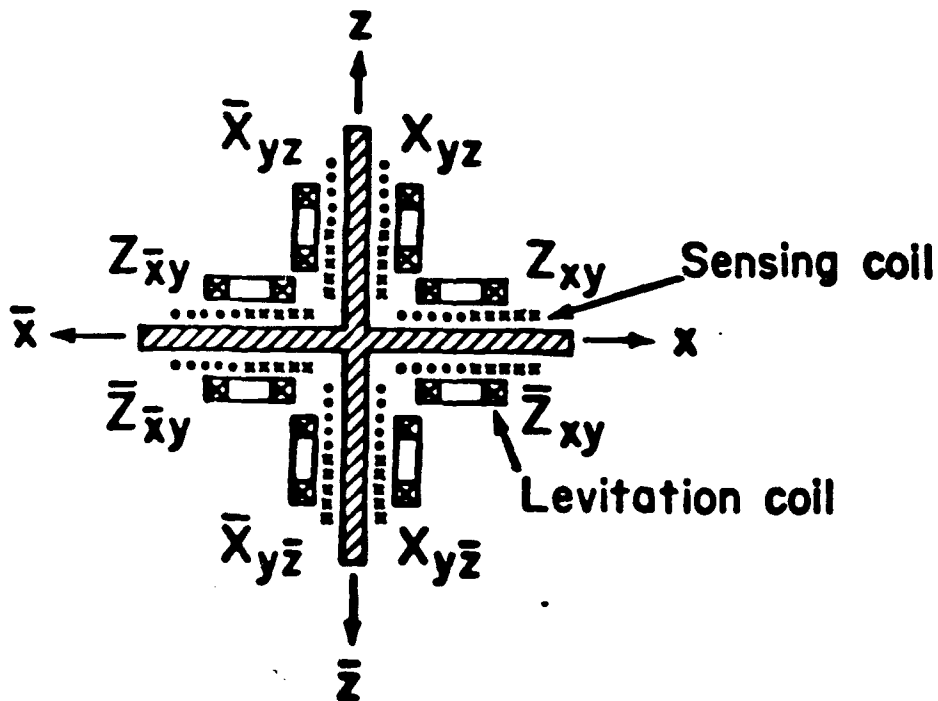
Proof mass (Niobium)

(a)



Coil form (Macor ceramic)

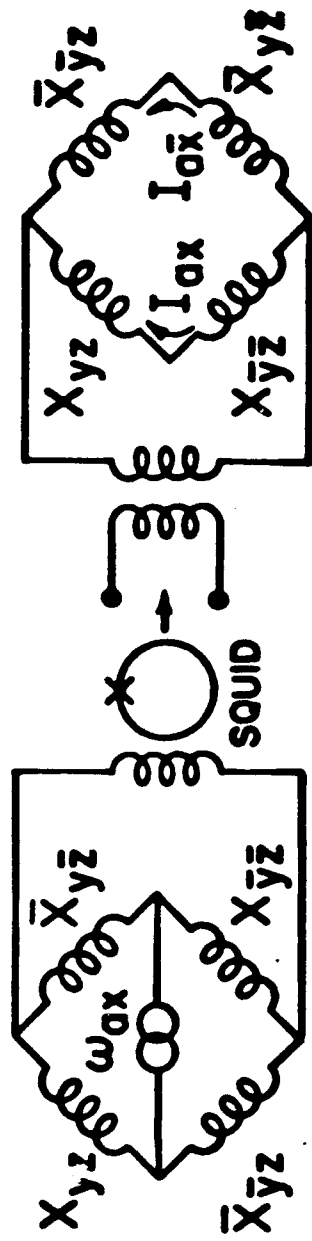
(b)



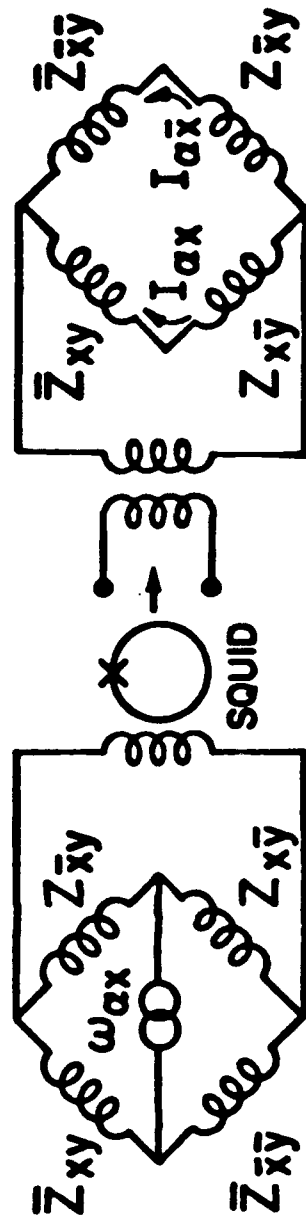
Coils (24 sensing coils + 24 levitation coils)

(c)

Superconducting Circuit



(a)



(b)

Sensing coils \longrightarrow Feedback \longrightarrow Levitation coils

Intrinsic Spectral Noise

$$S_g(f) = \frac{4}{m} \left[K_B T \frac{2\pi f}{Q(f)} + \frac{(2\pi f_0)^2}{2\beta} E_A(f) \right]$$

$$S_a(f) = \frac{4}{I} \left[K_B T \frac{2\pi f}{Q(f)} + \frac{(2\pi f_0)^2}{2\beta} E_A(f) \right]$$

Design Parameters

proof mass	m	0.1 kg
resonance frequency	f_0	1 Hz
temperature	T	1.5 K
quality factor	Q	10^4
amplifier noise	E_A	$3 \times 10^{-30} \text{ JHz}^{-1}$
energy coupling factor	β	$\sim \frac{1}{2}$
moment of inertia	I	$3 \times 10^{-5} \text{ Kg m}^2$

Acceleration Noise

$$S_g^{1/2}(f) = 4 \times 10^{-14} g_E \text{ Hz}^{-1/2}, \quad f = 0.1 \text{ Hz}$$

$$S_a^{1/2}(f) = 3 \times 10^{-11} \text{ rad s}^{-2} \text{ Hz}^{-1/2}, \quad f = 0.1 \text{ Hz}$$

PAPER TITLE: DEVELOPMENT OF SUPERCONDUCTING GRAVITY GRADIOMETER FOR
SPACE APPLICATIONS

SPEAKERS NAME: Vol Moody

Questions and Comments:

Warren Heller: 1. Is the common mode acceleration signal output from the gradiometer available?

2. Have you performed an analysis, relating the dimensional tolerances of the six-axis proofmass to the expected level of cross axis error coefficients expected?

SPEAKERS RESPONSE: 1. Yes, there is a redundancy in the detection of linear acceleration with the gradiometer and the accelerometer.

2. No, we expect cross coupling. The coefficients will be measured and calibrated out using a six-axis shaker.

PLATFORM REQUIREMENTS AND ERROR COMPENSATION FOR A SUPERCONDUCTING
GRAVITY GRADIOMETER

H. J. Paik

Dept of Physics and Astronomy

University of Maryland

College Park, Maryland 20742

ABSTRACT

Requirements of the platform for 10^{-4} E Hz $^{-1/2}$ gradiometer will be discussed. Platform stabilization and error compensation by use of a six-axis superconducting accelerometer and a six-axis shaker will be discussed.

● PLATFORM REQUIREMENTS AND ERROR COMPENSATION FOR A SUPERCONDUCTING GRAVITY GRADIOMETER

H. J. Paik
2/12/86

- I. Error Model of a S/C Gravity Gradiometer
- II. Passive Gravity Stabilized Platform
- III. Gradiometer Errors on the Passive Platform
- IV. Platform Stabilization and Error Compensation
- V. Platform Requirements for Spaceborne Gradiometer

● (Colorado Springs, Colorado)

I. Error Model of a S/C Gravity Gradiometer

1. Finite baseline error:

$$\delta \Gamma_L = -\frac{1}{24} (\hat{\ell} \cdot \vec{\nabla})^4 \phi$$

2. Misposition error:

$$\delta \Gamma_{\vec{r}} = (\hat{n} \cdot \vec{\nabla}) (\hat{n} \cdot \vec{r} \cdot \delta \vec{r})$$

3. Misorientation errors:

$$\delta \Gamma_{\hat{n}} = (\delta \hat{n}_{\hat{n}} + \delta \hat{\ell}) \cdot (\vec{r} - \vec{a} \vec{r}) \cdot \hat{n}$$

4. Misalignment errors:

$$\delta \Gamma_{\vec{a}} = \delta \hat{n} \cdot \frac{1}{2} (\vec{r} - \vec{a}) - \delta \hat{n}_{\hat{n}} \times \hat{n} \cdot \vec{r}$$

5. Scale factor errors:

$$\delta \Gamma_{\sigma} = \hat{n} \cdot (\delta \sigma_r \vec{r} - \delta \sigma_c \vec{c}) \cdot \hat{n}$$

6. Scale factor mismatch error:

$$\delta \Gamma_{\delta \sigma} = \delta \sigma_s \frac{1}{2} \hat{n} \cdot (\vec{r} - \vec{a})$$

7. Non-linearity errors:

$$\delta \Gamma_N = h_{cc} \frac{1}{2} (\hat{n} \cdot \vec{a})^2 + h_{dd} (\hat{n} \cdot \vec{c} \cdot \hat{n})^2 \\ + h_{cd} (\hat{n} \cdot \vec{a}) (\hat{n} \cdot \vec{c} \cdot \hat{n})$$

8. Temperature sensitivity errors:

$$\delta \Gamma_T = h_{Tc} T_c + h_{Td} T_d$$

9. Magnetic field sensitivity errors:

$$\delta \Gamma_B = h_{Bc} B_c + h_{Bd} B_d$$

Number of error coefficients:

$$26 / \text{axis} \times 3 \text{ axis} = 78 > 48$$

II. Passive Gravity Stabilized Platform

Transfer functions :

$$\vec{a}_z = \vec{A}_z$$

$$\vec{a}_h = \frac{\omega_p^2 + j\omega\tau_p^{-1} - (1 - l_0/l_p)\omega^2}{\omega_p^2 - \omega^2 + j\omega\tau_p^{-1}} \vec{A}_h$$

$$\vec{\theta}_p = \frac{-1}{\omega_p^2 - \omega^2 + j\omega\tau_p^{-1}} \frac{1}{l_p} \vec{A}_h \times \hat{z}$$

$$\vec{\Omega}_p = \frac{-j\omega}{\omega_p^2 - \omega^2 + j\omega\tau_p^{-1}} \frac{1}{l_p} \vec{A}_h \times \hat{z}$$

$$\vec{\alpha}_p = \frac{\omega^2}{\omega_p^2 - \omega^2 + j\omega\tau_p^{-1}} \frac{1}{l_p} \vec{A}_h \times \hat{z}$$

Coupling of environmental noise :

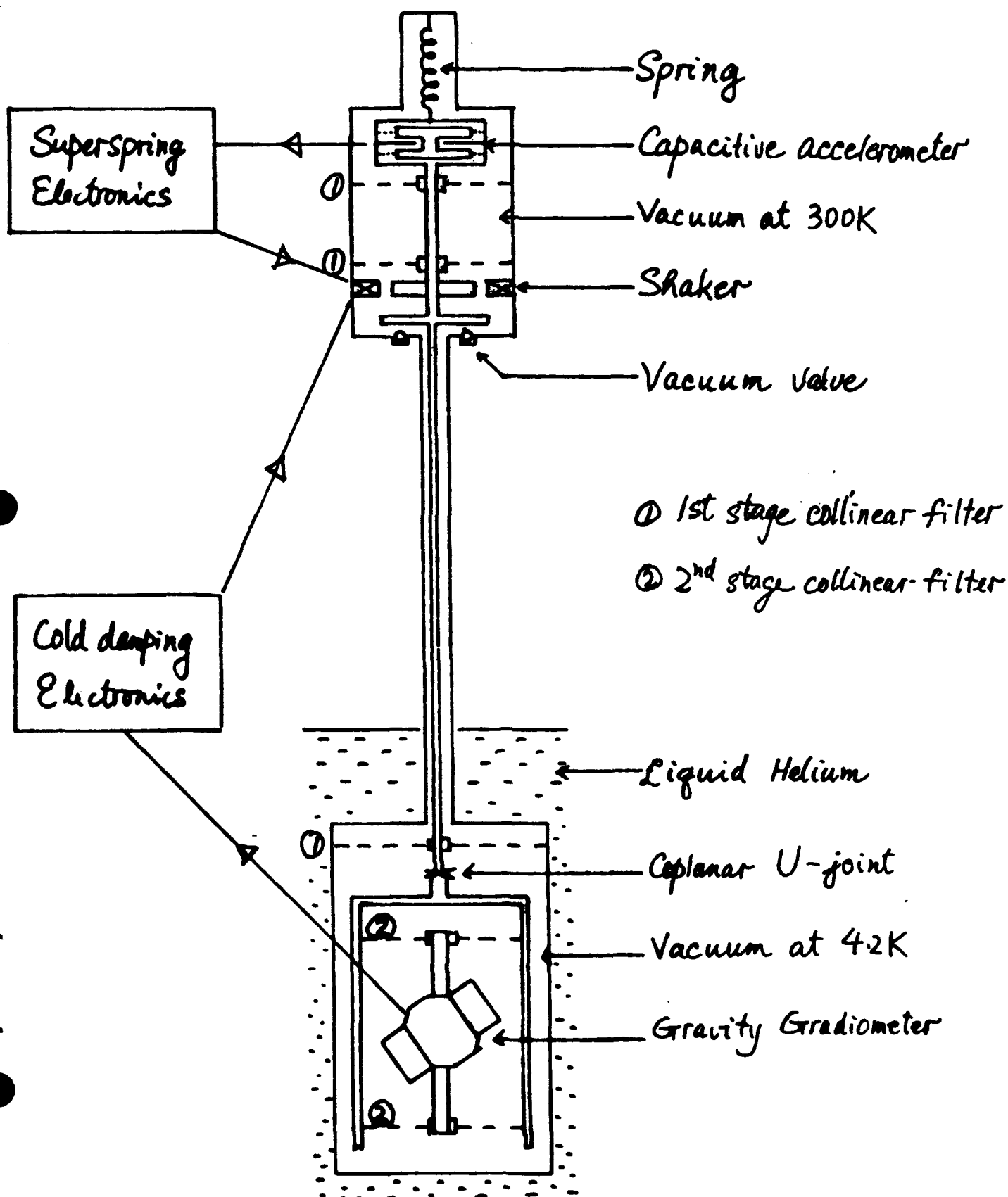
$$\begin{aligned} \delta\Gamma = & \frac{1}{l} (\delta\hat{n}_z + \delta\sigma_s \hat{n}) \cdot (g_E \vec{\theta}_p \times \hat{z} - \vec{a}) \\ & + \delta\hat{n}_{\perp \hat{z}} \times \hat{n} \cdot \vec{\alpha}_p \\ & + 2 [(\hat{n} \cdot \vec{\alpha}_E) \hat{n} - \vec{\Omega}_E] \cdot \vec{\Omega}_p \end{aligned}$$

The first term vanishes almost.

$$\therefore (\delta\hat{n}_z + \delta\sigma_s \hat{n}) \cdot \vec{a}_z = 0$$

$$\text{and } g_E \vec{\theta}_p \times \hat{z} - \vec{a}_h = 0 !$$

New Pendulum Suspension



Residual errors:

$$\delta \Gamma = \frac{-j\omega\tau_p^{-1}}{\omega_p^2 - \omega^2 + j\omega\tau_p^{-1}} \frac{1}{2} (\delta \hat{n}_- + \delta \sigma_s \hat{n}) \cdot \vec{A}_h$$

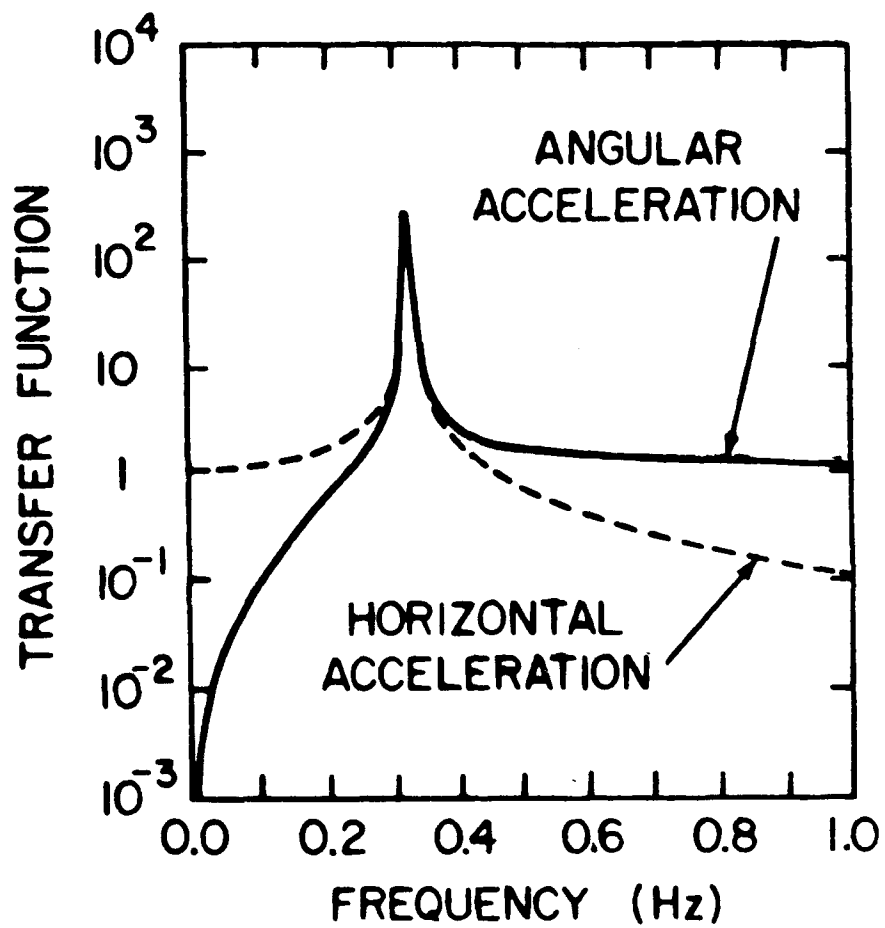
$$+ \frac{\omega^2 \delta \hat{n}_{\perp} \times \hat{n} + j\omega 2 [(\hat{n} \cdot \vec{\Omega}_E) \hat{n} - \vec{\Omega}_E]}{\omega_p^2 - \omega^2 + j\omega\tau_p^{-1}} \cdot \frac{1}{\tau_p} \vec{A}_h \times \hat{z}$$

When $|\delta \hat{n}_{\perp}| \approx 10^{-3}$,

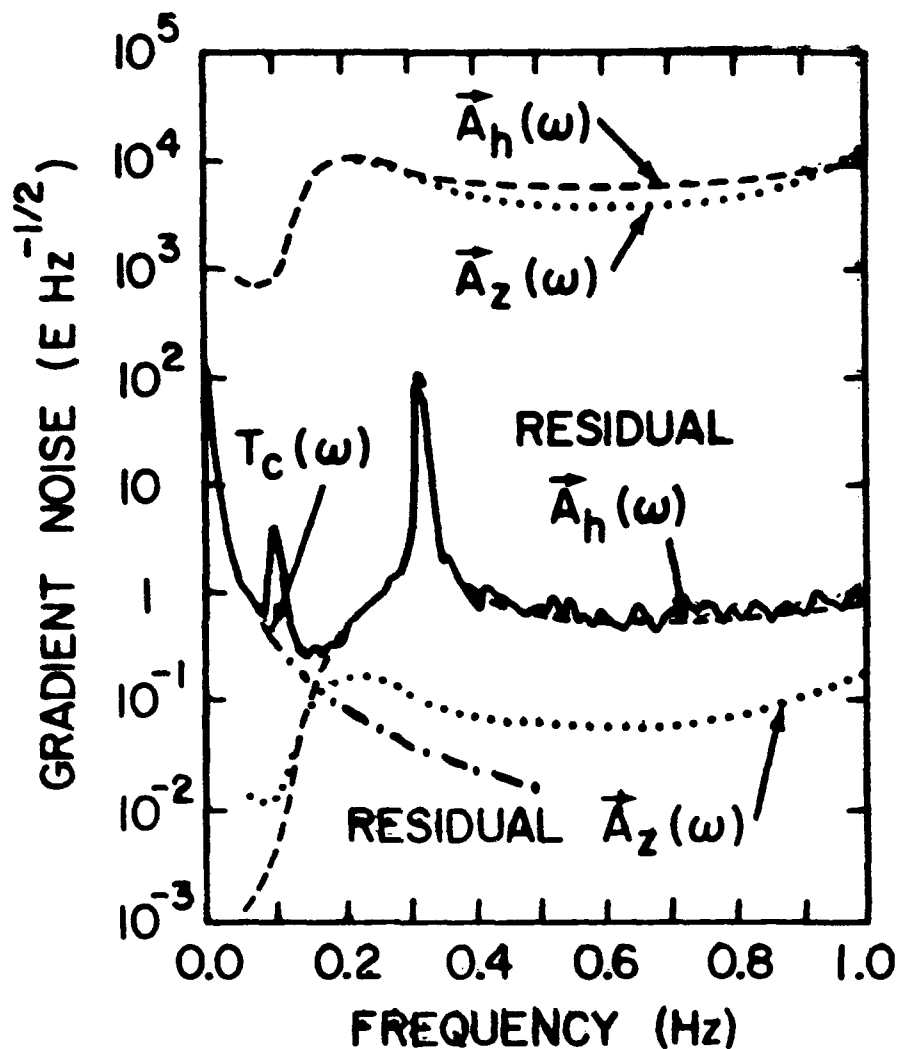
the angular acceleration term dominates
for $\omega/2\pi > 10^2 \text{ Hz}$.

The pendulum action provides a high-pass
filter for \vec{A}_h .

\Rightarrow 6-dimensional isolation is obtained
for low-frequency signals!



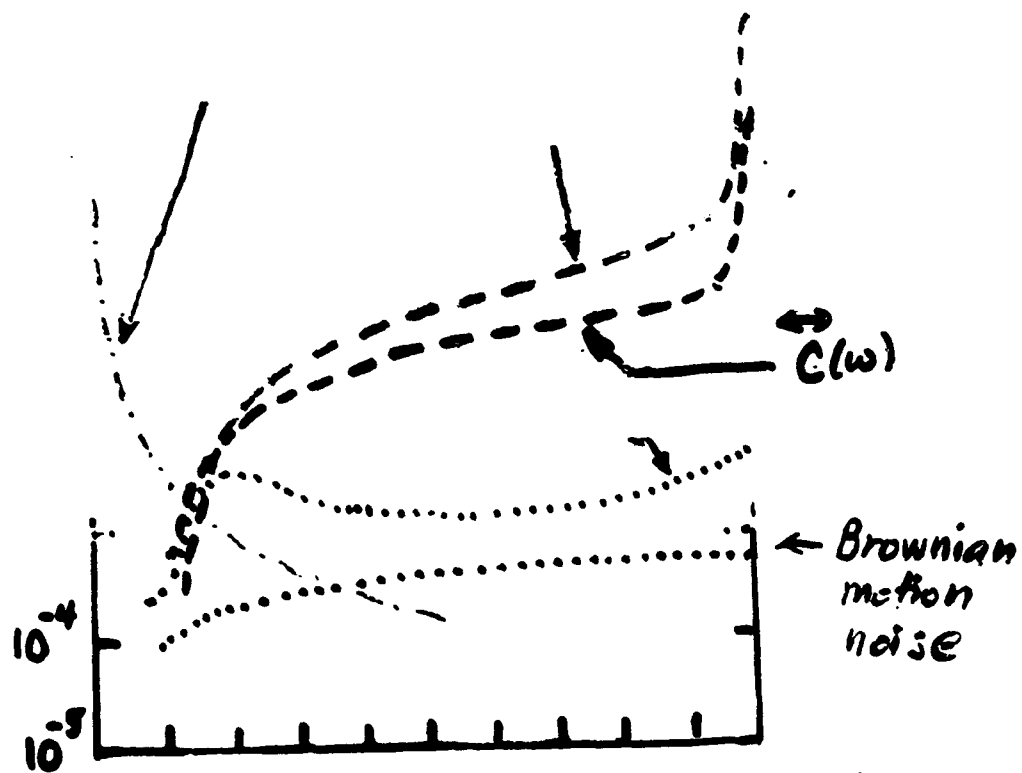
III. Gradiometer Errors on the Passive Platform



$$\omega_p / 2\pi = 0.3247$$

$$|\delta \hat{n}_{\hat{r}}| = 1.8 \times 10^{-3}$$

$$|(\delta \hat{n}_x + \epsilon \tau_s \hat{n}) \cdot \hat{z}| = 3 \times 10^{-5}$$



→ 1.0 Hz

→ 10^{-4}

→ 10^{-6}

TV. Platform Stabilization and Error Compensation

Horizontally stabilized pendulum suspension:
(in g-environment)

Remove \vec{A}_h by active isolation at pivot

$\Rightarrow \lesssim 10^{-2} \text{ Hz}^{-1/2}$ could be obtained.

Six-axis stabilized platform:

(in g- or Og- environment)

Six-axis accelerometer outputs

\Rightarrow Matrix box (signal mixing)

\Rightarrow Feedback to Six-axis shaker

Error Compensation:

(Three-axis gradiometer outputs
Six-axis accelerometer outputs)

\Rightarrow Compute errors

\Rightarrow Subtract from Gradiometer outputs

V. Platform Requirements for Spaceborne Gradiometer

Error Sources	Error Mechanism	Option	Required Control/Knowledge	
			$10^{-2} \text{ E Hz}^{-1/2}$	$10^{-4} \text{ E Hz}^{-1/2}$
Linear accel. $\vec{a}(f)$	$-\frac{1}{2} \delta \hat{n} \cdot \vec{a}(f)$	10^{-4} 10^{-7}	$2 \times 10^{-9} g_E \text{ Hz}^{-1/2}$ $2 \times 10^{-6} g_E \text{ Hz}^{-1/2}$	$2 \times 10^{-11} g_E \text{ Hz}^{-1/2}$ $2 \times 10^{-8} g_E \text{ Hz}^{-1/2}$
Altitude Error $\delta h(f)$	$(\hat{n} \cdot \vec{\nabla})$ $\hat{n} \cdot \vec{\Gamma}_E \cdot \delta \vec{h}(f)$		$7 \text{ m Hz}^{-1/2}$	$7 \times 10^{-2} \text{ m Hz}^{-1/2}$
Attitude Error $\vec{\theta}(f)$	$\vec{\theta}(f) \times \hat{n}$ $\vec{\Gamma}_E \cdot \hat{n}$	Inertial Geographic*	$4 \times 10^{-6} \text{ rad Hz}^{-1/2}$ $1.5 \times 10^{-3} \text{ rad Hz}^{-1/2}$	$4 \times 10^{-8} \text{ rad Hz}^{-1/2}$ $1.5 \times 10^{-4} \text{ rad Hz}^{-1/2}$
Attitude Rate E. $\vec{\Omega}(f)$	$2 \vec{\Omega}_0 \cdot \vec{\Omega}(f)$ $-2(\hat{n} \cdot \vec{\Omega}_0)(\hat{n} \cdot \vec{\Omega}(f))$	Inertial Geographic	$3 \times 10^{-6} \text{ rad s}^{-1} \text{ Hz}^{-1/2}$ $4 \times 10^{-9} \text{ rad s}^{-1} \text{ Hz}^{-1/2}$	$3 \times 10^{-7} \text{ rad s}^{-1} \text{ Hz}^{-1/2}$ $4 \times 10^{-11} \text{ rad s}^{-1} \text{ Hz}^{-1/2}$
Attitude Acc. E. $\vec{\alpha}(f)$	$-\delta \hat{n}_{+1} \times \hat{n} \cdot \vec{\alpha}$	10^{-4}	$10^{-7} \text{ rad s}^{-2} \text{ Hz}^{-1/2}$	$10^{-9} \text{ rad s}^{-2} \text{ Hz}^{-1/2}$
Dynamic Range	$\frac{\Gamma_{\max}}{\delta \Gamma}$	Inertial Geographic	3×10^5 10^3	3×10^7 10^5

* Local geographic orientation reduces the Attitude error only for signals near dc, as per R^2 law experiment.

PAPER TITLE: PLATFORM REQUIREMENTS AND ERROR COMPENSATION FOR A SUPERCONDUCTING GRAVITY GRADIOMETER.

SPEAKERS NAME: Ho Jung Paik

Questions and Comments:

Alan Zorn: You promised earlier to discuss the effect of self-gradients on a satellite-based cryogenic-gradiometer with $10^{-3} \text{ E/Hz}^{1/2}$ accuracy. Is this a good time?

SPEAKERS RESPONSE: Yes, self-gradients contribute a DC effect, and we do not consider them.

Alan Zorn: But, self-gradients are not constant (eg-outgassing, transfer of mass within helium cooling system, etc) and would certainly appear at $10^{-3} \text{ E/(Hz)}^{1/2}$

SPEAKERS RESPONSE: We can locate such moving items far from the sensing elements. We have been assured that the helium cooling system will not affect such accuracy. The next speaker may be willing to further expound on this question.

Warren Heller: Please comment on the practicality of your requirement to control jitter to 10^{-13} rad (or even 10^{10} - less stringent case).

SPEAKERS RESPONSE: With the co-rotating scheme that I proposed, the angular stability of the dewar should be very good. Our angular accelerometer can be tuned to measure angular acceleration down to $10^{-13} \text{ rad/s}^2/(\text{Hz})^{1/2}$. For $10^{-4} \text{ E/Hz}^{1/2}$, the required angular velocity sensitivity is $4 \times 10^{-11} \text{ rad/s/Hz}^{1/2}$ for the worst case which is for a local geographic orientation. This will be no problem for our angular accelerometer.

TLC FOR A MAGNETICALLY FLOATED GRAVITY GRADIOMETER

D. Sonnabend

Jet Propulsion Laboratory

California Institute of Technology

4800 Oak Grove Drive

Pasadena, California 91109

ABSTRACT

The proposed NASA Gravity Gradiometry Mission, a very low altitude satellite, carrying a cryogenic gradiometer under development at the University of Maryland, poses some unique technical challenges. Like some other highly sensitive inertial instruments, this one can deliver its promised performance only in orbit, and thus cannot be fully tested in the laboratory. Even in orbit we face problems from vibration, acceleration, rotation, and local gravity noise. Our approach to this is based on a magnetic isolation system, under development at JPL, and in cooperation with other efforts at Marshall and Goddard. The paper will discuss how we will float the whole experimental dewar, and measure the instrument's altitude and operating parameters.

JPL

TLC FOR A MAGNETICALLY FLOATED GRADIOMETER

dave sonnabend
JET PROPULSION LABORATORY

ds-14gg-1

JPL

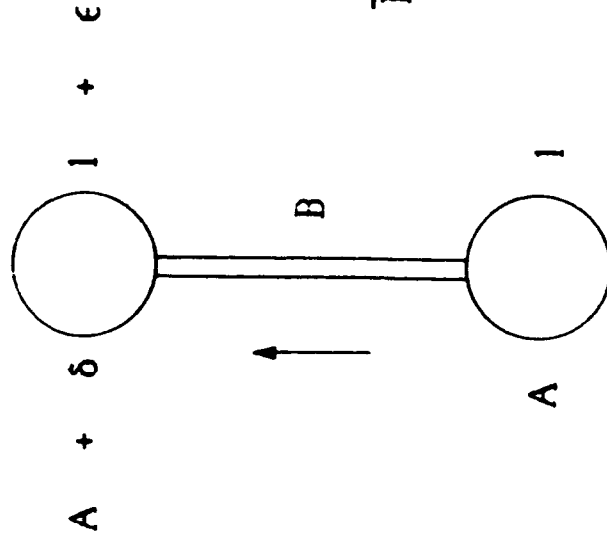
GRADIOMETER TEST and OPERATION PROBLEMS

- ACCELERATION
- VIBRATION
- ROTATION
- GRAVITY NOISE

ds-14gg-2

$$\Delta A = (1 + \epsilon)(A + \delta) - A = \delta + \epsilon A = BH$$

$$\epsilon_{\text{MAX}} < \left| \frac{B\Delta H}{A} \right|$$



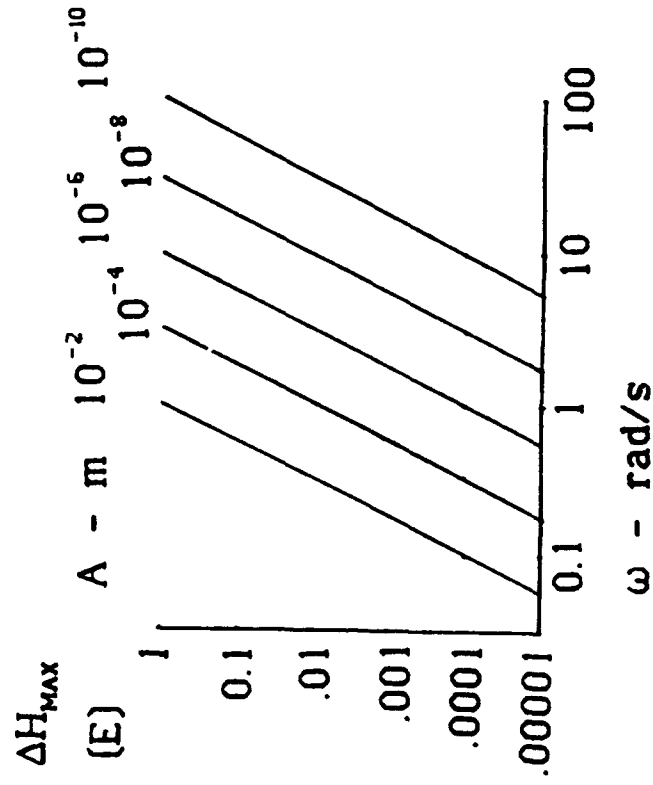
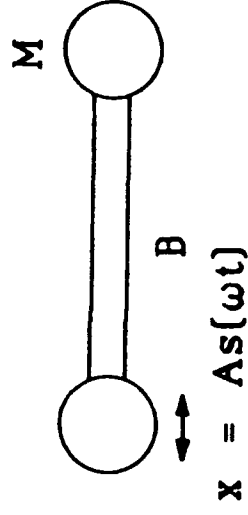
CASE	$\frac{\Delta H}{E}$	$\frac{A}{m/s^2}$	ϵ_{MAX}
LAB (1g)	1	10^{-4}	2×10^{-11}
STS	10^{-3}	10^{-10}	2×10^{-9}
FLOAT	10^{-4}	10^{-10}	2×10^{-4}

VIBRATION

JPL

$$\text{STRAIN} = \frac{\Delta B}{B} = \frac{M\ddot{x}}{ES}$$

$$\Delta H = \frac{\Delta \ddot{B}}{B} = \frac{MA\omega^4 s(\omega t)}{ES}$$

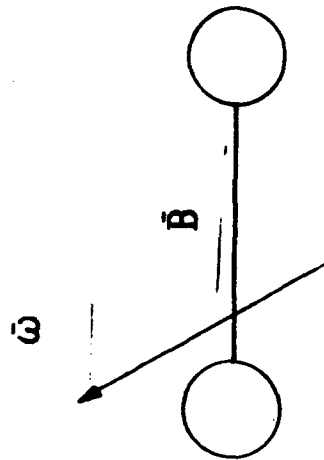


$$\begin{aligned} M &= 1 \text{ kg} \\ S &= 5 \times 10^{-4} \text{ m}^2 \\ E &= 2 \times 10^{10} \text{ N/m}^2 \text{ (steel)} \end{aligned}$$

JPL

ROTATION

$$\vec{z} = (\vec{H} + \vec{\omega}\vec{\omega} - 3\omega^2\vec{I}) \cdot \vec{B}$$



$$\Delta H = 2\omega\Delta\omega$$

CASE	ω rad/s	ω^2 E	$\Delta\omega$ rad/s ($\Delta H = 10^{-4}E$)
1 rad/s	1	10^3	5×10^{-14}
STS	4×10^{-4}	160	1.25×10^{-10}
EARTH	7.3×10^{-5}	5.3	7×10^{-10}
"STOP"	2.3×10^{-7}	5×10^{-14}	2.3×10^{-7}

JPL

DISTURBANCE LEVELS

Object	Mass kg	Distance m	GM/r ³ E
Whole Earth	5.976 x 10 ²⁴	6.367 x 10 ⁶	1544
Equivalent Earth	1	.0351	1544
Equivalent Earth	23,100	1	1544
1 km ³ Mountain	3 x 10 ¹²	1000	200
Building	30,000	10	2.0
Boulder	10,000	4	10.4
Small Car	1000	2	8.34
Calibrated Disturbance	15	1	1.0
Standard Object	1	1	.0667
Man Next to Instrument	70	0.7	13.6
Shuttle Crew Member	70	15	.0014
Internal Component	0.1	.03	.247

COMMON MODE BALANCING GRADIOMETER WITH MONOCRYSTALLINE SILICON SUSPENSION
FOR HIGH SENSITIVITY GRAVITY MEASUREMENTS

Jean-Paul Richard

Department of Physics and Astronomy

University of Maryland

College Park, Maryland 20742

ABSTRACT

Noise in a room temperature gradiometer with a new low frequency common mode balancing monocrystalline silicon suspension and laser instrumentation is analyzed.

The potential sensitivity as limited by the noise associated with damping in silicon and interferometric position sensing is projected at 2×10^{-4} Eotvos/ Hz^{1/2}.

Common mode BALANCING Gradiometer
with monocrystalline silicon suspension
for high sensitivity gravity measurements.

J.P. Richard. Univ of Md.

Potential of some (new) techniques
for gradiometry.

Fundamental noise limits.

Research toward ACTUAL Design
seems justified.

The G.V. DETECTOR - GRADIOMETER CONNECTION

Inductance
Modulation (Stanford)
Transducer.

Stanford
Md
Cryogenic gradiometer

Capacitance
Transducer
(dc biased)

(Frascati)
Rome
Japan
Md

SAO/Frascati
Ac biased capacitance
gradiometer.

Monocrystals

(Moscow)
Regina
Rochester
Md

Lasers

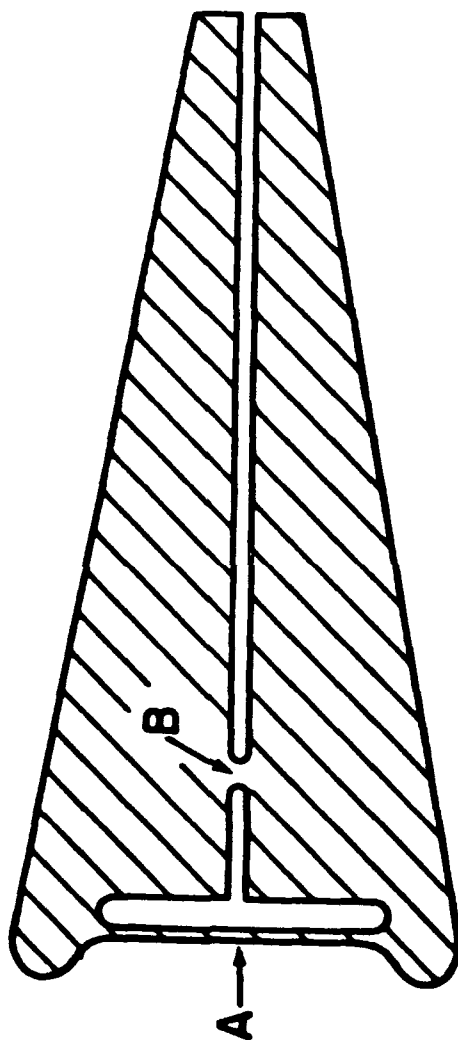
(Hughes)
Munich
MIT
Glasgow
Caltech.

non cryogenic
monocrystalline
suspension
+
Laser sensing of
mass position.

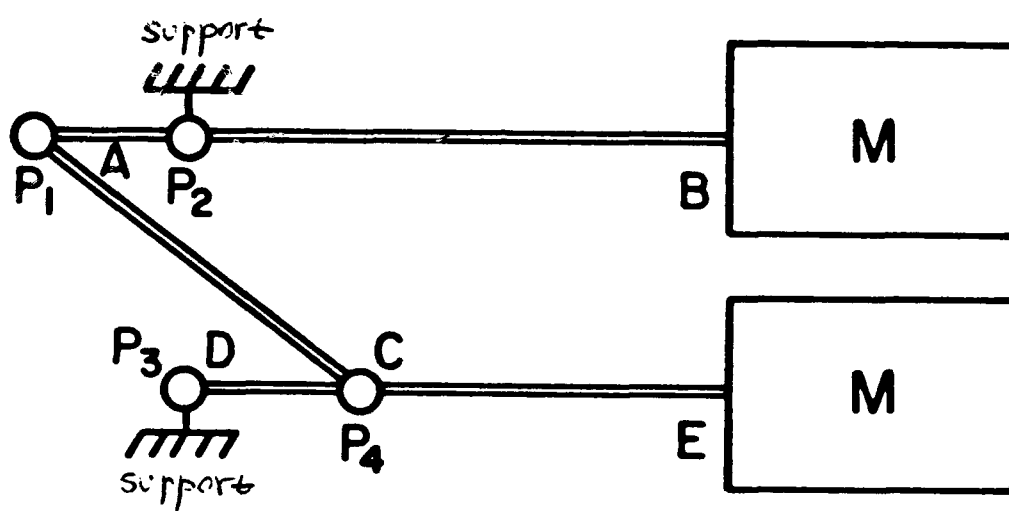
Common mode balancing
suspension. (Wai)

Items

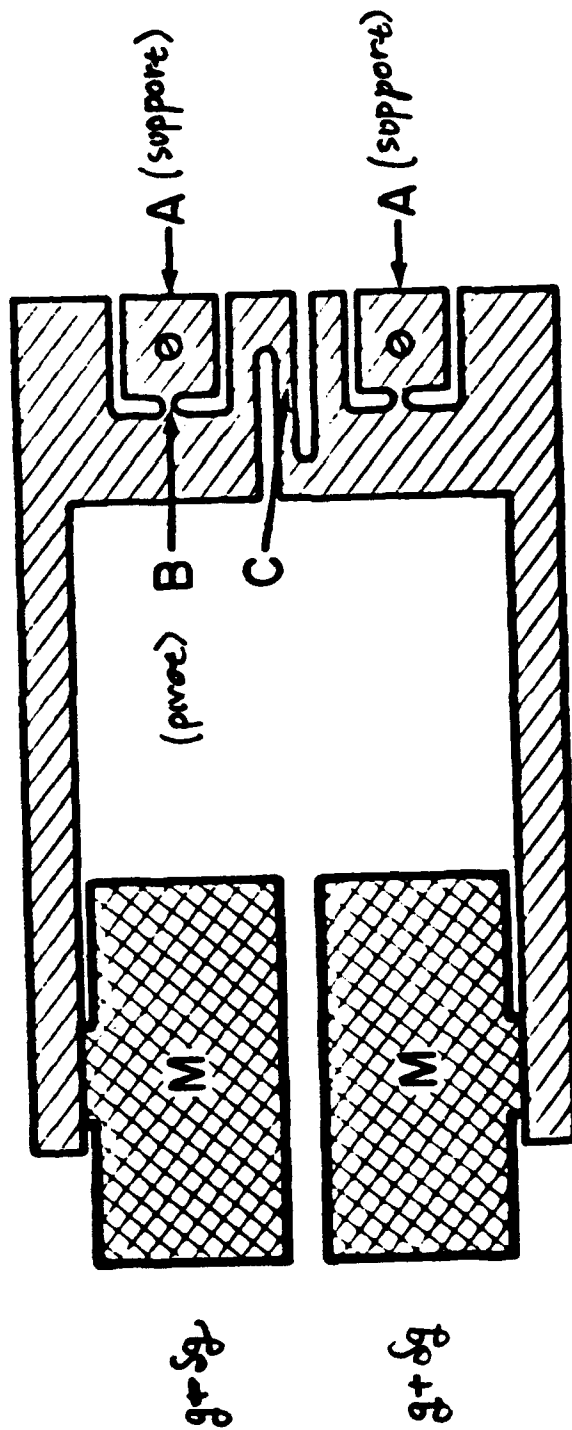
- Monocrystal quality factors: $\left(\text{Silicon } Q \sim 10^8 \right)$
at $t = 300K.$
- Common mode balancing suspension
(with low frequency.)
- Thermal noise level associated with monocrystalline
silicon suspension.
- Shot noise and back action noise of laser sensing
of mass position.



Test for Quasi frictionless pivots (B).
 $Q \geq 100,000$ for AL



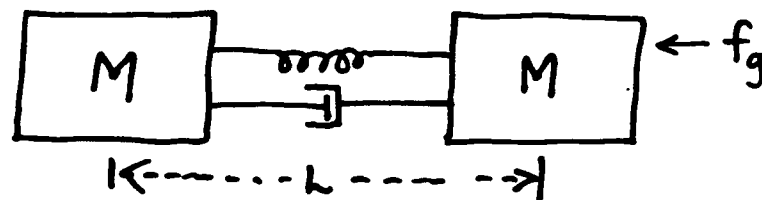
Common balancing gradiometer.
 (P_1 - P_4 = frictionless pivots)



Common mode balancing Test model.

Al. $f = 8 \text{ Hz}$. $Q \sim 1000$

Smallest measurable gravity gradient
as limited by thermal noise in suspension



Smallest gravity gradient which can be measured:

$$\tau_{\min}^2 = \frac{4 K_B \omega_0 T_g}{M L^2 Q}$$

K_B : Boltzmann's constant

ω_0 : gradiometer radial frequency

T_g : gradiometer temperature

M : proof masses

L : gradiometer baseline

Q : quality factor of proof mass suspension

Suspension thermal noise
Smallest measured gradient.

Assumed

$$\begin{array}{|l} L = 20 \text{ cm} \\ M = 1 \text{ Kg} \end{array}$$

$$| \omega_0 = 2\pi \times 25$$

$$\begin{array}{|l} \text{ALuminum suspension} \\ Q = 10,000 \\ T_{\min} = 8 \times 10^{-2} \text{ E} / \sqrt{\text{Hz}} \end{array}$$

$$\begin{array}{|l} \text{silicon suspension} \\ Q = 10^8 \\ T_{\min} = 8.1 \times 10^{-4} \text{ E} / \sqrt{\text{Hz}} \end{array}$$

$$| \omega_0 = 2\pi$$

$$\begin{array}{|l} \text{silicon suspension (common mode bal)} \\ Q = 10^8 \\ T_{\min} = 1.6 \times 10^{-4} \text{ E} / \sqrt{\text{Hz}} \end{array}$$

$$\begin{array}{|l} \omega_0 \sim 10^{-2}, \quad Q \sim 160,000 \\ T_{\min} = 1.6 \times 10^{-4} \text{ E} / \sqrt{\text{Hz}} \end{array}$$

Interferometer noise (compared to Thermal noise)

Amplitude noise in The Laser output.

Limit : shot noise in arrival rate of photons
+ noise generated in the process of detection

$$x^2(\nu) = \frac{h c \lambda}{\pi^2 \epsilon P b^2 e^{-(b-1)(1-R)}}$$

ϵ : quantum efficiency

P : Laser power

b : # of reflections

R : reflectivity

minimum for $b = 2/(1-R)$

for : $R = 99.5\%$, $b = 400$, $\epsilon = 50\%$, $P = 0.001 \text{ W}$

$$x^2(\nu) = 9.2 \times 10^{-34} \text{ m}^2/\text{Hz}.$$

Signal displacement at $T' = 1.6 \times 10^{-4} \text{ E}$

$$x_g^2 = \left(\frac{T' L}{\omega_0^2} \right)^2 = 6.5 \times 10^{-31} \text{ m}^2 \gg \text{amplitude noise.}$$

└ largest of ω at ω_0

Interferometer noise (compared to Thermal noise)

Radiation pressure noise (back action) (Poisson noise)

spectral power density of
stochastic radiation pressure force:

$$f^2(\nu) = \frac{4 b h P}{\lambda c} \Delta \nu$$

b # of reflections
for $b=400$, $P = .001 \text{ W}$

P: Laser power

$$f^2(\nu) = 7 \times 10^{-36} \text{ N}^2/\text{Hz}.$$

Thermal noise force (at $T_{\min} = 1.6 \times 10^{-4} \text{ E}/\sqrt{\text{Hz}}$)

$$f^2(\nu) = 4 \kappa_B T_g \gamma \quad \gamma = \frac{m \omega_0}{Q} = \frac{M \omega_0}{2Q}$$

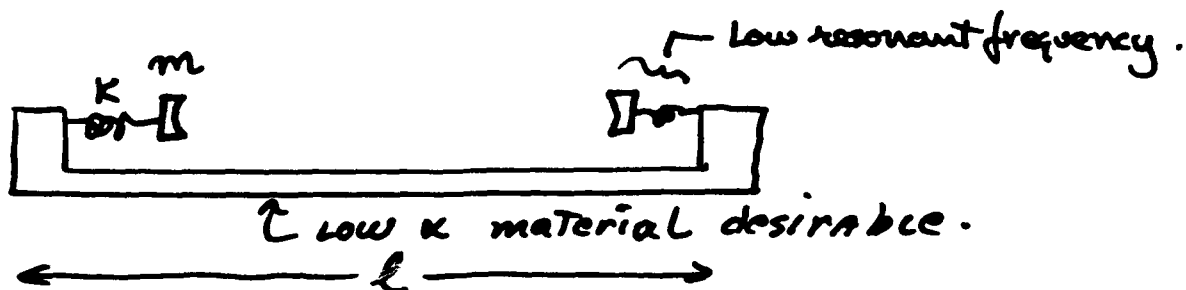
$$f^2(\nu) = 5 \times 10^{-28} \text{ N}^2/\text{Hz}$$

>> Radiation pressure noise.

In these limits, Interferometer noise is
below the thermal noise of $1.6 \times 10^{-4} \text{ E}/\sqrt{\text{Hz}}$.

Temperature control requirement ^(for) ^(space) ^(Experiment)

model



$$\omega \gg \omega_0$$

ω : signal frequency.

T_T : gradient noise due to temperature fluctuations

$$\frac{T_T(\omega)}{T} = \alpha \omega_0^2 T(\omega) \quad \left\{ \begin{array}{l} T_T(\omega), T(\omega) \\ \text{spectral amplitudes} \end{array} \right.$$

$$\alpha = (1/\ell)(dl/dT)$$

$T(\omega)$: Temperature fluctuations

$$\omega_0 = \sqrt{K/m}$$

Potential set of parameters

$$\alpha = 10^{-5}/K, \quad \omega_0 = 10^{-2}, \quad T(\omega) = 10^{-4} K$$

$$\frac{T_T(\omega)}{T} \sim 10^{-13}$$

or

lower α material with higher ω_0 or $T(\omega)$ also acceptable.

**PAPER TITLE: COMMON MODE BALANCING GRADIOMETER WITH MONOCRYSTALLINE
SILICON SUSPENSION FOR HIGH SENSITIVITY GRAVITY MEASUREMENTS**

SPEAKERS NAME: Jean-Paul Richard

Questions and Comments:

Dave Sonabend: Don't use invar for your structure, magnetostrictive strain is worse than temperature strain in routine materials.

Andrew Lazarewicz: With such a high Q, isn't your bandwidth very narrow?

• **SPEAKERS RESPONSE:** The mechanical Q is sharp, so is the mechanical bandwidth narrow. The instrument bandwidth is not limited by the mechanical bandwidth. Note that both signal and noise is amplified within the mechanical bandwidth, so S/N may not be improved (notable exception: shot noise). In fact, most gravitational signals of interest are outside the mechanical bandwidth in question.

Jim Faller: Why not measure the length of the bar with an independent laser & thereby take out (servo out) temp-effects: Servo to keep fixed & then measure distance with a laser to "measure" gradients.

LIQUID-SUPPORTED TORSION BALANCE AS GRADIOMETER

J. E. Faller

P. T. Keyser

Joint Institute For Laboratory Astrophysics

University of Colorado

Boulder, Colorado 80309

ABSTRACT

We employ a liquid-supported torsion balance as a fixed-site long-term curvature variometer. The traditional fiber is replaced by liquid support and electrostatic positioning. Thus the torsion constant is adjustable by varying the voltage applied to the torque electrodes, while the centering voltage remains constant. The sensitivity of this type of gradiometer will be discussed, along with critical parameters for success. Preliminary data will be presented.

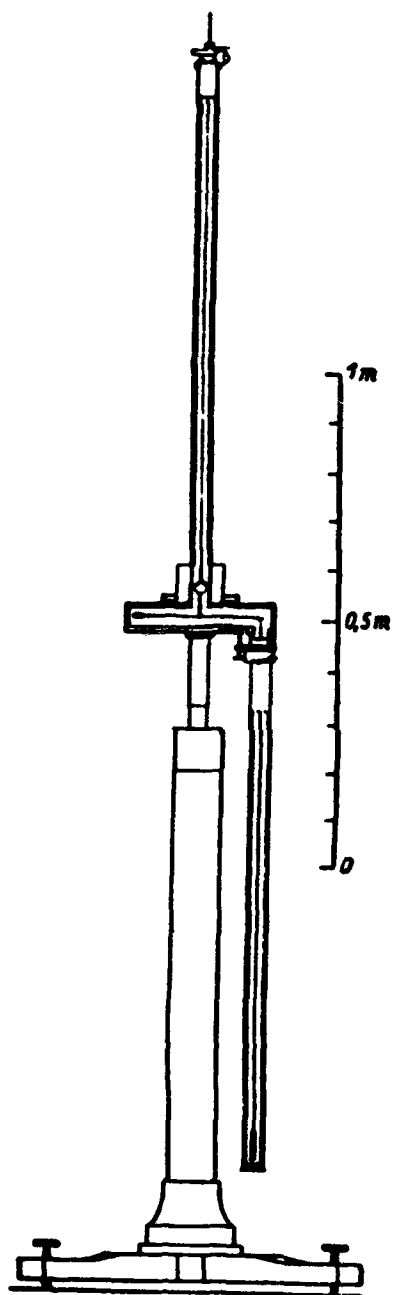
Liquid-Supported Torsion Balance as Gradiometer

P. T. Keyser and J. E. Faller

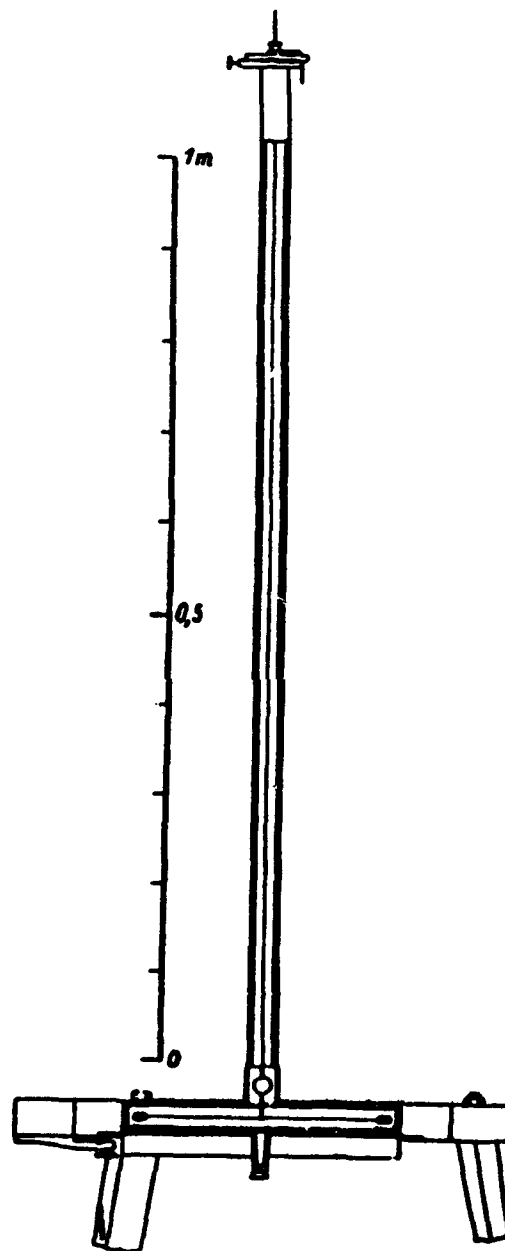
Joint Institute for Laboratory Astrophysics,
University of Colorado and National Bureau of Standards,
Boulder, Colorado, 80309-0440

We employ a liquid-supported torsion balance as a fixed-site long-term curvature variometer. The traditional torsion fiber is replaced by liquid support and electrostatic positioning. Thus the torsion constant is adjustable by varying the voltage applied to the torque electrodes, while the centering voltage remains constant. The sensitivity of this type of gradiometer will be discussed, along with critical parameters for success. Preliminary data will be presented.

The world's first gradiometers were the fiber-supported torsion balances (FSTB's) used by Baron Roland von Eötvös in the late nineteenth century.¹ A wide variety of supported mass configurations were developed (the two basic ones are shown in Figure 1) and such torsion balance gradiometers were used in geophysical research through about 1940, at which time gravimeters replaced them.² Torsion balances themselves were invented in the late eighteenth century and have been, and still are, used in a variety of applications for measuring very small forces. In our own work on the Einstein Equivalence Principle we have constructed,



(Gradiometer)



(Curvature Variometer)

FIGURE 1.

Baron Roland von Eötvös' FSTB Gradiometers (1896)
 [Ref. 1, pp. 369-370]

ostensibly as an auxiliary instrument, a pair of torsion balance gradiometers to monitor longterm ($T \approx 1$ day) changes in what may be loosely called the "horizontal gravity gradients" (more precisely: in the curvatures of the gravity level surface). However, due to the often bizarre and always subtle problems associated with the use of fibers,³ and due to our desire to increase the sensitivity of the torsion balance, we have used a radically different design. FSTB's have an inherently limited sensitivity to mass-dependent forces as may be seen by noting that the supported weight (test masses and beam) is proportional to the cross-sectional area of the fiber, while the observed angle is proportional to the square of the area. This results in a maximum sensitivity as determined by the fiber material (yield strength versus elasticity) and by the resolution of the detection system.

To overcome this sensitivity limit, the supported object can be immersed in a liquid, to decrease the load on the fiber, as John Henry Poynting first suggested.⁴ However, to completely avoid the use of fibers, the recently-perfected liquid-supported torsion balance (LSTB) uses an electrode array to provide the centering and restoring torque usually provided by the fiber.⁵ Our LSTB curvature variometer is pictured in Figure 2. An advantage of this "electrostatic fiber" is that the voltage applied to the center electrode may be (and usually is) much larger than that applied to the torque electrodes, which allows the centering and torquing forces to be effectively independent. (The force between two electrodes is proportional to the square of the applied voltage, and for spherical electrodes the force is almost in inverse proportion to the gap between the upper and lower electrodes.) Furthermore, the torque voltage is readily adjustable so that we can, for

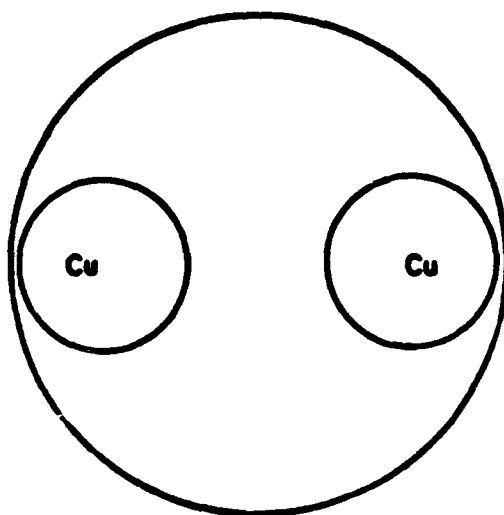
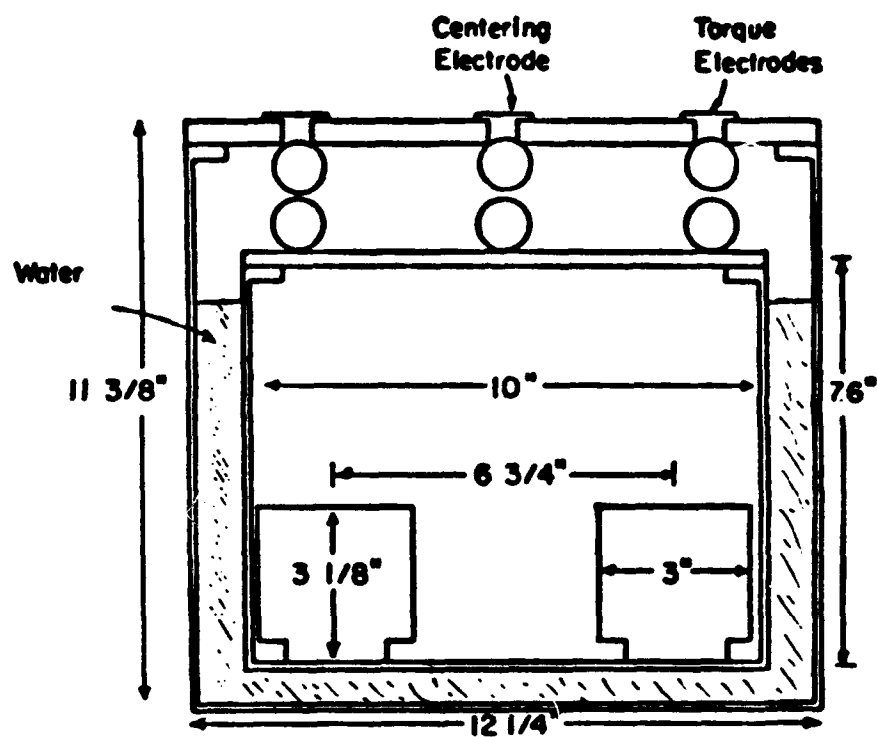


FIGURE 2.
Schematic of our LSTB Gradiometer (1986)

example, let the system thermally equilibrate with high torque voltage ("stiff fiber") and then simply lower the torsion constant to the correct value for critical damping (the optimum operating point). Similarly, we can quickly establish the true "zero" of the system so as to be able to measure the dc curvature values. A polyatomic inert gas (such as well-filtered N_2) used as the fill gas maximizes the dielectric strength of the electrode gaps and thus yields the maximum stiffness of the electrostatic fiber.

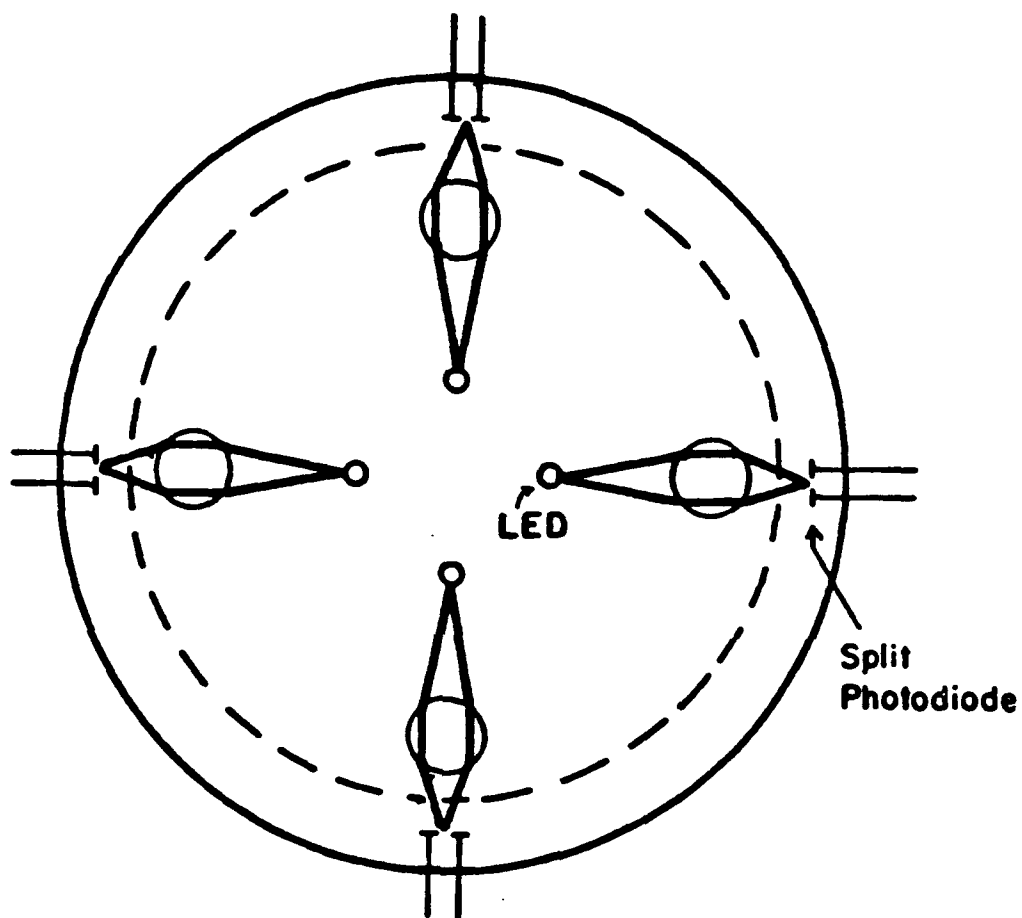
In a LSTB there are only a few undesirable mechanical oscillation modes, most of which have frequencies much higher than the torsional oscillation frequency ($T \approx 10$ min), and all of which are rapidly damped by the liquid. By contrast, FSTB's are plagued with a great number of high-Q modes which readily couple to the torsion mode.⁶ The bobbing mode of a LSTB ($T \approx 1$ sec) has never been observed to couple, while the off-centering mode ($T \approx 20$ min) is rarely excited and is highly damped. There are two tilting modes ($T \approx 1$ sec) one of which (or both, if they are degenerate) will of necessity couple to the torsion mode. This may be most readily seen by noting that a book (held shut with a rubber band) may be flipped into the air about any of three principal axes - and about two of those the rotation is stable. About the axis with the intermediate moment of inertia (or about the two axes of equal moments of inertia) the motion is unstable.⁷ Due to various practical constraints, in any real LSTB the moment of inertia about the torsional axis will always be smaller than the other two moments, and hence the torsional oscillation is always stable. Moreover, the coupling of the tilting mode(s) to the torsional mode only results in short episodes of small high-frequency "noise" (and the tilt modes are rarely excited).

We use a transmission-optics variant of the Gauss optical lever as our angle detection system. The infrared LED (noted in Figure 3) is a point source and the lens is a (borosilicate glass) rod with its axis vertical. The rays from the LED pass through the rod perpendicular to its axis and are focused into a vertical line. The focal plane (i.e., the line image) is made to coincide with the plane of the split photodiode. The two currents generated in the photodiode halves are converted to voltages in low-current-noise preamplifiers and their sum and difference formed. The four sums and four differences are combined in appropriate ways to generate radial translation (off-centering) and angular azimuth signals. The net gain is such that we have a measured sensitivity of about 30 mV/arcsec, using 4.5 mA in the LED.

The second derivatives of U , the scalar gravity potential, form a tensor, whose nine components are reduced by the constraints imposed by the curl of g and the divergence of g to five linearly independent components. Of these five we happen to be interested only in those two which correspond to masses near the instrument horizon, that is the two curvature values. In fact the azimuthal torque on a LSTB is given by

$$(1) \quad N = 1/2 \sin(2\alpha)(I_x'x' - I_y'y')(U_{yy} - U_{xx})$$

where α is the azimuth of the instrument relative to the axes of the principal radii of curvature, U_{xx} and U_{yy} are the two principal curvature values (so, e.g., $R_x = g_z/U_{xx}$), and the I 's are the two horizontal moments of inertia. Because of the symmetry of our float this reduces to (along the sensitive axes which are at $\pm 45^\circ$ to the line joining the test masses):



(LED's and Photodiodes attached to tank, lenses attached to float)

FIGURE 3.

Schematic of Optical Position-Sensing System

$$(2) \quad N = (mr^2)(U_{yy} - U_{xx})$$

where m is the mass of each test mass (2.935 kg) and r is its radius (8.65 cm). For an external (point or spherical) mass M located on the sensitive axis (x or y) at a distance R from the axis of the torsion balance, we have for the torque

$$(3) \quad N = (mr^2)(2GM/R^3)$$

For our apparatus, with an external mass $M = 150$ kg at $R = 2$ m (corresponding to $U = 2.5$ EU, $1 \text{ EU} = 10^{-9} \text{ sec}^{-2}$) we find a torque of about 0.55 mdyne-cm. Our critically-damped torsion constant is 1.09 dyne-cm/rad (at a voltage of about 55 V rms, electrode gap about 0.1 in.), so that the resultant angle is 0.50 mrad or 104 arcsec. This gives a sensitivity of over 40. arcsec/EU, or to put it another way the 2.5 EU signal is over 40 times the rms noise (from all sources) in our apparatus.

The noise sources may be conveniently characterized as internal or uncorrelated (i.e., uncorrelated with any external signal) and external or correlated. Tests have shown that the external noise sources have a very small effect.

The noise is observed to be insensitive to atmospheric pressure (the tank is sealed and fairly rigid). We have carefully avoided materials (or inclusions) of high magnetic susceptibility, and we keep all large magnets well away from the apparatus, so that the only significant noise of magnetic origin is due to eddy currents produced by rotating magnetic fields. It is quite possible to produce rotating fields of sufficient frequency and intensity to cause the float to rotate (at up

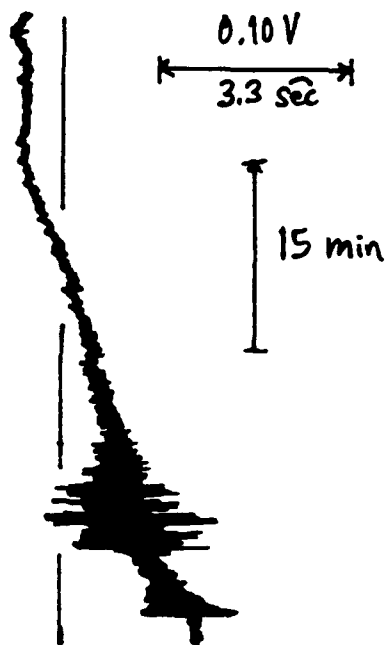
to 1 rpm), and we do so on occasion, but the ordinary 60 Hz rotating magnetic fields produced by lab motors have no observable effect. (In addition, we have obtained 62-mil high-permeability MIL-N14411C 80%-Ni magnetic shields which we plan to install.) Ordinary floor vibrations (people jumping at $R = 2$ m, e.g.) have no observable effect, but large earthquakes (as in Figure 4) or pathological (badly unbalanced) machines (as in Figure 5) which produce large horizontal accelerations or large tilts of the floor do have an effect. Such noise is intermittent and readily identifiable, and causes no real difficulty.

Internal noise sources cause more difficulties, none insurmountable. The torque and center voltages are ac to avoid the possibility of static charge accumulation (though all exposed surfaces of the float are conducting and grounded, and tests with dc voltages never showed any effects attributable to static charge). The center voltage is regulated to $\Delta V/V = 10^{-2}$ and the torque voltage to $\Delta V/V = 5 \times 10^{-4}$. The (spurious) change of angle, $\Delta\theta$, that arises from a shift in torque voltage is $10^{-3}\theta$. The observed (gaussian) voltage noise in the optical detection system amounts to 15 mV (pp) - i.e., 0.5 arcsec.

The dominant noise sources are due to convection currents in the liquid, which may arise either from impurity concentration gradients or from thermal gradients. Nothing is more crucial to the success of a LSTB than the elimination of these two problems.

Water is the universal solvent, and we go to great lengths to purify the water. We use: predeionization, followed by $5\mu\text{m}$ filtration, UV sterilization, $1\mu\text{m}$ filtration, carbon filtration, deionization, and $0.22\mu\text{m}$ filtration. All but the first stage are in a recirculating system.

20 Sept 1985
Second Mexican Quake



6 Sept 1985, 03:47:29 GMT
43.2°N, 110.8°W; R = 4.6
(near Jackson, Wyoming)

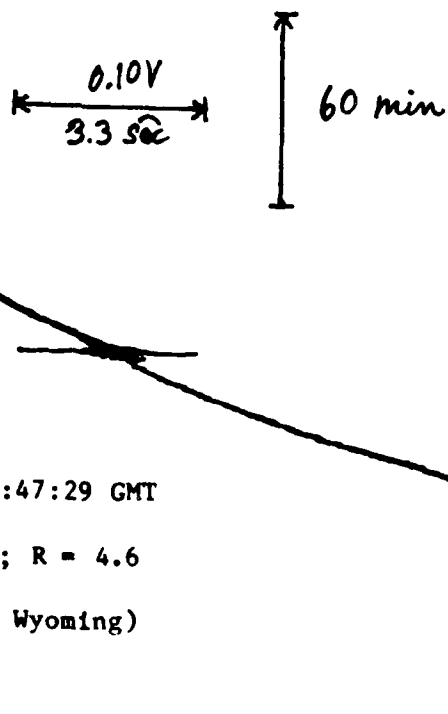


FIGURE 4.

Effects of Earthquakes on LSTB

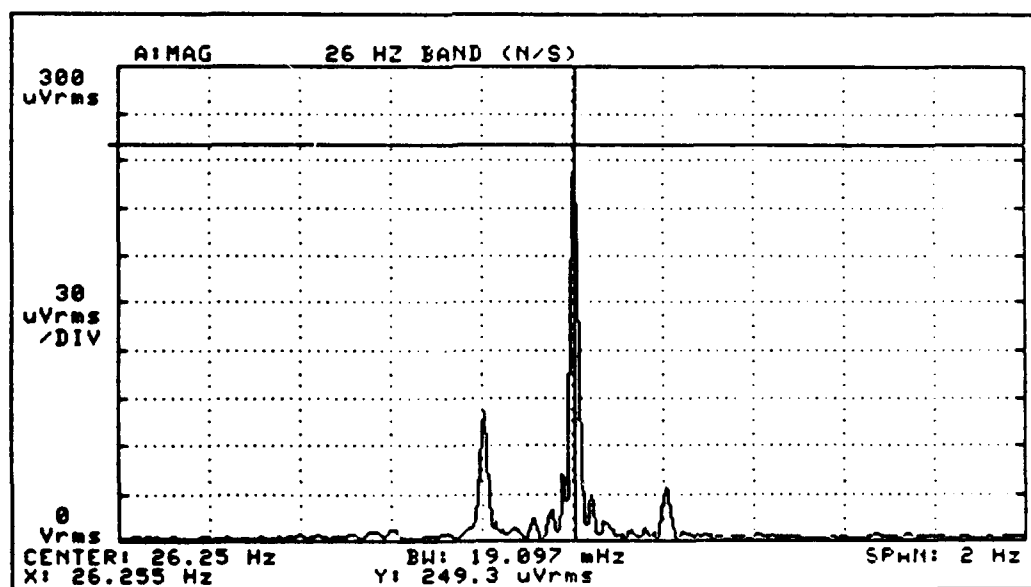
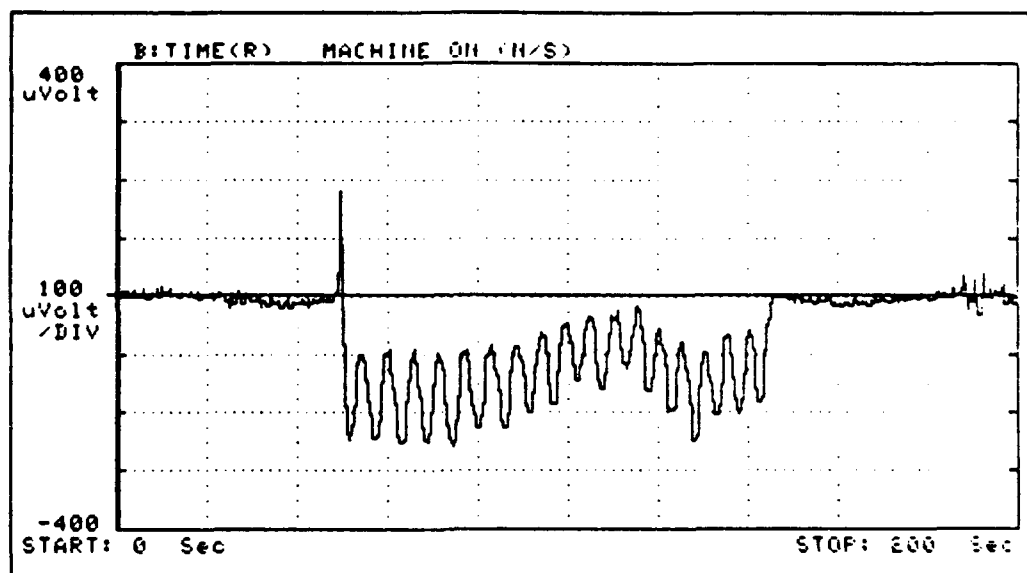


FIGURE 5.

Horizontal Floor Accelerations ($2 \mu\text{V}/\mu\text{m}$)

The resistivity of acceptable water is 10 MΩ-cm (though in practice we usually obtain 15 MΩ-cm). Experience shows that it is necessary to add a liquid non-ionic surfactant to the water to form a liquid surface monolayer which displaces the otherwise inevitable solid surface layer formed of residual (less than 1 ppm) impurities. We use Kodak Photoflo 2100 (not the premix Photoflo 200) or Triton X100, at about 500 ppm. In addition it is crucial to protect the aluminum from corrosive attack by the water. (Such attack is aggravated by dissolved oxygen, so we deoxygenate the water by bubbling filtered N₂ through it.) The main defense that we use against this otherwise inevitable corrosion is the application of a commercial chromate-conversion coating to the well-cleaned and unetched aluminum (as per MIL-C5541).⁸ We do not dissolve chromate ions in the water (which has also been shown to prevent corrosion effectively) as there is some indication that they react with our surfactants. Without this protective coating the LSTB fails ("locks up" in a weak surface gel) in about a week, but with the coating we can operate for eight months or more.

Water is used because it is cheap, safe, readily purified, and because it alone of all liquids has a maximum density point.⁹ Most thermal convection currents in a gravity field are driven by buoyancy and these buoyancy forces arise due to the temperature-dependent density of the liquid (similar to the principle of the hot-air balloon). At 3.98 °C the expansion coefficient of water is zero — so that small thermal gradients do not cause convection currents. There are five distinct sources of thermal gradient forces on a float. Two of these forces (which arise from the temperature-dependence of the surface-tension and the pressure) decenter the float and need not concern us here. The

other three forces (which are due to various types of convection currents) can torque the float. The dominant torquing convection current is the circumferential current in the water between the vertical walls of the float and tank. This is analogous to the "double-pane window" problem, where the idea is to minimize the heat flux.¹⁰ Here however we seek to minimize the convection (it can never go to zero unless the temperature gradient or the width of the gap is exactly zero). In the case of this circumferential current the maximum allowable ΔT (across the tank) for a specified $\Delta \theta$ (at critical damping) scales as:

$$(4) \quad \Delta T \propto (r_2 - r_1)^{-3}$$

so that (all else being equal) we should minimize this gap.

We go to great lengths to insulate and control the temperature of our apparatus. A multilayer cubical enclosure (alternating insulation and reflective metal cans) three feet on a side surrounds the one-foot cylindrical tank. Around the innermost of these outer cans is wrapped flexible hose through which temperature-controlled water flows. Around this same can is wrapped a heater connected to a proportional-integral controller (gain 120 dB, time constant 11000 sec, stability better than 0.1 m°C, resettability 1 m°C).¹¹ The temperature of this composite system is set to give 4.0 ± 0.1 °C at the waterline of the tank. (A serendipitous effect of operation at 4 °C is that the corrosive attack of water is slowed by over two orders of magnitude from its rate at 20 °C.) The net effect is a stability of better than 0.5 m°C on the tank over several days (Figure 6) and a sensitivity to room temperature fluctuations of less than 2 m°C/°C. We believe, in spite of all this, that

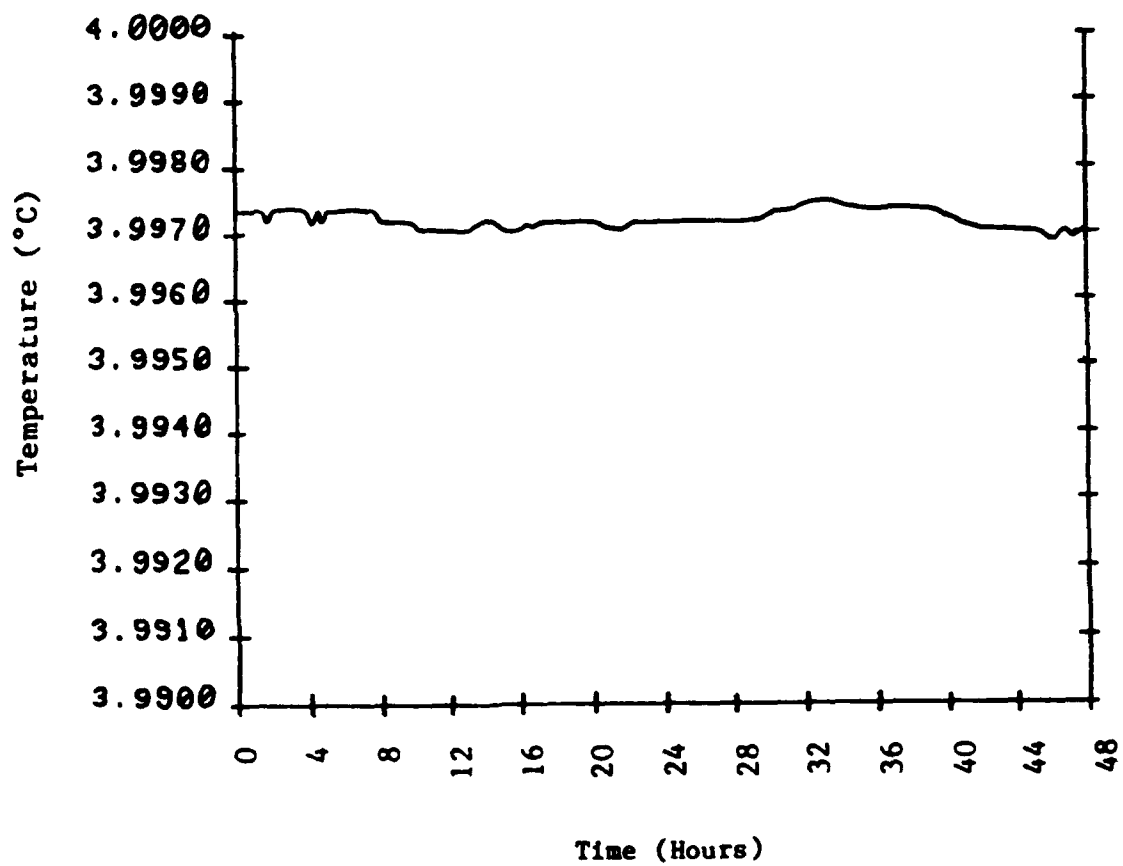


FIGURE 6.
Tank Temperature at the Waterline
(Start: 850915, 22:13)

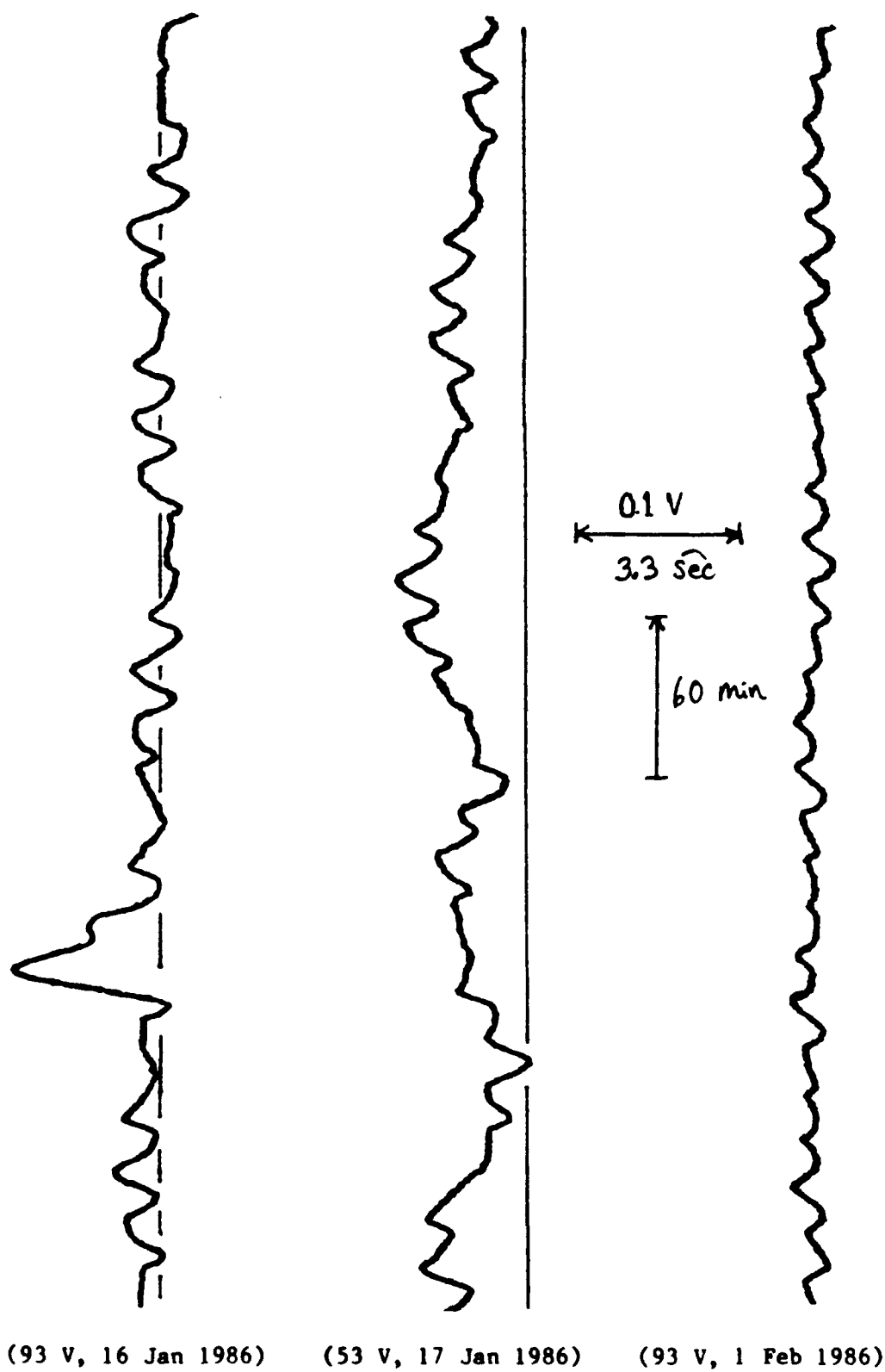


FIGURE 7.

Data from Symmetric LSTB

our dominant noise term is temperature-induced convection currents.

In Figure 7 we present sample data from a run with an identical system in which the two masses were replaced with a disk (of the same total mass and moment of inertia about z). In such a device no torque should arise from curvatures and so any signal is "noise" - torques due to floor vibrations (the 10-min period) or torques due to convection currents. Note that in two weeks (16 Jan to 1 Feb 1986) the "zero" has drifted almost 0.2 V or 0.4 arcsec/day or 0.01 EU/day. Some sample data from the gradiometer system are presented in Figures 8 through 11. As can be seen, a claimed sensitivity of 0.1 EU would not be amiss. The drift rate in Figure 11 is less than 75 mV/day or 2.5 arcsec/day or 0.062 EU/day. (This drift was measured during a period we now have reason to suspect marked the beginning of the degradation of the water, after eight months of operation. Before this it seemed to be about 5 times less, consistent with the data of Figure 7.) It must also be noted that the response time is vastly slower than the various dynamic gradiometers now available. In fact the damping time is almost 20 min (so that the response to a step will be 95% complete after about three such times or one hour) which is about two orders of magnitude slower.

Future plans include the construction of three new machined float-and-tank sets (the current sets are modified spun-aluminum cook pots). These new sets will have a 0.5 cm gap between the float and tank which should reduce the effect of the convection currents by a factor of about 100, and thus floor vibrations and electronics, not convection, should be the dominant noise sources. In addition, the larger tungsten-alloy masses will be at a greater radius for a gain of a factor of 2.64 in sensitivity to curvatures. The first set is ready and will be given a

preliminary test as soon as the larger masses are ready.

This work was supported by the National Bureau of Standards, the Sensor-Technology Division of the Belvoir Research Development and Engineering Center, and the Air Force Geophysics Laboratory.

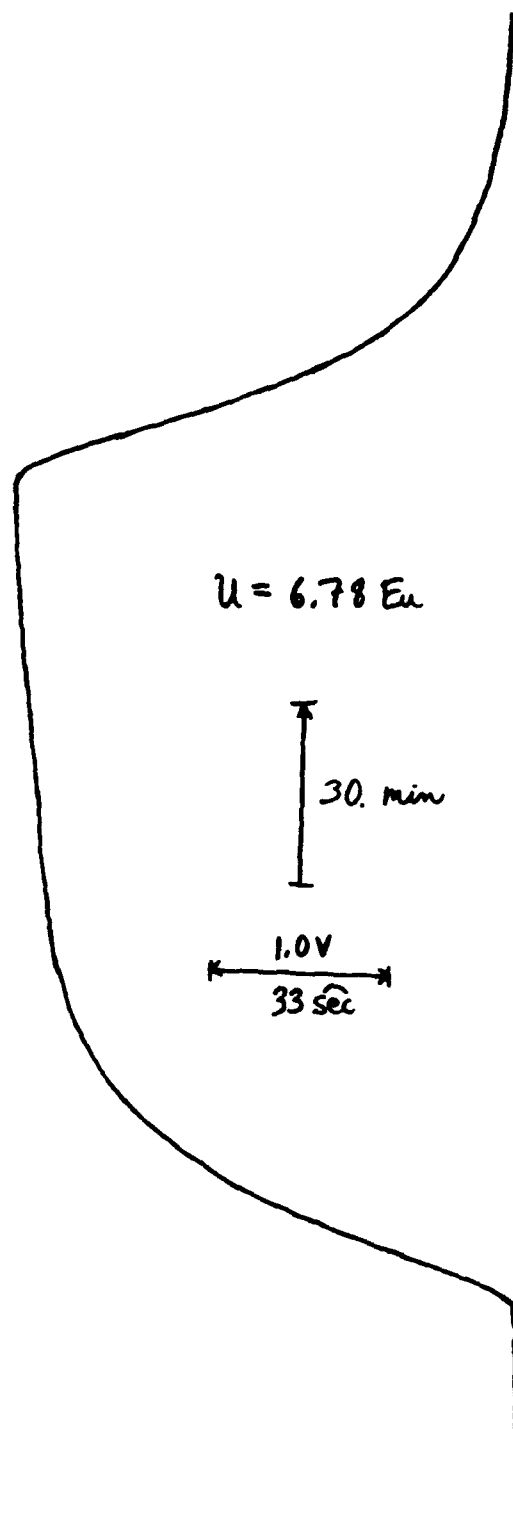


FIGURE 8.
Large Signal (17 Sept 1985)

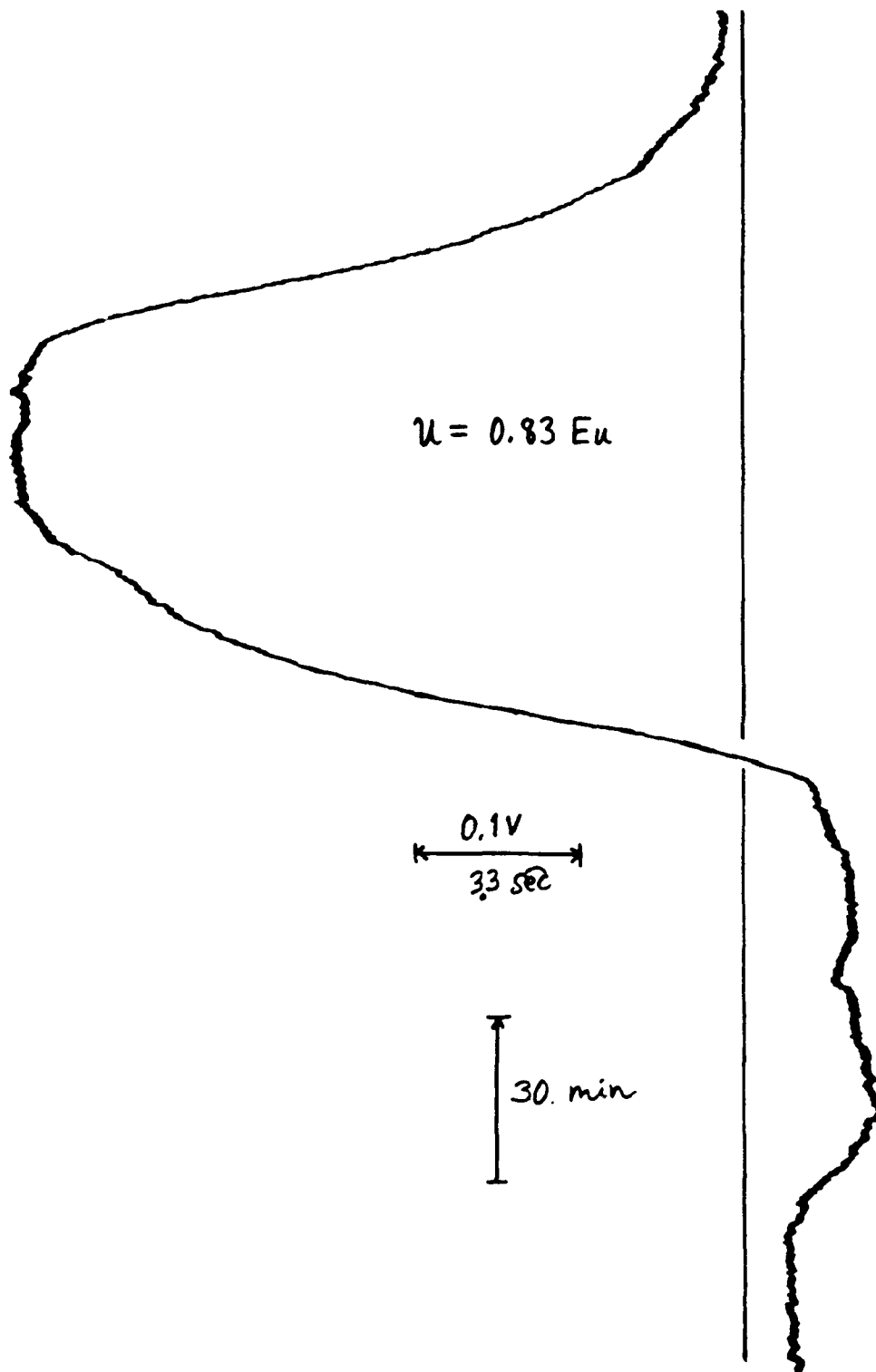


FIGURE 9.

Small Signal (8 Sept 1985)

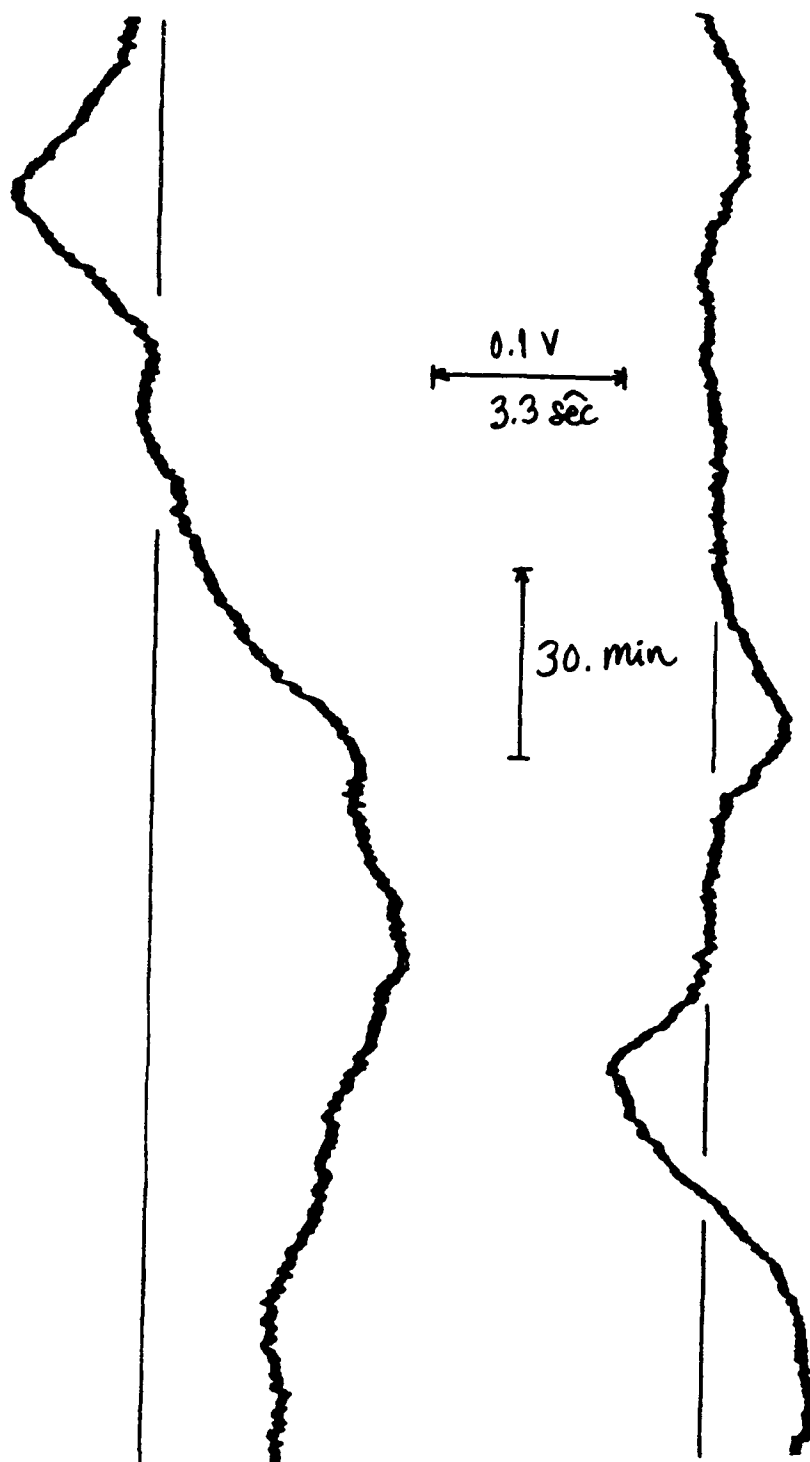


FIGURE 10.

Day (11 AM - 3 PM) and Night (1:30 AM - 5:30 AM)

(19 - 20 Aug 1985)

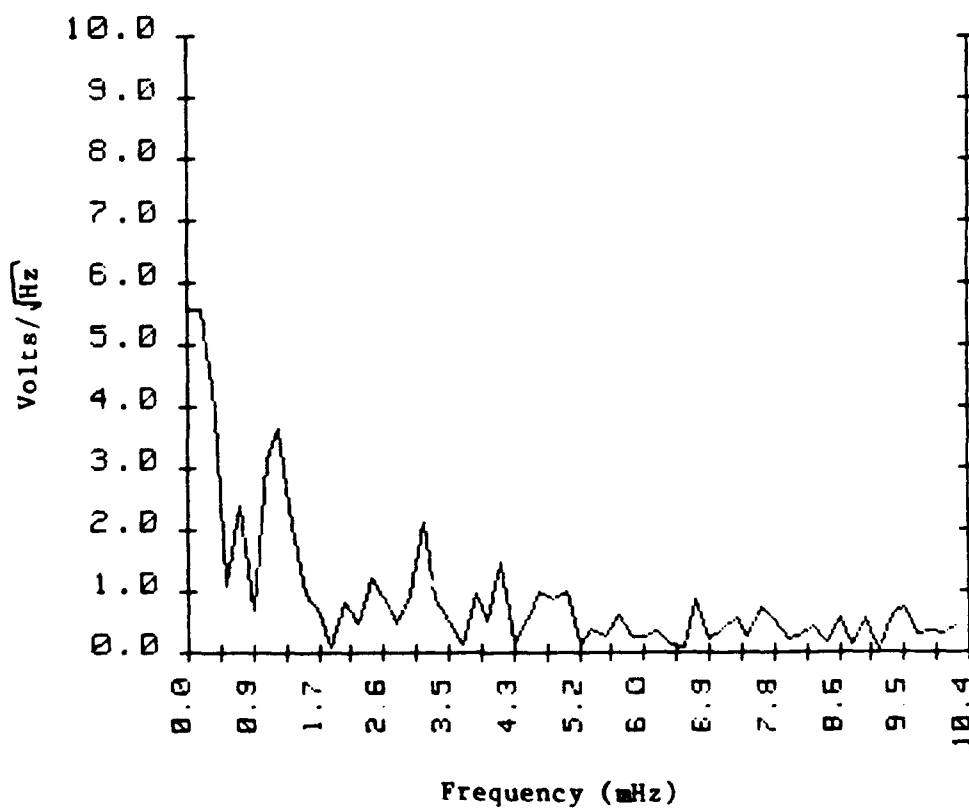
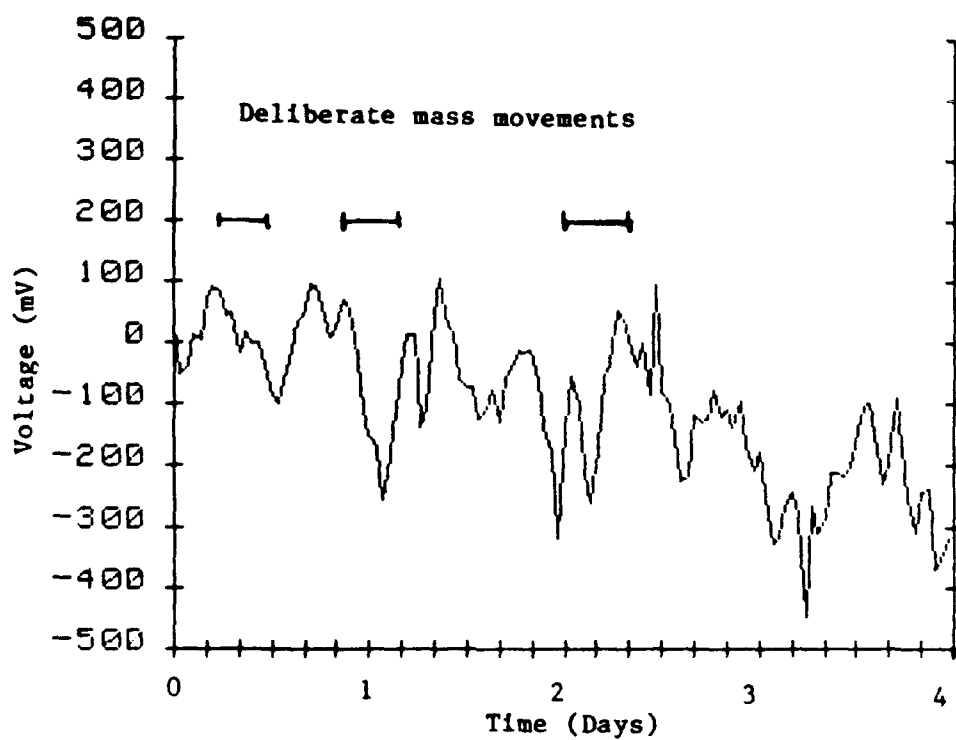


FIGURE 11.
Float Position and Fourier Transform
(Start 850819, 18:16)

¹Roland von Eötvös "Untersuchungen über Gravitation und Erdmagnetismus" Annalen der Physik und Chemie (Wiedmann) 59 (1896) 354-400.

²Karl Jung "Angewandte Geophysik" Handbuch der Experimental-Physik 25.3 (1930) 103-120; J. J. Jakosky Exploration Geophysics² (Los Angeles, California: Trija, 1950) 285 (I am indebted to Prof. Carl Kisslinger of CU for the latter reference).

³Herbert Tomlinson "The Influence of Stress and Strain on the Physical Properties of Matter" Philosophical Transactions of the Royal Society of London: A 177 (1886) 801-837 and "On Certain Sources of Error in Connection with Experiments on Torsional Vibrations" Philosophical Magazine 22 (1886) 414-419.

⁴J. H. Poynting The Mean Density of the Earth (London: C. Griffin, 1894) 8; G. K. Burgess Recherches sur la Constante de Gravitation (U of Paris Thesis; Paris: A. Hermann, 1901) and "A new Form of Cavendish Balance" Physical Review 14 (1902) 247-256; Károly Tangl "Vizsgálatok a gravitációról folyadékba merülő casavárási ingával" Matematikai és Természettudományi Értesítő 43 (1926) 342-352 (we have an English translation).

⁵G. M. Keiser and J. E. Faller "Eötvös experiment with a fluid fiber" Proceedings of the Second Marcel Grossman Meeting on General Relativity ed. R. Ruffini (Amsterdam:North-Holland, 1982) 969-976; R. Augustin, H. deBoer, H. Haars, and W. Michaelis "Ein haftreibungsfreies Quecksilber-Axiallager für die Präzisionsmessung sehr kleiner Drehmomente" Feinwerktechnik und Messtechnik 89 (1981) 280-283.

⁶O. V. Karagioz, V. V. Voronkov, V. P. Izmaylov "Effect of Swinging on Movement of a Torsion Pendulum" Determination of Gravity Constants and Measurement of Certain Fine Gravity Effects ed. Yuri D. Boul-

anger and Marat U. Sagitov (1974, NASA Technical Translation F15-722, microform # NA74-30831) 38-47; O. V. Karagioz, V. V. Voronkov, V. P. Izmaylov and N. I. Agafonov "Optimum Parameters of a Gravitational Variometer" Izvestiya, Earth Physics 11 (1975) 69-74 [translation of Russian original which is pp. 101-108].

⁷J. B. Marion Classical Dynamics of Particles and Systems² (New York: Academic Press, 1970) 399-401.

⁸Nelson J. Newhard "Conversion Coatings for Aluminum: Chemical Properties and Applications" Metal Finishing 70.7 (July 1972) 49-53 and idem 70.8 (August 1972) 66-69. I am indebted to John Krogulski of Aluminum Amchem Co. for this reference and for many useful discussions.

⁹Actually both heavy water and helium-4 have maximum density points. See respectively I. Kirschenbaum Physical Properties and Analysis of Heavy Water (New York: McGraw-Hill, 1951) and R. P. Behringer "Rayleigh-Bénard convection and turbulence in liquid helium" Reviews of Modern Physics 57 (1985) 657-687.

¹⁰G. K. Batchelor "Heat Transfer by free convection across a closed cavity between vertical boundaries at different temperatures" Quarterly of Applied Mathematics 12 (1954) 209-233; J. W. Elder "Laminar free convection in a vertical slot" Journal of Fluid Mechanics 23 (1965) 77-98. I am indebted to Prof. John Hart of CU for useful discussions on this issue.

¹¹M. A. Handschy "A general purpose temperature controller" Journal of Physics E: Scientific Instruments 13 (1980) 998-1001. I am indebted to Dr. Mark Handschy of CU for many useful discussions on temperature control.

PAPER TITLE: LIQUID-SUPPORTED TORSION BALANCE AS GRADIOMETER

SPEAKERS NAME: Paul T. Keyser

Questions and Comments:

* Peter Uginčius: Would your instrument be able to detect solid-earth tides?

SPEAKERS RESPONSE: Don't know. Depends on what U_{xx} , U_{xy} are for solid-earth tides.

1

DEVELOPMENT OF A HIGH-SENSITIVITY, NON-CRYOGENIC GRAVITY GRADIOMETER
FOR SPACE-BORNE USE

F. Fuligni*
E. C. Lorenzini

Smithsonian Astrophysical Observatory, Cambridge, MA 02138

F. Bordoni
B. V. Iafolla

*Istituto di Fisica dello Spazio Interplanetario, 00044 Frascati, Italy

ABSTRACT

The development of a one-axis, non-cryogenic gravity gradiometer is described. The instrument presently developed at IFSI/CNR (Frascati, Italy) consists of two displacement sensors, 50 cm apart in the instrument prototype. Since the sensitive axes of the sensors are orthogonal to the baseline the gradiometer measures the offline components of the gravity tensor. The proof masses, rectangular in shape, are connected to the main frame by a crank shaped attachment; every part being machined integrally from the same Al plate which constitutes the rigid baseline of the instrument. Displacements of each proof mass are measured by capacitive transducers whose outputs are sent to an FET amplifier with noise temperature $T_n = 100$ mk. A feedback loop provides a constant electric field on the moving plates, resulting in a dynamic range enhancement and sensitivity increase. A sensitivity of the order of 10^{-2} EU/Hz^{1/2} is expected, sufficient to perform significant measurements of the earth's gravity field from a low orbit spacecraft such as TSS-2. Results from preliminary laboratory tests of the instrument are also illustrated. On the ground, more exhaustive tests will be performed jointly with the Smithsonian Astrophysical Observatory by using a free fall technique in vacuum in order to isolate the instrument from seismic and acoustic noise.

Work Done Under the Sponsorship of:

PSN/CNR (Italian National Research Council)

Air Force Geophysical Laboratory
and
Hanscom Air Force Base

DEVELOPMENT OF A HIGH-SENSITIVITY

NON-CRYOGENIC GRAVITY GRADIOMETER

FOR SPACEBORNE USE

BY

F. FULIGNI, E. LORENZINI, E. BORDONI,

A.R. LAZAREWICZ, V. IAFOLLA

SMITHSONIAN ASTROPHYSICAL OBSERVATORY
60 GARDEN STREET, CAMBRIDGE, MA 02138

AND

IFSI/CNR (INSTITUTE OF SPACE PHYSICS)
00044 FRASCATI, ITALY

14th GRAVITY GRADIOMETER CONFERENCE
COLORADO SPRINGS, COLORADO 80201

11-12 FEBRUARY 1986

GENERAL DESCRIPTION

- SINGLE-AXIS, OFF-LINE, NON-CRYOGENIC GRAVITY GRADIOMETER
- TWO CONDENSER-PROBE DISPLACEMENT SENSORS INTEGRALLY MACHINED FROM THE SAME AL PLATE
- TO BE OPERATED IN VACUO AT A PRESSURE BETTER THAN 10^{-4} TORR
- TWO DIFFERENT MODELS OF THE INSTRUMENT ARE PLANNED
 - A 100 CM BASELINE, 500 GR SENSITIVE MASS FOR THE FLIGHT INSTRUMENT
 - A 50 CM BASELINE, 250 GR SENSITIVE MASS FOR THE PROTOTYPE

MECHANICAL CHARACTERISTICS OF THE PROTOTYPE

- OVERALL DIMENSIONS: 50 CM X 17 CM (BASELINE X WIDTH)
- INSTRUMENT TOTAL MASS (WITHOUT ELECTRONICS) : ~ 4 KG
- TWO SENSITIVE MASSES: 250 GR EACH
 - SENSITIVE MASSES ATTACHED TO THE MAIN FRAME BY CRANK SHAPED SUSPENSION (SEE FIG. 2) OBTAINED BY INTEGRALLY MACHINING AN AL PLATE
- MECHANICAL RESONANT FREQUENCY 30 HZ
- EACH SENSITIVE MASS IS THE CENTRAL PLATE (SEE FIG. 1) OF A DOUBLE-FACED CONDENSER, $GAP = 30\mu$, $C \approx 900$ pF.
- THE OUTER PLATES OF THE CONDENSER PROBE ARE SPLIT INTO TWO PARTS FORMING 4 CAPACITORS
 - 2 OF THEM ARE THE PICK-UP SENSORS INSERTED IN AN AC BRIDGE AT 20 KHZ
 - THE OTHER 2 ARE PART OF THE FEEDBACK CONTROL SYSTEM THAT PROVIDES A STATIC ELECTRIC FIELD

CONT'D

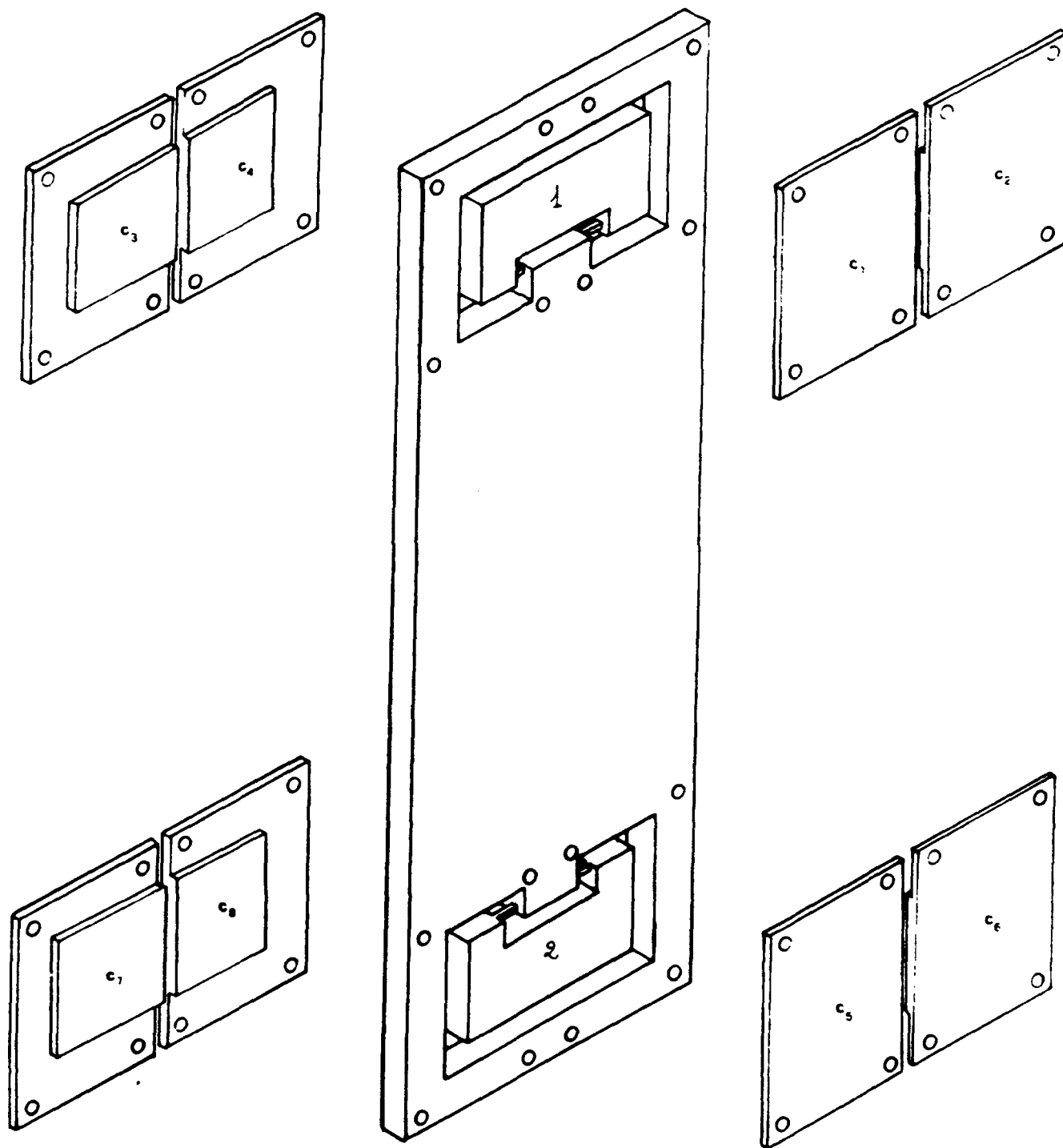


FIGURE 1

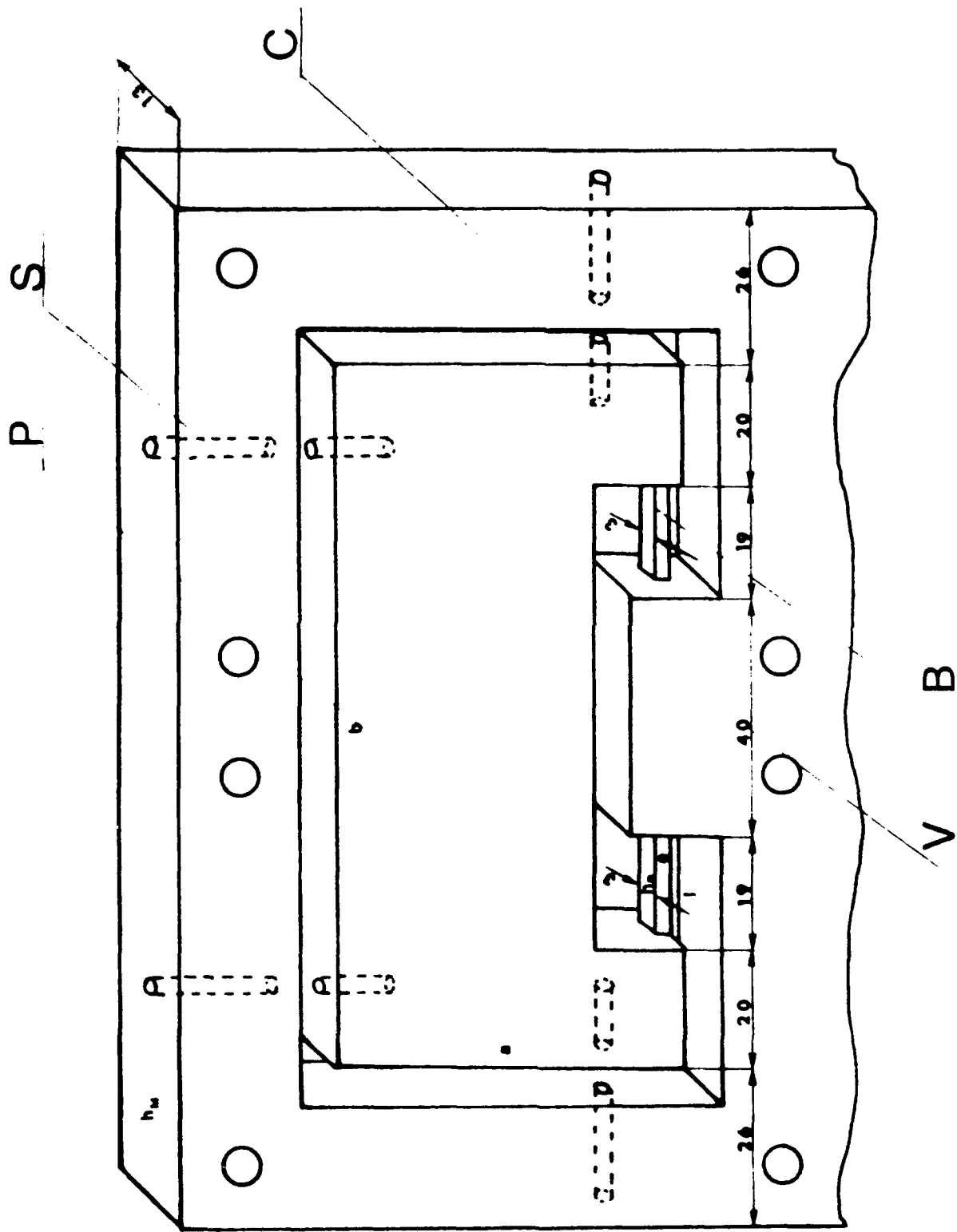


FIGURE 2

- THE STATIC ELECTRIC FIELD PROVIDES THE FOLLOWING CAPABILITIES:
 - DECREASING THE MECHANICAL RESONANT FREQUENCY
 - INCREASING THE DYNAMIC RANGE BY PRODUCING A RESTORING FORCE
- TESTS OF THE RESONANT FREQUENCY DECREASE PERFORMED WITH A 250 GR SENSOR.
MECHANICAL RESONANT FREQUENCY = 60 HZ
- RESULTS PRESENTED IN FIGURE 4 OBTAINED WITH THE ELECTRICAL CIRCUIT SHOWN IN FIGURE 3
 - RESULTS ARE IN ACCORDANCE WITH THE THEORY
 - A RESONANT FREQUENCY VARIATION OF 16 HZ HAS BEEN OBTAINED BY APPLYING 50 VOLTS DC
 - ON THIS BASIS THE PROTOTYPE SHOULD REACH A RESONANT FREQUENCY CLOSE TO ZERO

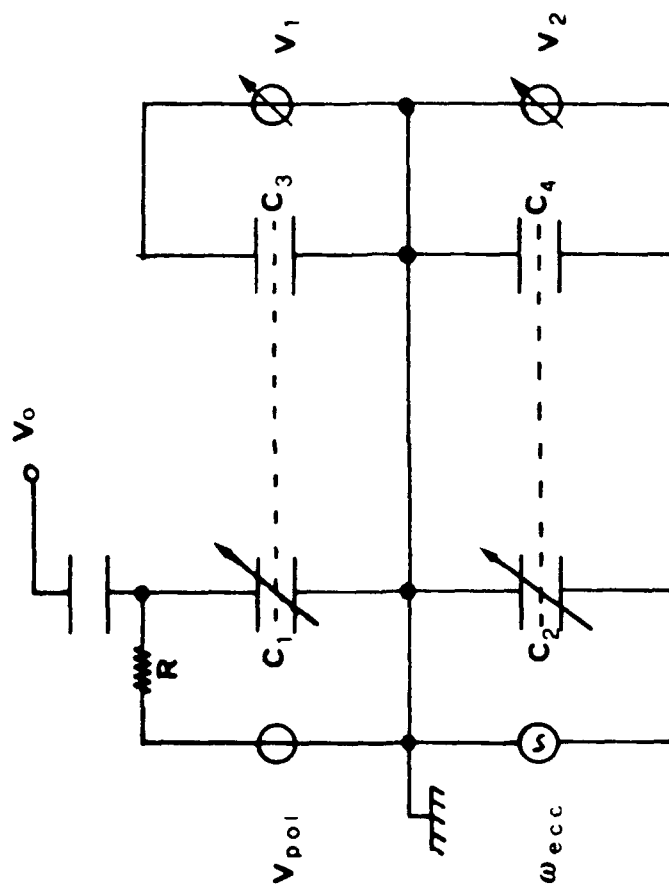


FIGURE 3

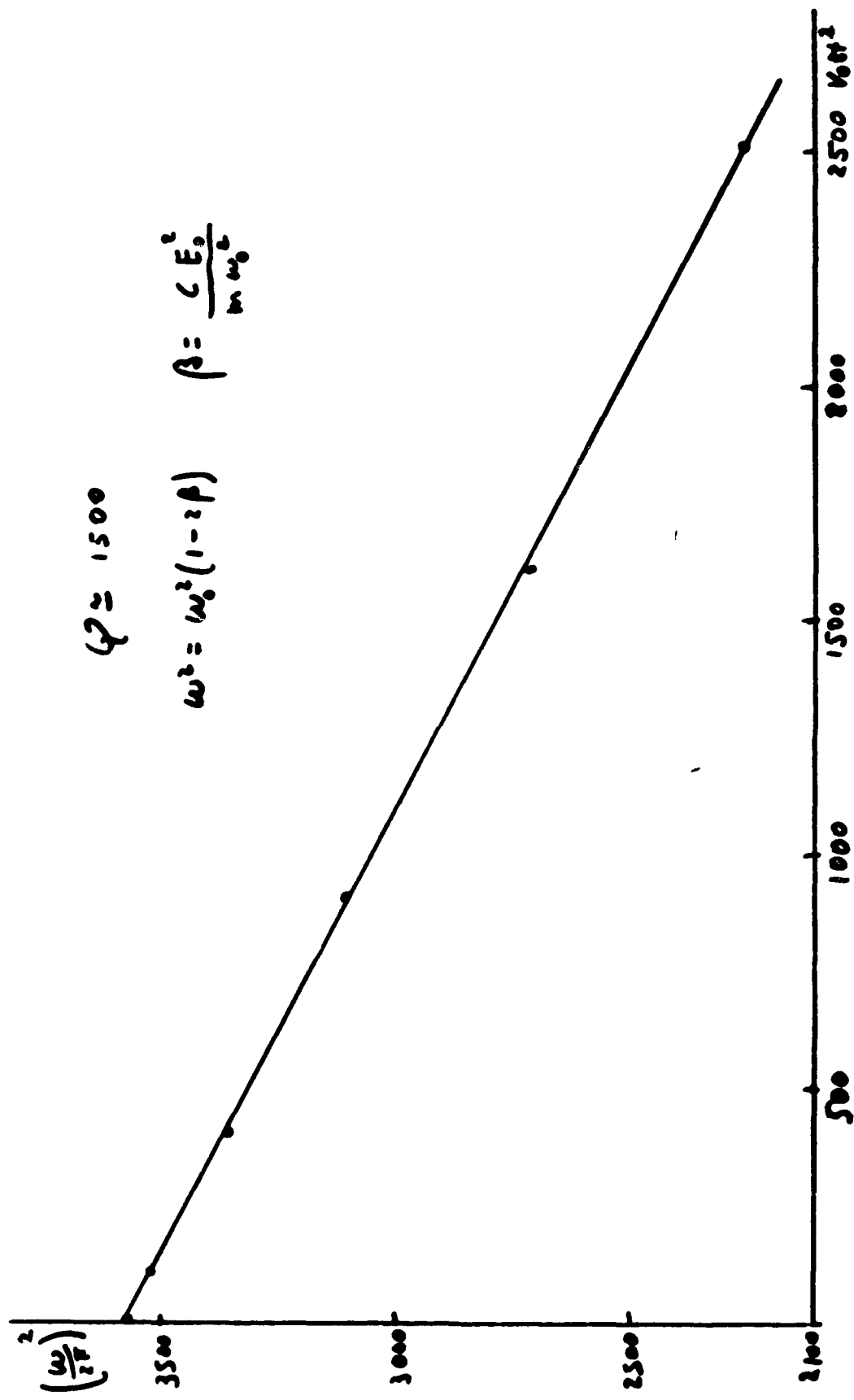


FIGURE 4

ELECTRIC CIRCUIT AND NOISE CHARACTERISTICS

- CONTROL FUNCTIONS GENERATED BY COMPUTER. THE ELECTRIC CIRCUIT OF THE INSTRUMENT IS SHOWN IN FIGURE 5

- PRELIMINARY RESULTS FROM SYSTEM PERFORMANCE TESTS, AS SHOWN IN

FIGURE 6, ARE LIMITED BY ENVIRONMENTAL NOISE

- EXPECTED SENSITIVITY ACCORDING TO

$$\Gamma^2 = \frac{\omega_o^2}{mL^2} \frac{\Delta f}{\omega_o} \left[\frac{4T}{Q} \frac{\omega_o}{\omega_o} + 2T_n \right] k$$

- PROTOTYPE CHARACTERISTICS AS FOLLOWS:

FET PREAMPLIFIER NOISE TEMPERATURE: $T_n = .1 \text{ } ^\circ\text{K}$; $\Delta F/\omega_o = 1$; $\omega_o \approx 10 \text{ RAD/SEC}$;

$L = 50 \text{ CM}$; $M = 250 \text{ GR}$; $Q = 1500$ GIVE AN EXPECTED SENSITIVITY OF $7 \times 10^{-2} \text{ EU IN } 10 \text{ SEC INTEGRATION TIME}$

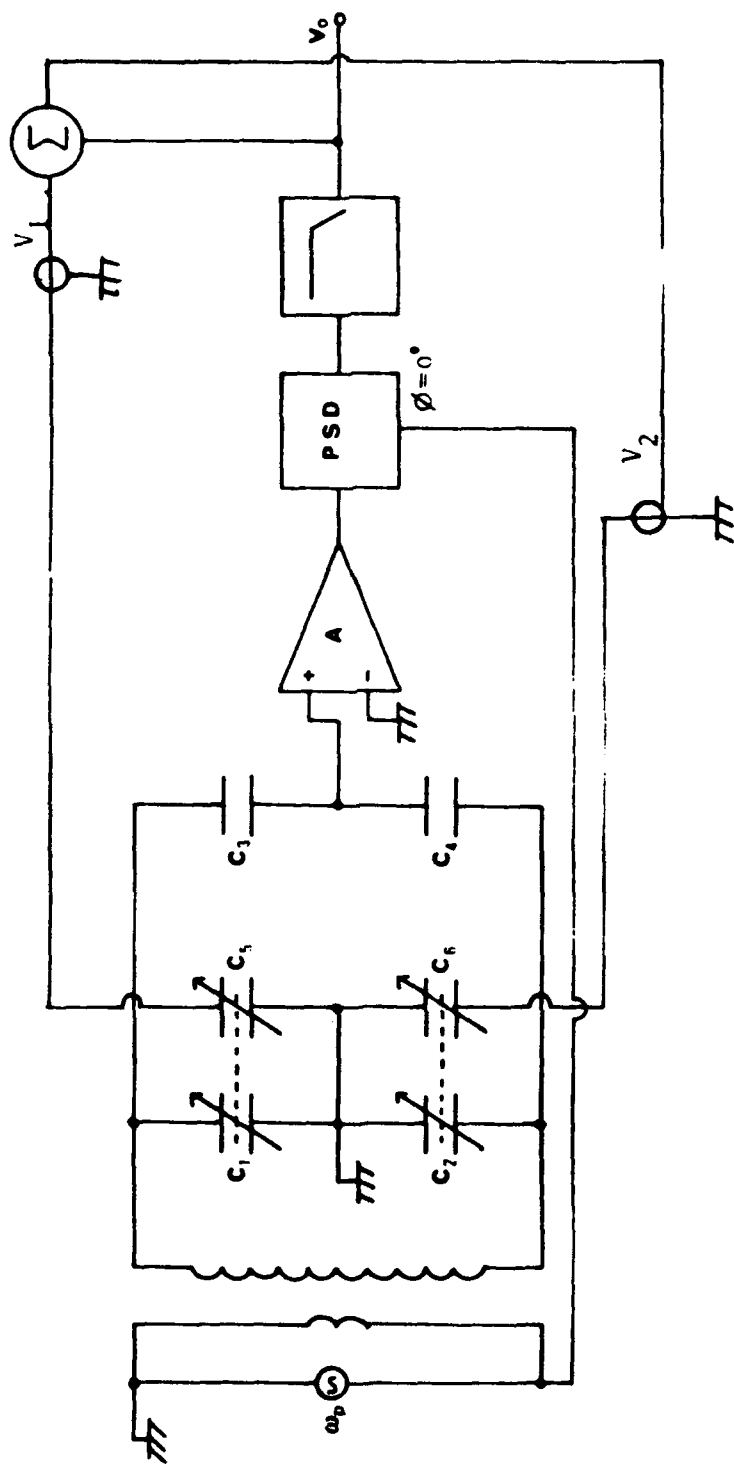


FIGURE 5

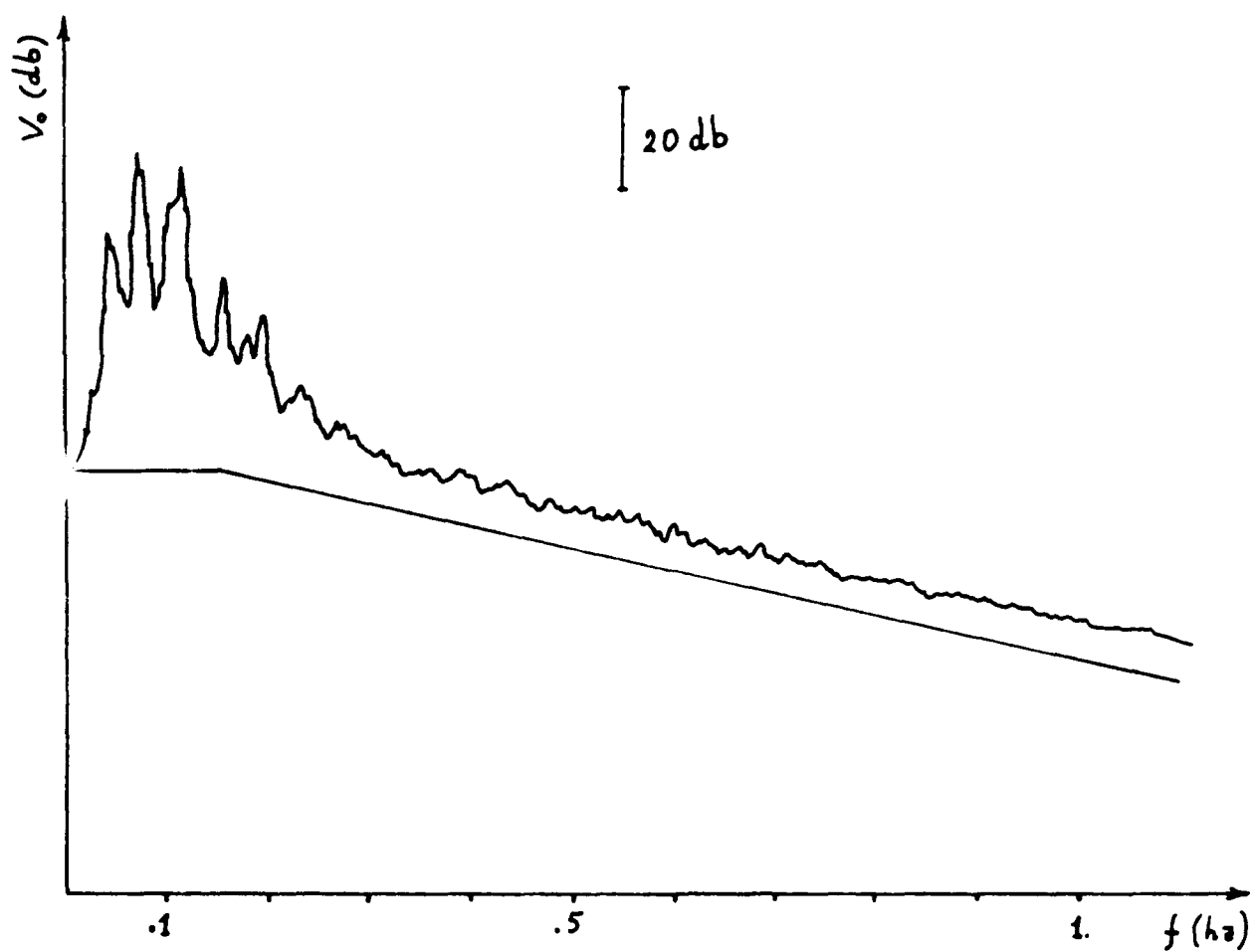
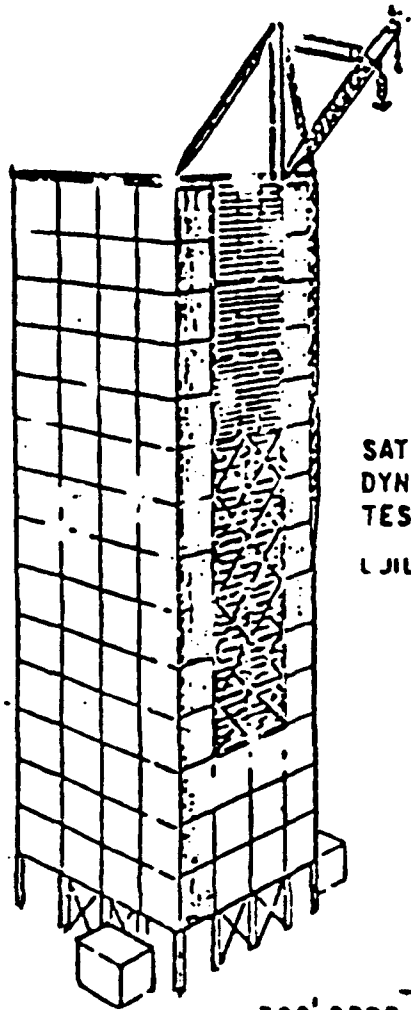


FIGURE 6

FREE-FALL TESTS IN THE NASA/MSEC DROP TOWER

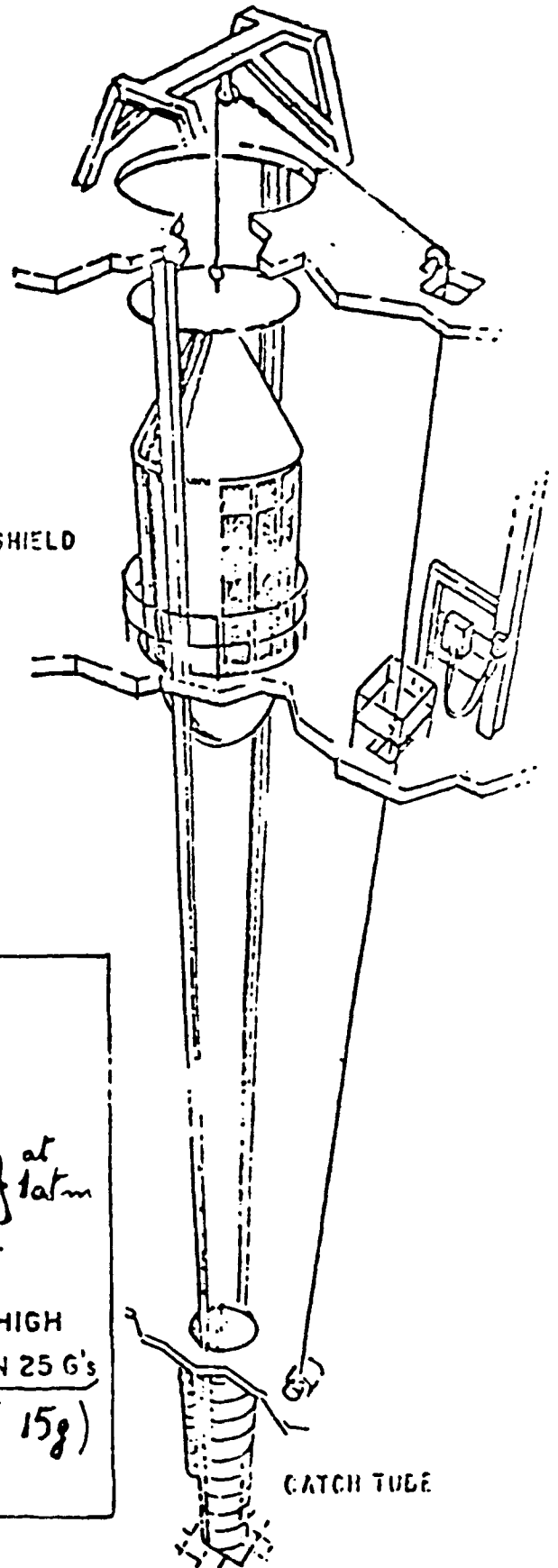
- FREE-FALL TECHNIQUE IS A CONVENIENT WAY TO ISOLATE THE INSTRUMENT FROM ENVIRONMENTAL NOISE
- THE NASA/MSEC DROP TOWER HAS BEEN SELECTED FOR GROUND TESTING OF THE INSTRUMENT PROTOTYPE
 - THE DROP TOWER IS 300' HIGH WITH A DROP TIME OF ~ 4 SEC
 - THE FREE-FALL ELEVATOR, AS SHOWN IN FIGURE 7, WILL BE AUGMENTED WITH A VACUUM CHAMBER AND NECESSARY AUXILIARY EQUIPMENTS: INSTRUMENT PACKAGE, GYRO PACKAGE, TELECOMMUNICATION RELAY FOR DATA TRANSMISSION
- THE GRAVITY GRADIOMETER WILL MEASURE ONE CROSS COMPONENT (e.g. Γ_{yz}) OF THE FIELD GRADIENT PRODUCED BY AN EXTERNALLY LOCATED PERTURBATION MASS
 - THE GEOMETRY OF THE EXPERIMENT IS DEPICTED IN FIGURE 8.
 - THE SIGNAL VS. TIME AND THE POWER SPECTRAL DENSITY OF THE SIGNAL ARE SHOWN IN FIGURE 9.

THE MSFC 300 FOOT DROP TOWER



SATURN V
DYNAMIC
TEST STAIRCASE
BUILDING 4550

300' DROP TOWER



DRAG SHIELD

CATCH TUBE

CAPABILITIES

PAYLOAD

PRESENT _____ 450 LBS.

FUTURE _____ 1000 LBS.

LOW GRAVITY TEST RANGE

MINIMUM _____ $10^{-3} G_0$

MAXIMUM _____ $4 \times 10^{-2} G_0$ } at 1 atm

DROP TIME (294') _____ 4.135 SEC.

TOTAL DROP WEIGHT _____ 4000 LBS.

MAXIMUM TEST PACKAGE _____ 3'DIA. X 3' HIGH

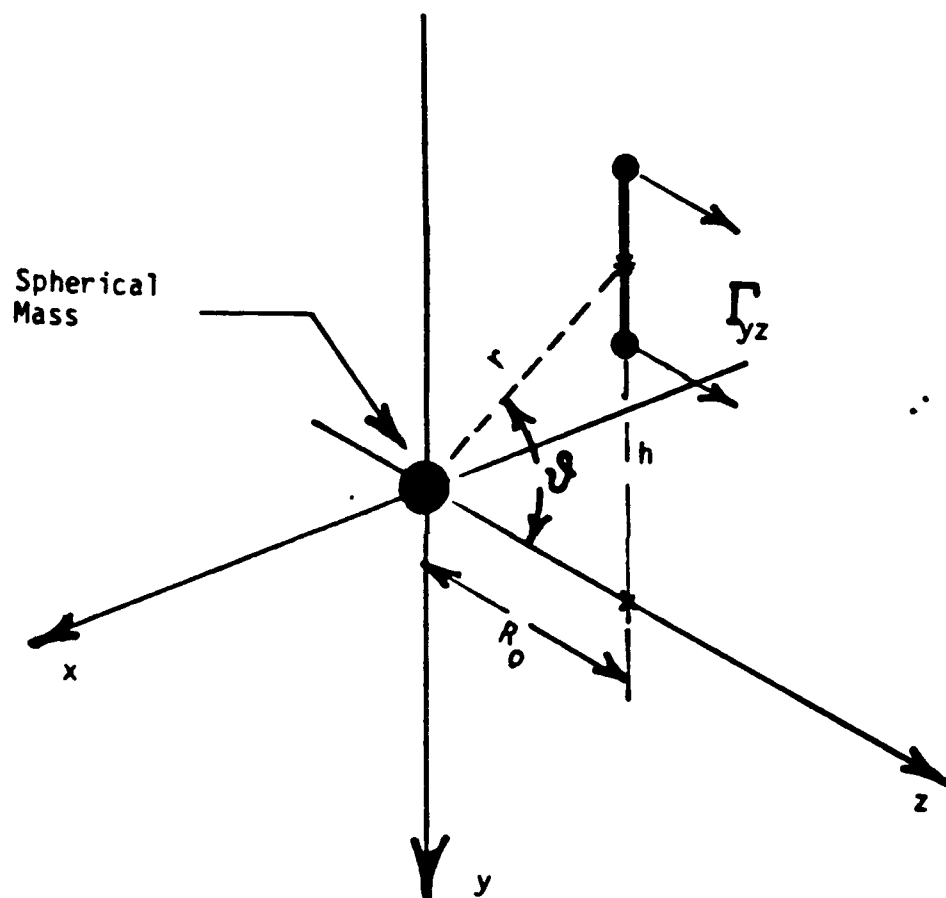
DECELERATION _____ LESS THAN 25 G's

INSTRUMENTATION CHANNELS _____ 6 $4(15g)$

NON-DESTRUCTIVE TESTING

ZERO TURN-AROUND TIME

FIGURE 7



GEOMETRY OF THE FREE-FALL EXPERIMENT

FIGURE 8

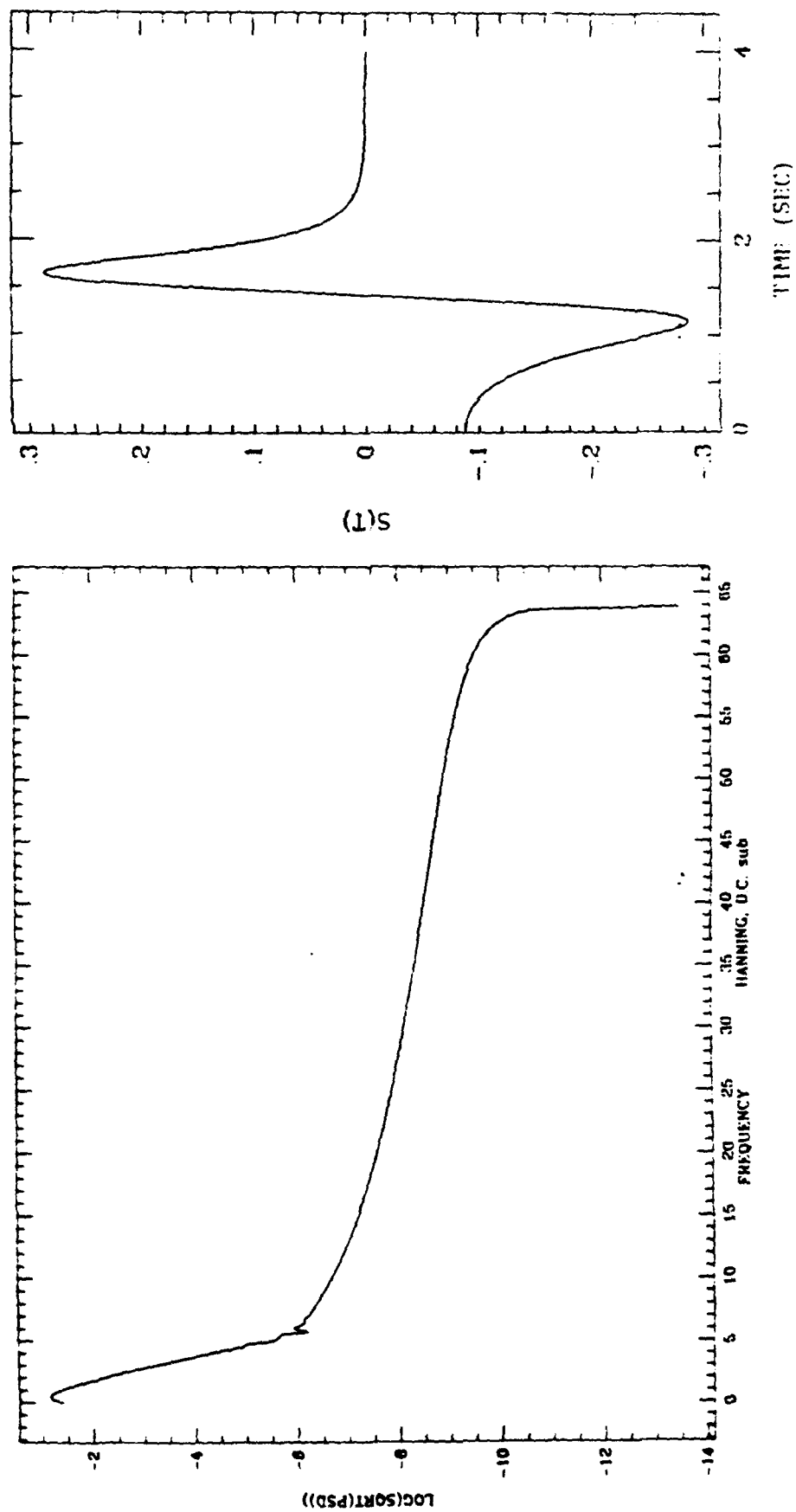


FIGURE 9

CONCLUSIONS

- RESULTS OF LABORATORY TESTS PERFORMED SO FAR INDICATE THAT THE PREDICTED INSTRUMENT PARAMETERS ARE ACHIEVABLE IN PRACTICE. THEREFORE THE EXPECTED SENSITIVITY OF 7×10^{-2} EU IN 10 SEC INTEGRATION TIME SHOULD BE ATTAINABLE BY THE PROTOTYPE.
- A BIGGER INSTRUMENT, 100 CM BASELINE, 500 GR SENSITIVE MASS, IS PLANNED FOR SPACEBORNE USE WITH AN EXPECTED SENSITIVITY OF 2.5×10^{-2} EU IN 10 SEC INTEGRATION TIME. POTENTIAL CARRIER IS THE TSS-2 (TETHERED SATELLITE SYSTEM)
- THIS INSTRUMENT CAN BE EXTENDED TO A MULTI-AXIS DESIGN AT THE EXPENSE OF GREATER COMPLEXITY IN THE INSTRUMENT ASSEMBLY

PAPER TITLE: DEVELOPMENT OF A HIGH SENSITIVITY, NON-CRYOGENIC GRAVITY GRADIOMETER

SPEAKERS NAME: Enrico Fuligni

Questions and Comments:

Dave Sonnabend: I don't believe nuisance dynamic angular rate in falling elevator can be measured to adequate accuracy.

SPEAKERS RESPONSE: Not sure.

Warren Heller: Common mode acceleration must be measured and controlled to one part in ten to the ninth. I did not see that this issue was addressed.

Ho Jung Paik: 1. Your basic design involving only two proof masses makes your device an angular accelerometer. At $10^{-2}E$ level, you need to compensate an angular acceleration to $10^{-11} \text{ rad s}^{-2}$. Which gyroscope would you use to compensate this noise?

2. Even if there is no angular acceleration, there will be a centrifugal acceleration due to angular velocity.

SPEAKERS RESPONSE: 1. There is no angular acceleration because the instrument will be tested in free fall.

2. The geometry of the instrument makes it insensitive to centrifugal acceleration.

Ho Jung Paik: That's not true. If you have an angular velocity 45° away from the baseline, you will be sensitive to the centrifugal acceleration. This will be true even if you employ 4 masses as Metzger does. It has been proven that the centrifugal acceleration cannot be taken out, even in principle in a second-order gradiometer, without stabilizing the platform.